UNIVERSITÀ DEGLI STUDI DI PADOVA

UNIVERSITÀ DEGLI STUDI DI PADOVA

Dipartimento di Scienze del Farmaco

SCUOLA DI DOTTORATO DI RICERCA IN SCIENZE MOLECOLARI

INDIRIZZO: SCIENZE FARMACEUTICHE

CICLO XXVI

SISTEMA INNOVATIVO VESCICOLARE pH SENSIBILE PER IL DIREZIONAMENTO DI siRNA AL TUMORE

Direttore della Scuola: Chiar.mo Prof. Antonino Polimeno

Coordinatore d'indirizzo: Chiar.mo Prof. Alessandro Dolmella

Supervisore: Dott. Stefano Salmaso

Dottorando: Elena Gallon

UNIVERSITÀ
DEGLI STUDI
DI PADOVA

UNIVERSITY OF PADUA

Department of Pharmaceutical and Pharmacological Sciences

DOCTORAL SCHOOL IN MOLECULAR SCIENCES

PHARMACEUTICAL SCIENCES CURRICULUM

XXVI CYCLE

NOVEL pH RESPONSIVE POLYMERIC VESICLES FOR siRNA DELIVERY TO THE TUMOR

School Director : Chiar.mo Prof. Antonino Polimeno

Curriculum Coordinator: Chiar.mo Prof. Alessandro Dolmella

Supervisor: Dott. Stefano Salmaso

Ph.D Student: Elena Gallon

Abbreviations

AIBN	Azobisisobutyronitrile
B16-F10-luc-G5 cells	Mouse melanoma cells transfected with SV40 promoter for luciferase
CAC	Critical Aggregation Concentration
$CDCl_3$	Deuterated chloroform
CF_3COOH	Trifluoroacetic acid
CO_2	Carbon dioxide
CPADB	4-cyanopentanoic acid dithiobenzoate
macro CTA	Macro Tranfer Agent
Da	Dalton
DAPI	4',6-diamidino-2-phenylindole
DCC	Dicyclohexylcarbodiimide
DCM	Dichloromethane
DCU	Dicyclohexylurea
DLS	Dynamic Light Scattering
DMAP	4-Dimethylaminopyridine
DMEM	Dulbecco's Modified Eagle Medium
DMF	Dimethylformamide
DMSO	Dimethyl sulfoxide
DP	Degree of Polymerisation
ds-siRNA	Double strand silencing ribonucleic acid

dsDNA	Double strand deoxyribonucleic acid
EDTA	Ethylenediaminetetraacetic acid
Et_2O	Diethyl ether
Et_3N	Triethylamine
EtOAc	Ethyl acetate
FBS	Fetal Bovine Serum
FR	Folate Receptor
GMA	Glicerol Methacrylate
GPC	Gel permeation chromatography
H_2SO	Sulfuric acid
ImHeMA	Imidazole hexyl methacrylate
K_2CO_3	Potassium carbonate
$K_3Fe(CN)_6$	Potassium hexacyanoferrate (III)
KB cells	Cells from human cervical carcinoma
KCl	Potassium chloride
MCF7 cells	Cells from human breast adenocarcinoma
MeOH	Methanol
$MgCl_2$	Magnesium chloride
$MgSO_4$	Magnesium sulfate
MTS	[3-(4,5-dimethylthiazol-2-yl)-5-(3-carboxymethoxyphenyl)-2-(4-sulfophenyl)-2H-tetrazolium, inner salt

MW	Molecular Weight
N_2	Nitrogen
NaCl	Sodium Chloride
NaH	Sodium hydride
NaOH	Sodium hydroxide
NHS	N-Hydroxysuccinimide
PBS	Phosphate Saline Buffer
PDI	Poly Dispersity Index
PEG	Polyethylene glycol
PEI	Polyethylenimine
pKa	Acid dissociation constant
PMS	Phenazine methosulfate
RAFT	Reversible addition−fragmentation chain-transfer polymeri-zation
RBCs	Red Blood Cells
RNAse	Ribonuclease
RP-HPLC	Reverse Phase – High Pressure Liquid Chromatography
t -Boc	Di-tert-butyl dicarbonate
TEMED	Tetramethylethylenediamine
TFA	Trifluoroacetic acid
THF	Tetrahydrofuran
TLC	Thin Layer Chromatography

Tris-HCl	Tris(hydroxymethyl)aminomethane hydrochloride
UV	Ultraviolet
VIS	Visible

Riassunto

Negli ultimi decenni sono stati sviluppati, in maniera sempre più consistente, *drug carriers* supramolecolari per la terapia tumorale capaci di aggregare in nanostrutture grazie all'utilizzo di polimeri "intelligenti". Questi sistemi sono stati progettati in modo tale da essere direzionati selettivamente al tessuto tumorale, mantenere l'efficacia terapeutica del farmaco caricato e ridurre gli effetti collaterali a livello sistemico. Polimeri con proprietà anfifiliche sono in grado di formare vescicole, chiamate anche polimerosomi, che possono essere caricate con farmaci idrofilici/idrofobici.

Il progetto di ricerca qui riportato ha avuto come fine ultimo la sintesi di un copolimero pH-sensibile a tre blocchi in grado di aggregare in vescicole utilizzate per il *delivery* di specifici *silencing RNA* (siRNA) alle cellule cancerose con lo scopo di rendere silenti specifici meccanismi coinvolti nel processo di progressione tumorale. Grazie alle sue nano-dimensioni, il sistema di *drug-delivery* colloidale è previsto andare incontro ad accumulazione passiva nel tessuto tumorale per *Enhanced Permeability and Retention Effect* (EPR) ed avere accesso selettivamente al comparto cellulare citosolico grazie al bioriconoscimento da parte della cellula tumorale. Una volta all'interno degli endosomi, la capacità delle vescicole polimeriche di rispondere in maniera differente ai diversi pH renderà possibile la disaggregazione del *carrier* e il rilascio del siRNA caricato.

I polimeri utilizzati sono stati sintetizzati in modo tale da rispondere con una rapida disaggregazione del nano-sistema una volta in contatto con l'ambiente acido caratteristico dei compartimenti endosomiali e lisosomiali, ottenendo quindi il rilascio del siRNA.

I polimeri a tre blocchi utilizzati presentano due monomeri idrofilici alle estremità, chiamati *poly-ethilenglycole* (PEG) 1.9 kDa - 3.5 kDa e *poly-glycerolmethacrylate (GMA),* e inoltre un blocco centrale pH sensibile, *poly-imidazole hexyl methacrylate* (ImHEMA) che guida la formazione e la disaggregazione delle vescicole. Il polimero ottenuto con PEG 3.5 kDa verrà coniugato all'agente direzionante acido folico per conferire proprietà di bioriconoscimento cellulare ai polimerosomi.

I polimerosomi sono stati preparati miscelando i polimeri ottenuti con 1.9 e 3.5 kDa in rapporti adeguati. I copolimeri in rapporto 90:10 w/w formano vescicole stabili a

pH 7.4 e temperatura ambiente con un diametro medio di 100 nm. La stabilità dei polimerosomi a 37°C è stata modulata aumentando il rapporto del copolimero PEG 3.5 kDa. Vescicole ottenute con rapporto di polimeri 90/10 w/w 1.9 kDa e 3.5 kDa sono state caratterizzate morfologicamente al microscopio elettronico a trasmissione TEM mettendo in evidenza forma sferica e alta omogeneità dimensionale. Le vescicole polimeriche caricano efficacemente sequenze di DNA doppia elica (dsDNA) con una resa molare del 14% come dimostrato da analisi spettrofotometriche. Il dsDNA viene rilasciato in 8 ore quando i polimerosomi vengono incubati a pH 5; a pH 7.4 invece il rilascio è risultato essere quasi nullo. La capacità del polimero di complessare il dsDNA è controllata dal pH esterno: studi di ritardo elettroforetico hanno evidenziato che il polimero e il dsDNA sono completamente associati per rapporti N (gruppi amminici del polimero) /P (gruppi fosfato del DNA) di 2/1 a pH 5. Nessuna formazione di complessi è stata osservata per N/P ratio fino a 20/1 a pH 7.4, condizioni cui l'unità imidazolica risulta pressochè neutra.

Studi di citotossicità eseguiti su cellule B16F10 da melanoma di topo hanno mostrato una buona biocompatibilità delle vescicole polimeriche a concentrazioni di 1, 2, 3 mg/mL. La alta attività emolitica del polimero a pH acido (pH 5) conferma la capacità del materiale nell'indurre la lisi della membrana endosomiale. In dettaglio, i risultati hanno mostrato un'attività emolitica pari al 70% a pH 5, mentre in condizioni fisiologiche (pH 7.4) non è stata rilevata alcuna lisi dei globuli rossi.

Le formulazioni polimeriche, con e senza agente di *targeting*, sono state incubate con cellule KB da cancro alla cervice uterina e cellule MCF7 da adenocarcinoma mammario, le quali rispettivamente sovreaesprimono e non sovraesprimono il recettore folato, in modo tale da studiare l'efficacia di direzionamento di polimerosomi aventi il folato sulla loro superficie. L'internalizzazione di vescicole caricate con dsDNA marcato per mezzo del fluoroforo *cyanine-3*, valutato mediante analisi fluorimetrica su lisato cellulare e per mezzo di citofluorimetria, ha dimostrato essere di circa 3 volte maggiore per cellule KB comparate a MCF7. Quindi, polimerosomi caricati con ds-siRNA per il silenziamento dell'enzima luciferasi sono state testate su cellule B16F10 trasfettate con il promotore per l'enzima e sovraesprimenti il recettore per il folato. L'esperimento ha mostrato una diminuzione

della bioluminescenza imputata all'attività luciferasica del 30% rispetto alle vescicole vuote.

I risultati riportati sono stati confermati grazie a studi di microscopia confocale eseguiti sulle stesse linee cellulari sopra descritte. Le immagini hanno evidenziato un accumulo di dsDNA marcato in modo significativamente più elevato in cellule KB e con una maggiore localizzazione della macromolecola nel compartimento nucleare.

Abstract

Supramolecular drug carriers based on physical assembly of "smart" polymers have emerged in last decades to obtain novel carriers for the tumor therapy. These systems are designed to target cancer tissue, preserve the therapeutic activity of loaded drug and reduce their systemic side-effects. Amphiphilic copolymers can be assembled in vesicles that can be loaded with hydrophilic and/or hydrophobic drugs.

The research project was aimed at synthesizing a triblock pH-responsive polymer to be assembled in vesicles for the delivery of specific siRNA to cancer cells to silence specific functions involved in the tumor progression. According to its nanometric size, the colloidal drug delivery system is intended to undergo passive accumulation in the cancer tissue by EPR effect and access selectively the cytosol by cancer cell biorecognition. Once the vesicles are localized in the endosomes, their pH responsiveness will guarantee for the disassembling of the carrier and the release of the siRNA payload.

The vesicles forming polymer was synthesized in order to respond to the acid environment in the endosomal and lysosomal compartments with prompt disassembly of the nanocarrier and consequent siRNA release. The triblock copolymers include two hydrophilic blocks at the terminal ends, namely 1.9 kDa or 3.5kDa PEG and poly-glycerolmethacrylate (GMA), and a central pH sensitive block, imidazole hexyl methacrylate (ImHeMA) that control the assembly and disassembly of the vesiscles. The polymer obtained with the 3.5kDa PEG is intended to be conjugated with the targeting agent folic acid to confer biorecongnition properties to the polimersomes. The vesicles were prepared by mixing the polymers obtained with 1.9 kDa and 3.5 kDa at adequate ratios. The copolymers with ratio 90:10 w/w polymers 1.9 kDa and 3.5 kDa self-assemble in vesicles at pH 7.4 with a mean size of 100 nm as detected by light scattering analysis and are very stable at room temperature. At 37°C the stability of vesicles was modulated by increasing the ratio of the copolymer 3.5 kDa PEG. Vesicles obtained with ratio 90:10 w/w polymers 1.9 kDa and 3.5 kDa were imaged by TEM microscopy showing a spherical shape and high size homogeneity. The polymeric vesicles were found to loads very efficiently double stranded DNA (dsDNA) sequences with a 14% molar loading yield as shown by UV-Vis spectrometry and release them in 8 hours when incubated at pH 5, while vesicles showed very limited DNA release at pH 7.4. The

physical assembly of the dsDNA with the pH responsive triblock copolymer was controlled by the environmental pH: gel retardation electrophoresis showed that the polymer and dsDNA completely associate at a N/P ratio of 2/1 at pH 5, while no association was observed up to a N/P ratio of 20/1 at pH 7.4 where the ImHeMA block is neutral.

Cell viability assay performed on B16F10 mouse melanoma cells showed a remarkable biocompatibility of the polymeric vesicles at concentration of 1, 2, 3 mg/mL. The high hemolytic activity of the polymer at acidic pH (pH 5) support for the capacity of the material to induce endosomal membrane disruption. The results displayed a 70% hemolytic activity at pH 5, while in physiological condition (pH 7.4) no red blood cell lysis was detected. Polymer formulations, with and without the folate-tipped terminal ends, were incubated with KB human cervical carcinoma cell line and MCF7 human breast adenocarcinoma cell line, that overexpress and do not express the folate receptor respectively, to investigate active targeting properties of the folate tipped vesicles. The uptake of vesicles loaded with cyanine 3 labeled dsDNA, that was evaluated by fluorescence spectroscopy on cell lisate and by cytometry, was 3 times higher in KB cells compared to MCF-7 cells. Vesicles loaded with double strand siRNA for the silencing of luciferase were investigated on luciferase transfected B16F10 cells that express the folate receptor. The decrease of bioluminescence in cell sample treated with siRNA loaded folate targeted vesicles was 30% with respect to control empty vesicles.

The above results were confirmed by confocal microscopy carried out with the same cancer cell lines. Confocal microscopy showed a significantly higher accumulation of the fluorescently labeled dsDNA in KB cells and a major localization of the macromolecule at the nuclear compartment.

1.INTRODUCTION

In recent years nanotechnology, described as manipulation of matter at the nanometric scale, has been applied to many different fields with encouraging results. The nanotechnology involves a variety of different files such as surface science, organic chemistry, molecular biology, semiconductor physics, micro fabrication, drug delivery and many more.

Nanocarriers represent a valuable outcome of the nanotechnological investigations and have been considered for potential biomedical exploitation such as cancer therapy, where they can carry therapeutic agents safely to a targeted organ, particular tissue or cell (1).

According to recent statistical analysis, cancer is one of the foremost causes of death worldwide with an overall mortality estimated of 1.596.670 diagnoses and 571.950 deaths in United States in 2011 alone (2) This disappointing report is in part ascribed to the lack of efficient and reliable therapies that allow to safely deliver therapeutic agents to the target sites selectively, without side effects involving the normal tissue. Nowadays, classical antitumor therapy involves the combination of surgical resection, radiation therapy and chemotherapy. These therapies are associated to high toxicity and patient mortality because of their unwanted effects on normal cells. Clinical benefits can stem from targeting anticancer agents selectively to disease tissues, from overcoming peculiar biological barriers and avoiding the accumulation in off target healthy tissues.

The word “nanoparticle therapeutics” refers to carriers made by structural components such as lipids and polymers (3) that provide for a container to load the therapeutic molecules. These systems represent a challenge in cancer therapy, where nanotechnology is significantly involved in proposing and screening solutions to evident delivery issues. Many different kinds of nanovectors were developed in the last decades, such as liposomes, micelles, dendrimers, nanospheres and nanocapsules, and more recently polymer based vesicles, namely polymersomes (Figure 1.1).

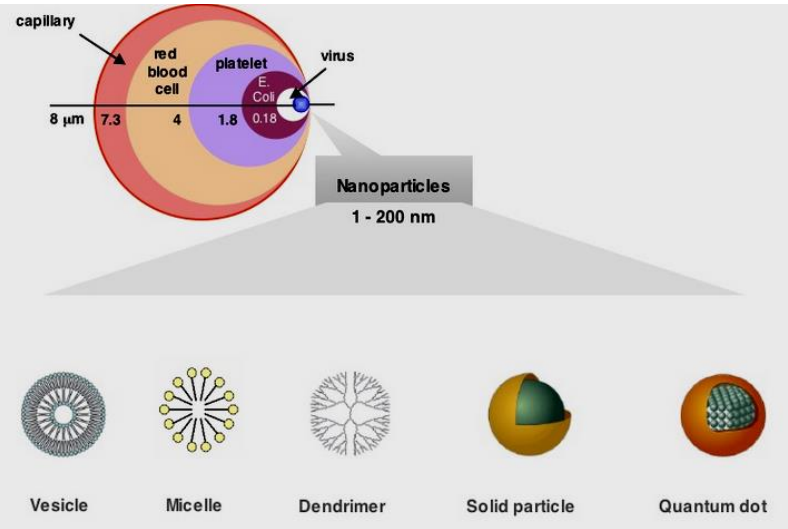

Figure 1.1. Representative nanovectors under development in the last decades.

These drug delivery systems, in virtue of their peculiar properties, have also been exploited for the delivery of macromolecules such as proteins and oligonucleotides with biological activity, which have emerged recently and can selectively target a variety of cellular processes involved in the carcinogenesis (4). These nanocarriers are particularly suitable for systemic administration because once the drug has been loaded is protected inside the vector. Thus the vehicle guarantees for the drug to reach the tumor site in the active form, avoiding possible enzymatic degradation in the bloodstream, which reduces the therapeutic efficacy. Moreover, nanocarriers protect the loaded drug from many phenomena that can reduce its activity and which take place during blood circulation. For instance, the extensive elimination attributed to lung blood filtration, renal filtration or biliary excretion; and the important tissue distribution which involves both liver and spleen (5).

Mechanisms as complement activation are also responsible for a drug reduced therapeutic effect. Indeed, xenobiotics recognized as pathogens are "covered" in vivo by a layer of proteins called opsonins. These adsorbed proteins are recognized by macrophages and trigger the xenobiotics (in our case the drug). Nanocarriers offer the advantage to protect drugs from all these degradative processes.

The distribution of biotherapeutics (proteins and oligonucleotides) in the tumor site is often very limited and not sufficient to guarantee a satisfying therapeutic effect. Furthermore, these biotherapeutics require an adequate access to the cytosolic

compartment to achieve their subcellular target (6). The access to the cytosol is a very relevant issue for most of therapeutic macromolecules that being very soluble, do not cross the cell membrane by simple diffusion as is the case of small drugs. Even when biotherapeutics are able to cross the cellular membrane by endocytosis, these drugs are rapidly directed to early endosomes, where the environment pH is rather acidic due to the activity of the ATP-dependent proton pumps (7). Therapeutic agents from early endosomes are transferred to late endosomes and finally to lysosomes for degradation (8). In 2-3 minutes, molecules that have been uptaken by cells migrate from early endosomes to late endosomes, and are exposed to the pH decreasing from 6.8-5.9 to 6.0-5.0. Once the therapeutic molecules dispose in the lysosomes, drugs are confined in a compartment with pH between 5.5-4.5. Inside these organelles, enzymes degrade the exogenous molecules thus prohibiting the biological activity of most of the therapeutic molecules.

In order to make the intracellular delivery of therapeutics possible, intelligent nanosystems were developed that are able to respond to biological signals or environmental alterations and provide controlled release at a specific site (6). Tumor sites present a variety of peculiar phatophysiological alterations such as abnormal pH profiles that can be exploited by "smart" responsive nanosystems to achieve site-selective deposition and confined action in the diseased site.

The PhD project presented in this thesis, an intelligent polymer based pH sensitive nanovesicular system have been developed for the systemic delivery of small sequences of siRNA (small interference RNA) that selectively inhibit the expression of intracellular proteins and involved in the tumor growth.

Many oncogenes were found to be involved in carcinogenesis and have been explored as targets for the treatment using RNA interference. The silencing of these oncogene products by RNAi technology has generated significant antiproliferative and/or proapoptotic effects in cell-culture settings and in animal models (9). The main obstacle to the use of oligonucleotides in cancer therapy stems from the very limited delivery to tumor cells for the free siRNA. In fact, when these oligonucleotide sequences are administered as un-formulated molecules, they undergo a very rapid degradation that reduce the activity. *In vitro* challenges of oligonucleotide delivery include the cellular uptake and escape from the internalizing endolysosomes that allow for the access to the cytosolic compartment where the molecular targets are; whereas *in vivo* challenges

concern avoiding clearance by the liver and spleen and the possibly selective-permeation of the target tissue (10). Encapsulation of siRNA in polymeric vesicles (named polymersomes) can provide protection against degradation, prolongs the plasma circulation time thus reducing the clearance, as well as enhance the cell entry and programmed oligonucleotides release into the cytosol according to an endosomolytic process (11).

Polymersomes are physically assembled vesicles are obtained by using polymers that must possess very peculiar physic-chemical features. Polymersomes are obtained with amphiphilic polymers, both diblock (12) and triblock copolymers (13), and possess an aqueous core, similarly to the liposomes, where hydrophilic macromolecules such as proteins and oligonucleotides can be loaded and protected from the external hostile environment. The loading of fragile therapeutic molecules in the core of these vesicles will preserve their activity until the release from the endosomal compartment into the cytosol.

1.1 CANCER: CLASSIC AND INNOVATIVE THERAPEUTIC TREATMENTS

1.1.1. CARCINOGENESIS

"Carcinogenesis is a multistep process in which cells accumulate multiple genetic alterations as they progress to a more malignant phenotype" (14). A cell can, as consequence of a variety of genetic alterations, turns into an aberrant cell and start dividing without precise control. This process leads to the development of solid tumors or an abnormal increase of circulating blood cells (liquid tumors). Cancer development as a multi-step process, was proposed by Berenblum and Schubik in 1948 (15) and supported by further studies. Three main phases could be pointed out: *initiation*, *promotion* and *progression*. *Initiation* involves one or more stable cellular genetic changes arising spontaneously or induced by exposure to a carcinogen. This is considered to be the first step in carcinogenesis, where the cellular genome undergoes mutations, creating the potential for neoplastic development (16), which predisposes the affected cell and its progeny to subsequent neoplastic transformation. The human DNA sequences involved in the transformation of cells in cancer cells are called oncogenes. *Promotion* consists of the survival and clonal expansion of cells that underwent the initiation process. Indeed,

initiated cell is stimulated to further proliferation, which disturbs the cellular equilibrium. This neoplastic transformation may involve more than one step and requires repeated and prolonged exposures to promoting stimuli (17). The stage of *progression* involves both the growth of solid tumors in size and the formation and diffusion of metastasis. In the first moment of this step, referred also as neoplastic conversion, the pre-neoplastic cells are transformed to a state in which they are more committed to malignant development. When this stage advances, cells lose their adherence property, detach from the tumor mass and invade closer tissues. The detached cells also enter the circulating blood and lymph and are transported to other organs/tissues away from the site of the primary growth and develop into secondary tumors at the new sites. These nucleation areas form *metastases*. The emergence of metastasis can enhance the tumor progression through different mechanisms: (a) invasion of local heathy tissues, (b) entry and neoplastic cells diffusion in the blood and lymphatic systems, and (c) the consequent origin of secondary tumor growth at distant sites (18).

Figure 1.2 describe the chronological steps involved in the carcinogenesis.

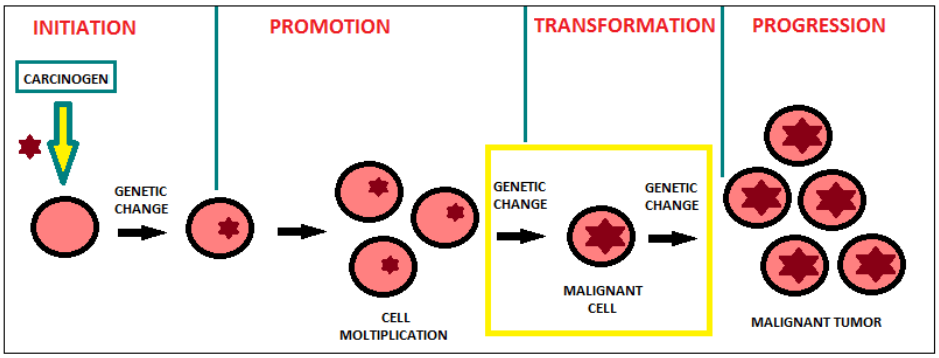

Figure 1.2. Steps involved in the carcinogenesis.

As mentioned above, carcinogenesis is mainly due to irreversible changes in a gene (mutation point), which predispose the cells to malignant transformation. Genes involved in this mechanism are mainly regulatory genes as oncogenes and anti-oncogenes. Oncogenes are positive regulators of carcinogenesis and in non-transformed cells, they are inactive (proto-oncogenes). Gene mutations can activate proto-oncogenes, resulting in the activation of the gene function. On the other hand, anti-oncogenes, named also tumor suppressor genes, are negative growth regulators. In healthy cells, they regulate cell proliferation by surveying cell cycle progression. Mutations in these genes result in a loss of gene function (the protein product will not be produced), which promotes

carcinogenesis (19). One of the mostly known example of tumor suppressor genes is the p53 that possess a fundamental role in maintaining the genomic stability and cell cycle equilibrium. In healthy cells, this gene promotes apoptosis, regulates cell cycle and induces cell differentiation. This suppressor gene participates in a cell cycle checkpoint signal transduction pathway that can cause either a G1 phase arrest or apoptotic cell death after DNA damage (20). Mutations in p53, resulting in loss of function, will cause suppression of apoptosis and promote cell division leading to neoplasm development (21). These kind of mutations in p53 gene are the most common genetic change observed in a large number of human diseases (22) and these alterations made these genes a good target for cancer treatment involving gene therapy.

1.1.2 PATHOPHYSIOLOGY OF CANCER

1.1.2.1 EPR effect and passive targeting

After the "*magic bullet*" concept proposed by Paul Ehrlich at the turn of the 20th century, underlying the need for drug to own a very specific activity and tropism, many attempts have been made to discover nontoxic and selective anticancer therapeutic agents. As an alternative, novel strategies that could deliver in a site-selective fashion conventional anticancer drugs were also widely investigated. This stimulate also the discovery of the tumor physiopathological unique features.

Blood vessels in most solid tumors possess peculiar characteristics that are not commonly observed in normal tissues. Such characteristics are:

- ✓ *extensive angiogenesis and hence high vascular density* (23);
- ✓ *extensive extravasation (vascular permeability) induced by various vascular mediators* such as a) bradykinin, responsible for ascitic fluid accumulation, and which is produced via the activated kallikrein-kinin cascade involving various proteolytic steps (24) b) nitric oxide (NO) generated by the inducible form of nitric oxide synthase (iNOS) (25), c) VPF/VEGF and other cytokines (25) (26), d) prostaglandins involving cyclooxygenases (24), e) matrix metalloproteinases (MMPs/collagenases) (27);
- ✓ *defective vascular architecture* (28);

- ✓ *impaired lymphatic clearance from the interstitial space of tumor tissues* (29)

These characteristics enhance the permeability of blood vessels in tumor tissues to macromolecular components such as plasma proteins and macromolecular therapeutics as well as nanocarriers. Furthermore, the impaired clearance of macromolecules and nanoparticles from the interstitial space of tumor tissue contributes to the retention of these drugs in the tumor for prolonged time and can increase their intra tumor concentration by 70-fold (30). This phenomenon is called enhanced permeability and retention effect (EPR) (31, 32) and its representation is reported in Figure 1.3.

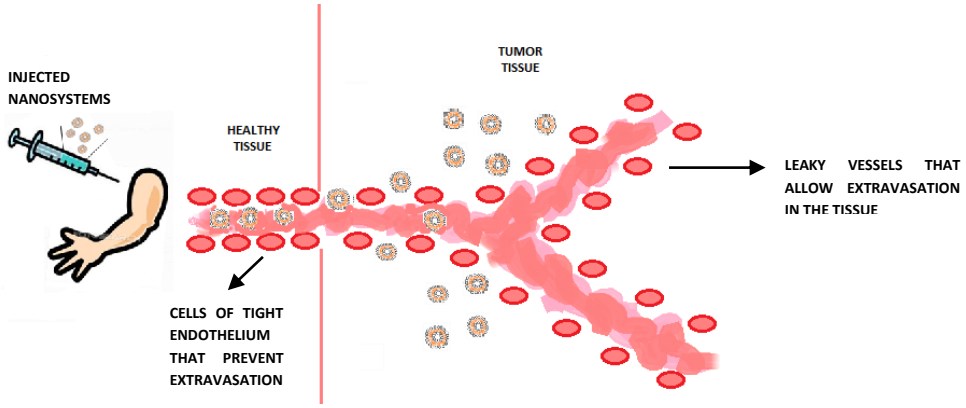

Figure 1.3. Representation of EPR effect.

According to the EPR effect, biocompatible macromolecules accumulate at much higher concentrations in tumor tissues than in normal tissues or organs. This EPR effect can be observed with macromolecules having an apparent size corresponding to molecular weight larger than 50 kDa which have long plasma half-lives (33). Most conventional drugs have a plasma half-life of less than 20 minutes in mouse or human. However, it takes at least 6 hours for drugs in circulation to undergo significant extravasation according to the EPR effect. In other words, any drug candidate must possess an adequate molecular size, above the renal clearance threshold, to circulate for an adequately long time.

Maeda *et al.* described the EPR effect for albumin, immunoglobulin G, and transferrin. Other smaller proteins of less than 30 kDa do not exhibit the EPR effect. A synthetic polymer-conjugated anticancer agent, SMANCS, which is poly(styrene-co-maleic acid/half-*n*-butyl ester) (SMA) conjugated with neocarzinostatin (NCS), was produced

with a size of 16 kDa (34) and did show the EPR effect only because *in vivo* it is bound to albumin, which confers an overall molecular size of about 80 kDa.

The EPR phenomenon was observed using a wide range of polymer conjugates such as poly(hydroxypropylmethacryl-amide) (HPMA) copolymer, polyethylene glycol, polyvinylalcohol, the lipid contrast agent Lipiodol (an iodized derivative of poppy seed oil used as an X-ray contrast agent) and other vegetable oils, and liposomes (35). Therefore, the EPR effect appears to be a key mechanism for tumor-selective drug delivery and and for anticancer drug design.

Especially, macromolecules, including SMANCS (chemical conjugate of the synthetic copolymer of styrene maleic acid + neocarzinostatin) and neocarzinostatin, injected subcutaneously, accumulate in regional lymph nodes (36). Furthermore, as compared to macromolecules, lipids and Lipiodol showed greater accumulation in tumors (31).

Transvascular migration of cancer cells observed in solid tumors is ascribed to the angiogenesis controlled by VEGF (25). In recent years attention has been focused on tumor angiogenesis control by vascular endothelial growth factor (VEGF), responsible of the tumor vessels architecture differentiation. In cancers, VEGF promotes rapid and random growth of vessels, characterized by structural leakage and high permeability. In this way it enhances the tumor growth because it supplies nutrients and oxygen to the tissue. Inhibition of angiogenesis using agents as endostatin and angiostatin has yielded promising results for tumor therapy. Angiogenesis inhibition has been in fact found to promote tumor cell death by apoptosis and necrosis.

It has been demonstrated that exogenously administered bradykinin and its potentiators such as kininase inhibitors can enhance (up to 100-fold) the dissemination of bacteria from the peritoneal compartment to the blood, the liver, the spleen, and the kidney. This effect is suppressed to 1/50-1/100 of the original level by bradykinin antagonists and the protease inhibitor ovomacroglobulin (37). Furthermore, NO derivatives such as peroxynitrite and $\cdot NO_2$ can activate MMPs, or collagenases (38). MMPs are known to facilitate cancer metastasis and to enhance angiogenesis to support growth of solid tumors. Recently it has been found that MMPs also facilitate the vascular permeability of solid tumor in mice, and this effect is inhibited by many MMP inhibitors. The activation of the bradykinin-generating cascade by MMPs has been described; evidences showed that the activation involve the participation of kallikrein. Maeda et al. reported that

plasmin can trigger the kallikrein-kinin cascade in tumor tissue, which is induced by urinary-type plasminogen activator produced by almost all types of solid tumor cells (39). It has been shown (40) that MMPs can activate plasminogen to yield miniplasmin. Miniplasmin would probably activate Hageman factor or prekallikrein. Thus, here again the generation of bradykinin may be mediated by $ONOO^-$ via MMP activation.

In addition, oxidative stress inactivates α_1-protease inhibitor, whose main target is neutrophil-derived elastase (41). In both inflammation and cancer, the proteolytic activity is greater than that in normal tissues, and thus these proteases would facilitate the dissemination of cancer cells in multiple ways. Prostaglandins, NO, and bradykinin exert their actions co-dependently, or by cross-talking, to up-regulate inflammatory mediators (42), so it may be beneficial to simultaneously suppress multiple mediators together.

In summary, we can exploit the specific features of the tumor vasculature to selectively deliver macromolecular anticancer drugs. One example could be the macromolecular pro-drug HPMA-doxorubicin conjugated PK-1 (43).

1.1.2.2 Active targeting and endocytosis

Active targeting takes advantage from ligand-receptor, antigen–antibody and other forms of molecular recognition to deliver a particle or drug to a specific site (44). In cancer therapy, ligands for active targeting are particularly used because they reduce or eliminate the potential drug toxicity to healthy tissue. Targeted nanoparticles delivering chemo-therapeutics are interesting because they can increase therapeutic efficacy and reduce potential side effects (45). Active targeting exploits the over-expression of receptors on the tumor cell surface (6) and many of these targeted nanosystems (Figure 1.5) have been tested with a variety of cancers. These nanosystems showed to be much more effective if compared to their non-targeted counterparts exibiting an increased cytotoxicity to tumor cells and a reduction of side effects (46). The main advantage of the targeted systems is that they are expressly instructed to access the cancer cell cytosol, which is missing in non targeted carriers even though both systems can undergo the EPR effect.

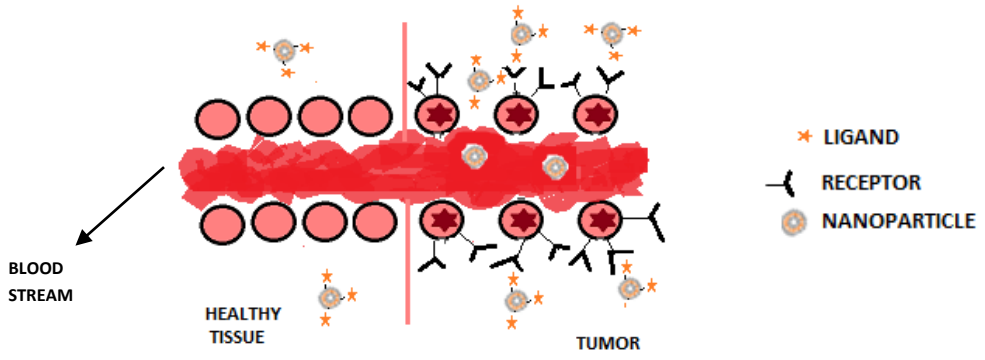

Figure 1.4. Ligand decorated nanoparticles are internalized not only by passive targeting but also by active targeting. This active targeting is more effective in the tumor tissue due to tumor cells overexpressing some receptors or antigens that allow for a better uptake of functionalized nanoparticles.

The mechanism through which functional molecules are internalized into the cells by interaction with specific receptors on cell surface is called receptor-mediated endocytosis (RME). RME is a well-known process for cellular uptake of many endogenous and exogenous ligands (47). Specialized receptor proteins have been identified to operate for the transport in the cytosolic compartment of nutrients (LDL-cholesterol, Tf-iron), growth factors (EGF, insulin), viruses (influenza), toxins (diphtheria), glycoproteins (galactose-terminating or mannose-terminating glycoconjugates) and negatively charged macromolecular ligands. Membrane receptors are heterogenous in structure but contain a common hydrophilic extracellular domain (ligand-binding domain), which possess a glycosylation site. After binding of the ligand to the receptor (or sometimes independently) at the cell surface and clustering in the coated pits, internalization of the receptor ligand complex occurs via a clathrin-coated vesicular intermediate (clathrin-dependent pathways) which enters the cytosol (48). Sometimes the receptors along with the bound ligand are internalized without the coating of the clathrin protein (clathrin-independent pathways). Clathrin from the plasma membrane was one of the first vesicular coat proteins to be identified by electron microscopy. It has a role in the endocytic process that it exert as vesicular coat and it cooperates in the sorting along the endocytic pathway (clustering of receptors in clathrin-coated pits). Uptaken carriers are guided through different pathways; based on this evidence, it is conceivable that the endocytic cargo is processed in accordance with the hypothesis that coat proteins mediate vesicular transport and protein sorting. However, some clathrin-independent endocytic pathways have recently been explored (48). In contrast to RME, which appears to be independent of cellular cytoskeletal components, uptake through the non-clathrin-coated pit and

macropinocytic pathway appears to involve components of the cytoskeleton. Caveolae are also coated invaginations of plasma membranes but differ in the receptor disposition from clathrin-coated vesicles in that they do not separate from the plasma membrane while unloading their cargo through a process termed *potocytosis* (49). An alternative model that reveals the underlying mechanism suggests that, similar to the clathrin-mediated pathway, caveolae generate from the plasma membrane and fuse with the endosome. Intracellular transport and processing after receptor-mediated endocytosis and transcytosis vary markedly among different receptor-ligand systems and different cell types, and determine the fate of drug-carrier composites to specific intracellular destinations. Endogenous ligands and receptors can follow one of at least four pathways:

- ✓ Receptors can provide for intracellular transport of ligand and return to the initial plasma membrane domain
- ✓ Receptors can move to lysosomes and, with the ligand bound to them, share the fate of the ligand (lysosomal disposition).
- ✓ Receptors can be recycled, along with the ligand, back to the site from where the receptor originated.
- ✓ Receptors can return to a different domain of the plasma membrane (transcytosis).

Followed by receptor-mediated internalization, the ligand-receptor complex is routed to an acidic compartment through a maturation and fusion mechanism, after internalization. This prelysosomal sorting compartment (compartment of uncoupling of receptor and ligand, CURL) is referred to as the endosome, or receptosome (50). Numerous events relevant to endocytic uptake of ligands and drug delivery occur in the endosomal and lysosomal compartment (pH 6-6.6 for endocytic vesicles, pH 5-6 for late endosomes, and pH 4-5 for lysosomal apparatus) and drive the intracellular migration of the ligand-coupled carriers to their respective destinations. The endosomal and lysosomal compartment possess different pH conditions: pH 6-6.6 for endocytic vesicles, pH 5-6 for late endosomes, and pH 4-5 for lysosomal apparatus that can promote and control the events taking place within these vesicles. These include ligand-receptor dissociation, sorting and transport of internalized molecules and receptors to lysosome, plasma membrane, or Golgi apparatus or to other cellular targets as well as partial hydrolysis of

some ligands (51). Like the plasma membrane, the lysosomal membrane is a natural barrier to macromolecular ligands and/or ligand-appended carrier composites and only low-molecular-weight molecules are released as a consequence of lysosomal degradation. The degradation of the ligand-coupled drug-carrier composites in lysosomes is a key step in designing an intracellular delivered system and constitutes the "lysosomotropic" approach to drug targeting.

The differences in the regulatory and metabolic requirements of metastatic cells compared with normal cells are reflected in the over-expression and up-regulation of the receptor portal systems which process these tumor-derived endogenous ligands: this is the only key-difference that can be reasonably addressed for specific anti-cancer drug targeting.

1.1.2.3 Folic acid and folate receptor

Folic acid is a low molecular weight pterin based vitamin of the group B (B9) required by eukaryotic cells for one-carbon metabolism and de novo nucleotide synthesis. Because animal cells lack key enzymes of the folate biosynthetic pathway, their survival and proliferation are dependent on their ability to acquire and utilize this vitamin (52).

It consists of 2-amino-4-hydroxy-6-methylpteridine bound to p-aminobenzoic acid (PABA) and terminates with a glutamic acid molecules, as reported in Figure 1.5.

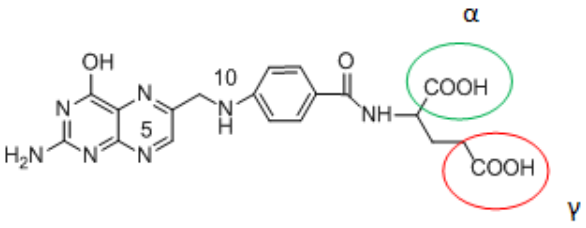

Figure 1.5. Chemical structure of folic acid.

Two carboxylic groups are present in the vitamin due to the glutamic acid and the one in α position is required for the biological activity. Together with B12 vitamin, folic acid acts as donator/acceptor of methylene groups in the methylation cycle that is central in regulating gene expression. For this reason, this vitamin is essential for synthesis of purine nucleotides (53).

Owing to the two carboxylic groups positioned at the distal end of the folate molecule, passive membrane permeability at physiological temperature and pH is minimal. To

circumvent this obstacle, nature has evolved two mechanisms for the cellular uptake of the vitamin. The first mechanism involves a low-affinity (K_D ~1-5 μm) membrane-spanning protein that transports reduced folates directly into the cell cytosol (54). The second mechanism uses a high affinity (K_D ~100 pm) glycoprotein receptor, generally referred to as the folate receptor (FR), which preferentially mediates the uptake of oxidized forms of folate (e.g. folic acid) into the cell by endocytosis (55).

Folate receptor (FR) is a glycosylphosphatidylinositol (GPI)-linked membrane glycoprotein with an apparent molecular weight of 38-40 kDa (56). Two membrane-bound isoforms of FR have been identified in humans, designated α and β. FR α-isoform has a dissociation constant (K_d) for folic acid of ~0.1 nM, which is approximately 10-fold lower than its K_d for reduced folates (e.g., 5-methyltetrahydrofolate) (57). The role of FR in cellular folate transport is not well understood, although a clathrin-independent "potocytosis" model has been proposed (58). FRs were found to be clustered in non-coated membrane regions called caveolae. Localization of FRs in caveolae and receptor internalization can be induced by receptor crosslinking and is regulated by cholesterol. From a mechanistic perspective, the FR functions to concentrate exogenous folates and various derivatives into the cell cytosol by endocytosis. As depicted in Figure 1.6, the endocytic vesicles (endosomes) that contain the FR-folate complex rapidly become acidified to ~pH 5 and thereby allow the FR to release the folate molecule (59).

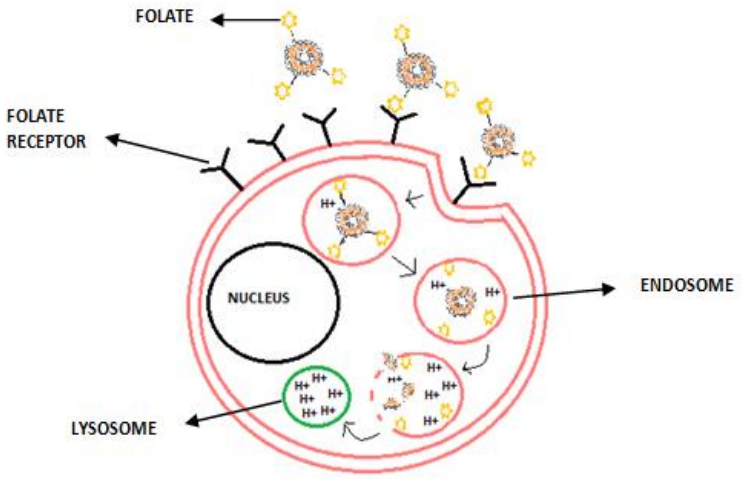

Figure 1.6. Endocytosis of folate–drug conjugates. Exogenous folate–drug conjugates bind specifically to folate receptors (FRs) presented on the surface of a target cell. The plasma membrane invaginates around the folate–FR complex to form an intracellular vesicle that is commonly referred to as an endosome.

While elevated expression of FR has frequently been observed in various types of human cancers, the receptor is generally absent in most normal tissues with the exceptions of choroid plexus, placenta, and low levels in lung, thyroid and kidney (60). Although FR type β has been found on CD34+ cells, the receptor curiously lack affinity for [^{3}H] folic acid and folate derivatives (61). FR type α is frequently over expressed in tumor cells in culture and epithelial lineaged tumors such as ovarian carcinomas. Several studies show that over 90% of ovarian carcinomas overexpress the FR (62). In a study, a monoclonal antibody against the type α receptor, LK26, was used to determine the frequency of FR over expression in human tumors by indirect immunohistochemical staining. High frequencies of receptor over expression were found in many types of tumors, including ovarian (52 of 56 cases tested), endometrial (10 of 11), colorectal (6 of 27), breast (11 of 53), lung (6 of 18), renal cell (9 of 18) carcinomas, brain metastases derived from epithelial cancers (4 of 5), and neuroendocrine carcinomas (3 of 21). FR type β is frequently over expressed in non-epithelial lineaged tumors such as sarcomas and acute myeloid leukemias but not in established cell lines of the same origin (63). The causes of FR over expression in cancers are unclear. Transfection and expression of FR on NIH/3T3 cells provide cells with the ability to survive in low folate medium and increased cell growth both in vitro and in vivo (64). Studies also show that high levels of FR expression are associated with increased biological aggressiveness of ovarian carcinomas as shown by a higher percentage of S-phase cells and increased resistance to chemotherapeutic agents (65). Thus FR elevation may be a useful prognostic factor.

The prevalence of FR over-expression among human tumors makes it a good marker for targeted drug delivery to these tumors. High affinity FR binding is retained when folate is covalently linked via its γ-carboxyl group to a foreign molecule. It has been known for nearly a decade that simple covalent attachment of folic acid to virtually any macromolecule produces a conjugate that can be internalized by FR-bearing cells according to the same process involving free folic acid (66). Many authors have seen into this small molecular weight molecule an ideal substitute to monoclonal antibodies for site specific drug targeting, where possible (Table 1.1).

Table 1.1. Comparison between folic acid and antibodies main properties.

Property	Folic acid	Antibody/protein
Molecular weight	441	160 000/ variable
Tumor permeability	High	Low
K_D for cell-surface receptor	10^{-10} M	10^{-10} to 10^{-6} M
Immunogenicity	Low	Low to high
Conjugation chemistry	Easy	Difficult
Receptor recycles	Yes	No
Stability to acids/bases/solvent	High	Low
Stability during storage	High	Variable
Lysosomal disposition	Low	High
Toxicity of targeting ligand	Low	Variable
Cost	Low	High

Particles conjugated with folate or folic acid and bound to a folate receptor are internalized by the cell and introduced to the cytoplasm. Once inside the cell, they start to interact with intracellular components (67).

Yoo and colleagues developed a folate conjugated nanoparticle developing biodegradable polymeric micelles loaded with doxorubicin. Micelles were assembled from a copolymer of poly(L-lactic-co-glycolic acid) (PLGA) and poly(ethylene glycol) (PEG). The advantageof using PLGA is its biodegradability after delivery of the payload, while PEG increases the circulation time of the particles. Doxorubicin was conjugated with chemical bond to the PLGA while the folate was bound to the PEG terminal end. The micelles were tested for cytotoxicity and cardiotoxicity (a side effect of Doxorubicine) compared to free doxorubicine on cell lines expressing folate receptor. The micelles showed increased cellular uptake, circulation time, and decreased cardiotoxicity (68). The targeting moiety managed to recognize between healthy and tumor tissue with greater specificity than untargeted doxorubicine and a decrease in cardiotoxicity was evaluated. A representation of the micelles is reported in Figure 1.7.

Figure 1.7. Folate-conjugated PLGA-PGA polymeric micelle loaded with encapsulated doxorubicin (68).

1.1.2.4 Classic antitumor therapy

Classical antitumoral therapy involves the use of chemotherapeutics. These agents are, in general, small molecules that interfere with the normal cell function by inhibiting the replication or inducing apoptosis (69). Because of their wide cytotoxicity, chemotherapeutic agents have been almost exclusively exploited for the treatment of cancer, where they exhibit deleterious effects mostly to rapidly proliferating cells (69). Paclitaxel, doxorubicin, daunorubicin, cisplatin, and docetaxel are examples of classic chemotherapeutics. Paclitaxel and docetaxel are taxanes, and they work stabilizing the microtubules during cell cycle, which prevents mitosis from progressing from metaphase to anaphase (70). Doxorubicin and daunorubicin belong to a class of chemotherapeutics known as the anthracyclines. Even if mechanisms of action of anthracyclines in cancer cells are not completely clear, a possible hypothesis could involve the drug intercalation between base pairs of the DNA/RNA strand, with consequent decreasing in replication of rapidly-growing cancer cells. These molecules are among the most effective drugs available, inducing the highest degree of cytotoxicity and used to treat most of tumors including aggressive lymphoma, breast cancer, and myeloblastic leukemia (71, 72). Doxorubicin has been shown to target the topoisomerase-II-DNA complex, disrupting the DNA and preventing cellular replication (73). Similarly, cisplatin, a platinum-compound, by modifying the cell DNA, activates signaling pathways that triggers apoptosis (74).

The main problem with using the above mentioned chemotherapeutics is their inability to differentiate between healthy and tumor tissue (75). The biological activity of the drugs is indiscriminate, being particularly harmful to any rapidly proliferating cells in the body such as hair, intestinal epithelial cells, and bone marrow (69). The most cytotoxic agents are the most effective but often result in severe side effects. Doxorubicin is considered to

be one of the most used and efficient anti-cancer drug available today but gives side effects such as, nausea, fatigue, and extensive and often fatal cardiotoxicity (71).

1.1.2.5 Gene therapy and siRNA interference

Gene therapy is a therapeutic strategy that allow the treatment of acquired and inherited diseases by the transfer of genetic material into specific cells of the patient.

Gene delivery refers to the use of DNA to obtain the expression of a protein that is not coded in the host genome, whereas delivery of RNA and antisense oligonucleotides are employed to decrease protein expression.

At the really beginning, gene therapy was employed to hit inherited monogenic disorders through the replacement of an abnormal gene with the one responsible of encoding the correct protein. Among the diseases that were considered for this type of therapeutic treatment, most clinical trials were performed in cystic fibrosis (76), hemophilia (77, 78) Duchenne muscular dystrophy (79), familiar hypercholesterolaemia (80), beta thalassemia (81), severe combined immunodeficiencies (SCID) (82) and chronic granulomatous disease (83).

Thereafter, gene therapies have been extended to a wide spectrum of acquired diseases, cancer included. Indeed, DNA damages introduced by the carcinogenesis process, can be exploited as target for anticancer gene therapy.

In particular, for this project we have focused on the exploitation of siRNA for therapeutic treatment. siRNA emulate a natural cellular process that involves the RNA interference (RNAi). "This physiologic process is a post-transcriptional mechanism of gene silencing through chromatin remodeling, inhibition of protein translation or direct mRNA degradation, and is ubiquitous in eukaryotic cells" (84,85). Previous biological studies showed that the introduction of exogenous double-stranded RNAs (dsRNA) in the cell cytosol can initiate a potent cascade of sequence-specific degradation of endogenous mRNAs that have homology with dsRNA introduced (86). Once in the cytoplasm, dsRNAs are processed by the enzyme RNase-III Dicer, which cleaves the long dsRNAs into sequences of 21–28 nucleotides.

These RNA duplexes are known as short interfering RNAs (siRNA). They associate with a multiprotein RNA-inducing silencing complex (RISC) present in the cytoplasm, guide the complex to a homologous target mRNA and trigger its endonucleolytic cleavage by Slicer (Argonaute-2), an enzyme located inside the RISC complex. As consequence, the

target mRNA is cleaved at a single site in the center of the duplex region between the guide siRNA and the target mRNA, resulting in gene silencing (Figure 1.8).

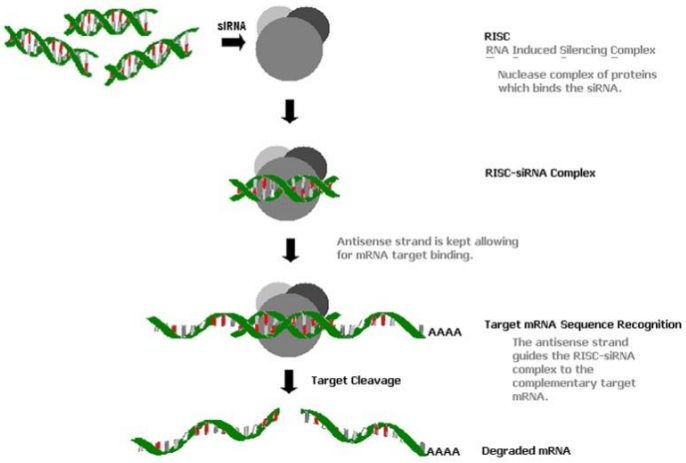

Figure 1.8. Mechanism of mRNA silencing.

The silencing process is highly sequence specific. Furthermore the process is very efficient because, since the antisense strand of the dsRNA is protected within the RISC complex, its catalytic activity is preserved and it can thus degrade additional copies of the target mRNA.

1.1.2.6 Molecular target: the α1 subunit of $Na^{+/}K^{+}$-ATPase pump

In 1957 Jens Christian Skou (87) demonstrated that the different concentrations in Na^{+}/K^{+} ions outside and inside of the two sides of the cellular membrane is maintained by an energy-dependent mechanism mediated by the Na+/K+-ATPase pump. The Na^{+}/K^{+}-ATPase pump is an enzyme that belongs to the P-type ATPase family of cation transporters, which reacts with Adenosine Triphosphate (ATP) involving a phosphorylation process, during the catalytic cycle.

Sodium pumps can be classified in two groups with distinct functions:

1) one is the ubiquitous trans-membrane enzyme that transports Na^{+} and K^{+} across the plasma membrane by hydrolyzing ATP (88, 89)

2) the second and majority of the cellular Na/K-ATPase is engaged in cellular activities different from pumping ions (90). These ones are located in caveolae and interact directly with multiple proteins including protein kinases, ion transporters, and structural proteins to exert their signal-transduction activity (91).

As mentioned above, when the Na/K-ATPase is located in the lipidic bilayer of the cell membrane it is responsible for maintaining the K^+ and Na^+ gradients between the intra and extracellular environment. These gradients are needed for the Na+ -coupled transport of various nutrients, as for instance glucose and aminoacids and contribute to regulate intracellular concentrations of ions. This regulating process is important because it is implicated in specialized cellular functions such as the muscle contraction and the transmission of nerve impulse, and for osmotic balance and the regulation cellular volume.

When the enzyme is located in the caveolae, flask-shaped invaginations of the plasma membrane (92), it plays a signal transducer role and modulates cell proliferation, cell adhesion and migration pathways.

In general, Na+/K+ pump is composed of two sub-units in equimolar ratios:

1) The ‘α catalytic sub-unit’ is a multicomponent transmembrane protein (10 membrane-spanning domains) which contains the binding sites for Na^+, K^+ and ATP. This sub-unit executes the functional properties of the Na+/K+ATPase. It binds and transports the cations, hydrolyzes ATP and is intermediately phosphorylated.

2) The 'β regulatory sub-unit' is a type II glycoprotein with a single transmembrane segment. This protein has several glycosylation sites, required for the biogenesis and activity of the enzyme complex; it is important for the structural and functional development of the α sub-unit and is also involved in the Na^+ and K^+ activation kinetics of mature pumps.

In nature exist 4 isoforms of α subunit (α1, α2, α3, α4) and 3 isoforms of β subunit (β1, β2, β3) (93, 94). In Figure 1.9 a simple model of Na^+/K^+ATPase with its pump function is reported.

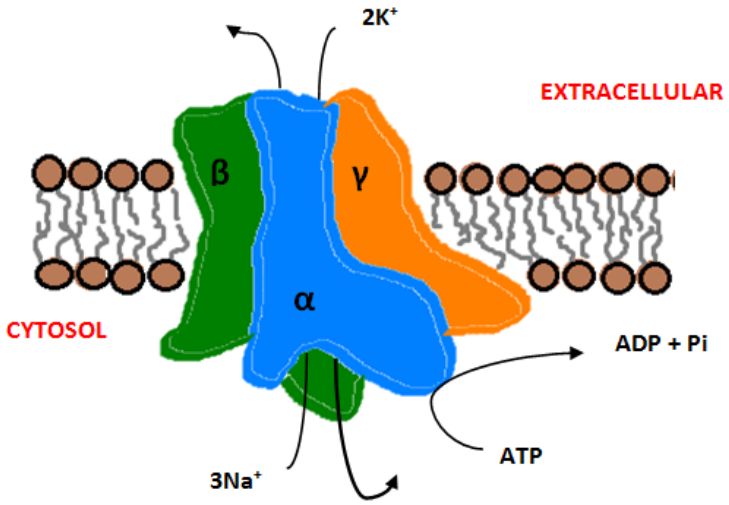

Figure 1.9. Isoforms of α and β subunits of Na/K-ATPase pump.

Many studies from literature (95) demonstrated that the activity of this enzyme can be affected in the course of malignant transformation such as cancer and this is even evident at the early phases of carcinogenesis (96). α and β isoforms are often involved in this mutation process, where β1 is very frequently down regulated in cells of human epithelial cancer (97), whereas α-subunits appear to be up-regulated in malignant cells (98).

As consequence, with the suppression or reduction of the sodium pump function correlated to the α or β subunits, a reduction in proliferation and migration of cancer cells is obtained (92).

In particular, studies demonstrated that α1-subunit of Na-K-pump present in the caveolae is overexpressed in many kinds of tumor, as glioblastoma and non-small cell lung cancer (92). A strategy to block the expression of ATPase α1 subunit could be the delivery of a gene knockdown agent such as siRNA. We can conclude that the sodium pump, and in particular its α1 subunit, could be an important molecular target for anticancer therapy and in particular for the siRNA vesicular system developed in the course of this thesis.

1.1.2.7 Nanocarriers for delivery of cancer therapeutics: state of the art

Nanocarriers used for systemic cancer therapy and their latest stage of development are summarized in Table 1.2 (99).

Table 1.2. Nanoscaled systems for systemic cancer therapy. Adapted from (99) with DOI:10.1038/nrd2614.

Platform	Latest stage of development	Examples
Liposomes	Approved	DaunoXome, Doxil
Albumin-based particles	Approved	Abraxane
PEGylated proteins	Approved	Oncospar, PEG-Intron, PEGASYS, Neulasta
Biodegradable polymer–drug composites	Clinical trials	Doxorubicin Transdrug
Polymeric micelles	Clinical trials	Genexol-PM*, SP1049C, NK911, NK012, NK105, NC-6004
Polymer–drug conjugate-based particles	Clinical trials	XYOTAX (CT-2103), CT-2106, IT-101, AP5280, AP5346, FCE28068 (PK1), FCE28069 (PK2), PNU166148, PNU166945, MAG-CPT, DE-310, Pegamotecan, NKTR-102, EZN-2208
Dendrimers	Preclinical	Polyamidoamine (PAMAM)
Inorganic or other solid particles	Preclinical (except for gold nanoparticle that is clinical)	Carbon nanotubes, silica particles, gold particles (CYT-6091)

*Approved in South Korea. PEG, polyethylene glycol.

PEG-containing proteins and PEG conjugated small molecules are considered nanosystems. Indeed, despite they are in some cases single molecules in solution, due to their size, they can be defined as nanoscale therapeutics, or even as nanoparticles if they have some degree of polymer–polymer interaction to induce some level of physical assembly.

Liposomes (~100 nm and larger) represent a very relevant class of drug vehicles widely exploited to deliver chemotherapeutic molecules. They have been approved for cancer treatment since mid-1990s, and are mainly used to encapsulate water soluble drugs. Liposomes can also intercalate hydrophobic drugs in a small content, allowing to improve the biodistribution profile that promotes higher disposition in the tumor site than the free drug (99).

However, conventional liposomes do not provide control over time of drug release, and in most cases do not achieve effective intracellular delivery of the drug molecules (100), therefore limiting their potential efficacy against multidrug resistant cancer cells.

A typical example of liposomes for cancer treatment shown in Table 1 is Doxil (Ortho Biotech). This liposome formulation coated with PEG contains the cytotoxic drug

doxorubicin. Doxil was originally approved for the treatment of AIDS-related Kaposi's sarcoma and is used in ovarian cancer and multiple myeloma.

The longer blood circulation time of drug loaded nanosystems compared to the unformulated free drug can significantly improve tumor uptake since it allows for longer extravasation time at the tumor site where the vessels are leaky compared to normal tissues (99). Moreover, it was found that polymeric carriers with a size larger than 10 nm up to few hundred nanometers will avoid renal clearance and penetrate in the tumor interstitium. Therefore, careful control of size is basic for the pharmacokinetics, biodistribution, tumor penetration and tumor accumulation of the nanocarrier with its drug payload.

Some of the nanocarriers that are under investigation in clinical trials also possess mechanisms to spatially and temporally control the release of the drug. The controlled release features base on the cleavage of specific chemical bonds linking the drug to a polymeric component of the carrier; on enzymes that are located within and outside cells. For instance, some interested enzymes could be lysozymes, esterases, or enzymes located only within cancer cells, for example, cathepsin b. Finally, the environment can control the dissociation of the nanocarrier matrix.

Polymersomes, although they represent a quite recent system for drug delivery, are under development as "innovative products" for a wide range of diagnostic and therapeutic applications. An example is represented by the privately-held biotechnology company Vindico Pharmaceuticals Inc. Vindico's polymersomes have been extensively utilized in medical applications, including as implantable biomaterials in drug delivery devices, bioresorbable sutures, adhesion barriers, and as scaffolds for injury repair via tissue engineering. These vesicles are made of "biodegradable polymers that enable: 1) high permeability to small drug molecules; 2) maintenance of neutral pH environments upon degradation; 3) facility in forming blends with other polymers; and 4) suitability for long-term delivery afforded by slow erosion kinetics" (reported by Vindico Pharmaceuticals Inc.). All these features allowed the company the utilization of their polymersomes for in *vivo* studies (101).

1.2 ENVIRONMENTALLY RESPONSIVE CARRIERS FOR CANCER THERAPY

In last decades highly specific biological pharmaceutical agents have been introduced in medicine, including proteins (monoclonal antibodies, hormones, growth factors, enzymes, synthetic oligopeptides) and nucleic acids (plasmid DNA, antisense oligonucleotides, siRNA, miRNA) that can be used to treat a huge spectra of tumors (6). However, as previously mentioned, these therapeutics needs to be delivered to their subcellular site of action in order to be active. Controlled release carriers sensitive to specific environmental features can make their effect possible. These "smart" drug delivery systems include polymer-drug conjugates, polymer micelles, polymer–drug polyplexes, nanohydrogels and have been investigated to ameliorate the efficacy of a variety of drugs by providing protection from clearance and enzymatic degradation, as well as offering the possibility for controlled release (102, 103). Recently many intelligent systems were developed, but the most interesting are the ones able to answer to biological signals for tissue specific targeting or controlled drug release. The design of these systems needs to consider parameters as the stability, administration, absorption, metabolism, and bioavailability at target site. Level control and localization of biotherapeutics within the body allow to decrease drug doses potentially harmful for their side effects.

The idea of stimuli-responsive drug delivery was firstly suggested in the late 1970s with the use of thermosensitive liposomes for local release of drugs through hyperthermia (104). In the last decade research has been carried out on stimuli-responsive materials for drug delivery, especially regarding their design and application as nanocarriers. Stimuli-responsive nanodevices may be sensitive to specific endogenous stimuli, such as a lower interstitial pH, a higher glutathione concentration or an increased level of particular enzymes such as matrix metalloproteinases (104). Inside the cell, pH sensitivity can either trigger the release of the carried drug into late endosomes or lysosomes, or promote the escape of the systems from the lysosomes to the cell cytoplasm. At the tissue level, microenvironmental changes associated with cancer are exploited as well as pathological conditions such as ischemia, inflammatory diseases or infections. Exogenous physical stimuli can be also applied to target the drug delivery system, as for instance the use of magnetic fields to target metallic nanoparticles. Drug release profiles can also be achieved by thermo-, light- or ultrasound-sensitive nanoparticulate systems (104).

In the next sections examples of stimuli-responsive drug-delivery nanocarriers are reported, divided into exogenous an endogenous stimuli-responsive drug delivery systems.

1.2.1 EXOGENOUS STIMULI-RESPONSIVE DRUG DELIVERY: EXTERNALLY APPLIED STIMULI

1.2.1.1 Thermoresponsive systems

Thermoresponsive drug delivery has been explored since a long time in oncology. Thermoresponsiveness is usually controlled by a nonlinear sharp change in the properties of one or more components of the nanocarrier material with temperature. The variation in the surrounding temperature causes the release of the delivered drug. Ideally, thermosensitive nanocarriers should retain their drug load at body temperature (~37 °C), and rapidly deliver the drug within a locally heated tumor (~40–42 °C). Thermoresponsive systems that have received considerable interest are liposomes, or polymeric micelles, or nanoparticles (usually using poly(N-isopropyl acrylamide), PNIPAM) that exhibit a Lower Critical Solution Temperature (LCST) (104). Under this transition temperature, polymers present in the aqueous dispersion are soluble, whereas above the LCST, they become hydrophobic, collapse and aggregate. For liposomes, thermo-responsiveness usually comes from a phase transition of the constituent phospholipids and the consequent conformational variations in the lipid bilayers. In vivo, heat is generally provided by using temperature-controlled water sacks, radiofrequency oscillators or microwave applicators. In the past few years, the focus has been on rapid and quantitative drug-release performance. Thermosensitive liposomes (TSLs) are maybe the most advanced thermoresponsive nanosystems, as shown by their use in several clinical trials. Doxorubicin loaded TSLs (ThermoDox, Celsion Corporation), in association with hyperthermia or radiofrequency ablation, now are investigated in phase II trials for the treatment of breast cancer and colorectal liver metastasis, and passed to phase III trials for the treatment of hepatocellular carcinoma. More recently, improved liposomal formulations have been shown to release their loads quickly after applying hyperthermia (~40-45 °C) (105). An alternative approach was developed with leucine zipper peptide–liposome hybrids, which combine the advantages of traditional TSLs with the dissociative, unfolding properties of a temperature-sensitive peptide (104).

Promising results were obtained also by Al-Ahmady (106) et al. using thermoresponsive bubble-generating liposomal systems. These rely on the creation of permeable defects in the lipid bilayer by means of the generation of carbon dioxide bubbles through decomposition of ammonium bicarbonate at mild hyperthermia (~42 °C). After this effect, as reported in Figure 1.10, the payload can be released in the interested district.

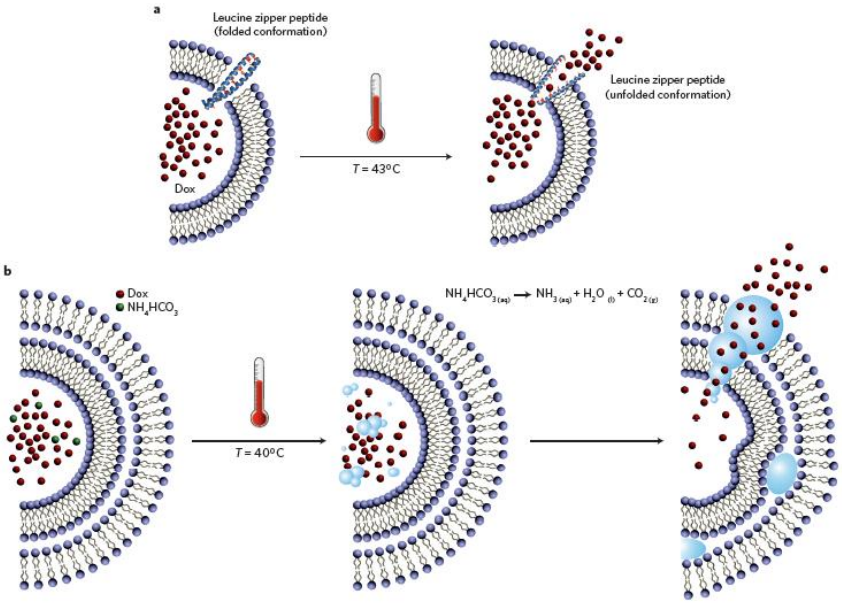

Figure 1.10. Temperature-based actuation mechanisms for liposomal drug delivery. a) The temperature-triggered unfolding of a leucine zipper peptide inserted in the membrane of a doxorubicin (Dox)-carrying liposome opens a channel through which the drug is released. b) Drug-permeable pores can also be created by the temperature-triggered generation of bubbles from the decomposition of encapsulated ammonium bicarbonate. Adapted from (104) with DOI:10.1038/nmat3776.

1.2.1.2. Magnetically responsive systems

Magnetical guidance is typically obtained by focusing an extracorporeal magnetic field on the biological and tissue target during the injection of a magnetically responsive nanocarrier. This concept has demonstrated great potential in experimental cancer therapy because of improved accumulation of drug inside solid-tumor models. Candidate nanosystems for such a therapeutic approach are core – shell nanoparticles (a magnetic core made of magnetite (Fe_3O_4) coated with silica or polymer) (107, 108), magnetoliposomes (Fe_3O_4 or maghemite (Fe_2O_3) nanocrystals encapsulated in liposomes (109) and porous metallic nanocapsules (110). Magnetically guided nanocarriers have

also found application in the delivery of oligonucleotides, including siRNA and genes. These experiments are generally performed using nanoassemblies with cationic coatings to condense nucleic acids, which results in higher transfection efficiencies under a permanent magnetic field. This technique led to improved effectiveness in the transfection of siRNA in vitro and/or in vivo when directed against prostate (111) and breast (112) cancers. The use of magnetically responsive nanoparticles is generally limited to accessible tumor nodules, but is not suitable for metastasis or disseminated tumors. Although most of these tumors are suggested for direct surgery, some are not surgically removable because they are too hemorrhagic or localized too near to healthy tissues, with high risk of injury these last ones (it could be the case of some brain cancers). In such cases, magnetically responsive nanoparticles could be a valid therapeutic option. However, the magnetic approach is prevented by the complexity involved in the set-up of external magnetic fields, which need adequate focusing and deep penetration into the tissues to reach the disease area and give the desired effect. In this respect, efforts to identify the best magnetic and irradiation technologies are required.

1.2.1.3. Ultrasound-triggered drug delivery

Ultrasounds are an effective method to obtain spatiotemporal control of drug release at the desired site, preventing deleterious side effects to healthy tissues. A second advantage is their non-invasiveness, the absence of ionizing radiations, and the easy regulation of tissue penetration depth by regulating frequency, duty cycles and time of exposure.

Ultrasound waves can cause the release of the drug from nanocarriers through the thermal and/or mechanical effects generated by cavitation phenomena or radiation forces. Indeed, it has been shown that physical forces associated with cavitation can induce the destabilization of the nanosystem, drug release (113) and transient increase in vessel permeability, leading to the cellular uptake of therapeutic molecules (114). All these effects can be achieved when low ultrasound frequencies (kHz range) are used. However, ultrasound mediated enhancement of vessel permeability can generate drawbacks such as metastatic dissemination. For this reason, other ultrasound contrast agents as microbubbles, which efficiently interact with ultrasonic waves, have been used at diagnostic frequencies to reduce the threshold required for cavitation. However, short lifespan and absence of extravasation may still limit the use of microbubbles for tissue targeting. To solve this aspect, perfluorocarbon (PFC) nanoemulsions that convert into

microbubbles under the action of therapeutic ultrasounds were developed. The bubbles are formed through vaporization of droplets and are subjected to cavitation, triggering the drug release in the tumor site (Figure 1.11). This has resulted in significant therapeutic efficacy and suppression of metastatic process (115).

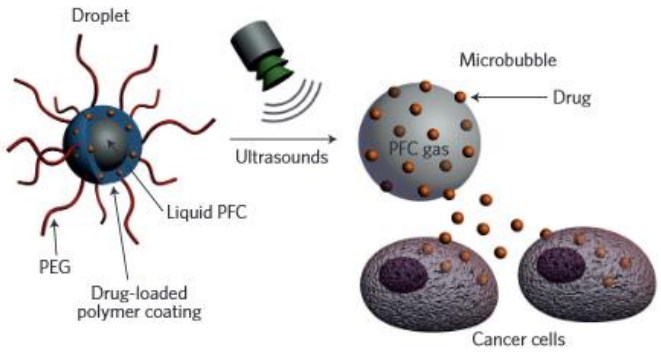

Figure 1.11. Drug delivery from echogenic perfluorocarbon (PFC)-containing nano-emulsions. Adapted from (104) with DOI:10.1038/nmat3776.

1.2.1.4. Light-triggered drug delivery.

A large variety of photoresponsive systems has been developed in the past few years to achieve drug release in response to illumination to a specific wavelength (in the ultraviolet, visible or near-infrared (NIR) regions) (116) The different strategies available are able to exercise an on–off drug-release event triggered by photosensitiveness-induced structural modifications of the nanocarriers. For instance, the ultraviolet–visible photoisomerization of the azobenzene group (and its derivatives) - from trans to cis on irradiation at 300 - 380 nm, and from cis to trans by shining light in the visible region - enables control of drug release in developed cyclodextrins and derivative.

In the field of light-triggered drug delivery, the main disadvantage is given by the low penetration depth (~10 mm) that results from the strong scattering properties of soft tissues in the ultraviolet-visible region of the spectrum (below 700 nm). Unfortunally, conventional light-induced drug delivery can be applied only to regions of the body that can be directly illuminated (as eyes and skin). Anyway, using photosensitive groups that answer to higher wavelengths or exploiting two-photon technology (117), it is possible to replace the classical light source by a NIR laser (700–1,000 nm range) with deeper tissue penetration, lower scattering properties and minimal damage to tissues. In this way these light sensitive nanosystems become promising for clinical applications. An application of

these techniques are doxorubicin-loaded gold nanospheres, which showed faster drug release when irradiated at 808 nm, allowing anticancer activity and reducing systemic toxicity compared to the treatment with the free-drug (118).

1.2.1.5. Electroresponsive systems

Weak electric fields (typically about 1 V) can be used to have drug release. For instance, nanoparticles based on polypyrrole - a conductive polymer - showed release profiles that could be tuned by synergistic processes consisting of electrochemical reduction–oxidation and electric-field-driven movement of charged molecules (119). Montmorillonite, a mineral made of hydrate silicate of calcium, aluminium, magnesium and sodium, when introduced in a chitosan nanohydrogel, could provide drug release using electrostimulation, and preserved responsiveness and reversibility after consecutive on–off exposure to the electric field. An electric field also activated the reversible disaggregation of polymersomes that obtained by host–guest complexation between β-cyclodextrin and ferrocene attached at the terminal ends of a pair of different homopolymers (120) (Figure 1.12).

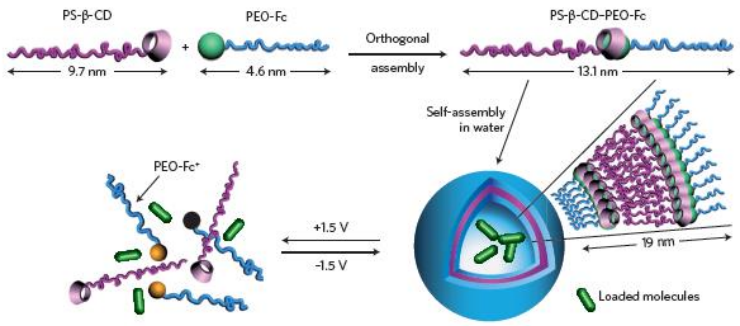

Figure 1.12. Voltage-responsive vesicles. Structure of polystyrene-β-cyclodextrin (PS-β-CD) and poly(ethylene oxide)-ferrocene (PEO-Fc), and representation of the voltage-responsive controlled assembly and disassembly of PS-β -CD–PEO-Fc supramolecular vesicles. Adapted from (104) with DOI:10.1038/nmat3776.

In a similar way, an oxidizing voltage was used to activate the disaggregation of a vesicle membrane (composed of redox-responsive self-assembled amphiphilic rod-coil tetraaniline-PEG) into smaller micelles, which could reaggregate on the application of a reductive voltage (121). Electroporation - the application of voltage to cause the formation of pores in cell membranes and thus increasing their permeability to drugs - has been shown to be an efficient strategy to obtain drug delivery. In recent studies

electroporation has been applied to nucleic acid delivery to cancer, using PEG-coated silica nanoparticles with opposite polarities to enhance gene transfection (122) or by using transferrin-decorated liposomes loaded with exogenous oligonucleotides (123).
Although the positive trend obtained in such kind of therapy, the limitation on electroresponsive nanocarriers is again the low tissue penetration depth and the need to avoid undesired tissue damage.

1.2.2 ENDOGENOUS STIMULI-RESPONSIVE DRUG DELIVERY

In this section systems that take advantage of microenvironmental alterations in pH, redox potential, concentrations of enzymes or specific analytes will be discussed.

1.2.2.1. pH-sensitive systems

The variation in pH have been exploited to control the delivery of drugs in specific organs (as the gastrointestinal tract) or intracellular compartments (as endosomes), or in order to cause the release of the drug after a change in the environmental pH in pathological situations, such as cancer or inflammation (104). Two main strategies can be used for the purpose. The first is the use of polymers (polyacids or polybases) which present ionizable groups that according pH variation are subjected to conformational or solubility changes in response to environmental. The second is the design of polymeric systems with acid-sensitive bonds. Cleavage of this bonds allows the release of molecules anchored at the polymer backbone, the modification of the charge of the polymer or the exposure of targeting ligands. Many anticancer drug-delivery systems exploit the difference of pH existing between healthy tissues (~7.4) and the extracellular environment of solid tumors (6.5–7.2). This acidic pH in tumoral tissues is due to an irregular angiogenesis in fast-growing tumors, which causes a rapid deficit of nutrients and oxygen and as result a pH switch towards a glycolytic metabolism. Acidic metabolites are produced and an acidic pH is obtained in the tumor interstitium. It is clear that efficient pH-sensitive systems must give a sharp response to a slight change of pH in the tumor tissue. For instance, swelling of chitosan nanospheres induced by the amino-group protonation (pKa ~6.3) brings to the release of encapsulated tumor necrosis factor alpha (TNFα) acidic environment of tumor tissues (124). A second example is given by the disassembly at pH 6.4–6.8 of PEG–poly(β-amino ester) micelles with campthotecin release. In ischemic

areas the release of protein drugs was achieved with piperidine- and imidazole-modified PEG–poly(β-amino ester) micelles (125).

Once reached the cell compartment, the acidification of endosomes (pH ~5–6) can be exploited in order to obtain a controlled and sustained release. Small pH variations toward acidic values can cause nanoparticle expansion with release of their payloads. This effect has been obtained either by masking the hydroxyl groups in the polymer backbone with acid-labile protecting groups (126) or using dimethylaminoethyl methacrylate monomer units that can be protonated. In this manner it was possible obtain a tuned DNA release kinetics within the endosomal pH range (127). On the other hand, the acid-sensitive bonds can be exploited in the polymer backbone (such as hydrazone (128), acetals (129) or the presence of acid-degradable crosslinkers to obtain the disaggregation of the nanocarrier. Drugs covalently conjugated to polymer backbones (128) or protein scaffolds (130) can also be released exploiting this acidic sensitive linkages.

However, a strong acidic pH, as the one inside lysosomes, can be harmful to many drugs. For this reason systems have been designed able to escape the endosomal compartment by exploiting the proton sponge effect (where an increase in osmotic pressure caused by polymers leads to endosomal swelling and rupture). To obtain this, copolymers obtained with amine-containing polymers (such as poly-l-lysine, poly(β-amino esters) (131)) have been used to buffer the endosomal pH. For example, lipid-coated poly(β-amino ester) nanoparticles combined the endosomal escape and the delivery of mRNA in vivo with a good transfection after intranasal administration (132). The charge-reversal behavior of chitosan has also been exploited for pH-triggered drug release (133). PEG-coated liposomes with a positive charged surface were used to enhance the interaction with membrane of endosomes (134). pH sensitivity to the nanosystem can be obtained also through caging polymer chains that undergo phase transition in lysosomal acidic conditions, releasing the payload (135).

1.2.2.2. Redox-sensitive systems

Redox senstive systems can be obtained exploiting the different concentrations of GSH found in extracellular (~2–10 μM) and intracellular (~2–10 mM) compartments, and in tumour tissues compared with healthy ones. cit Disulphide bonds, susceptible to cleavage by glutathione (GSH), can be used to obtain drug carriers that can change their conformation, and release their content in cytosolic compartment, following redox

stimuli. Degradable micelles have been developed with self-assembled amphiphilic copolymers containing disulphide bonds a disulphide bond at the connection of the two polymer blocks (136). GSH-sensitive crosslinking agents could also be incorporated in the shell or in the core (137) of the micelles, leading to micelle disassembly followed by specific intracellular release of hydrophobic drugs. Redox-sensitive systems can also be obtained with thiol-cleavable bonds (138) or quinone-lipid conjugate (139).

1.2.2.3. Self-regulated systems

A last option in developing of stimuli responsive systems, could be the exploitation of specific analytes concentration in order to achieve self-regulated drug delivery. This strategy could be important in the non-invasive management of diabetes, which requires a system that triggers the release of insulin according to glucose levels in the blood. A quite common strategy to design glucose-responsive systems exploit the capability of phenylboronic acid (PBA) to combine reversibly with *cis*-diol units. The equilibrium in aqueous solution between neutral (hydrophobic) and charged (hydrophilic) PBA is shifted towards the second one when charged PBA form complexes with glucose, resulting in the swelling of PBA containing polymers. As consequence the release of insulin from poly(ethylene glycol)-block-poly(acrylic acid-co-acrylamidophenylboronic acid) micelles (140) and poly(ethylene glycol)-b-poly(styrene boroxole) polymersomes is obtained (141). Anyway, this kind of responsiveness required high glucose concentrations (up to 50 mg/ml), quite far from the concentration present in physiological conditions (1–3 mg/ml). A greater glucose sensitivity was obtained by rearrangement of the polymer structure with introduction of non-responsive solubilizing groups (142). When these molecules are introduced, the interaction of PBA with the glycopolymer is weakened in the presence of glucose by competition, resulting in a matrix swelling and insulin release.

Despite the huge progresses achieved in this field, the translation of stimuli-responsive drug-delivery systems from the bench to the bedside is not so easy. This could be due to their sophisticated designs, which makes the potential pharmaceutical development more complex, especially in terms of the manufacturing, reproducibility and quality control (104). Moreover, non trivial optimizations and improvements are often required and have to be studied for the translation of each stimulus from preclinical experimental models to daily clinical practice. In particular, endogenous triggers are really difficult to control

because they may vary from one patient to another. The pH in the interstitium of a tumor or the presence of reducing agents in the blood stream can also be rather dishomogeneous among patients.

Although systems responsive to external stimuli are interesting and promising, major improvements would be needed to improve both tissue-penetration depth and focusing of the physical trigger in order to avoid damages at normal tissues. At the moment, the two stimuli-responsive nanosystems that have reached the clinical stage (Table 1.3 (104)) are responsive to exogenous stimuli, whereas no immediate success is expected for the many systems responsive to external stimuli under development.

Table 1.3. Stimuli responsive drug-delivery systems in clinical trials. Adapted from (104) with DOI:10.1038/nmat3776.

Stimulus	Nanocarrier	Drug (trade name)	Targets	Clinical status
Temperature	Liposomes	Doxorubicin (ThermoDox)	Unresectable hepatocellular carcinoma	Phase III, the HEAT study
			Recurrent chest-wall breast cancer	Phase II, the DIGNITY study
			Colorectal liver metastases	Phase II, the ABLATE study
			Painful bone metastases, breast carcinoma, non-small-cell lung cancer, small-cell lung cancer, adenocarcinoma	Phase II
			Bone metastases, pancreatic cancer, metastatic liver cancer	Phase I
Magnetic	Magnetic fluid MFLAS1	NanoTherm AS1, MagForce Nanotechnologies	Glioblastoma	European Union regulatory approval
	Iron-oxide magnetite		Prostate and pancreatic carcinoma	Phase I
	Iron and carbon particles	Doxorubicin/MTC–DOX	Unresectable hepatocellular carcinoma	Phase II and Phase III
			Hepatocellular carcinoma	Phase I and Phase II
			Cancer metastatic to the liver	Phase I and Phase II

*ClinicalTrials.gov identifiers are given if available; ClinicalTrials.gov

As we can deduce from the above table, the thermosensitive liposomes ThermoDox are at present in clinical trials for the treatment of breast cancer (phase II) and hepatocellular carcinoma (phase III). Iron oxide NanoTherm has been approved for the treatment of glioblastoma. ThermoDox have been recently suspended because it did not show to overcome the threshold of 33% in life span, nevertheless these trials have demonstrated the safety profile of the liposomes, which were well tolerated by patients. Iron oxide-based MTC–DOX (magnetic target carrier–doxorubicin, developed by FeRX) entered phase II and III clinical trials for the treatment of liver cancer and unresectable hepatocellular carcinoma, respectively, but no updated data have been published since 2005 (104).

1.3 POLYMER VESICLES

1.3.1 AMPHIPHILIC POLYMERS AND NANOSTRUCTURE FORMATION

Development of drug delivery systems based on water-soluble polymers is one of the main goal of research in the fields of polymer chemistry and physics, since water is the solvent of first choice if we want to deliver natural macro-molecules, such as protein and DNA (143). If polymers are designed as amphiphilic materials, they should be able to assemble, form nanosized structures and stabilize systems susceptible to macrophase separation. Amphiphilicity is the key feature that influences a variety of properties of water soluble polymers in aqueous solutions. Totally hydrophilic compounds are soluble in water while the hydrophobic ones are not. Moreover, amphiphilic compounds possess an intermediate feature, being able to stabilize the unprofitable interactions between water and hydrophobic fractions of the molecules.

First attempts to describe the principles of spatial organization of amphiphilic polymers led to the development of a simple (at first sight) Hydrophobic - Polar (HP) (144). The inspiration to this model came studying the different existing protein conformations, where protein design experiments showed that groups of hydrophylic (more polar, P) and hydrophobic (less polar, H) amino acids have an important role in determining the final secondary (145) or tertiary protein structure (146). Taking inspiration from proteins, the HP model was transferred on copolymers, that distinguishes only two kinds of monomers, namely hydrophilic (P) and hydrophobic (H). This scheme allowed simulation studies about the thermodynamics and stability of aggregated systems obtained with these macromolecules. The obtained result is a minimalist model, based on the physical principle of Hydrophilic/Hydrophobic definition.

The disadvantage of this HP model is that it does not take into account the fact that the monomer units themselves, which are considered as hydrophilic, consists actually of hydrophilic and hydrophobic parts, and are actually amphiphilic. Possibly, the spatial of amphiphilic polymers will organize at the interface between hydrophobic and hydrophilic media.

A second model, reported in Figure 1.13, concerns a two-dimensional thermodynamic classification for amphiphilic monomers, which took into account three possible preferential dispositions of a monomer unit in two non-miscible liquids. This model is

based on an affinity scale to polar and non polar phases and allows to study the behavior of a selected monomer (147).

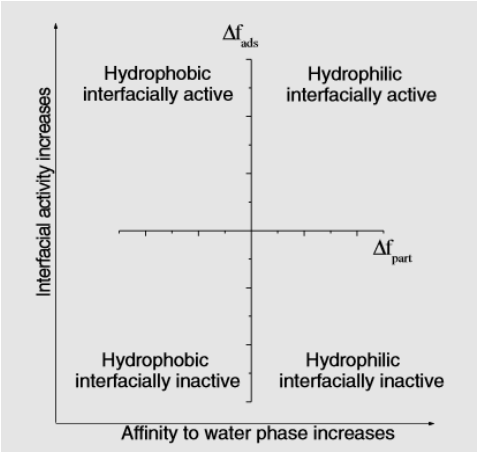

Figure 1.13. Two dimensional diagram of phase affinity and interfacial activity, general view. Adapted from (147) with DOI:10.1007/12_051.

In this model, each monomer is defined by two dimensional coordinates: the abscissa corresponds to the affinity to the polar (water) or the non polar phase (hexane) while the ordinate corresponds to the interfacial activity. The standard free energy of partition beetween water and hexane is used as a control for the abscissa axis (ΔF_{part}), whereas the standard energy of adsorption at the interface is used for the ordinate axis (ΔF_{ads}). On the bases of this diagram, studies performed by Okhapkin and colleagues (143) on synthetic monomers N-vinylcaprolactam (VCL), N-vinylpyrrolidone (VP), N-isopropylacrylamide (NIPA) and 1-vynilimidazole (Vim), showed that the interfacial activity increases as the hydrophobicity of the amino acid residues increases. Since the amino acids possess two major hydrophilic groups, namely the amino and carboxyl groups that are constant in all aminoacids, it can be concluded that the increase in hydrophobicity enhances the amphiphilic character of aminoacids. Thus, it was shown that many building blocks of natural and synthetyc polymers are amphiphilic and interfacially active, and are able to provide spontaneous nanostructures assembly in aqueous solution (143).

1.3.2 POLYMERSOMES

Amphiphilic polymers, by structure, are mostly copolymers since they are made of repetitive hydrophilic blocks and a hydrophobic blocks. In the previous section, we

underlined that amphiphilic polymers can form nanostructures in aqueous conditions. Furthemore, all block copolymers, if made of suitable amphiphilic proportions, can self-assemble into vesicles when hydrated (148). The hydrophobic blocks of each polymer chain tend spontaneously to associate with each other to minimize direct exposure to water, whereas the more hydrophilic blocks stick toward the water phase in and out the vesicle, are hydrated by water. The assembly of the copolymer generate a layer with two interfaces with water. It must be highlighted here that the generation of micelles or a bilayer of a vesicle is strongly dictated by the hydrophilic and hydrophobic weight ratio of the polymer blocks as described below. The colloidal system generated is rather similar to a liposome and for this reason it is named polymersome (148). Liposomes are assembled with components with Molecular Weight of less than 1 kDa, whereas copolymers have MW of at least 5-10 kDa.

In the case of liposomes, phospholipids aggregate forming vesicles in many aqueous solutions, because water exalts their amphiphilicity, while they fail to do so in solvents that do not exalt their amphiphilicity (as chloroform). Solubility of amphiphilic polymer also depends in general on chain MW, which suggests that vesicles can also be assembled using weakly hydrophobic polymers (12).

Lipids and small amphiphiles can differ considerably for what concern their hydrophilic component, also named head group, but the most of the times they contain one or two strongly hydrophobic chains composed of multiple ethylene units $(–CH_2–CH_2–)n$ (with n = 5 to 18 typically). The minimal concentration at which lipids and polymers aggregate to give liposomes, or polymersomes, or micelles can be provided measuring the CAC or CMC (Critical Aggregation Concentration or Critical Micelle Concentration respectively):

$$C_{CAC/\mathrm{CMC}} = \exp(-n\varepsilon_h/k_bT),$$

where k_bT is the thermal energy and ε_h is the effective interaction energy of the monomer with the bulk solution. Only at concentrations of the amphiphilic component above $C_{CAC/\mathrm{CMC}}$ colloidal aggregates can form. For ethylene groups at the physiological temperature T_{biol}, $\varepsilon_h \approx 1$ to 2, $k_BT_{biol} \sim 4$ to 8 pN·nm. Thus values of C_{CMC} for lipids and related amphiphiles in aqueous solutions range from micromolar to picomolar (148)

As reported above, copolymers have the amphiphilic character as lipids but consist of polymer chains where a series of two or more blocks are covalently linked (Figure 1.14).

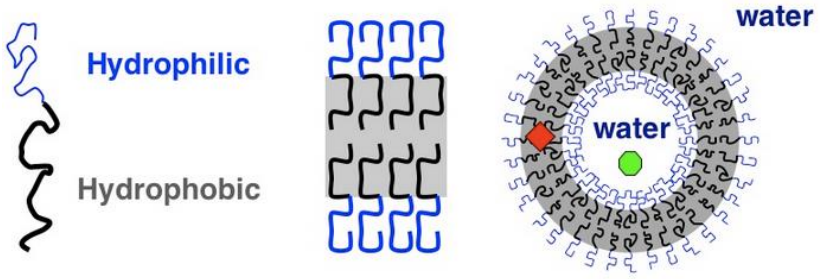

Figure 1.14. Schematic representation of block copolymers and polymersomes.

One of the earliest examples of a semi synthetic diblock copolymers that self-assembles in aqueous conditions is a dipeptide construct PolyStyrene$_{40}$ (PS_{40})-poly(isocyano-L-alanine-L-alanine)$_m$ (149). Under acidic conditions and for m = 10, vesicles with diameters ranging from tens to hundreds of nanometers were observed. (Figure 1.15).

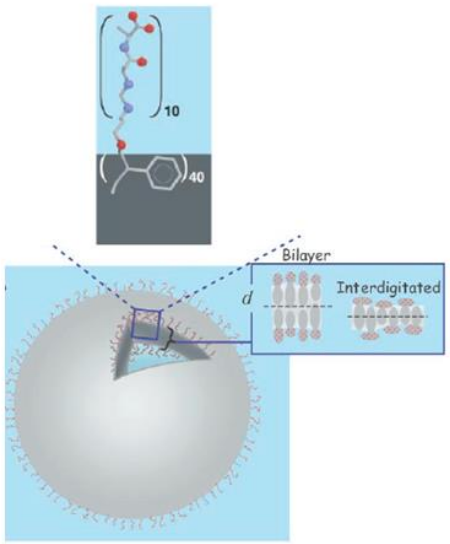

Figure 1.15. Example of vesicles obtained with block copolymer PS_{40}-poly (isocyano-L-alanine-L-alanine)$_{m..}$ Adapted from (12) with DOI:10.1126/science.1074972.

A fully synthetic diblock copolymers of PEO_m-PBD_n (PEO, polyethylen oxide; PBD, polybutadiene) and the hydrogenated homologue of PBD, namely the poly(ethylethylene) (PEO-PEE), led to formation of polymer vesicles first referred to as polymersomes (150) . The effective shape of obtained vesicles can be predicted thank to the hydrophilic fraction *f*. Liposomes have a *f* value around 50% referred to their total mass. In general, in order

to obtain polymersomes $f_{hydrophilic} \approx 35\% \pm 10\%$ (151). Polymers with $f_{hydrophilic} \approx 45\%$ are expected to form micelles, whereas molecules with $f_{hydrophilic} \approx 25\%$ generally form inverted microstructures (12). These general rules allow to design polymers with adequate hydrophilic/hydrophobic balance depending on the colloidal structures that are desired. How the polymer chain chemistry and the MW affect these rules have not been fully elucidated. However, copolymers complying these rules and assembling in polymersomes have MWs ranging from ~ 2700 to 20.000 g/mol. Furthermore, cryogenic transmission electron microscopy (cryo-TEM) of 100 to 200 nm vesicles showed that membrane thickness increases with MW increase from 8 to 21 nm (152, 153). Lipid membranes of liposomes have a far more limited range of tickness (3 to 5 nm). Polymersome membranes thus offer a novel opportunity to study membrane properties and membrane associated proteins as a function of the membrane tickness. Polymersomes can be generated with a low permeability membrane, able to retain encapsulated molecules over periods of months. These polymersomes had ~100-nm in size and were prepared by extrusion techniques similar to those exploited to prepare liposomes (154) as well as with ~10 μm giant vesicles. Figure 1.15 shows that lateral diffusivity (12, 155) as well as apparent membrane viscosity studies (12, 151, 156) point out that membrane fluidity decreases increasing MW of the polymer. Moreover, the decreases are most relevant when the chains are long enough to entangle (Figure 1.16).

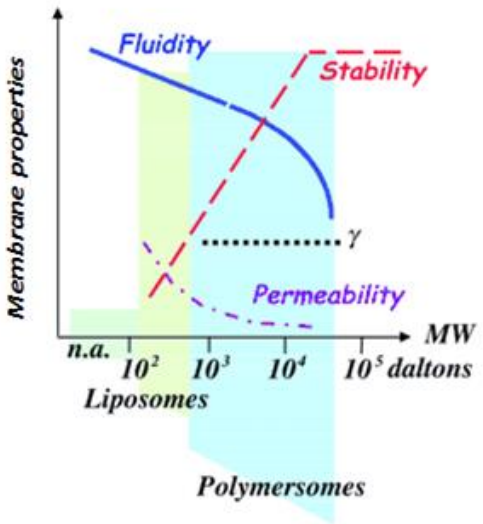

Figure 1.16. Schematic of membrane properties versus amphiphile molecular weight. Adapted from (12) with DOI:10.1126/science.1074972.

Measurements of the area elasticity gives an indirect measure of ε_h as γ (~ 25 mN/m) and shows that the elasticity of the membrane is independent from the MW of the polymer.

Also water permeation through the polymersome membranes has been measured (156) and compared to phospholipid membranes. A considerably reduced transport rate was obtained in the case of polymersomes. These results are in agreement with early measurements on liposomes made by Bangham on a narrow MW-series of lipids (157). What we can deduce from these studies is that liposome membranes appear fluider than stable. In this context, cholesterol is a useful component for membranes because it both toughens and fluidizes the cell membranes (158). To investigate the effect of polymer structure on the strength and fluidity of polymeric membranes, several triblock copolymers have been investigated in detail, and the differences in membrane properties have offered important insights.

Polymersomes are versatile carriers because they allow loading of both hydrophilic and hydrophobic drugs. Hydrophobic agents can be trapped in the hydrophobic layer while hydrophilic therapeutics can be disposed into the aqueous core. In addition, the hydrophilic corona can be used to easily conjugate biomolecules with the external faceing layer in order to selectively target specific cell types. Literature reports samples of polymer vesicles obtained with ABC triblock copolymers (159, 160).

A and C are two different hydrophilic blocks and B is the hydrophobic block which can mimic the characteristic structure of the physiological membrane with a surface hydrophilic section (head groups of phospholipids), an hydrophobic internal core (alkyl chains of phospholipids), and another hydrophilic section (head groups of phospholipids). The phase segregation and the organization of amphiphilic polymers that self-assemble into polymeric membranes yielding polymersomes affect the interaction of the colloidal system with cells. Thus the interface features of the system is paramount in dictating its biological properties. In particular, it has been demonstrated that by systematically varying the blocks of the triblock copolymer by varying the monomers or the block length, polymersomes can undergo rapid endocytosis, can induce cell apoptosis or can exhibit relatively slow cellular uptake and low cytotoxicity (160). Thus the polymer blocks features possess a double role: on one side they dictate the arrangement of the polymer chains to yield the polymersomes, on the other side they are the primary

responsible for the surface properties of the vesicles that will interface with the biological environment after administration.

To ensure efficient therapeutic activity, delivery systems must be able to circulate for long periods of time in the bloodstream and avoid the elimination by the mononuclear phagocytic system (MPS, also known as reticulo-endhotelial system). Hydrophobic or charged nanoparticles usually are removed by the immune system and rapidly cleared. Coating surface techniques involving hydrophilic polymers have been used to solve this problem and often require additional conjugation efforts to coat the preformed carriers with polymers (e.g.: nanoparticles or liposomes). Due to their amphiphilic nature, polymeric vesicles already possess an hydrophilic shielding layer as soon as they are assembled. An example is given by polymersomes assembled with an appropriate synthesized biocompatible hydrophilic block, usually poly(ethylene glycol) (PEG) or 2-methacryl-oyloxyethyl phosphorylcholine (PMPC) (161).

Due to their ability to load simultaneously hydrophilic and hydrophobic therapeutics, these nano-sized carriers are also good candidates for combinational-therapies, that is regarded as a promising frontier for the treatment of cancer. Compared to lipid-based vesicles, polymersomes are in general more stable. Liposomes have been widely exploited as delivery vehicles despite their limits including the short circulation time and lack of efficient mechanism for controlled drug release. On the contrary, polymersomes offer a more versatile system. The stability of the polymersomes can be programmed by designing and synthesizing proper block copolymers. Furthermore, polymersomes are more flexible than liposomes for what concern the modulation of their physical features and their biological behavior. Polymeric vesicles for this reason have been recently explored as novel in vivo delivery vehicles.

Furthermore, in virtue of their versatility, polymersomes can be generated using positively charged polymers (162), which is very helpful for the formulation and delivery of oligonucleotides. An efficient non viral vector for gene delivery or oligonucleotide delivery should ideally guarantee for specific and efficient cell transfection, for high level and period of expression and for low immunogenicity. Unfortunately, a non viral vector that satisfies these requirements has not been produced yet. On the other hand, while viral vectors have great transfection activity, they can also transfer viral genome traces, which trigger severe immunogenic responses. For this reason, non-viral vectors are regarded as a

safer alternative to viruses. In virtue of their stability, the polymeric vesicles can protect oligonucleotides or proteins and they can be easily functionalized to integrate mechanisms for targeting as well as controlled release. Encouraging early results in clinical trials with polymer conjugates have promoted the development of synthetic systems the intracellular delivery according to a viral mimic activity.

1.3.3 pH SENSITIVE POLYMERSOMES

In order to achieve effective controlled release or site-selective uptake, the materials designed for the assembly of polymersomes can be tailored to respond to external physic-chemical stimuli, such as pH variations, alteration of the environment redox potential, temperature changes (163) (Figure 1.17).

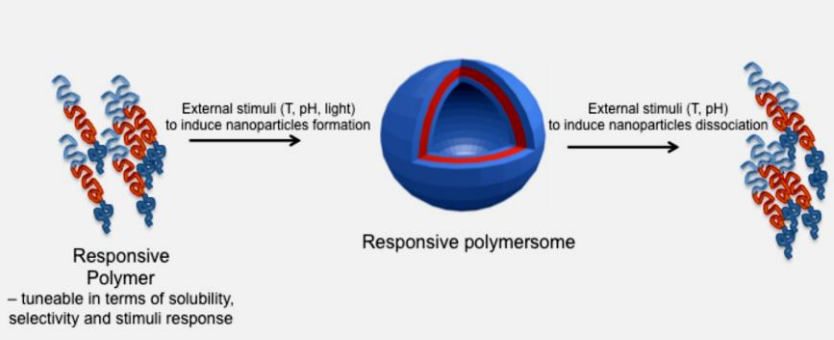

Figure 1.17. Schematic representation of the assembly and the dissociation of stimuli-responsive polymersomes.

Among the realm of the stimuli-sensitive systems, pH responsive nanocarriers have been the most investigated because of the wide range of pH gradients available in different tissues and subcellular compartments in physiological and pathological conditions, which can be used to activate the programmed response of the carriers.

Controlled drug release can be triggered in tumor tissues or intracellularly in the endosomal or lysosomal compartment in virtue of their peculiar lower pH with respect to the blood. In order to be effective, these systems are required to respond to a rather narrow pH range. The responsiveness to environmental pH shift can be achieved with protonable polyionic materials including polyacids or polybases in the blocks of the copolymer used to assemble polymersomes. The capability of these polymers to respond is provided by peculiar functional groups that can switch their ionization state between

protonated and deprotonated depending on the external environment. The ionic/non ionic conversion dictated by the external environment can affect the solubility and the special conformation of the copolymer (164).

Functional "titratable" groups with pKa from 3 to 11 are generally exploited to synthesized pH responsive polymers for the assembly of pH sensitive polymersomes. They include a variety of small molecules that are used to generate monomers for the material polymerization. These small molecules usually possess carboxylic acids or primary secondary and tertiary amine (165).

Different methods can then be exploited to induce the assembly of the pH responsive polymers into polymersomes. General methods of assembly include the processing of the polymer in organic solvents or a mixture of organic solvent/water or aqueous media (166). The "solvent-switch" method is representative of this family of techniques to assemble polymersomes and has been used because often the amphiphilic block copolymers are not directly water soluble. This method involves the dissolution of the copolymer in an organic solvent suitable for the polymer blocks and and miscible with water. Then slowly the organic solution is diluted with water (167, 168). The hydrophilic blocks of the polymeric chains are hydrated once the polymer assemble in water and form the external coronas, while the hydrophobic block associates to minimize the contact surface with water and form the polymersome membrane core. The "solvent- switch" method requires the removal of the organic co-solvent by dialysis.

An alternative technique to the "solvent-switch" method involves the rehydration of a dry polymeric film by the addition of a buffer solution containing the therapeutic molecules (169). The copolymer is firstly dissolved in a highly volatile organic solvent, such as chloroform, and then it is evaporated obtaining a copolymer thin film. The film is then rehydrated, leading to vesicles formation.

The systems obtained with these procedures have usually micrometer-sizes and tend to have wide distribution in particle size (170, 171). Some examples of innovative methods that allow the formation of polymersomes using charged polymers have been reported in literature. Here we mention the work of Du and Armes (166) which obtained vesicles with tunable membrane permeability at different pH. The amphiphilic block copolymer poly (ethylene oxide)-b-poly[2-(diethylamino)ethylmethacrylate-s-3-(trimethoxysilyl) propyl metha-crylate] [PEO-b-P(DEA-s-TMSPMA)] was synthesized in THF/water

mixture using PDEA. The PDEA block is responsible for the pH response of the vesicles since it is protonated and becomes hydrophilic at low pH, which increase the polymersome membrane permeability. By increasing the pH, the PDEA block becomes hydrophobic and gradually decreases the membrane permeability by strong hydrophobic interactions. This allows both controlled encapsulation and release. Poly[3-(trimethylsilyl) propyl methacrylate] (PTMSPMA) was added as a cross-linking agent in order to preserve the vesicular morphology.

The complete removal of the organic solvent from formed vesicles can be problematic, can require long time and may originate following toxicity, therefore recently solvent-free preparation have been investigated. A reported example is the formation of vesicles from poly(2-methacryloyloxyethylphosphorylcholine)-block-poly[2-(diisopropylamino)ethyl methacrylate] (PMPC-block-PDPA) used for the delivery of Doxorubicin (166). MPC is the biocompatible and hydrophilic monomer, and DPA is the hydrophobic and responsive monomer. When the pH of the PMPC-block-PDPA solution is lower than the pKa of PDPA, the PDPA becomes hydrophilic due to the protonation of the tertiary amine and becomes fully soluble in water. By increasing the pH, the block loses its protons, turns hydrophobic and spontaneously form vesicles in aqueous media.

1.3.4 POLYMERSOME APPLICATION FOR RNA INTERFERENCE DELIVERY

Small interfering RNA (siRNA), discovered only in the 1990s, has rapidly been applied as a potential therapeutic for a wide array of diseases (77, 78, 172). siRNA molecules, double-stranded RNA typically of 20−25 nucleotides in length, act to down-regulate expression of a specific target genes. This down-regulation is obtained with participation of the cell own RNA interference machinery. A single strand of the siRNA molecule with a precise sequence, typically the antisense strand, is incorporated into endogenous protein complex RISC (RNA-induced silencing complex) assembly in the cytosol, which then is able to degrade complementary messenger RNA (mRNA) (173).

The advantage of RNAi technology is that it can be used to target different genes responsible for different cellular pathways. This is particularly relevant for a complex disease as cancer. The major cellular pathways that have been identified as altered in cancer include the receptor protein tyrosine kinase (PTK) pathway, adenomatous polyposis coli (APC) pathway, glioma-associated oncogene (GLI) pathway,

phosphoinositide 3-kinase (PIK3) pathway, SMAD pathway, hypoxia-inducible transcription factor (HIF) pathway, retinoblastoma (Rb), p53 pathway, and apoptosis (APOP) pathway (9, 174). All these and even more pathways are good candidates for the application of siRNA as therapeutic molecule. Most of the cancer genes exploited as targets for RNAi candidates are involved in pathways involved in tumor growth. While mRNAs expressed from mutated cancer oncogenes can be directly targeted by exogenous RNAi, the process of siRNA interference can also be used to target and silence gene products that negatively regulate the function of endogenous tumor suppressor genes thus counterbalancing the deregulated growth of tumors. Anyway, RNAi can also work on proteins involved in cellular senescence, or protein stability and degradation.
Table 1.4 summarizes some of the genes that have been targeted by RNAi until now (9).

Table 1.4. Genes involved in oncogenesis. Adapted from (9) with DOI: 10.1038/sj.gt.3302694.

Oncogenesis pathways	
PTK pathway	EGFR/ErbB1, ErbB2/HER2/Neu, ErbB3/HER3, IGF-1R, RET, K-ras, R-ras, CSF-1R/c-fms, PDGFR-β, FLT-3, Met, EphA2, BRAF, Pim-2, ABL, c-Kit, c-Src
APC pathway	(Met, β-catenin, c-Myc
GLI pathway	N-Myc, Cyclin-D1
PI3K pathway	PI3K, AKT, IKK-β, NF-$\kappa\beta$
SMAD pathway	EWS/FLI-1
HIF-1 pathway	HIF-1α, XBP-1
Cell cycle regulators	
RB pathway	HPV E7, E2F4
P53 pathway	HPV E6, Hdmx, Notch-1, Delta-like-1, Jagged-1
Cyclins, CDKs, Check points	Cyclin B1, cyclin D1, Chk1
APOP pathways	FLIP, BCL-2, BCL-XL, Survivin, XIAP
Cell senescence	Telomerase, Id1
Protein stability and degradation	Cks-1, Skp-2, βTRCP1, cathepsin L

PTK, protein tyrosine kinase; APC, adenomatous polyposis coli; GLI, glioma-associated oncogene; PI3K, phosphoinositide 3-kinase; HIF, hypoxia-inducible transcription factor; APOP, apoptosis; EGFR, epidermal growth factor receptor; ErbB2/Her2/neu, erythroblastic leukemia oncogene 2; ErbB3/HER3, erythroblastic leukemia oncogene 3; IGF-1R, insulin-like growth factor-1 receptor; PDGF-Rβ, platelet-derived growth factor receptor β; FLT-3, FMS-like tyrosine kinase-3; Met, met proto-oncogene (hepatocyte growth factor receptor); EphA2, erythropoietin-producing hepatocellular (EPH)A2; BRAF, gene for the B-type Raf kinase; Pim-2, proto-oncogene Pim-2 (serine threonine kinase); ABL, Abelson murine leukemia oncogene; Kit, tyrosine protein kinase oncogene; Src, Rous sarcoma oncogene; Myc, myelocytomatosis oncogene; Akt, v-akt murine thymoma viral oncogene homolog; IKK-β, IkappaB kinase β; NF-$\kappa\beta$, nuclear factor $\kappa\beta$; EWS, Ewing's sarcoma gene; FLI-1, friend leukemia integration-1; XBP-1, X-box-binding protein1; HPV, human papillomavirus; E2F4, E2 factor 4; HdmX, human double minute X; Chk1, checkpoint kinase 1; FLIP, Fas-associated death domain-like interleukin-1β-converting enzyme (FLICE)-like inhibitory protein; Bcl-2, B-cell lymphoma2; Bcl-xL, B-cell lymphoma xL; XIAP, X chromosome-linked IAP; Id1, Inhibitor of DNA binding/differentiation; Cks-1, cyclin-dependent kinase subunit 1; Skp2, S-phase kinase protein-2; βTRCP, β-transducin repeats-containing proteins.

Although RNAi has always been a fascinating process in the field of research, effective delivery of siRNA molecules to tumors and cancer cells presents a number of unique challenges (175, 176). First, RNA is rapidly degraded in the presence of serum and any ribonuclease (RNase). Consequently, effective delivery of the siRNA molecules requires the protection from degradation (177, 178). Secondly, because siRNA is a quite big

molecule (~13 kDa) and highly negatively charged, its intracellular delivery has to be assisted because he has not access into cells as free molecule.

Finally, siRNA has to reach the cytosolic compartment in order to assemble with the RISC protein complex. In most cases means that the siRNA must escape the endosomal intracellular compartments to be released in the cytosol. The above cited requirements are needed both for delivery of siRNA in vitro and in vivo. However, for the case of in vivo delivery, we have also to consider that siRNA has to arrive to the appropriate tissue in the body, evading host immune response and phagocytosis, colloidal stability, toxicity, and avoiding filtration in the kidneys (172).

It is conceivable that adequate and efficient non viral carriers for siRNA delivery are paramount to guarantee the biological activity of the siRNA at the site of action. For this reason, siRNA complexes with positively charged liposomes (lipoplexes), polymers polyplexes, and polymersomes are under investigation. With oligonucleotides encapsulated inside the aqueous lumen of polymersomes, protection from the external environment has been clearly demonstrated and it was shown to be an efficient strategy. Furthermore, polymer vesicle coronas, composed of a dense PEO brush layer, have been shown to effectively prohibit the opsonization of the vesicles and therefore reduce the host immuneresponse and clearance from the body (179, 172). An example of siRNA loaded polymersomes is given by Kim et all. (10) which used various block copolymers such as PEG-polycaprolactone (OCL), PEG-polylactic acid (OLA), and inert PEG-polybutadiene (OB). Polymersomes were prepared according a co solvent dialysis method, which exploits the miscibility of DMSO (where copolymer are dissolved) with water (suitable environment for siRNA). Briefly, to a DMSO copolymers solution, the siRNA in PBS was added. Following, dialysis was performed in order to have a graduated polymersomes formation with a parallel siRNA encapsulation. This method showed a siRNA encapsulation efficiency up to 30% by the prepared polymersomes.

Pangburn et al. (172) prepared polymersomes for siRNA delivery using poly(1,2-butadiene)-b-poly(ethylene oxide) according the film rehydration method. Copolymers were placed in a vial with chloroform to form a polymer concentrated solution and shaken for 24 hours. The film was then prepared drying the solvent and an aqueous solution of the oligonucleotides was added to the film that was in this manner rehydrated forming the loaded vesicles. These polymersomes showed an encapsulation efficiency of even 50%.

The use of polymeric vesicles has some advantages if compared to siRNA delivery by liposomes. Firstly, as reported in previous sections, polymersomes are bigger than liposomes and can allow a higher loading of siRNA. Furthermore, polymersomes can circulate in vivo longer than lipid vesicles (10). Finally, polymers can be synthesized *de novo* with the features needed and desired, whereas number of phospholipids is limited in the market.

A last very important example of nanocarriers for siRNA delivery, although it does not concern polymersomes, is given by cyclodextrin based targeted polyplexes. Cyclodextrins are toroidal shape molecules with structure similar to a truncated cone. They have an hydrophobic inner cavity and a hydrophilic outer surface (180). In literature many interesting in vivo studies are reported using this nanovector for RNAi application. Bartlett et all. inoculated mice with an Ewing's sarcoma family tumors (EFT) and treated them with targeted Transferrin-PEG-polyplexes-cyclodextrins loaded with a siRNA sequence for tumor suppression (siEFBP2). As result, a significant inhibition against implanted malignant cells was obtained (181). The biodistribution and the pharmacokinetic profiles of these cyclodextrins loaded with ^{64}Cu-labelled siRNA targeting luciferase were also investigated on NOD/scid mice bearing luciferase transfected Neuro2A tumour cells. The in vivo bioluminescence imagining showed that targeted cyclodextrines reduced the luciferase expression increase by 50% compared to non targeted polyplexes (182).The following step was the evaluation of the best dosing schedule for the system. This aspect was studied injected the loaded system into A/J mice bearing a subcutaneous Neuro2A tumour cell line. Results showed that tumor growth inhibition was achieved when the siRNA concentration threshold inside the cells was reached. The best therapeutic performance was obtained by three single administrations over three consecutive days of 2.5 mg/kg siRNA formulated with the transferrin targeted cyclodextrins (183). To conclude, Davis showed the absence of severe side effects after administration of siRNA loaded transferrin-PEG polyplexes to cynomolgus monkeys. The siRNA loaded ciclodextrins were injected to healthy animals at 3 to 27 mg/Kg per siRNA, reaching in this way a 100 times higher concentration than the one which showed efficacy in the mouse model. The animals did not show any alteration as loss of weight or modified food consumption. Moreover, serum markers and coagulation parameters were

in the physiological range and only the highest dose exhibited mild toxicity to kidney and liver. No response in terms of complement activation were underlined (184).

The above described studies are a good example to show that targeted siRNA loaded nanosystems, if well designed, have a really good chance to reach the phase of clinical trials in the field of anticancer therapy.

1.4 REVERSIBLE ADDITION FRAGMENTATION CHAIN TRANSFER POLYMERIZATION (RAFT)

The generation of novel materials and polymers require the exploitation of very sophisticated techniques to produce them in small and subsequently at large scale. The production of polymers is critical for what concern the capacity to fully control their physic-chemical features and the process has to be reproducible.

Among the most recent chemical strategies to synthesize polymers, Reversible Addition-Fragmentation Chain Transfer (RAFT) radical polymerization was set up by Commonwealth Scientific and Industrial Research Organization (CSIRO) and firstly reported in 1998 by Chiefari J (185).

A RAFT polymerization system consists of an equilibrium between the addition and fragmentation reactions that occur in the presence of a chain transfer agent, conventionally named as a RAFT agent. RAFT agents provide the living feature to this process by their high transfer constant, which provides the rapid exchange between the dormant and active species. Thus their structure needs to be chosen based on the features and reactivity of the chosen monomer (186). This is usually obtained using thiocarbonylthio compounds of generic structure as shown in Figure 1.17.

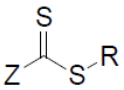

Figure 1.17. General structure of RAFT agents.

The key features of RAFT agents are a reactive C=S double bond and a weak S-R single bond. Transfer constants are strongly dependent on “Z” and “R” substituents. The R group is the free radical leaving group and it is chosen so that it undergoes b scission from the RAFT-adduct radical and it is still able to re-initiate polymerization. The reactivity of the transfer agent is highly influenced by the Z group. It should be able to

activate or deactivate the thiocarbonyl double bond in order to provide radical addition and to modify the stability of the intermediate radicals.

A variety of functionalities can be used to synthesize polymers containing end or side chain functionality in a one-step process (187).

Initiation and radical-radical termination processes take place as in a conventional radical polymerization. The most common used initiator are peroxy- and azo- compounds, such as AIBN, that decomposes thermically to provide two radical species and release N_2. In the early stage of the process the radical reacts with a monomer unit to generate a radical specie that starts an active polymerizing chain (Pn*). The propagating radical reacts with the C=S bond of the transfer agent to produce a carbon-centered radical. This radical specie undergo b-scission and is converted to a poly-RAFT agent while liberating a new radical that consists of the 'leaving group'(R) of the RAFT agent. As mentioned before, R is a key group since it must be able to reinitiate polymerization when in contact with new monomer and create a new propagating chain (Pm*). The central step in the RAFT polymerization process is the establishment of equilibrium between active and dormant species. To achieve control over polymerization it is required that the dormant species concentration is favored than that of the active one but in rapid exchange with one another. In this way the radical-radical termination is minimized and all the chains have equal probability to grow, ensuring polymers with narrow polydispersity (M_w/M_n) and low termination rate, usually < 10%. Scheme 1.1 summarize the steps involved in the RAFT polymerization process.

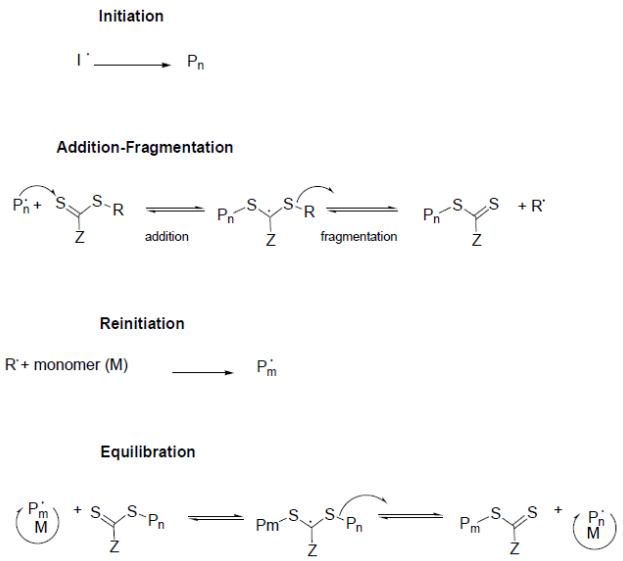

Scheme 1.1. Schematic representation of the mechanism of the RAFT polymerization.

Since radicals are not formed nor destroyed during the chain-transfer reaction, RAFT is usually carried out with an external source of free radicals (initiator). The concentration of the active species is maintained low related to the dormant species. This is obtained with the control of amount of initiator and capping agent, which should limit termination steps and increase polymer length. Termination rate is of second order as in conventional free radical polymerizations, while propagation steps show a dependency of first order with respect to the radical species concentration. Thus, if we reduce the concentration of radical species will promote propagation over termination.

Transfer agent addition to the reaction mixture can affect the polymerization kinetics through an "inhibition period", where the polymerization is slow or absent, or through a "rate retardation", which consists of a polymerization rate slower than the one of the same reaction without the use of the RAFT agent. Inhibition can be ascribed to a pre-equilibrium phase, known as initialization, where the RAFT agent is converted to a polymeric RAFT agent. RAFT agents that mostly generate this inhibiting phenomena of polymerization are the ones that stabilize the radical adduct, e. g. Z=phenyl or other aromatic compounds. This issue can be solved using more reactive RAFT agents, e.g. trithiocarbonates. The "R" group of the RAFT agent co-determines the stability of the adduct during the initializing phase. A transfer agent with a weak leaving group or inefficiently reactive will not be able to control the polymerization or will induce strong inhibiting phenomena. The advances in RAFT polymerization procedures, the knowledge of mechanism and structure-reactivity correlations have made possible the production of narrow polydisperse polymers with high conversion and commercially acceptable polymerization rates. The opportunity to carry out the reaction with a wide range of monomers, solvents and initiators make this technique extremely fascinating for the production of polymer with complex design, like stars, blocks and hyper branched materials, polymeric micelles and vesicles (188). In particular with blocks copolymer, that are the main point for polymersome assembly, the RAFT polymerization process allow to fully control features as the molecular weight and numbers of monomers of each single block since the growth of the polymer can be stopped at the end of each block and re-started with the following block.

1.5 AIM OF THE PROJECT

The aim of this thesis was the development of a novel pH sensitive targeted polymeric vesicular system for the delivery of siRNA to specific cancer cells. In virtue of the specific features of the polymers used to assemble the vesicles, once inside the cells, siRNA is released in order to carry out the RNA silencing process to inhibit the translation of aberrant proteins involved in carcinogenesis. As a molecular target, we aim to silence the synthesis of the α1 Na^+/K^+ ATPase subunit that has been reported to have a role in the tumor growth and homeostasis. The polymeric nanosystem assembled using pH responsive block copolymers is designed to achieve the tumor site in virtue of the EPR effect. Then the vesicles are internalized by cancer cells according to receptor mediated endocytosis involving the interaction between a selected ligand (folate) conjugated on the surface of the vesicles and folate receptor over expressed on target cell surface.

The project was supported by the *European NanoSci ERA-net* transnational collaborative funding scheme and was developed in collaboration with the University of Nottingham (UK) and the Centro de Investigacion Principe Felipe (CIPF) of Valencia (Spain).

A new family of N-alkyl imidazole monomers was designed to produce pH-responsive block copolymers able to assemble in drug nanocarriers. Molecules with imidazole moieties are common in biology and are known to possess useful tunable acid/base behavior. The amino acid histidine, for example, exhibits a wide range of pKa values associated to its imidazole side-chain, ranging from 2.3 to 9.2, depending on its specific location and proximity to other residues within proteins (189). In addition, N-alkyl imidazole moieties are present in a number of clinically prescribed drugs, ranging from antifungal lanosterol 14 α-demethylase inhibitors - e.g. ketoconazole, miconazole, and clotrimazole - to nitroimidazole antibiotics such as metronidazole and tinidazole (190). With a pKa in the 6.5–7.5 range, N-alkyl imidazoles appeared to be ideal precursors for the synthesis of pH responsive drug nanocarriers. An imidazole based monomer should, when present in a block co-polymer, alter the aggregation state of polymers across this pH range in virtue of its protonated/deprotonated shifting that dictates a hydrophilic/hydrophobic switching. In turn, this should result in conformational changes of the polymers when migrating from the systemic circulation (pH 7.4), to more acidic conditions such as those found in hypoxic tumor tissue (pH 6.5–7.0) or

endosomal/lysosomal acidic conditions (from 6.5 to 4.5) following cellular uptake (191). The pH response of these systems may thus provide from local entrapment of drugs in the carriers at physiological pH and the controlled release of therapeutically relevant loaded molecules under acidic conditions.

We intend to generate such polymeric vesicles by using amphiphilic di- and triblock pH responsive polymers. The first designed polymers for this purpose were diblock copolymers; literature reports a variety of studies where amphiphilic diblock co-polymers were investigated to obtain polymersomes (12). Nevertheless, the diblock copolymers produced for this project and consisting of polyglicerolmethacrylate and polyC_6-imidazole-methacrylate blocks generated vesicles with limited stability. However, the physico-chemical characterization of this first set of materials provided valuable information that were successfully exploited to generate the triblock copolymers.

The triblock copolymers were generated from the diblock and were constituted by two hydrophilic terminal blocks, polyethilenglycole (PEG) and polyglicerolmethacrylate (polyGMA), and a central pH sensitive polyC_6-imidazole-methacrylate that promotes the self-assembly of the polymeric vesicles at neutral pH and dictates the dissociation of the vesicles under acidic pH.

Once the polymeric vesicles have been endocitosed, the endosomal transit exposes polymersomes to such an environment that the midazole side chains of the pH sensitive block of the polymer will be protonated, inducing the dissociation of polymersomes. As a result, the therapeutic payload, namely siRNA, will be released inside the cytosolic compartment. Figure 1.18 schematizes the delivery mechanism intended for the carrier proposed in this thesis.

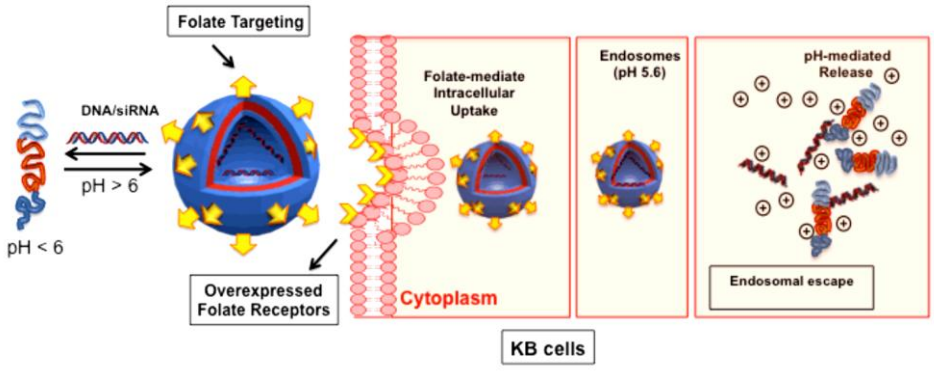

Figure 1.18. Graphical representation of one of the delivery mechanism for the pH responsive polymersomes proposed in this thesis. Adapted from (205) with DOI: 10.1039/c3py00744h - Reproduced by permission of the Royal Society of Chemistry.

The aim of the project is thus to generate novel materials with peculiar physico-chemical features, assess the assembling properties of the newly synthesized triblock copolymers, evaluate the loading and pH controlled release of model dsDNA and siRNA, and the targeted delivery of oligonucleotides to model cancer cells over expressing the folate receptor by a variety of spectroscopic and microscopic techniques. The biopharmaceutical properties of the carriers will also be investigated by delivering biologically active siRNA to the cells which will prove the capacity of the polymeric vesicles to protect the activity of the fragile siRNA, the targeting efficiency and the cytosolic release of siRNA.

2. MATERIALS AND METHODS

2.1 REAGENTS

- Tetrahydrofuran anhydrous (THF), azobisisobutyronitrile (AIBN), imidazole, ethylene carbonate, sodium hydride (NaH), sodiumhydroxide (NaOH), methacryloyl chloride, carbon disulfide, glycidyl methacrylate, 6-chloro-1-hexanol, acetic anhydride, magnesium sulfate, K_2CO_3 (potassium carbonate), N,N dimethylamino pyridine (DMAP), dimethyl formamide anhydrous (DMF), dimethylsulfoxide anhydrous (DMSO), tetrahydrofuran anhydrous (THF), chloroform, dichloromethane (DCM), ethyl acetate (EtOAc), methanol (MeOH), diethylether (Et_2O), petroleum ether (b.p. 40-60 0C), triethylamine (Et_3N), 2,2'-dithiopyridine, propylamine, PEG2000SH, β-alanine, acetic acid, low melting point agarose gel, Blue/Orange (loading dye) 6X, SafeView (nucleic acids staining), (3-(4,5-dimethylthiazol-2-yl)-2,5-diphenyltetrazolium bromide) were obtained at the highest purity available from Sigma- Aldrich, Alfa Aesar, Promega and Fisher Scientific, NBS biological, Gibco BRL companies and used without further purification unless stated.
- Folic acid, N,N'-Dicyclohexylcarbodiimide, N-Hydroxysuccinimide, were obtained from Fluka (Buchs, Switzwerland).
- Vectashield® mounting medium with 4'6-diamidine-2-phenylindole (DAPI) was provided by Vector Laboratories Inc (Burlingame, CA).
- Fluoresceine-DHPE and Rhodamine-DHPE were bought from VWR International PBI s.r.l. (Milan, Italy).
- Double strand DNA 19 nucleotides, cyanin-3 labelled DNA were obtained by biomers.net GmbH (Ulm, Germany)
- siRNA Luciferase GL3 Duplex and control siRNA with 21 nucleotides were provided by Fisher Scientific (Madrid, Spain)
- Quant-iT™ RiboGreen® RNA Assay Kit for siRNA quantification was bought by Life Technologies S.A. (Madrid, Spain)
- Folate receptor alpha, monoclonal primary Antibody from mouse 1 mg/mL in PBS 804-439-R100 and secondary antibody 1 mg/mL in PBS, Alexa fluor 488

labeled α-mouse monoclonal antibody were purchased from Enzo Life Sciences Inc.

- All products for cell biology comprising Dulbecco's modified Eagle medium (DMEM), L-glutamine, trypsin, antibiotic and antimicotic solution, bicinchoninic acid, solution of copper (II) sulfate, fetal bovin serum (FBS), phosphate saline buffer with and without Ca/Mg and plastics Greiner were obtained from Sigma-Aldrich (St. Louis, MO, USA). Chamber slides BD Falcon™ for confocal microscopy were bought from SACCO S.r.l. (Cadorago, Italy).
- Cell lines from human breast cancer (MCF7) and cervical cancer (KB) come from cell bank ATCC-USA.
- B16-F10-luc-G5 Bioware® Cell Line from mouse melanoma were obtained from Xenogen Corporation (Alameda, California)
- All aqueous solutions were prepared using deionized water (milliQ-grade, 0.06 μSiemens cm-1) obtained trough Millipore MilliQ (MA, USA).
- Salts for buffer preparation and paraformaldehyde were provided by Riedel-de-Haen (Seelze, Germany), Fluka Analytical (Buchs SG, Switzerland) and Sigma-Aldrich (St. Louis, MO, USA).

2.2 INSTRUMENTATION

- Spectrophotometric analysis were carried out with spectrophotometer UV-Vis λ25 Perkin Elmer (Norworlk, CT, USA).
- Multiwell plate detections were carried out with Microplate Autoreader Biotek Instruments inc., mod. EL311SK (Highland, Vermont U.S.A.) and Victor^2 Wallac plate reader Perkin Elmer (Norworlk, CT, USA).
- HPLC system Jasco, equipped with two pumps PU-2080 Plus, a detector UV-2075 Plus and Hercule 200 JMBS, and analytic column Luna (C18, 5 μ, 300 Å, 250 x 4.6 mm) from Phenomenex (Torrance, U.S.A.) was used for reverse phase chromatographic analysis (RP-HPLC).
- Samples were maintained under stirring with Rotating stirrer, MOD 708, of ASAL S.r.l..
- Lyophilization was carried out with freeze-dryier Hetossic HETO Lab Equipment.

- Solvents were evaporated with Rotavapor R114 of BÜCHI Labortechnik AG (Postfach, Switzerland).
- pH measurements were carried out with pHmeter Seven Easy S20-K Mettler Toledo with electrode Mettler Toledo Inlab 413 (Schwerzenbach, Switzerland) and pHmeter Fischerbrand Hydrus600.
- Centrifuges were carried out with CENTRIKON T-42K Kontron Instruments, Z300 Hemle and with ALC microcentrifughette 4214 della ALC international (Cologno Monzese, Italy).
- Polymerizations were carried out using standard Schlenk techniques under a nitrogen atmosphere. Thin layer chromatography (TLC) was performed using pre-coated plates (silica gel 60 ALUGRAM SIL G/UV254) and eluted in the solvent system indicated. Compounds were visualized by using UV light (254 nm) or stained with a basic solution (10% w/w K_2CO_3 in water) of $KMnO_4$. Across Organic 60 Å (0.035-0.070 mm) silica gel was used for column chromatography.
- ^{1}H and ^{13}C NMR spectra were recorded on a Bruker DPX400 Ultrashield spectrometer and Bruker Spectrospin AMX 300 MHz (Fallanden, Switzerland). All NMR data were processed using MestreNova 6.2.1 Software. All chemical shifts are reported in ppm (d) relative to tetramethylsilane. The following abbreviations were used for NMR peak multiplicities: s = singlet, bs = broad singlet, d =doublet, t = triplet, m = multiplet.
- Polymersomes size analysis were performed by *Dynamic Light Scattering* Zetasizer NanoZS (Malvern Instruments Ltd, UK) or *Dynamic Light Scattering* Particle Sizing System NICOMP 380ZLS (Santa Barbara, CA, USA).
- Gel electrophoresis of dsDNA/polymer mixtures were performed with an Amersham Biosciences miniVE Electrophoresis and Electrotransfer Unit system, GE Healthcare (Milan, Italy). Gel images were obtained with UV transilluminator ChemiDoc™ XRS + imaging system with Image Lab™ image acquisition and analysis software (Bio-Rad Laboratories, Headquarters, CA).
- Transmission electron microscopy (TEM) was performed using a Tecnai G2 (FEI, Oregon, USA). Samples were placed on copper grid, the excess was removed with filter paper and then stained with uranyl acetate (1% in deionized water).

- Biological studies were carried out in biological safety cabinet Space, cells were grown using the incubator from PBI International and imaged with optical microscope Axiovert 40CFL Zeiss.
- Buffers were filtered with Millipore systems (Bendford, MA, USA) using 0.22 μm cellulose acetate filter.
- Fluorimetry analyses were performed using a LS 50 B Perkin-Elmer fluorimeter (Norworlk, CT, USA).
- Cytometric analyses were performed using a BD FACSDiva flow cytometer (Becton, Dickinson and Company, Buccinasco, Milan) and results were processed with BD FACSDiva Software.
- Pictures of confocal microscopy were obtained using confocal microscope Leica TCS SP5 Leica Microsystems GmbH (Wetzlar, Germany) and software Leica Application Suite advanced fluorescence 2.0.2 for image elaboration.
- Bioluminescence studies were performed using a Victor^2 Wallac plate reader Perkin Elmer (Norworlk, CT, USA).

2.3 METHODS

2.3.1 SYNTHESIS OF MONOMERS, INTERMEDIATES AND BLOCK CO-POLYMERS

A novel family of N-alkyl imidazole monomers and block copolymers was synthesized to produce the pH-responsive domains of the intended nucleic acids nano-carriers.

2.3.1.1 Synthesis of glycerol methacrylate monomer (GMA)

Glycidyl methacrylate (10.0 g, 70.4 mmol, 9.34 mL) in H_2SO_4 (0.5 equiv.) and distilled water (420 mL) was stirred at 60ºC for 2 hours. The reaction was monitored by TLC. After completion, the mixture was extracted with DCM (3 x 150 mL), washed with brine, dried over $MgSO_4$ and then concentrated to give the crude product. Purification by silica gel flash chromatography, eluting with EtOAc 100%, provided the monomer (8.50 g, 53.0 mmol, 75%). ^{1}H NMR (400 MHz, DMSO-d6): δ 6.06 (q, J = 1.8 Hz, 1H, CH_2=C), 5.68 (q, J=1.6Hz, 1H, CH_2=C), 4.93 (d, J=5.3Hz, 1H, OH-CH2), 4.66 (t, J= 5.7Hz, 1H, $OHCH_2$), 4.13-3.99 (m, 2H, CH_2OC), 3.70 (m, 1H, CH), 3.38 (m, 2H, CH_2OH), 1.89 (s, 3H, CH_3). ^{13}C NMR (400 MHz, $CDCl_3$): δ 167.13 (1C), 136.41 (1C), 126.25 (1C), 69.63

(1C), 66.54 (1C), 63.02 (1C), 18.39 (1C). ESI-Tof mass spectrometry: expected for m/z [M-H]+1 161.08 Da, found 161.26 Da.

2.3.1.2 Synthesis of 2-(1H-imidazol-1-yl) ethyl-methacrylate monomer (ImEMA)

- *Synthesis of 6-chlorohexyl acetate*

A solution of 6-chloro-1-hexanol (40.0 g, 293 mmol), acetic anhydride (44.0 g, 428 mmol), Et_3N (88.0 g, 870 mmol) and DMAP (3.5 g, 29 mmol) in DCM (100 mL) were reacted at 0 °C for 30 minutes and then left to react for an hour at room temperature. The volume of DCM was reduced to ~70 mL, then the mixture was poured in a separating funnel containing 200 mL of H_2O. The aqueous layer was extracted twice with Et_2O (2 × 150 mL) and the organic layers were combined and washed with water (2 × 150 mL) then dried over $MgSO_4$. The mixture was filtered and the solvent was removed under reduced pressure to give (49.4 g, 276 mmol, 94%) of crude product as pale yellow oil that was used for the next step without further purification. ^{1}H-NMR (400 MHz, $CDCl_3$): δ 3.98 (t, J = 6.6 Hz, 2H, CH_2), 3.47 (t, J = 7.1 Hz, 2H, CH_2), 1.97 (s, 3H, CH_3), 1.71 (m, 2H, CH_2), 1.57 (m, 2H, CH_2), 1.40 (m, 2H, CH_2), 1.31 (m, 2H, CH_2). ^{13}C-NMR (101 MHz, $CDCl_3$): δ 171.48 (1C) 64.68 (1C), 45.25 (1C), 32.72 (1C), 28.65 (1C), 26.64 (1C), 25.40(1C), 21.43 (1C).

- *Synthesis of 6-(1H-imidazol-1-yl)-hexan-1-ol*

NaH (6.59 g, 276 mmol) was suspended in 200 mL of anhydrous DMSO. Imidazole (18.0 g, 264 mmol) was added under stirring, at room temperature. The mixture was heated to 100 °C and then 6-chlorohexyl acetate (49.40 g, 276 mmol) was added. The reaction was carried out for 3 hours at 100 °C and monitored by ^{1}H NMR in $DMSO_{d6}$. The reaction mixture was added to a solution (500 mL) of K_2CO_3 (111 g, 803 mmol) at room temperature, under vigorous stirring. The product was extracted (5 x 100 mL) with EtOAc, washed with basic water and dried over $MgSO_4$. After removal of $MgSO_4$ by filtration, the product was recovered from EtOAc solution by rotary evaporation of solvent. The product was added to 250 mL of NaOHaq 10% (w/v) and the mixture heated to 70 °C and reaction was continued for 2 hours at 70 ºC, until complete deacetylation of the alcohol was confirmed by ^{1}H NMR. The mixture was then extracted with DCM (3 × 200 mL) and dried over $MgSO_4$. After removal of $MgSO_4$ by filtration, the solvent was removed under reduced pressure and the crude product (21.0 g, 125 mmol, 45%) was

used in the next step without further purification. ^{1}H NMR (400 MHz, $CDCl_3$): δ 7.39 (s, ^{1}H, H-aromatic), 6.96 (s, ^{1}H, Haromatic), 6.85 (s, ^{1}H, H-aromatic), 3.89 (t, J = 7.1 Hz, 2H, CH_2N), 3.55 (t, J =6.4 Hz, 2H, CH_2OH), 1.72 (m, 2H, CH_2), 1.49 (m, 2H, CH_2), 1.34 (m, 2H, CH_2), 1.25 (m, 2H, CH_2).^{13}C NMR (101 MHz, DMSO-d6): δ 137.63 (1C), 128.70 (1C), 119.66 (1C), 61.01 (1C), 46.35 (1C), 32.82 (1C), 31.10 (1C), 26.27 (1C), 25.42 (1C). ESI-Tof mass spectrometry: expected for m/z [M-H]+1 169.25 Da, found 169.85 Da.

- *Synthesis of 6-(1H-imidazol-1-yl) hexyl methacrylate hydrochloride (ImHeMA)*

6-(1H-imidazol-1-yl)-hexan-1-ol (21 g, 125 mmol) was dissolved in DCM (40 mL) and kept at -20 °C. A solution of methacryloyl chloride (26.0 g, 250 mmol, 24.5 mL) in DCM (50 mL) was added dropwise under stirring over 1 hour. The reaction was stirred at this temperature 30 minutes, then left at room temperature overnight. Purification was carried out firstly by precipitation of the monomer in petroleum ether and then by flash column chromatography on silica gel eluting with 100% EtOAc and subsequently with EtOAc/MeOH 3:1. The volatiles were removed under reduced pressure and the product (21.3 g, 78.0 mmol, 63%) stored at -20 °C. ^{1}H NMR (400 MHz, $CDCl_3$): δ 9.22 (s, 1H, H-aromatic), 7.81 (s, 1H, Haromatic), 7.67 (s, 1H, H-aromatic), 5.99 (m, 1H, C=CHH), 5.66 (m, 1H, C=CHH), 4.19 (t, J = 6.6 Hz, 2H, OCH_2), 4.05 (t, J = 7.1 Hz, 2H, NCH_2), 1.89 (s, 3H, CH_3), 1.81 (m, 2H, CH_2), 1.60 (m, 2H, CH_2), 1.35 - 1.23 (m, 4H, CH_2). ^{13}C NMR (101 MHz, DMSO): δ 166.38 (1C), 136.17 (1C), 135.27(1C), 125.78 (1C), 121.85 (1C), 119.71 (1C), 63.98(1C), 48.18 (1C), 29.46 (1C), 27.83 (1C), 25.16 (1C), 24.70 (1C), 18.17 (1C). ESI-Tof mass spectrometry: expected for m/z [M-H]+1 238.17 Da, found 238.92 Da.

2.3.1.3 Synthesis of Reversible Addiction-Fragmentation Chain Transfer (RAFT) Agent / macro Chain Transfer Agent (CTA)

- Synthesis of 2-cyanopropan-2-yl 2-hydroxyethyl carbonotrithioate

2-mercaptoethanol (2.80 g, 70.4 mmol) was added dropwise to a suspension of NaH (60% w/w, stabilized in mineral oil) (5.0 g, 64 mmol), in Et_2O (50 mL) cooled to 5-10°C using an ice bath, over 15 minutes. Then, the mixture was further cooled at 0°C and carbon disulfide (7.30 g, 96.1 mmol) was added dropwise. After 2 hours, the product was

filtered, washed with Et_2O and dried overnight under reduced pressure. The product (7.0 g, 40 mmol, 57%) was used in the next step without further purification.
^{1}H NMR (400 MHz, DMSO-d6): δ 4.66 (s, 1H), 3.46 (t, J = 5.6 Hz, 2H), 3.11 (t, J = 7.2 Hz, 2H).

- Synthesis of 2,2'- (disulfaneyl-bis (carbonothioylsulfanedyl) bis (hydroxyethane)

Sodium 2- hydroxyethyl carbonotrithioate (7.0 g, 40 mmol) was dissolved in 50 mL of deionized water. $K_3Fe(CN)_6$ (14.4 g, 44.0 mmol) was slowly added under constant stirring. The crude product was isolated by precipitation as yellow viscous oil, dissolved in Et_2O and dried over $MgSO_4$. The solution was then filtered and the volatiles removed under reduced pressure. The yellow residue (5.70 g, 18.5 mmol, 46%) was used for the next step without further purification. ^{1}H NMR (400 MHz, DMSO-d_6): δ 5.20 (s, 2H), 3.67 (t, J = 6.1 Hz, 4H), 3.49 (t, J = 6.1 Hz, 4H).

- Synthesis of 2-cyanopropan-2-yl 2-hydroxyethyl carbonotrithioate

2,2'-(disulfanediylbis(carbonothioylsulfanediyl)]bis(hydroxyethane) (5.70 g, 18.5 mmol) and AIBN (4.6 g, 28 mmol) were dissolved in EtOAc (60 mL) and the resultant solution was degassed by bubbling N_2 over 30 minutes. Then, the mixture was left overnight at 80 °C, under stirring. The formation of the RAFT agent was monitored by TLC (petroleum ether/EtOAc 7:3) and ^{1}H-NMR in DMSO-d6. After completion, the solvent was removed under reduced pressure and the yellow residue was purified by flash chromatography on silica gel, before eluting with petroleum ether/EtOAc 9:1 and then petroleum ether/EtOAc 7:3. The product (6.50 g, 29.3 mmol, 78%) was obtained as orange insoluble oil. ^{1}H NMR (400 MHz, DMSO-d6): δ 5.08 (m, 1H, OH), 3.62 (t, J = 5.92 Hz, 2H, CH_2), 3.50 (t, J = 6.60 Hz, 2H, CH_2). 13C NMR (100 MHz, $CDCl_3$): δ 217.53 (1C, C=S), 120.13 (1C, C-N), 60.04 (1C, C-OH), 42.51 (1C, CH_2), 38.86 (1C, CH_2), 26.87 (2C, CH_3).

2.3.1.4 Synthesis of RAFT macro Chain Transfer Agent (CTA)

- *Synthesis of poly[GMA] macro-CTA*

GMA (2.40 g, 14.9 mmol), 2-cyanopropan-2-yl 2-hydroxyethyl carbonotrithioate (94.0 mg, 0.43 mmol) and AIBN (35.0 mg, 0.21 mmol) in DMF (6 mL) were sealed in a Schlenk tube, deoxygenated by argon bubbling for 30 minutes and then heated at 70 ºC. The conversion of the polymer was calculated via ^{1}H NMR following the decrease of the integrals of the monomer vinyl signals (6.03 and 5.68 ppm) using the singlet at 7.95 ppm

of the DMF as an internal standard. Polymerization was stopped after 150 minutes at 87% conversion. The polymer was purified by precipitation in THF.

^{1}H NMR (400 MHz, DMSO-d6): δ 4.90 (broad s, ^{1}H, OH), 4.66 (broad s, ^{1}H, OH), 3.92 (broad s, ^{1}H, CH), 3.69 (broad s, 2H, CH_2) , 3.39 (broad, 2H, CH_2,), 1.80 (broad s, 2H, CH_2,), 0.85 (broad d, 3H, CH_3).

The number of the repeat units in a polymer is defined by the Degree of Polymerisation (DP) and it is provided by the general formula:

$$DP_n = M_n/M_0$$

where M_n is the number- average molecular weight, whereas M_0 is the molecular weight of the monomer unit.

DP [GMA] = 30

- *Synthesis of mPEG$_{1.9\ kDa}$ macro-CTA*

mPEG-OH$_{1.9\ kDa}$ (2.20 g, 1.16 mmol) was dried from water by azeotropic distillation with toluene under reduced pressure. mPEG-OH$_{1.9\ kDa}$ was dissolved in DCM (30 mL) and CPADB (969 mg, 3.47 mmol), DMAP (0.05 g, 0.4 mmol) and DCC (716 mg, 3.47 mmol) were added. The mixture was left to react overnight. The precipitate was filtered to remove the DCU by-product and the solution added dropwise under stirring to 100 mL of petroleum ether to give mPEG$_{1.9\ kDa}$ macro-CTA as a pink powder.

^{1}H NMR (400 MHz, D_2O): d 7.90 (s, 2H, CH-Ar), 7.57 (m, 1H, CH-Ar), 7.40 (m, 2H, CH-Ar), 4.26 (t, 2H, CH_2O), 3.66 (bs, 204H, PEG repeating unit), 3.38 (s, 3H, OCH_3), 2.72–2.60 (m, 4H, CH_2CH_2C), 1.94 (s, 3H, $CN(C)CH_3$).

- Synthesis of t-Boc–NH–PEG$_{3.5\ kDa}$ macro-CTA

t-Boc-NH-PEG-OH$_{3.5\ kDa}$ (400 mg, 0.114mmol) was dissolved in DCM (10mL) and CPADB (0.096 g, 0.350 mmol), DMAP (0.009 g, 0.07 mmol) and DCC (0.071 g, 0.34 mmol) were added. The mixture was left to react overnight, the resultant precipitate was filtered to remove the DCU by-product and the solution added dropwise under stirring to 100 mL of petroleumether to give t-Boc–NH–PEG$_{3.5}$ kDa macro-CTA as a pink powder.

^{1}H NMR (400 MHz, D2O): d 7.90 (s, 2H, CH-Ar), 7.57 (m, ^{1}H, CH-Ar), 7.40 (m, 2H, CH-Ar), 4.27 (t, 2H, CH2O), 3.65 (bs, 342H, PEG repeat unit), 2.63 (m, 4H, $COCH_2CH_2C$), 1.94 (s, 3H, CN(C) CH_3), 1.72 (s, 9H, t-Boc).

2.3.1.5 Synthesis of diblock co-polymers

- *Synthesis of poly[GMA]$_{30}$-block-poly[ImHeMA]*

Two syntheses of this block co-polymer, using the same poly[GMA]$_{30}$ macro-CTA, were performed with the aim of obtaining a different degree of polymerization (DP) on the poly[ImHeMA] block.

1) ImHeMA (1.30 g, 11.3 mmol), p[GMA]$_{30}$ macro-CTA (0.60 g, 3.74 mmol of GMA repeating units) and AIBN (10.0 mg, 0.06 mmol) in DMF (5 mL) were sealed in a Schlenk tube, deoxygenated by argon bubbling for 30 minutes and then heated at 70 ºC. The experimental degree of polymerization was calculated by ^{1}H-NMR following the decrease of the integrals of the monomer vinyl signals (d= 5.99 and 5.66 ppm) using the singlet at d= 7.95 ppm of the DMF as an reference. The polymer was obtained by precipitation in Et_2O.

^{1}H NMR (400 MHz, MeOD): δ 9.14 (bs, 1H, H-Ar), 7.80 (bs, 1H, H-Ar), 7.65 (bs, 1H, H-Ar), 4.38 (bs, 2H, CH_2OC), 3.99 (bs, 2H+3H, $CHCH_2$+ NCH_2), 3.65 (t, 2H, CH_2OH), 2.00 (bs, 2H+ 2H, CH_2+CH_2), 1.70 (bs, 2H, CH_2), 1.48 (bs, 2H, CH_2), 0.95 (bs, 6H, CH_3+CH_3).

DP[ImHeMA] = 42

2) ImHeMA (1.30 g, 11.3 mmol), poly[GMA]$_{30}$ macro-CTA (0.30 g, 1.87 mmol of GMA repeating units) and AIBN (5.00 mg, 0.03 mmol) in DMF (5 mL) were sealed in a Schlenk tube, deoxygenated by argon bubbling for 30 minutes and then heated at 70 ºC. The experimental degree of polymerization was calculated by ^{1}H-NMR following the decrease of the integrals of the monomer vinyl signals (d= 5.99 and 5.66 ppm) using the singlet at d= 7.95 ppm of the DMF as an internal standard. Polymer was obtained by precipitation in THF/petroleum ether 1:1.

^{1}H NMR (400 MHz, MeOD) δ 9.09 (bs, 1H, H-Ar), 7.75 (bs, 1H, H-Ar), 7.61 (bs, 1H, H-Ar), 4.33 (bs, 2H, CH_2OC), 3.95 (bs, 2H+3H, $CHCH_2$+ NCH_2), 3.60 (t, 2H, CH_2OH), 1.95 ((bs, 2H+ 2H, CH_2+CH_2), 1.69 (bs, 2H, CH_2), 1.45 (bs, 2H, CH_2), 0.89 (bs, 6H, CH_3+CH_3).

DP[ImHeMA] = 682.1.5

- *Synthesis of diblock co-polymer $mPEG_{1.9\ kDa}$-block-poly[ImHeMA]$_{67}$*

ImHeMA (3.570 g, 12.69 mmol), $mPEG_{1.9\ kDa}$ macro-CTA (4) (330 mg, 0.151 mmol) and AIBN (12 mg, 0.08 mmol) in DMAC (10 mL) were sealed in a Schlenk tube, deoxygenated by argon bubbling for 30 minutes and then heated at 65 °C. The conversion of the polymer was calculated via ^{1}H NMR following the decrease of the integrals of the monomer vinyl signals (5.99 and 5.66 ppm) relative to the broad singlet of the $PEG_{1.9\ kDa}$ repeat unit protons (3.71 ppm). Polymerization was stopped at 50% of conversion. The desired polymer was recovered by precipitation in Et_2O–petroleum ether (1 : 1 v/v) and used for the next reaction as a macro-chain-transfer agent (CTA) without further purification.

^{1}H NMR (400 MHz, D2O): d 8.82 (bs, ^{1}H, H-Ar), 7.51 (bs, 2H, H-Ar), 4.32 (bs, 2H, CH_2OC), 4.04 (bs, 2H, NCH_2), 3.71 (bs, 204H, PEG repeat unit), 3.66 (t, 2H, CH_2O), 3.35 (s, 3H, CH_3), 2.00 (bs, 2H, CH_2), 1.70 (bs, 3H, CH_3).

- *Synthesis of diblock co-polymer t -Boc-NH-$PEG_{3.5\ kDa}$-block-poly[ImHeMA]$_{20}$ (8).*

ImHeMA (910 mg, 3.30 mmol), t -Boc-$PEG_{3.5\ kDa}$ macroCTA (150 mg, 0.04 mmol) and AIBN (3.00 mg, 0.02 mmol) in DMAC (5 mL) were sealed in a Schlenk tube, deoxygenated by argon bubbling for 30 minutes and then heated at 65 °C. The conversion of the polymer was calculated via ^{1}H NMR following the decrease of the integrals of the monomer vinyl signals (5.99 and 5.66 ppm) relative to the broad singlet of the t-Boc-$PEG_{3.5kDa}$ repeat unit protons (3.71 ppm). Polymerization was stopped at 54% of conversion. Polymers were obtained by precipitation in Et_2O–petroleum ether (1 : 1 v/v) and used in the next reaction as a macro-CTA.

^{1}H NMR (400 MHz, D_2O); d 8.57 (bs, 1H, H-Ar), 7.43 (bs, 2H, H-Ar), 4.20 (bs, 2H, CH_2OC), 4.00 (bs, 2H, NCH_2), 3.71 (bs, 342H, PEG repeat unit), 2.23–1.84 (bs, 2H, CH_2), 1.65 (s, 9H, t-Boc), 1.44–1.28, 1.02–0.86 (bs, 2H, CH_2).

2.3.1.6 Synthesis of tryblock co-polymers

- *Synthesis of triblock co-polymer $mPEG_{2kDa}$-poly[GMA]-block-poly[ImHeMA] through pyridyl intermediate conjugate*

1) The diblock copolymer poly[GMA]-block-poly[ImHeMA] underwent aminolysis reaction in order to cleavage the RAFT agent from the polymer and obtain a free thiol group able to react with mPEG-SH_{2kDa} (192). 100 mg of block copolymer (6.48×10^{-3}

mmol) were solubilized in 500 µL of MeOH and the mixture was deoxygenated by N_2 bubbling for 20 minutes. 17.13 mg of 2-2'-dithiodipyridine (0.0778 mmol) and 5.30 µL of propylamine (1171.79 mM) were added under stirring to the polymer solution to obtain a final molar ratio of 2,2'-dithiodipyridine/propylamine/polymer of 12:10:1. The reaction was left under stirring overnight.

After solvent removal under reduced pressure, the polymer was firstly solubilized in 2 mL of water acidified at pH 3 adding 1M HCl. Then the pH was led to 12 adding 1 M NaOH to induce polymer fractionated precipitation. Diblock copolymer pirydil intermediate conjugate activation yield (%) was determined by ^{1}H NMR and determining the amount of thiopyridine conjugated through a colorimetric assay. In detail, 4.8 mg of polymer were solubilized in 750 µL of MeOH (0.415 mM) in presence of the reducing agent DL-dithiothreitol 0.1 M. The released 2-thiopyridine was quantified by spectrophotometric analysis at λ= 370 nm.

2) During the second step of the synthesis, the above activated diblock copolymer (76.6 mg) was solubilized in 1.7 mL of MeOH (4.96×10^{-3} mM). mPEG-SH_{2kDa} (36.98 mg, 0.0198 mM) and Et_3N (6.9 µL, 0.0496 mM) were added to the mixture to obtain the final molar ratio mPEG-SH $_{1.9kDa}$ /Et_3N/ poly[GMA]-block-p[ImHeMA]-thiopyridine of 4:10:1. The mixture was deoxygenated by N_2 bubbling for 20 minutes and was left reacting for 12 hours under stirring. The solvent was removed under reduced pressure and the crude product was solubilized in water acidified at pH 3 adding HCl 1M. Then the pH was led to 12 adding 1 M NaOH obtaining a colloidal opalescent suspension consisting in the partially soluble product mPEG$_{2kDa}$-block-poly[GMA]-block-poly[ImHeMA]. The unreacted mPEG-SH_{2kDa} was eliminated by 24 hours dialysis with *float a-lyzer*® membrane cut off 100 kDa against water pH 12. The triblock copolymer was obtained by lyophilization of the purified colloidal suspension and the yield of mPEG-SH_{2kDa} conjugation was determined by ^{1}H NMR amalysis.

- *Synthesis of triblock co-polymer mPEG$_{2\ kDa}$-block-poly[ImHeMA]$_{67}$-block-poly[GMA]$_{36}$*

Diblock co-polymer mPEG$_{2kDa}$-block-poly[ImHeMA]$_{67}$ macro-CTA (2.18 g, 0.11 mmol), GMA (1.13 g, 7.08 mmol) and AIBN (9.6 mg, 0.06 mmol) in DMAC (5 mL) were sealed

in a Schlenk tube, deoxygenated by argon bubbling for 30 minutes and then heated at 65 °C. The conversion of the polymer was calculated via ^{1}H NMR following the decrease of the integrals of the monomer vinyl signals (6.35 and 5.68 ppm) using the broad singlet (8.82 ppm) of the aromatic repeat unit protons of the imidazole ring as an internal standard. Polymerization was stopped at 50% conversion and the desired material obtained by precipitation in Et_2O–petroleum ether (1:1 v/v). The dithioester end-group was removed by reaction with AIBN (mPEG$_{2kDa}$-block-poly[ImHeMA]$_{67}$-block-poly[GMA]$_{36}$/AIBN = 1/20) at 80 °C in DMSO for 3 hours and the resulting polymer recovered by repeated precipitations in THF.

^{1}H NMR (400 MHz, D_2O): d 7.64 (bs, ^{1}H, H-Ar), 7.13 (bs, 1H, H-Ar), 6.88 (bs, 1H, H-Ar), 3.91 (bs, 2H, CH_2OC), 3.83 (bs, 2H, NCH_2), 3.66 (t, 2H, CH_2O), 3.50 (bs, 204H, PEG repeat unit), 3.35 (bs, 3H + 2H, CH_3 + CH_2), 1.63 (bs, 2H, CH_2), 1.48 (bs, 2H, CH_2), 1.29 (bs, 3H, CH_3), 1.19 (bs, 3H, CH_3).

- *Synthesis of triblock co-polymers t-Boc-NH-PEG$_{3.5kDa}$-block-poly[ImHeMA]$_{20}$-block-poly[GMA]$_{58}$.*

Block copolymer macroCTA t-boc-NH-PEG$_{3.5kDa}$-block-poly[ImHeMA]$_{20}$ (586 mg, 0.04 mmol), GMA (370 mg, 2.43 mmol) and AIBN (164 mg, 0.02 mmol) in DMAC (5 mL) were sealed in a Schlenk tube, deoxygenated by argon bubbling for 30 minutes and then heated at 65 °C. The conversion of the polymer was calculated via ^{1}H NMR following the decreasing of the integrals of the monomer vinyl signals (6.35 and 5.68 ppm) using the broad singlet (8.57 ppm) of the aromatic repeat unit protons of the imidazole ring as internal standard. Polymerization was stopped at 60% conversion. Polymers were obtained by precipitation in Et_2O–petroleum ether (1:1 v/v). The dithioester end-group of the block copolymer was removed by reaction with AIBN (molar ratio polymer (t-boc-NH-PEG$_{3.5kDa}$-block-poly[ImHeMA]$_{20}$-block-poly[GMA]$_{58}$/AIBN = 1/20) at 80°C in DMSO for 3 hours and the polymer was recovered by precipitation in THF.

^{1}H NMR (400 MHz, D2O): d 8.32 (bs, 1H, H-Ar), 7.37 (bs, 2H, H-Ar), 4.15 (bs, 4H, CH_2 + CH_2), 3.99 (bs, 4H, CH_2 + CH_2), 3.71(bs, 342H, PEG repeat unit), 2.30–1.93 (bs, 2H + 2H, CH_2 + CH_2), 1.70 (s, 9H, t-Boc), 1.20–0.83 (bs, 6H, CH_3 + CH_3).

- *Synthesis of folate-terminated triblock co-polymers α-Folate-NH-PEG$_{3.5\ kDa}$-block-poly[ImHeMA]$_{20}$-block-poly[GMA]$_{58}$.*

The conjugation of Folic Acid to the triblock co-polymer t-boc-$PEG_{3.5\ kDa}$-block-poly[ImHeMA]$_{20}$-block-poly[GMA]$_{58}$ was carried out following protocols reported elsewhere by three steps reaction (193, 194).

1) t-boc-$PEG_{3.5\ kDa}$-block-poly[ImHeMA]$_{20}$-block-poly[GMA]$_{58}$ (20 mg, 0.0011 mmol) was dissolved in a 1 : 1 (v/v) CF_3COOH–DCM mixture (1 mL/1 mL) at room temperature. The solution was stirred at room temperature for 2 hours and then TFA and DCM were removed by evaporation under reduced pressure. The reaction was monitored by ^1H NMR in MeOD by following the disappearance of the t-Boc protons at 1.44 ppm. The reaction yielded NH_2-$PEG_{3.5\ kDa}$-block-poly[ImHeMA]$_{20}$-block-poly[GMA]$_{58}$ ^1H NMR (400 MHz, MeOD): d 9.02 (bs, 1H, H-Ar), 7.70 (bs, 1H, H-Ar), 7.61 (bs, 1H, H-Ar), 4.48 (bs, 4H, CH_2 + CH_2), 4.29 (bs, 3H, CH_2 + CH), 3.91 (bs, 2H, CH_2), 3.64 (bs, 342H, PEG repeat unit), 1.94 (bs, 2H + 2H, CH_2 + CH_2), 1.42–0.93 (bs, 6H, CH_3 + CH_3).

2) folic acid (100.0 mg, 0.226 mmol) was dissolved in anhydrous DMSO (2 mL). NHS (26 mg, 0.23 mmol) and DCC (47 mg, 0.23 mmol) were added to the folic acid solution (folic acid/NHS/DCC 1:1:1 molar ratio). The reaction was carried out overnight at room temperature in the dark. N-Hydroxysuccinimidyl-ester-activated folic acid was precipitated by dropwise addition to 40 mL of cold Et_2O under stirring. The obtained yellow precipitate was washed with Et_2O (3 × 30 mL) and then dried under vacuum.

3) NH_2-$PEG_{3.5kDa}$-block-poly[ImHeMA]$_{20}$-block-poly[GMA]$_{58}$ was dissolved in anhydrous DMSO and N-hydroxysuccinimidyl-ester-activated folic acid (1.8 mg, 0.0034 mmol) was added to the polymer solution (1 : 4 polymer/activated folate molar ratio). The reaction was performed overnight under stirring at room temperature in the dark. The product was recovered by dropwise precipitation in Et_2O and dried after solvent removal. The resulting dried product was dissolved in 2 mL high purity water (resistivity > 18 M_Ω); the solution was acidified by 5 M HCl addition in order to precipitate the free folic acid (which is not soluble under acidic conditions). The polymer aquous solution was recovered by centrifugation (5 minutes, 14 000 rpm) and then dialyzed (MWCO 3500 Da) and water was removed by lyophilization.

Folate-$PEG_{3.5}$-block-poly$(ImHeMA)_{20}$-block-poly$[GMA]_{58}$ was characterized by spectrophotometric methods. The conjugate was dissolved in high purity water, then diluted to 0.5 mg/mL in 20 mM phosphate buffer, 150 mM NaCl, at pH 7.0 and the absorbance at 363 nm was measured to quantify the folate concentration in the modified polymer. The folate concentration was derived using the ε_M of folic acid reported in the literature (6197 $mol^{-1}cm^{-1}$) (195) The polymer solution was also diluted in water and tested by the iodine assay in order to determine the PEG concentration based on a calibration curve obtained with PEG (196). The quantification tests showed a conjugation yield of folic acid of 96% and thus a 1 : 1 folate/polymer molar ratio.

The presence of residual free folic acid in the synthesized conjugate was tested by reverse phase high-performance liquid chromatography (RP-HPLC). The system was equipped with a RP-C18 column eluted with 10 mM ammonium acetate buffer, pH 6.5 (eluent A) and acetonitrile (eluent B), in a gradient mode from 10 to 40% of eluent B in 40 minutes (197). The UV detector was set to 363 nm. Free folic acid was not detected in the chromatogram confirming the high degree of purity of the conjugate folate-$PEG_{3.5\ kDa}$-block-poly$[ImHeMA]_{20}$-block-poly$[GMA]_{58}$.

2.3.2 POLYMER TITRATION AND TURBIDIMETRY ASSAYS

2.3.2.1 Titration assay of poly$[GMA]_{30}$-block-poly[ImHeMA]

Apparent pKa values of poly$[GMA]_{30}$-block-poly[ImHeMA] (1) and (2) were determined from mid-points between titration start and equivalence points, using first derivatives of the titration curves to aid in measurement of equivalence points. Poly$[GMA]_{30}$-block-poly[ImHeMA] (1) and (2) were dissolved in deionized water (1 mg/ mL solution). The titration was performed by adding 10 μL aliquots of 0.1 M NaOH under stirring, starting from pH ~3 until pH ~11. The back titration was started from the pH value reached at the end of the titration by adding 10 μL aliquots of 0.1 M HCl until pH 3 was achieved. Variations of pH were registered after each addition.

2.3.2.2 Turbidimetry assay of poly$[GMA]_{30}$-block-poly[ImHeMA]

To a highly dilute polymer solutions 10 μL aliquots 0.1 M NaOH were added and the intensity of light scattered by the dispersed particles of aggregated polymer was plotted as function of the amount of precipitan. Scattered light was measured by Uv-Vis spectroscopy. Poly$[GMA]_{30}$-block-poly[ImHeMA] (1) and (2) (1 mg/mL) was dissolved

in 150 mM aquous NaCl. The value of turbidity (%T) registered at 500 nm was found to be 100% at pH 3, then, the NaOH was added until ~pH 10, registering the % T at each addition.

2.3.2.3 Titration assay of $mPEG_{1.9kDa}$-block-poly[ImHeMA]$_{67}$-block-poly[GMA]$_{36}$

Polymer $mPEG_{1.9\ kDa}$-block-poly[ImHeMA]$_{67}$-block-poly[GMA]$_{36}$ (20 mg) was dissolved in 150 mM aquous NaCl (1 mg/mL). Potentiometric titration was carried out by adding 10 μL aliquots of 0.1 M NaOH under stirring over a pH range of 3-10. The back titration was started from the pH value reached at the end of the titration by adding 10 μL aliquots of 0.1 M HCl until pH 3 was achieved. Variations of pH were recorded after each addition.

2.3.2.4 Turbidimetry assay of $mPEG_{1.9\ kDa}$-block-poly[ImHeMA]$_{68}$ and $mPEG_{1.9\ kDa}$-block-poly[ImHeMA]$_{67}$-block-poly[GMA]$_{36}$

$mPEG_{1.9kDa}$-block-poly[ImHeMA]$_{68}$ and $mPEG_{1.9kDa}$-block-poly[ImHeMA]$_{67}$-block-poly[GMA]$_{36}$ (1 mg/mL) were dissolved in 150 mM aqueous NaCl. The value of turbidity (T, %) was registered at 500 nm and was found to be 100% at pH 3. Transmittance was recorded after each addition of 10 μL aliquots of 0.1 M NaOH.

2.3.3 POLYMERSOME ASSEMBLY

Polymersomes formulations were prepared using: a) $PEG_{1.9kDa}$-block-poly[ImHeMA]$_{67}$-block-poly[GMA]$_{36}$; b) different $PEG_{1.9kDa}$-block-poly[ImHeMA]$_{67}$-block-poly[GMA]$_{36}$/ $PEG_{3.5kDa}$-block-poly[ImHeMA]$_{20}$-block-poly[GMA]$_{58}$ mixtures [99:1, 95:5, 90:10 w/w%]; c) 90:5:5 w/w % $PEG_{1.9kDa}$-boly-poly[ImHeMA]$_{67}$-block-poly[GMA]$_{36}$/$PEG_{3.5kDa}$-block-poly[ImHeMA]$_{20}$-boly-poly[GMA]$_{58}$ / Folate-$PEG_{3.5kDa}$-block-poly(ImHeMA)$_{20}$-block-poly[GMA]$_{58}$ mixture following a protocol adapted from prior literature (166, 198).

Polymer solutions (1 mg/mL) were prepared in 20 mM phosphate buffer, 150 mM NaCl, at pH 5 and the pH was increased to 6.5 and pH 7.4 by addition of suitable aliquots of 0.1 M NaOH solution. The slow increase of the pH induced the self-assembly into polymersomes.

The resulting colloidal dispersions were analyzed by DLS at 25°C to determine the mean size ± standard deviation (SD). ζ-potential measurements were performed after diluting samples 10-fold in high purity mQ water.

2.3.4. KINETIC STABILITY STUDIES

Polymersomes formulations obtained with $mPEG_{1.9kDa}$-block-poly[ImHeMA]$_{67}$-block-poly[GMA]$_{36}$/ t-boc-$PEG_{3.5kDa}$-block-poly[ImHeMA]$_{20}$-b-p[GMA]$_{58}$ mixtures [99:1, 95:5, 90:10 w/w%] (1 mg/mL) generated in 20 mM phosphate, 150 mM NaCl, at pH 5, 6.5 and 7.4 were tested for stability over time by Dynamic Light Scattering (DLS) at scheduled intervals up to 5 hours at 37°C.

Polymersome formulations obtained with 90:10 w/w% of $mPEG_{1900}$-block-poly[ImHeMA]-block-poly[GMA]/ Folate-$PEG_{3.5kDa}$-block-poly[ImHeMA]$_{20}$-block-poly[GMA]$_{58}$, 90:5:5 w/w% of $mPEG_{1.9kDa}$-block-poly[ImHeMA]-block-poly[GMA]/ t-boc-$PEG_{3.5kDa}$-block-poly[ImHeMA]$_{20}$-block-poly[GMA]$_{58}$ / Folate-$PEG_{3.5kDa}$-block-poly [ImHeMA]$_{20}$-block-poly[GMA]$_{58}$ and 90:10 w/w% of $mPEG_{1.9kDa}$-block-poly[ImHeMA]-block-poly[GMA]/ t-boc-$PEG_{3.5kDa}$-block-poly[ImHeMA]$_{20}$-block-poly[GMA]$_{58}$ (1 mg/mL) generated in 20 mM phosphate, 150 mM NaCl, pH 7.4, were incubated at 37 °C and analyzed by dynamic light-scattering (DLS) at scheduled time intervals. The choice of using the 90:5:5 w/w% ratio of $mPEG_{1.9kDa}$-block-poly[ImHeMA]-block-poly[GMA]/ t-boc-$PEG_{3.5kDa}$-block-poly[ImHeMA]$_{20}$-block-poly[GMA]$_{58}$ / Folate-$PEG_{3.5kDa}$-block-poly [ImHeMA]$_{20}$-block-poly[GMA]$_{58}$ was determined by the preliminary stability study performed with dsDNA loaded polymersomes.

The 90:10 w/w% $mPEG_{1.9kDa}$-block-poly[ImHeMA]-block-poly[GMA]/ t-boc-$PEG_{3.5kDa}$-block-poly[ImHeMA]$_{20}$-block-poly[GMA]$_{58}$ and 90:5:5 w/w % $mPEG_{1.9kDa}$-block-poly[ImHeMA]-block-poly[GMA] / t-boc-$PEG_{3.5kDa}$-block-poly[ImHeMA]$_{20}$-block-poly[GMA]$_{58}$/Folate-$PEG_{3.5kDa}$-block-poly(ImHeMA)$_{20}$-block-poly[GMA]$_{58}$ formulations (1 mg/mL) were incubated in 20 mM phosphate, 150 mM NaCl, pH 7.4, in the presence of 10% v/v of fetal bovine serum for 8 hours at 37 ºC. At scheduled times, the samples were analyzed by DLS.

2.3.5 BLOCK CO-POLYMER pH RESPONSE

$mPEG_{1.9kDa}$-block-poly[ImHeMA]$_{67}$-block-poly[GMA]$_{36}$ and t-boc-NH-$PEG_{3.5kDa}$-block-poly[ImHeMA]$_{20}$-block-poly[GMA]$_{58}$ solutions (1 mg/mL) were prepared in D_2O, 150 mM NaCl. The pH was set by adding aliquots (5 μL) of NaOD (100 mM in D_2O). Analysis was carried out by ^{1}H-NMR (400 MHz or 500 MHz), 1024 or 256 scans for each sample submitted.

pH responsiveness of polymersomes prepared according the pH-switching method described above with $mPEG_{1.9kDa}$-block-poly[ImHeMA]$_{67}$-block-poly[GMA]$_{36}$ was evaluated also through DLS analysis. Polymersomes were prepared in phosphate saline buffer 20 mM NaCl 150 mM pH 7.4 and the formulation was splitted in three parts. The pH of the three formulations was corrected to reach the values of 7.4, 6.5 and 5. The size and polydisperity index (PDI) of vesicles was collected up to 96 hours at scheduled times.

2.3.6 POLYMER CRITICAL AGGREGATION CONCENTRATION (CAC)

The CAC of $mPEG_{1.9kDa}$-block-poly[ImHeMA]$_{67}$-block-poly[GMA]$_{36}$ was determined using pyrene as a fluorescent probe. The polymer vesicle dispersion was prepared as with the method described above in 20 mM phosphate, 150 mM NaCl, pH 7.4 was diluted with the same buffer yielding different polymer concentrations ranging from 0.2 to 100 μg/mL. Pyrene (5 μL) dissolved in acetone (0.18 mM) was added to 0.75 mL of the polymer dispersions. The samples were incubated overnight at room temperature in the dark to allow equilibration. Prior to the measurements, the dispersions were incubated at 37 °C for 15 minutes. The excitation spectra of pyrene were recorded at 37 °C from 300 to 360 nm with the emission wavelength set at 390 nm. The excitation and emission band slits were 4 and 2 nm, respectively. The intensity ratio of I_{338}/I_{333} was plotted *versus* the logarithmic concentration of the polymer to determine the CAC.

2.3.7 POLYMERSOMES LABELLING WITH FLUORESCENT PROBES

Polymersomes were loaded with 5(6)carboxyfluorescein (hydrophilic probe) and N-(fluorescein-5-thiocarbamoyl)-1,2-dihexadecanoyl-snglycero-3-phospho-ethanol-amine triethyl-ammonium salt (fluorescein-DHPE) used as hydrophilic and hydrophobic probes, respectivelly. A mixture of 90:10 w/w% $mPEG_{1.9kDa}$-block-poly[ImHeMA]$_{67}$-block-poly[GMA]$_{36}$ / t-boc-$PEG_{3.5kDa}$-block-poly[ImHeMA]$_{20}$-block-poly[GMA]$_{58}$ was

prepared at 1 mg/mL in 20 mM phosphate, 150 mM NaCl, pH 5 and 1 mL solution was added of 0.1 mg of 5(6)carboxyfluorescein or 2 μL of 5 mg/mL fluorescein-DHPE in chloroform. The pH of the solutions was increased to 7.4 by stepwise addition of 0.1 M NaOH to induce the polymersome assembly and excess 5(6)carboxyfluorescein and fluorescein-DHPE were removed by dialysis against 20 mM phosphate,150 mM NaCl, pH 7.4, for 24 hours using a regenerated cellulose dialysis membrane with 3500 Da MW Cut-Off. The dialysis method was validated by treating the 5(6)-carboxyfluorescein or fluorescein-DHPE in polymer-free solutions at the same concentration used for the loading procedure. The validation test showed that after 24 hours, complete release of the fluorescent probes occurred. After dialysis, the polymer formulations were analysed with a spectrofluorimeter (λ_{ex} 490 nm and λ_{em} 520 nm) and 5(6)carboxyfluorescein and fluorescein-DHPE were quantified referring to a standard calibration curve. The results of the analysis were reported in terms of Loading Capacity mol% (LC% = moles of loaded fluorophore / moles of polymer %) and Encapsulation Efficiency wt% (EC%= loaded fluorophore /initial fluorophore concentration).

2.3.8 ELECTROPHORETIC MOBILITY SHIFT ASSAY

dsDNA sequence used for the loadind studies (Section 3.1.2.14) was used to study the retardation induced by association with the triblock copolymers on a gel electrophoretic setting. The study was performed with mPEG$_{1.9kDa}$-block-poly[ImHeMA]$_{67}$-block-poly[GMA]$_{36}$ at pH 5 in 0.08 M citrate buffer and in 20 mM phosphate, 150 mM NaCl, pH 7.4. Polyacrylamide gel was prepared at 12% w/v concentration of acrylamide monomer, according to the following recipy: 3 mL of 30% w/v Acrylamide/Bis-acrylamide in water solution, 1.5 mL 0,08 M citrate buffer pH 5, 54 μL of ammonium persulfate 10% w/v in water, 5 μL of N,N,N′,N′-Tetramethylethylenediamine (TEMED, 0.775 g/mL) and 3 mL of deionized water. All the reagents were mixed in the water volume under magnetic stirring. 3 μL of a solution containing 2.9×10^{-10} mol of dsDNA were mixed to 7 microliters of a mPEG$_{1.9kDa}$-block-poly[ImHeMA]$_{67}$-block-poly[GMA]$_{36}$ solution at increasing concentration in order to prepare the mixtures at different N/P ratios (0.1:1, 0.5:1, 1:1, 2:1, 3:1, 5:1, 20:1). The N/P ratio was calculated assuming the mPEG$_{1.9ka}$-block-poly[ImHeMA]$_{67}$-block-poly[GMA]$_{36}$ nitrogen content to be 5.26×10^{-5}

Mols/mg. The samples prepared at different N/P ratio were loaded into the wells of the polyacrylamide gel.

The first well was loaded with 6 microliters of a low range DNA-Ladder dissolved in 10 mM Tris-HCl pH 7.6, 1 mM EDTA, concentration 0.5 mg DNA/ml and composed of 11 chromatography-purified individual DNA fragments (from 10 to 300 base pairs). The second well was loaded with 3 microliters of the above dsDNA solution and a third one with 7 microliters of the polymer at the same concentration used to generate the different N/P ratios. All the volumes inside the wells were adjusted to the total volume of 10 μL with the 0,08 M citrate buffer pH 5 used to prepare and run the gel. To all the wells, 5 μL of gel loading buffer, containing bromophenol blue, xylene cyanol FF and glycerol in water, were added. The gel was run at 100 mV for 1 hour. After the gel was run, it was dipped in a staining medium containing the DNA intercalating agent Gel Red® 10000X diluted 3300 fold to make a 3X staining solution in H_2O for 1 hour. The gel was imaged with the UV-Transilluminator. The same gel electrophoresis assay was performed at neutral conditions using 45 mM Tris-borate/1 mM EDTA buffer pH 7.4.

2.3.9 DNA LOADING STUDIES

A dsDNA, 19-bp oligonucleotide, sequence was used as a model to simulate ds-siRNA. The sequences chosen for the experiment were GAGATGTAAGGCCAGGCCG and its complementary strand. When hybridized, the dsDNA had a total molecular weight of 11.5 kDa. dsDNA was loaded into polymer dispersions at different N/P feed ratios, where N is the number of imidazole groups of the triblock copolymer and P is the number of phosphate groups of DNA. N/P feed ratios of 10:1 and 1:1 were investigated. To a solution of 90:10 w/w% of $mPEG_{1.9kDa}$-block-poly[ImHeMA]$_{67}$-block-poly[GMA]$_{36}$ / t-boc-$PEG_{3.5kDa}$-block-poly[ImHeMA]$_{20}$-block-poly[GMA]$_{58}$ mixture (1 mg/mL) in 20 mM phosphate, 150 mM NaCl pH 27 or 265 μL of dsDNA solution (100 μM in 10 mM TRIS HCl, 50 mM NaCl, 1 mM EDTA, pH 7.8) were added to achieve 10:1 N/P and 1:1 N/P feed ratio, respectively. The polymer was induced to self-assemble by increasing the pH to 7.4. The assembly into colloidal nanostructures was confirmed by DLS as reported above. Non encapsulated dsDNA was removed from polymersome assemblies using a Float-A-lyzer® system equipped with a 100 kDa MW cut-off membrane. The dialysis of dsDNA-loaded polymersomes was performed for 24 hours against 20 mM phosphate, 150

mM NaCl, pH 7.4. The purification method was validated by introducing in the device free dsDNA or empty polymersomes at the same concentration used for the loading test. dsDNA was completely removed by dialysis in 24 hours while the polymer was totally retained.

z-potential of polymersome formulations loaded with dsDNA diluted 10 times in high purity mQ water was determined.

dsDNA loading quantification within the polymer assemblies was performed by UV-vis spectroscopy. The dsDNA loading polymersome dispersion was diluted 1:5 in 20 mM phosphate, 0.15 M NaCl at pH 7.5, the pH was decreased to 5 by 1 M HCl addition in order to disassemble the polymers and eliminate the contribution of larger particle scattering and the solutions underwent UV-Vis spectroscopic analysis at 263 nm.

2.3.10 DNA RELEASE STUDIES

DNA release studies were performed in 20 mM phosphate, 150 mM NaCl at pH 7.4 and 5.0. Two (1 mg/mL) dsDNA-loaded 90:10 w/w % $mPEG_{1.9kDa}$-block-poly[ImHeMA]$_{67}$-block-poly[GMA]$_{36}$ / t-boc-$PEG_{3.5kDa}$-block-poly[ImHeMA]$_{20}$-block-poly[GMA]$_{58}$ based formulation samples in PBS pH 7.4 were prepared with a 1:1 N/P feed ratio. 1 mL of the first sample was transferred in a Float-A-lyzer® 100 kDa MW Cut-Off and dialyzed against 20 mM phosphate, 150 mM NaCl at pH 7.4. One mL of the second sample was acidified to pH 5 with 0.1 N HCl and dialyzed against in a Float-A-lyzer® 100 kDa MW Cut-Off 20 mM phosphate, 150 mM NaCl at pH 5. The release study was performed at 37 °C. At scheduled times 100 microliters of each sample were withdrawn, adequately diluted with 20 mM phosphate, 150 mM NaCl pH 5 and spectrophotometrically monitored at 263 nm for DNA concentration. The variation of concentration was plotted versus time.

2.3.11 siRNA LOADING STUDIES

Because of ds-siRNA sensitivity to degradation by RNAses, all the buffers employed for the procedure were autoclaved before use to degrade RNAses traces and polymer solutions were filtered using 0.22 μm filters before polymersomes assembling.

Polymeric vesicles were loaded with ds-siRNA luciferase GL3 duplex with a specific sequence for the inhibition of the intracellular luciferase synthesis. To a solution of a 90:10 w/w % $mPEG_{1.9kDa}$-block-poly[ImHeMA]$_{67}$-block-poly[GMA]$_{36}$ / t-boc-$PEG_{3.5kDa}$-

block-poly[ImHeMA]$_{20}$-block-poly[GMA]$_{58}$ mixture (1 mg/mL in 20 mM phosphate, 150 mM NaCl, pH 5) 70 μL of ds-siRNA 100 μM in 60 mM KCl, 0.2 mM $MgCl_2$, 6 mM HEPES-pH 7.5 were added. The co-polymer was induced to self-assemble by increasing the mixture pH to 7.4. The generation of colloidal nanostructures was confirmed by DLS analysis. Non-encapsulated ds-siRNA was removed from polymeric assemblies using a Float-A-lyzer® system equipped with a 100 kDa MW cut-off membrane. The dialysis of ds-siRNA loaded polymersomes was performed for 24 hours using 20 mM phosphate, 150 mM NaCl, pH 7.4 as releasing buffer.

The intercalating reagent Quant-iT™ RiboGreen® was used to quantify the ds-siRNA encapsulation yield in polymersomes. The assay was performed on a black 96 wells plate transferring 170 μL of the ds-siRNA loaded polymersome suspensions per well at the two different concentrations of 1 mg/mL and 0.5 mg/mL in PBS pH 7.4. 10 μL of 0.5 M HCl were added to the polymer suspensions in the wells followed by 10 μL of the intercalating reagent solution. Three minutes after the acidification, the pH was increased to 7.4 with 10 μL of 0.5 M NaOH to allow for intercalation. The samples underwent fluorescence analysis (λ_{ex} 485 nm/ λ_{em} 530 nm) that was performed using the microplate reader. The ds-siRNA concentration was derived by substracting the emission intensity of the polymer contribution associated to ds-siRNA free polymersomes from the emission intensity associated to the ds-siRNA loaded polymersomes. A calibration curve with known dilutions of siRNA and same samples treatment was prepared in RNAses free 10 mM Tris-HCl, 1 mM EDTA, pH 7.5.

2.3.12 TRANSMISSION ELECTRON MICROSCOPY (TEM)

dsDNA-free and dsDNA-loaded 90:10 w/w % mPEG$_{1.9kDa}$-block-poly[ImHeMA]$_{67}$-block-poly[GMA]$_{36}$ / t-boc-PEG$_{3.5kDa}$-block-poly[ImHeMA]$_{20}$-block-poly[GMA]$_{58}$ polymersomes were prepared according to the previously described protocol with final polymer concentrations of 2 mg/mL in 20 mM phosphate, 150 mM NaCl, pH 7.4 and analyzed by TEM. Samples were observed in negative staining mode, using small copper grid (400 mesh), covered by a "holey film" carbon layer. Samples were deposited on the grids and the contrast staining was performed with a uranyl acetate solution 1% w/v.

2.3.13 CELL CULTURE

KB cells (human cervical carcinoma) were grown at 37 °C, in 5% CO_2 atmosphere, using folic acid free DMEM medium supplemented with 15% FBS, 2 mM L-glutamine, 100 IU/mL penicillin, 100 μg/mL streptomycin and 0.25 μg/mL of amphotericin B (Sigma-Aldrich). MCF7 (human breast adenocarcinoma) were grown at 37 °C, in 5% CO_2 atmosphere, using RPMI-1640 medium supplemented with 10% FBS, 100 IU/mL penicillin, 100 μg/mL streptomycin and 0.25 μg/mL of amphotericin B. B16-F10-luc-G5 from mouse melanoma were grown at 37 °C, in 5% CO_2 atmosphere, using DMEM medium supplemented with 10% FBS, 2 mM L-glutamine, 100 IU/mL penicillin, 100 μg/mL streptomycin. These cells were transfected with the North American Firefly Luciferase gene whose expression is under the control of SV40 promoter.

2.3.14 FOLATE RECEPTOR EXPRESSION IN KB AND MCF7 CELL LINE

KB and MCF7 cells were seeded in 25 cm^2 cell colture flasks at a density of 5×10^5 cells/well and grown for two days at 37°C and 5% CO_2. Medium was then removed, cells washed with PBS and detached from the flasks by scraping. Cells were pipetted and tranferred in tubes for cytometric analysis and centrifuged at 1000 rpm for 3 minutes. The supernatant was removed leaving a cell pellet in a minimal volume (100 μL) of PBS. Two μl of primary antibody for folate receptor detection in PBS (1 mg/mL, 804-439-R100 - Folate receptor alpha, monoclonal Antibody from mouse) were added to cell samples and incubated at room temperature for 5 minutes. Then, 2 μL of secondary antibody in PBS (1 mg/mL, Alexa fluor 488 labeled α-mouse monoclonal antibody) were added to cell samples and incubated at room temperature in the dark for 5 minutes. After incubation, samples were centrifuged at 1000 rpm for 5 minutes and repeatedly washed with PBS to remove the secondary antibody excess and resuspended in 300 μL of PBS buffer. Untreated cells were also prepared while the controls were prepared by treating the cells with the secondary antibody only. Samples were analyzed by flow cytometry using λ_{ex} and λ_{em} of 499/519 nm respectively.

2.3.15 $mPEG_{1.9KDA}$-BLOCK-POLY[IMHEMA]$_{67}$-BLOCK-POLY[GMA]$_{36}$ AND FOLATE-$PEG_{3.5KDA}$-BLOCK-POLY[IMHEMA]$_{20}$-BLOCK-POLY[GMA]$_{58}$ BIOCOMPATIBILITY STUDY

The effects of $mPEG_{1.9kDa}$-block-poly[ImHeMA]$_{67}$-boly-poly[GMA]$_{36}$ and Folate-$PEG_{3.5kDa}$-block-poly[ImHeMA]$_{20}$-block-poly[GMA]$_{58}$ were evaluated by MTS (3-(4,5-dimethylthiazol-2-yl)- 5- (3- carboxymethoxyphenyl)-2-(4-sulfophenyl)-2H-tetrazolium, inner salt) cell viability test using B16-F10-luc-G5 cells. Cell viability was detected after 24 and 48 hours. Cells were seeded in 96-wells plate at density of 10000 cell/well and treated with increasing concentrations [1, 2 and 3 mg/mL] of the two triblock co-polymers. After the established incubation times, 10 µL of a mixture 20:1 3-(4,5-dimethylthiazol-2-yl)-5-(3-carboxymethoxyphenyl)-2-(4-sulfo-phenyl)-2H-tetrazolium/ Phenazine methosulfate (MTS/PMS; 2 mg/mL MTS, 0.92 mg/mL PMS) were added to each well and the plate incubated for 2 hours at 37°C. Then, the medium was removed and DMSO was added to each well and the plate was shaken for 4 hours. The absorbance was measured at 492 nm by microplate reader. The cytotoxicity was expressed as the percentage of cell viability refers to untreated cells.

2.3.16 POLYMER HEMOLYTIC ACTIVITY

Heparinized blood from mices was diluted with PBS at pH 7.4 to 2% w/v hematocrit in a 15 mL tube. The tube was gently shaken and centrifuged at 3000 rpm for 10 minutes at 4°C for three times, removing the supernatant after each centrifugation. The pellet was used to prepare 3 red blood cell (RBCs) suspensions in three phosphate saline buffers at pH 7.4, 6.5, 5.5. $mPEG_{1.9kDa}$-block-poly[ImHeMA]$_{67}$-block-poly[GMA]$_{36}$ was dissolved in PBS at pH 7.4, 6.5, 5.5 at concentrations 0.5, 1, 2, 3 mg/mL and 100 µL of each dilution were transferred in a 96 multiwell plate. 80 kDa Dextran was used as negative control, whereas polyethylenimine (PEI) was used as positive control. 1% w/v Triton X-100 was employed as reference for 100% hemolysis. 100 µl of the RBCs dilutions at one of the three different pH values were added to each sample prepared in the well with the corresponding pH and the plate was incubated at 37°C for 1 hour. Afterwards, the plate was centrifuged at 3000 rpm for 10 minutes at room temperature and the supernatant of each well was transferred in a second plate. The absorbance at 570 nm was measure with

a microplate reader and the absorbance was correlated to the hemolitic properties of the polymer at different pH conditions.

2.3.17 CELLULAR UPTAKE STUDIES

2.3.17.1 Fluorescence spectroscopy on cell lisates

KB and MCF7 cells were seeded in a 12 well plate at a density of 5×10^5 cells per well. dsDNA–cyanine 3 loaded polymer assemblies obtained with 90 : 5 : 5 w/w of polymers $mPEG_{1.9kDa}$-block-poly[ImHeMA]-block-poly[GMA] / t-boc-$PEG_{3.5kDa}$-block-$poly[ImHeMA]_{20}$-block-$poly[GMA]_{58}$/Folate-$PEG_{3.5kDa}$-block-$poly(ImHeMA)_{20}$-block-$poly[GMA]_{58}$ and control 90 : 10 w/w of polymers $mPEG_{1.9kDa}$-block-$poly[ImHeMA]_{67}$-block-$poly[GMA]_{36}$ / t-boc-$PEG_{3.5kDa}$-block-$poly[ImHeMA]_{20}$-block-$poly[GMA]_{58}$ (500 mL of 1 mg/mL) were added to the cells in the wells, and incubated at 37°C for 2 hours in the dark to prevent photo-bleaching of labelled DNA. A control solution containing PBS (500 mL, 20 mM phosphate, 150 mM NaCl, pH 7.4) was also added to specific wells. After incubation, polymer dispersions were discharged and wells were washed with PBS. Cells were detached by treatment with 1% (w/v) trypsin in PBS. Cell suspensions from each well were transferred in microtubes and recovered by centrifugation at 1000 rpm for 5 minutes. The pellets were treated with 6 mL of 0.1% v/v Triton X-100 and lysates were analysed by fluorimetry (λ_{ex} 550, λ_{em} 570).

2.3.17.2 FACS analysis

The study was performed at the University of Padova using KB and MCF7 cells only for an incubation time of 30 minutes at 37°C. The same study was performed at Centro de Investigacion Principe Felipe of Valencia on B16-F10-luc-G5 cells evaluating the internalization of the folate targeted vesicles over time up to 5 hours both at 3°C and 4°C. Cells were seeded in a 6 well plate at a density of 28×10^4 cells/well. The medium was then removed, cells were washed twice with PBS and 1 mL of a 1 mg/mL of dsDNA-cyanine loaded polymer assemblies obtained with 90:5:5 w/w% of $mPEG_{1.9kDa}$-block-$poly[ImHeMA]_{67}$-block-$poly[GMA]_{36}$ / t-boc-$PEG_{3.5kDa}$-block-$poly[ImHeMA]_{20}$-block-$poly[GMA]_{58}$/Folate-$PEG_{3.5kDa}$-block-$poly(ImHeMA)_{20}$-block-$poly[GMA]_{58}$ and 90 : 10 w/w of polymers $mPEG_{1.9kDa}$-block-$poly[ImHeMA]_{67}$-block-$poly[GMA]_{36}$ / t-boc-$PEG_{3.5kDa}$-block-$poly[ImHeMA]_{20}$-block-$poly[GMA]_{58}$ was added to the wells. Cells were incubated at 37 °C and 4°C. At incubation times of 0, 15 minutes, 30 minutes, 2 hours

and 5 hours wells were washed with PBS and cells collected in cytometer tubes scraping on ice. After incubation, the polymer dispersions were discharged and wells washed with PBS. To detach cells from the wells, 300 µL of 1% v/v trypsin were added and cells were incubated 4 minutes at 37°C. One mL of PBS containing $CaCl_2$ and $MgCl_2$ was added to each well and cells were recovered, centrifuged at 1000 rpm for 5 minutes. The cellular pellet was resuspended, washed twice with PBS and centrifuged eliminating the supernatant. Samples were recovered in 300 µL of 1% w/v freshly prepared paraformaldehyde in PBS and analyzed by flow cytometry (λ_{ex} 550, λ_{em} 570).

2.3.18 CONFOCAL MICROSCOPY

Glass BD Falcon™ chamber slides were pretreated with a poly-D-lysine hydrobromide solution (0.2 mg/mL) in strile water to increase cell attachment. The poly-D-lysine solution was sterilized with a 0.22 µm filter and added to each well. Chamber slides were incubated for 1 hour at room temperature in the safety cabinet and afterwards the poly-D-lysine solution was removed. Wells were rinsed three times with PBS and KB and MCF7 cells were seeded at a density of 10×10^4 cells/well and grown for 24 hours at 37°C and 5% CO_2. The medium was then removed, cells were washed with PBS and 500 µL of Cyanine 3 labeled ds DNA loaded polymersomes were prepared with 90:5:5 w/w% of $mPEG_{1.9kDa}$-block-poly[ImHeMA]$_{67}$-block-poly[GMA]$_{36}$ / t-boc-$PEG_{3.5kDa}$-block-poly [ImHeMA]$_{20}$-block-poly[GMA]$_{58}$ / Folate-$PEG_{3.5kDa}$-block-poly(ImHeMA)$_{20}$-block-poly [GMA]$_{58}$ and 90 : 10 w/w of polymers $mPEG_{1.9kDa}$-block-poly[ImHeMA]$_{67}$-block-poly[GMA]$_{36}$ / t-boc-$PEG_{3.5kDa}$-block-poly[ImHeMA]$_{20}$-block-poly[GMA]$_{58}$ polymer mixture (non targeted polymersomes) in PBS pH 7.4 as described previously were added to each well and incubated at 37°C in the dark for 30 minutes. Polymersome suspension was the removed and wells were gently washed three times with PBS. Cells were fixed with 500 µL of freshly prepared 1% w/v paraformaldehyde for 20 minutes at 4°C, washed with PBS and incubated with 200 µL of 5 µg/mL fluorescein-DHPE in PBS for 10 minutes in the dark. Cells were washed three times with PBS, chamber slides were disassembled and 20 µL of Vectashield® mounting medium containing DAPI for nuclei staining were added to each slide. Finally, slides were covered with coverslips. Samples were analyzed by confocal microscopy using an immersion lens. Lasers with an emission

wavelength at 405, 488 e 561 nm were used to detect DAPI, fluorescein-DHPE and cyanine-3 labeled DNA.

2.3.19 SILENCING STUDIES

B16F10 cells from mouse melanoma, transfected with luciferase and over expressing folate receptor (199, 200) were seeded in a 96 well plate at a density of 10×10^4 cells/well. ds-siRNA-loaded polymer assemblies obtained with 90:5:5 w/w% of $mPEG_{1.9kDA}$-block-poly[ImHeMA]$_{67}$-block-poly[GMA]$_{36}$ / t-boc-$PEG_{3.5kDa}$-block-poly[ImHeMA]$_{20}$-block-poly[GMA]$_{58}$ / Folate-$PEG_{3.5kDa}$-block-poly(ImHeMA)$_{20}$-block-poly[GMA]$_{58}$ and control 90:10 w/w % $mPEG_{1.9kDa}$-block-poly[ImHeMA]$_{67}$-block-poly[GMA]$_{36}$ / t-boc-$PEG_{3.5kDa}$-block-poly[ImHeMA]$_{20}$-block-poly[GMA]$_{58}$ (100 μL of 1 mg/mL) in PBS pH 7.4 were added to the wells, and incubated at 37 °C for 30 minutes. Cells were also treated with ds-siRNA free targeted polymersomes, targeted polymersomes loaded with a scrambled ds-siRNA sequence, free luciferace silencing ds-siRNA and free scrambled ds-siRNA as controls. After incubation, polymer dispersions were discharged and replaced with DMEM medium supplemented with 10% FBS. Cells were grown for 24 and 48 hours. Afterwards, 16 μL of the luciferin (150 μg/mL) in PBS was added to each well and the Luciferase activity was spectrofotometrically quantified using a microplate reader at λ_{em} 535 nm.

3. RESULTS AND DISCUSSION

3.1 SYNTHESIS OF MONOMERS, INTERMEDIATES AND BLOCK CO-POLYMERS

3.1.1 SYNTHESIS OF GLYCEROL METHACRYLATE MONOMER (GMA)

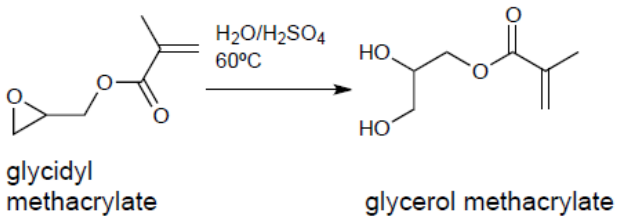

Scheme 3.1. Reaction of the glycidyl methacrylate in acidic water, at 60° C to yield the glycerol methacrylate.

The synthesis of GMA monomer was carried out using protocol already reported (201, 202) in the literature for the hydrolysis of epoxides. Hydrolysis of epoxides is one of the most exploited methods for synthesizing vicinal diols. The reaction can be performed under mild conditions by using solid or solid-supported Lewis acids, one-electrontransfer reagents and a variety of recently discovered reagents (202).

Glycidyl methacrylate was left to react in water at 60 ºC in the presence of aqueous H_2SO_4 (0.5 equiv.) to yield the expected product. ^{1}H-NMR, ^{13}C-NMR and mass spectroscopy analysis confirmed the GMA structure. Hot water and high-diluted H_2SO_4 were used as nucleofilic-acid catalysts and solvents and were efficient in promoting the ring opening of the epoxide to yield the diol.

3.1.2 SYNTHESIS OF IMIDAZOLIC MONOMER

The preparation of the pH-sensitive block co-polymers involved the synthesis of polymers featuring a pKa in the 6-7 ranges. The polymers were generated with a central block bearing pendant imidazolic groups. Here, the synthesis of 6-(1H-imidazol-1-yl) hexyl-methacrylate hydrochloride monomers is discussed. These monomers were chosen because of their aromatic amine functionality with a pKa in the range of interest for intratumoural and endosomal protonation. In fact, the imidazole is an analogous to

histidine (pKa 6.5) (190). The imidazole side chain of this amino acid exhibits a non charged, neutral status in physiologic environment at pH 7.4 (namely the blood) thus relatively small shifts in pH may change its ionization status with the protonation of the aromatic ring that can occure in the slightly acid tumor interstitium or in net acid environment of the intracellular endosomes and lysosomes. Hence, the idea to synthesize block co-polymers from histidine-alike monomers to prepare polymersomes that are designed to release nucleic acids/drugs at acidic pH into tumors.

The synthesis of the ImHeMA was performed according to a three step protocol.

Step 1:

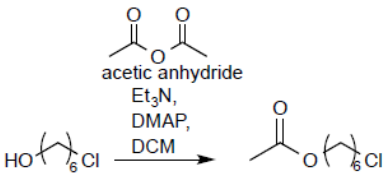

6-chlorohexyl-acetate

Scheme 3.2. Reaction of the 6-chloro-1-hexanol with the acetic anhydride to give the 6-chlorohexyl acetate.

The first intermediate synthesised was 6-chlorohexyl acetate, following an adaption of reported methods (203). Commercially available, 6-chloro-1-hexanol and acetic anhydride were reacted in DCM in the presence of DMAP, that was employed as nucleophilic catalyst, and Et_3N to yield the acetylated product. The reaction was carried out for 30 minutes at 0ºC, then for an hour at room temperature. An extraction with Et_2O and water was performed to remove the water-soluble Et_3NH^+ $^-O\text{-}COCH_3$ salt and the DMAP catalyst. The solvent was changed from DCM to Et_2O for the low solubility of Et_3NH^+ $^-O\text{-}COCH_3$ salt in Et_2O, which facilitated the extraction process. Evaporation of the organic phase under reduced pressure gave the product that was used without further purification in Step 2. 6-chlorohexyl acetate was fully characterized by ^{1}H-NMR, ^{13}C-NMR, and mass spectroscopy.

Step 1 of synthesis allowed to protect the hydroxyl group of 6-chlorohexanol, forming the acetate derivate, in order to guarantee the reaction with the imidazole at the chlorine bearing carbon in the next step.

It is well known that reactions of alcohols with an excess of anhydride proceed in inert solvents at 0ºC. Furthermore, DMAP, by activating the acetic anhydride, provides a strong catalytic effect to the process (204). Its catalytic effect is due to the dimethylamino group that acts as electrondonor substituent, which increases the nucleophilicity and the basicity of the pyridine nitrogen.

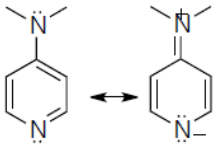

Scheme 3.3. Effect of dimethyl amino group on the pyridine nitrogen

Et_3N, employed to deprotonate the starting alcohol, leads to the formation of the Et_3N ammonium salt. The general mechanism of the reaction is exemplified in Scheme 3.4.

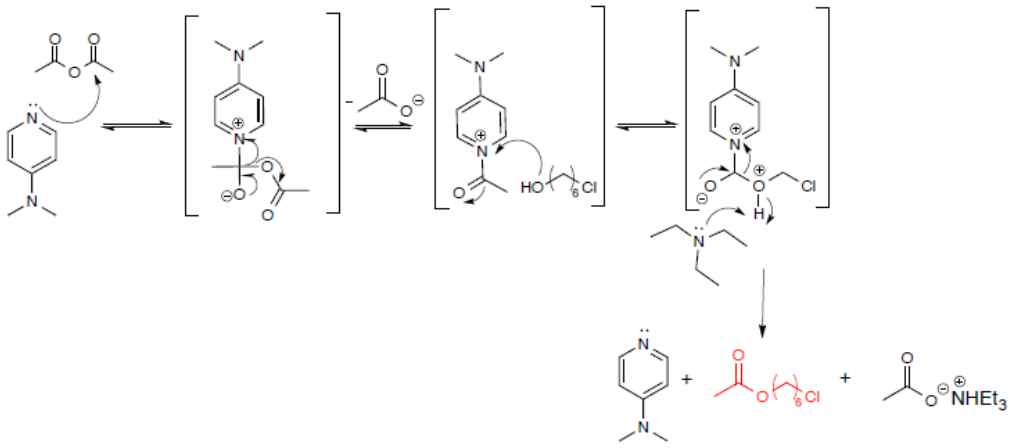

Scheme 3.4. Mechanis of the reaction between 6-chloro-1-hexanol and acetic anhydride with DMAP and Et_3N as catalysts, to give 6-chlorohexyl acetate.

Step 2:

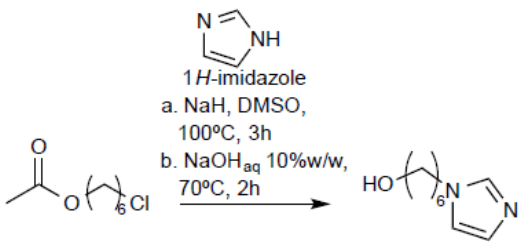

Scheme 3.5. Reaction of the 6-chlorohexyl acetate with the imidazole to give the 6-(1H-imidazol-1yl) hexan-1-ol.

Initially, imidazole was treated with the strong base NaH. The resulting imidazolium sodium salt was N-alkylated with the α-ω O-acetyl chloroalcohol, 6-chlorohexyl acetate, in DMSO at 100 °C for 3 hours, followed by hydrolysis in 10% aqueous NaOH to give the alcohol intermediates. Imidazole, acting as a "weak Brønsted acid", was deprotonated by NaH yielding the imidazolium sodium salt derivative with the development of H_2. (Scheme 3.6) The process was carried out at room temperature.

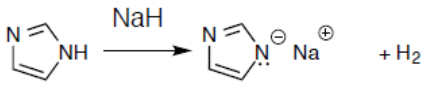

Scheme 3.6. Mechanism of the reaction between imidazole and NaH to form the imidazolium sodium salt, as nucleophilic intermediate with high reactivity with 6-chloro acetate.

The reaction between the imidazolium sodium salt and 6-chlorohexylacetate is a classic example of nucleophilic substitution (SN_2) in anaprotic polar solvent (DMSO). (See Scheme 3.7). In the reaction, the nucleophilic nitrogen of the imidazole react with the carbon bearing the chlorine, with following elimination of Cl^-, as leaving group, to form 6-(1H-imidazol-1-yl) hexyl acetate and NaCl.

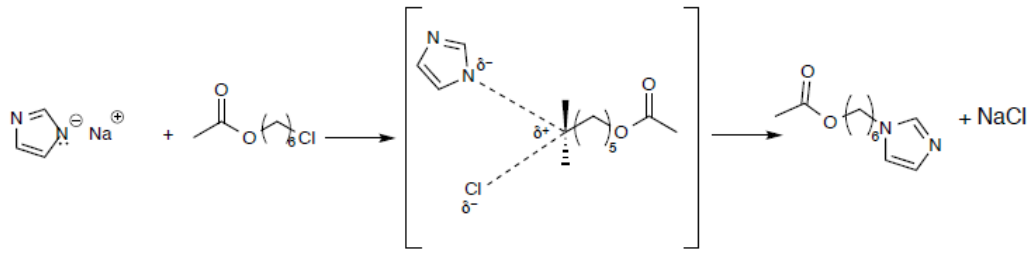

Scheme 3.7. Mechanism of the SN2 reaction between imidazolium sodium salt and 6-chloroacetate.

Deacetylation reaction of the acetate derivative was performed by hydrolysis with aqueous NaOH at 70ºC and yielded the 6-(1H-imidazol-1-yl) hexan-1-ol. Esters can be easily hydrolysed in alkaline aqueous solutions and in these conditions the process is always irreversible.

Step 3:

6-(1H-imidazol-1-yl) hexan-1-ol could react with methacryloyl chloride using Et_3N, as catalyst, to form the methacrylic monomer ImHeMA as reported in Scheme 3.8.

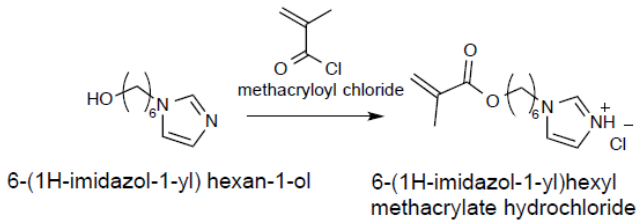

Scheme 3.8. Reaction of the imidazolic alcohol and methacryoloyl chloride to obtain the ImHeMA monomer.

The use of standard acid scavengers for this latter step was found to reduce dramatically the yields (< 10%) and shelf life of the monomer (205). This last step was then carried out exploiting the imidazole ring of the reagent as a base, yielding the desired monomer as its hydrochloride salt. This methodology allowed to minimize a number of side-reactions previously observed when Et_3N was also employed and led to a simplification in the purification process by flash column chromatography.

Furthermore, obtaining the ImHeMA as a salt allowed to an easier solubilization in aqueous media. The molecule was also found to be chemically stable at -20 °C for several months as confirmed by the ^{1}H-NMR analysis and mass spectroscopy.

3.1.2 SYNTHESIS OF REVERSIBLE ADDICTION-FRAGMENTATION CHAIN TRANSFER (RAFT) AGENT / (CTA)

Controlled/living radical polymerisations (CRP) were carried out using the glycerol methacrylate monomer and the imidazolic monomer synthesized in the previous sections to obtain a well-defined AB diblock co-polymers. In particular, in this work RAFT polymerization was chosen for its experimental simplicity compared to other polymerization techniques and because it allows for the precisely control molecular weight of the polymers. RAFT polymerization, as previously described in Chapter 1, involves the use of a chain transfer agent (CTA), where the transfer of the S=C(Z)S- moiety from the RAFT agent provides the living character to the process (185). The reaction of the CTA with a radical monomer results in a polymer containing the same S=C(Z)S-functionalities from the initial RAFT agent. Moreover, this polymer is capable, under appropriate conditions, to reinitiate, acting as a macroCTA, a new polymerization reaction. In this study, a series of hydrophilic macroCTAs were synthesized to obtain a starting material that can be used to grow the pH responsive imidazole based monomers, producing a variety of well-defined block co-polymers.

3.1.2.1 Synthesis of 2-cyanopropan-2-yl 2-hydroxyethyl carbonotrithioate RAFT Agent

This RAFT agent was synthesised following and adapting previously reported procedures for the same kind of products (206).

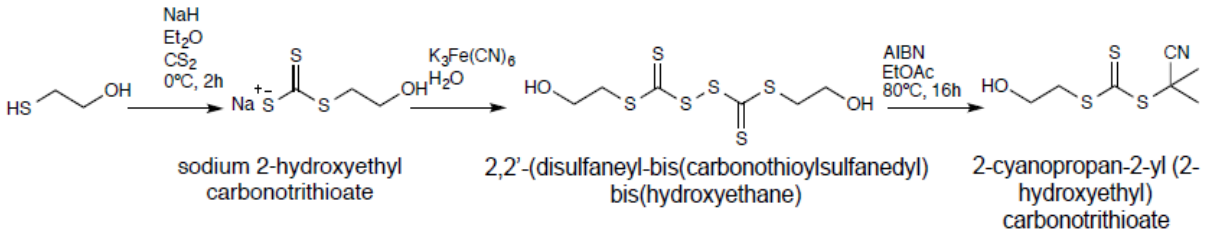

Scheme 3.9. Synthesis of 2-cyanopropan-2-yl 2-hydroxyethyl carbonotrithioate.

Firstly, 2-mercaptoethanol was treated with NaH in Et_2O at 0°C, then carbon disulfide was added dropwise to yield the trithio-salt intermediate. This Na^+ salt was oxidised by using $K_3Fe(CN)_6$ to give the 2,2'(disulfanediylbis(carbonothioylsulfanediyl)] bis(hydroxyethane) intermediate. 'Radical-induced' decomposition of this intermediate via reaction with AIBN gave the 2-cyanopropan-2-yl 2-hydroxyethyl carbonotrithioate desired as confirmed by ^{1}H-NMR and ^{13}C-NMR.

3.1.2.2 Synthesis of poly[GMA] macroCTA

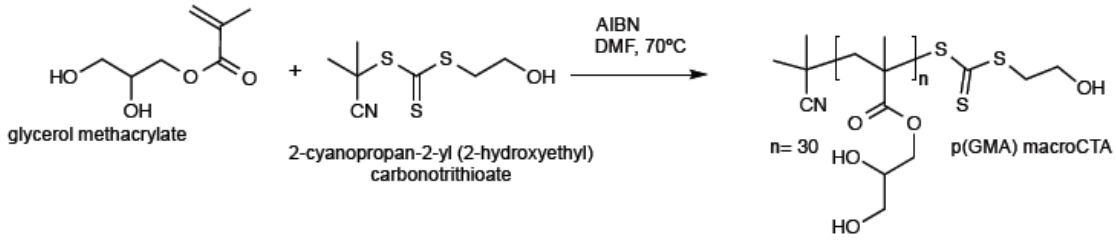

Scheme 3.10. RAFT polymerization of GMA to obtain the poly[GMA] macro-CTA.

The polymerization of GMA was performed using glycerol methacrylate (GMA) monomer, AIBN as radical initiator and 2-cyanopropan-2-yl 2-hydroxyethyl carbonotrithioate as RAFT agent. The molar ratio of the reagents was: [Raft Agent]: [AIBN]: [GMA] = 1: 0.5: 35. The reaction was monitored by ^{1}H-NMR to determine the conversion. Aliquots of the reaction mixture were withdrawn every 30 minutes until 150 minutes, when the polymerization was stopped.

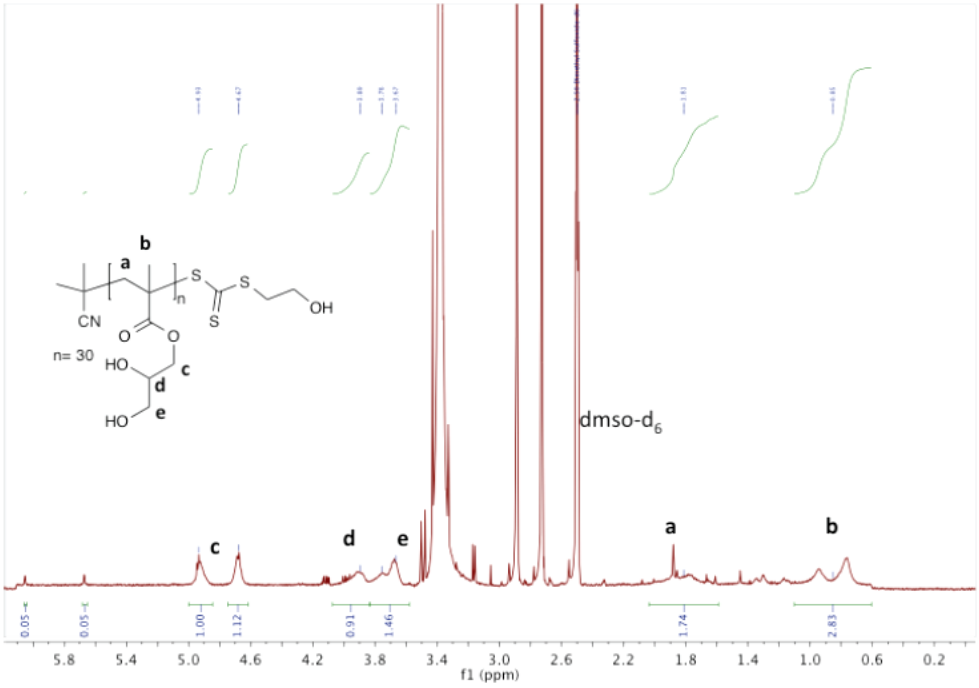

Figure 3.1. ^{1}H-NMR spectrum of poly[GMA] macro-CTA in dmso-d_6 with peak assignment. [5% of unreacted monomer signals was detected on the spectrum]

Figure 3.1 shows the ^{1}H-NMR spectrum of the final product. The rate of polymerization was calculated by comparing the integral variation (arbitrary units, A.U.) of one of the vinylic protons in the starting monomer to the integral of the CH of the solvent, DMF, used has internal standard. DMF, at the ^{1}H-NMR in dmso-d_6, provide three singlet peaks placed at 7.95 ppm and 2.73 ppm. The peak at 7.95 ppm was chosen as reference peak because it does not overlap with the peaks of the growing polymer or the starting monomer. DMF has a very high boiling point (153ºC), therefore it can be assumed that its concentration is constant during our polymerization, performed at 70 ºC, and its signals can be used as reference to measure the decreasing in the vinylic proton integral. The conversion of the monomer during the polymerization was determined by comparing the value of the vinyl integral at time = 0 and the value of the integral of the sample at every given time. The polymerization was stopped at 87% conversion when the DP was 30.

3.1.3 SYNTHESIS OF POLY[GMA]-BLOCK-POLY[IMHEMA]

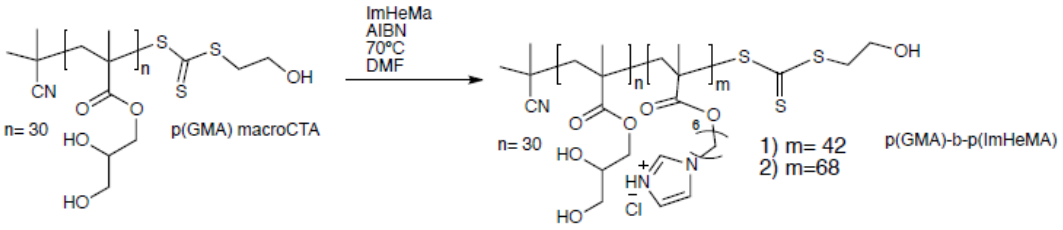

Scheme 3.11. RAFT polymerization scheme starting from poly[GMA] to obtain the poly[GMA]-block-poly[ImHeMA] diblock co-polymer.

Two block co-polymers were generated using the poly[GMA] as the hydrophilic block and macro-CTA and the newly synthesized ImHeMA monomer, with different polymerization degree of the latter, to understand the influence of this monomer on the properties of the final diblock copolymers. The reagent conditions used were:

1) poly[GMA]: [ImHeMA]= 1: 6

2) poly[GMA]: [ImHeMA]= 1: 3

The synthesis of both materials was carried out following a RAFT polymerization method, using DMF as solvent and AIBN as radical initiator. The two reactions showed different polymerisation rates. The Polymerization of co-polymer (1), with a higher ratio of ImHeMA, was found to be slower and its kinetic plot showed a higher deviation from a linear first order kinetic compared to polymer (2). The plot showed an initial faster rate of polymerization that, after 180 minutes, drastically decreased. Polymerization of co-polymer (2), instead, proceeded faster and was stopped at theroic 90% conversion, after 150 minutes. Conversely, the synthesis of polymer (1) was stopped at 75% conversion, after 25 hours. Polymerization rate was calculated in both reactions by ^{1}H NMR using the solvent DMF as internal standard and shown in Figure 3.2. In particular, it was observed the decreasing in the intensity of the signal, corresponding to the vinyl protons of the ImHeMA monomer, versus the singlet at 7.95 ppm (in dmso-d_6) of the DMF.

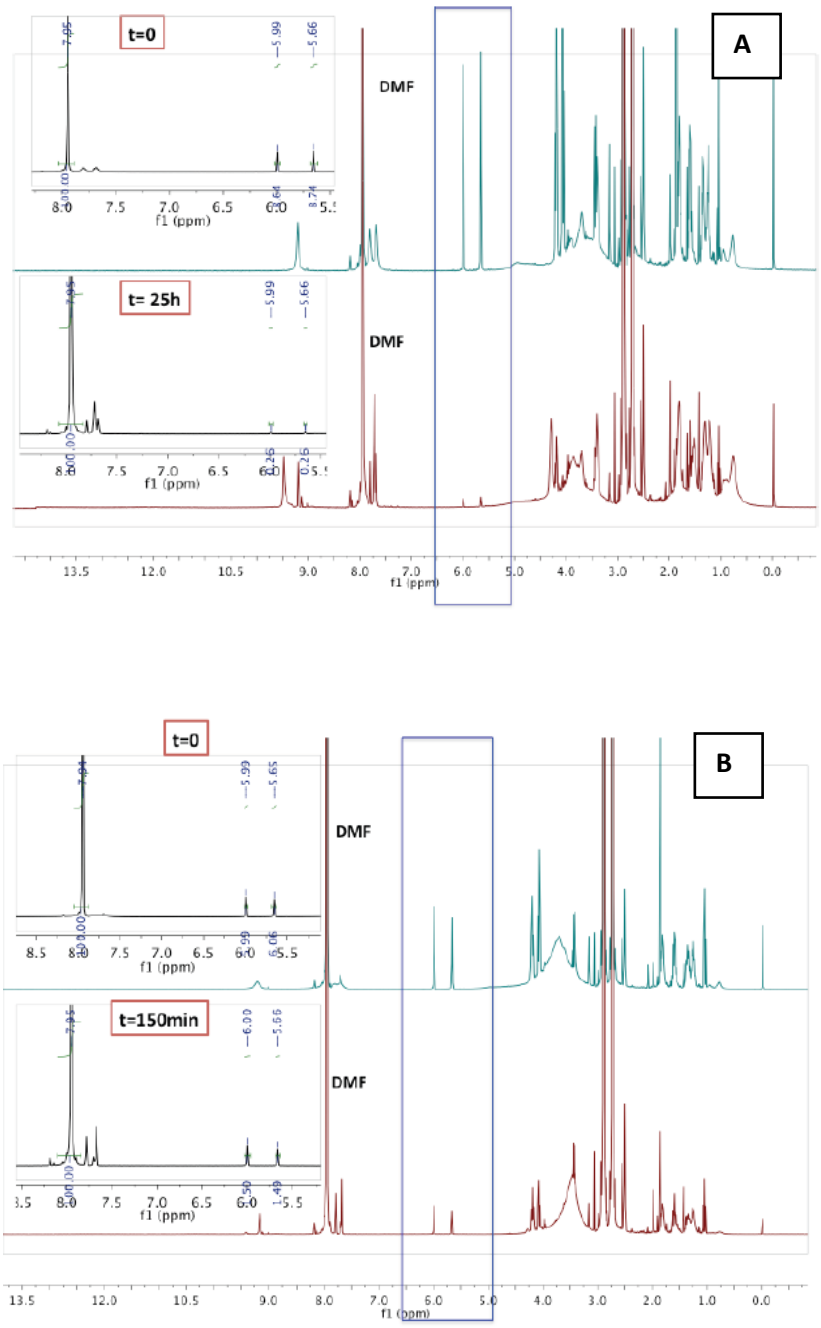

Figure 3.2. ^{1}H-NMR stacked spectra in DMSO-d_6 of the poly[GMA]-block-poly[ImHeMA] (1) (Panel A) and (2) (Panel B) at t=0 and t= end (when the reaction was stopped). The peaks used to determine polymer conversion are highlighted in blue (d=6.00 and 5.66) relative to the vinyl protons of the ImHeMA.

GMA/ImHeMA molar ratio in the final diblock co-polymers was obtained comparing the integral of protons corresponding to -OCH_2 of the polyGMA macroCTA block to protons vinyl protons of ImHeMA, corresponding to same protons in the poly[ImHeMA] block.

As shown in Table 3.1, the final molar ratio of both materials was found to be different than the one estimated in the kinetic study. ^{1}HNMR analysis, in fact, indicated a final molar ratio [GMA]:[ImHeMA] of 1: 1.4 for the co-polymer (1) and 1: 2.25 for the co-polymer (2).

Table 3.1. Molar ratio of GMA/ImHeMa in co-polymer (1) and (2).

	FINAL RATIO[a]	M_n p(GMA)* (kDa)	M_n p(ImHeMA)* (kDa)	w/w% p(GMA)*	w/w% p(ImHeMA)*
polymer 1	1: 1.4	4802	9912	33	67
polymer 2	1: 2.25	4802	15930	23	77

[a] Calculated ^{1}H-NMR
*Theoretical molecular weight

It is not fully clear why the molar ratios of the monomers forming the two blocks differed from those expected, but it might be due to the difficulty to integrate correctly the signal representative of the solvent, used as reference, which is proximal to the polymer peaks. Gel Permeation Chromatography (GPC) analyses to determine the molecular weight and polydispersity index (PDI) of these samples was difficult to perform due, likely, to solubility limits of the materials in the chromatographic eluents or to polymer interactions with the stationary phase of the column. Nevertheless, both polymerizations were relevant to provide useful materials. Further studies were performed to prove their ability of self-assembly in pH-swop conditions and select which one was more suitable to generate a definitive system to be used for biological applications.

3.2 REPRESENTATIVE TITRATION AND TURBIDIMETRIC ASSAYS OF POLY[GMA]-BLOCK-POLY[IMHEMA] (1) AND (2)

Potentiometric acid/base titration and back titration on poly[GMA]-block-poly[ImHeMA] diblock copolymers (1) and (2) were carried out to evaluate the apparent pKa of these materials. Titration was performed in all cases by adding aliquots of 10 μL of 0.1 M NaOH and recording the pH value after each addition, to a 1 mg/mL polymer solution at pH 3. The titration curve was obtained plotting the pH data in function of the volume of the titrant added. The point of inflection ("equivalence point") was determined as the maximum value in the first derivative of the curve. The equivalence points were 6.29 for poly[GMA]-block-poly[ImHeMA] co-polymer (1) and 6.47 for poly[GMA]-block-

poly[ImHeMA] co-polymer (2). The back-titrations were carried out on the same solution used for direct titration, starting at pH 10.5; 10 μL aliquots of 0.1M HCl were added and pH values recorded after each addition until ~pH 3 was reached. The plotted data generated by back-titration showed an equivalence point at 9.27 for poly[GMA]-block-poly[ImHeMA] copolymer (1) and pH 8.52 for poly[GMA]-block-poly[ImHeMA] co-polymer (2).

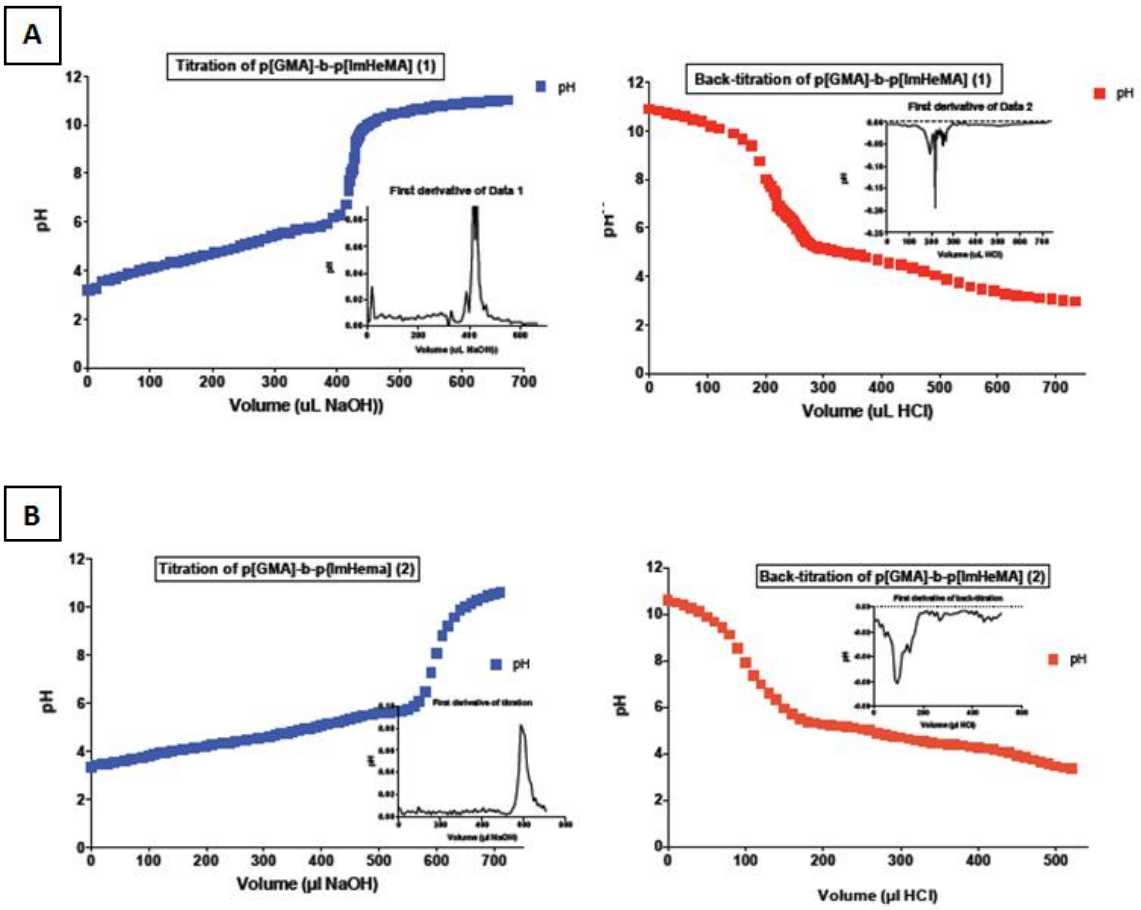

Figure 3.3. Titration (■) and back-titration (■) curves of poly[GMA]-block-poly[ImHeMA] co-polymer (1) (Panel A) and (2) (Panel B).

The apparent pKa were derived as the mean value between titration and back titration "equivalent points". Apparent pKa was 7.5 for co-polymer (1) and 7.78 for co-polymer (2). A precipitation of all polymers was observed during the titrations from low pH and solutions became turbid. Turbidity rose with the increase of the pH due to deprotonation of the imidazole lateral groups of the polymers. It suggested the presence of aggregation phenomena that is triggered at pH above the pKa found for these materials.

Aggregation phenomena could make more difficult the access of the titrant to the amino group of the imidazole in the pH-responsive block, causing a delay in the protonation/deprotonation process. For this reason, the pKa of the polymer is commonly named "apparent pKa" due to the effect of aggregation on the deprotonation of the polymer.

Poly[GMA]-bock-poly[ImHeMA] diblock co-polymer (1) and (2) resulted poorly soluble in aqueous media. A turbidimetric analysis was carried out to determine their "cloud point". The "cloud point" for these materials is the pH at which they are no longer completely soluble, but they start to aggregate (207). This technique has been widely used to understand the behaviour of pH-sensitive polymeric materials, especially in view of a practical application of these materials in more complex drug delivery systems. The basis of the assay is that the turbidity of a dispersion of scattering particles (e.g. polymer chains in water) is an increasing function of the relative refractive index (n) and particle volume (Vp). Therefore, an increase in the turbidity with the increasing of the pH correlates with *n* or *Vp* (or both) increase. Variation of the transmittance at λ 500 nm (due to light scattering) was recorded as a function of pH for 1 mg/mL polymeric solution, starting at pH 3 (Figure 3.4). Aliquots of 5 µL of 0.1 M NaOH were added to the polymer solution and the pH was measured after each addition, allowing few seconds under stirring for equilibration.

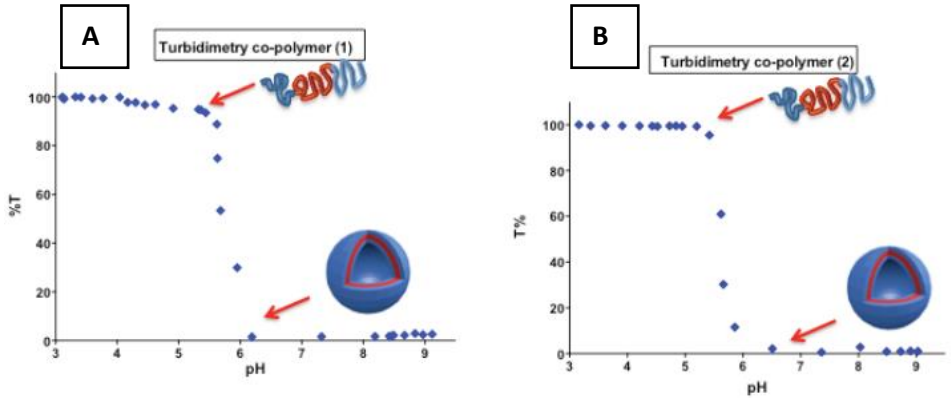

Figure 3.4. Representative turbidimetric assay for poly[GMA]-block-poly[ImHeMA] co-polymer (1) (panel A) and (2) (panel B).

All the experiments were performed in doublicate and the cloud point calculated as the mean values of the two results. The cloud point found for poly[GMA]-block-poly[ImHeMA] co-polymer (1) was pH 5.6 and pH 5.4 for poly[GMA]-block-poly[ImHeMA] co-polymer (2). These results confirmed that the co-polymer with a

higher hydrophilic/hydrophobic ratio (co-polymer 1) has a solubility with a slightly wider pH range in aqueous media with respect to co-polymer (2). Through all these early stage pH-studies we confirmed ImHeMA being a highly hydrophobic monomer. Its physic-chemical features confirm that the polymer responds to pH environmental variations with physical aggregation, which underlines the hydrophilic/hydrophobic conversion. The data however do not support for the assembly of the two polymers into nanovesicles.

3.3 SYNTHESIS OF THE TRIBLOCK CO-POLYMER PEG$_{1.9KDA}$-BLOCK-POLY[GMA]-BLOCK-POLY[IMHEMA] THROUGH PIRYDIL INTERMEDIATE CONJUGATE

Solubility of the previously described AB block co-polymers, as revealed by all the studies performed at different pH conditions, was good. However, the results obtained from these block co-polymers confirmed that improved solubility and stability of the polymer system was required to allow the generation of more soluble amphiphilic materials with self-assembling properties. The polymers might be stable in the blood stream at physiologic conditions (pH 7.4) to protect the DNA or siRNA in transit in the body, and hydrophilic in the acidic conditions of the cellular endosome compartment where, as the aim of the study dictates, they will be delivered. Therefore, an ABC triblock co-polymer was synthesized starting from poly[GMA]-block-poly[ImHeMA] (1) by reaction with a mPEG$_{2kDa}$-SH to improve the polymer solubility at higher pH. poly[GMA]-block-poly[ImHeMA] (1) was chosen between the two polymers for the synthesis of the ABC co-polymer in virtue of its higher hydrophilic/hydrophobic ratio, which provide slightly higher solubility in aqueous media.

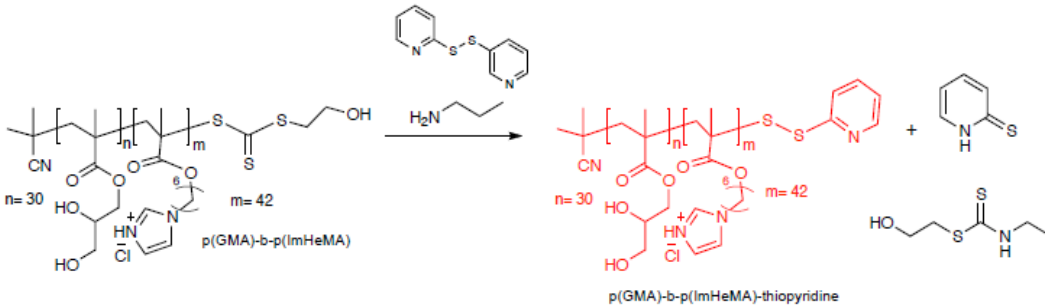

Scheme 3.12. Reaction of poly[GMA]-block-poly[ImHeMA] with propylamine and 2-2-dithiopyridine to yield the poly[GMA]-block-poly[ImHeMA] pyridyl conjugate product.

The first step of this reaction involved the simultaneous removal of the RAFT agent though propylamine addition and the conjugation of 2,2'-dithiopyridine to the polymer

thiol group (Scheme 3.12). Propylamine, through the aminolysis, promotes the conversion of the RAFT-end group to a stable reactive thiol suitable to be attacked by the pyridil group to yield a pyridyl disulfide-terminated co-polymer. The aminolysis route has possible drawbacks, as the thiol group can undergoes further oxidation to disulfide, leading to bimodal polymer populations (208). Therefore, to overcome this disadvantage the reaction was performed in the presence of a thiol-reactive compound as the 2-2'-dithiopyridine to have a pyridyl disulfide protective group before the reaction with the $mPEG_{2kDa}SH$. Pyridyl disulfide, as widely reported in the literature, is an efficient active group for selective exchange-reactions with thiols under mild conditions. The pyridyl disulfide group, in fact, presents a high reactivity towards the attack of free thiol derivates (209). Therefore, it is an advantageous functional group towards disulfide-thiol exchange reactions used particularly in biological applications for the preparation of cleavable conjugates of biomolecules such as protein or thiol-activated oligonucleotide (210).

The reaction mixture was stirred overnight at room temperature and under nitrogen. After evaporation of the solvent, the product was recovered by dissolving the solid residue in acidic water (obtained by adding 1 N HCl to deionised water until pH 3) and, then, increasing the pH by adding 1 N NaOH. Precipitation with this method was possible because the polymer was completely deprotonated, therefore more hydrophobic, at high pH as demonstrated by pH studies previously reported (Section 3.2). From ^{1}H-NMR spectra of the final product it was not possible to identify the signals corresponding to the pyridyl protons. This could be explained considering the small molar fraction of the end-group compared to the whole polymer. In fact, the peaks corresponding to pyridyl protons might be partially covered by the imidazole peaks of the polymer-repeating unit. Therefore, it was not possible to determine the functionalization degree of the product at this stage by NMR, whereas a "colorimetric assay" by UV-vis was performed. The disulfide bond of the poly[GMA]-block-poly[ImHeMA]-thiopyridine was reduced by using an excess of DL-dithiothreitol (DTT), a strong reducing agent as shown in Scheme 3.13 The released thiopyridine was quantitatively detected by spectrophotometric analysis at 370 nm.

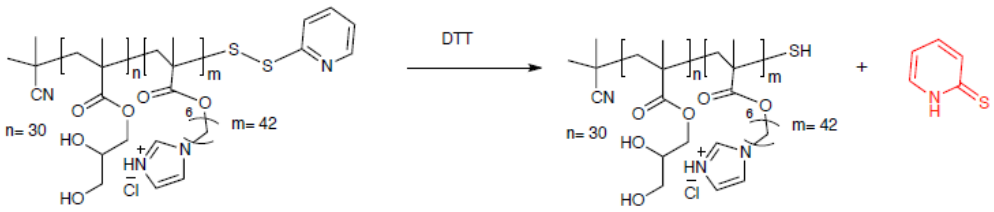

Scheme 3.13. Schematic representation of 2-thiopyridine cleavage from poly[GMA]-block-poly[ImHeMA]-thiopyridine co-polymer using DTT.

The concentration of 2-thiopyridine released from the polymer was obtained using the molar extinction coefficient value (ε_M = 5027 $mol^{-1}cm^{-1}$) derived from a calibration curve of 2-thiopyridine in methanol (Figure 3.5) and the co-polymer activation yield was derived as a ratio between the 2-thiopyridine in solution and the polymer dissolved.

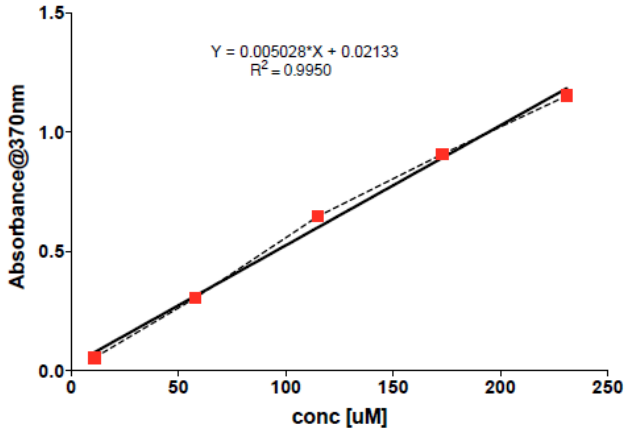

Figure 3.5. Calibration curve of the 2-thiopyridine in MeOH.

The co-polymer activation yield was found to be only 48%. However the copolymer was used for the second step of the synthesis, namely the conjugation of the mPEG-SH to the activated terminal end of poly[GMA]-block-poly[ImHeMA]-thiopyridine.

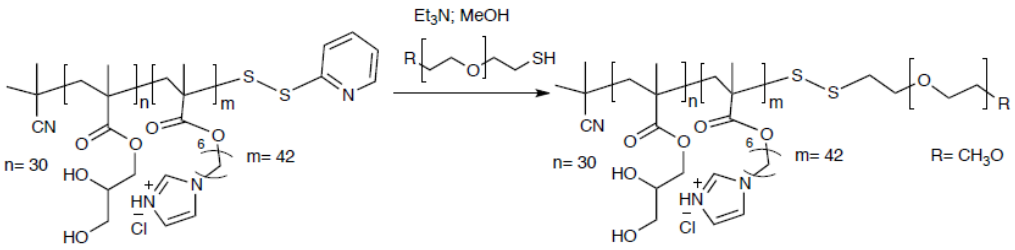

Scheme 3.14. Conjugation of mPEG-SH_{2kDa} to poly[GMA]-block-poly[ImHeMA]-thiopyridine .

In the second step, the activated polymer with a disulfide end functionality was reacted with the free thiols of the $mPEG_{2kDa}SH$ and allowed the generation of the triblock co-polymer. The reaction was carried out as shown in Scheme 3.14. This is a thioldisulfide exchange reaction, and it requires the presence of an organic base, Et_3N, in order to form the thiolate that will react selectively with the disulfide bond. Purification of the product was done in two steps. At first, a precipitation was carried out following the same method used for the precipitation of the poly[GMA]-block-poly[ImHeMA]-S-S-pyridyl co-polymer. MeOH was evaporated under reduced pressure and the solid residue was dissolved in acidic deionized water (pH 3) and, then, 1 N NaOH was added. A small amount of precipitate was observed while the aqueous solution became opalescent, probably due to the formation of colloidal assemblies of the triblock copolymer. This evidence supported for the generation of a more soluble copolymer with self-assembling capacity. Both the precipitate and the suspension, recovered after centrifugation, were freeze-dried and analyzed by ^{1}H-NMR. Figure 3.6 shows the spectra of the opalescent suspension containing $mPEG\text{-}SH_{2kDa}$-poly[GMA]-bkock-poly[ImHeMA] and the precipitate obtained by centrifugation. The signal of the mPEG backbone was expected to be at about 3.6 ppm and the terminal methoxyl group of the CH_3-O-PEG- chain at slightly lower value (region highlighted in red).

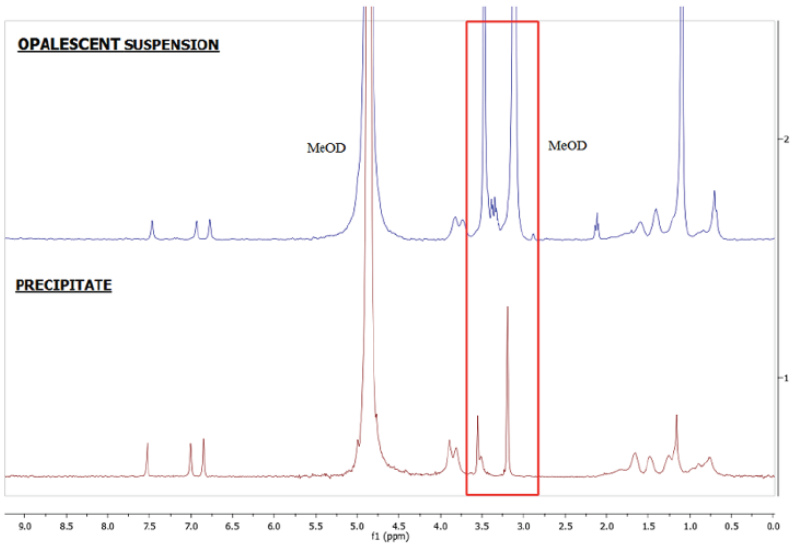

Figure 3.6. Stacked ^{1}H-NMR in MeOD of opalescent material containing $mPEG\text{-}SH_{2kDa}$-poly[GMA]-block-poly[ImHeMA] and the precipitate derived from the conjugation of mPEG-SH to poly[GMA]-block-poly[ImHeMA]. Highlighted in red the region in the spectrum where PEG is expected.

Chemical shift and intensity of the peaks are reported in Table 3.2. The peak at 3.67 ppm in the spectra of the suspension phase is attributed to the mPEG and overlaps the signal corresponding to the ester -OCH_2- of the poly[GMA] block. The same pattern of peaks was not visible in the spectrum of the precipitate. The suspension was shown to contain the triblock co-polymer and the excess of mPEG-SH, while the precipitate was determined to be unreacted poly[GMA]-block-poly[ImHeMA]-S-S-pyridyl co-polymer.

Table 3.2. Chemical shift and integration of the peaks in the precipitate and suspension obtained after precipitation of $mPEG_{1.9kDa}$-p-(GMA)-b-p(ImHeMA)

Chemical shift (δ)	Precipitate Integral (A.U.))	Suspension Integral (A.U.)
7.65	1.00	1.00
7.13	1.03	1.05
6.97	0.97	1.07
3.93	6.09	6.02
3.67	**2.66**	**35.05**
1.78	3.75	4.96
1.60	2.31	5.15
1.28	5.73	35.41
0.88	4.80	7.73

The crude material of the opalescent suspension isolated from the conjugation of the mPEG-SH to the poly[GMA]-block-poly[ImHeMA]-S-S-pyridyl co-polymer was dissolved in 20 mM phospate saline buffer, 150 mM NaCl pH 5 and the pH was increased to 8 with NaOH 0.1M. The polymeric dispersion underwent size analysis as shown in Figure 3.7. From the dynamic light scattering analysis it was evident that the polymer was self-organized in a colloidal system with an average size of about 50 nm. According to this evidence, the polymeric dispersion was then dialyzed using a membrane with a 100 kDa C.O. (cut-off) to remove the excess of unreacted $mPEG_{2kDa}$-SH.

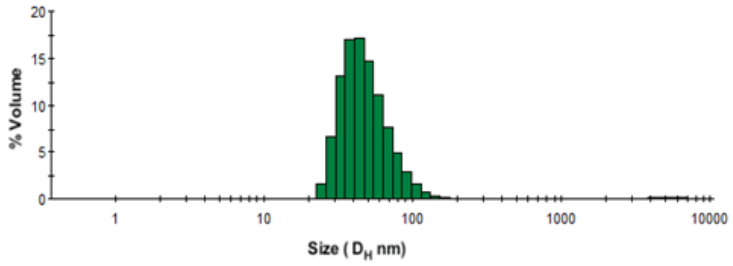

Figure 3.7. DLS analysis (Size distribution by % Volume) of the polymeric suspension of poly[GMA]-block-poly[ImHeMA]-$PEG_{1.9kDa}$ before dialysis. DLS confirmed the presence of assemblies.

The diameter of the co-polymer assembly was larger than the pores of the membrane and the vesicles were retained inside, while mPEG-SH, considerably smaller then the dyalisis membrane pores, could diffuse outside. The cut-off of the membrane allowed the diffusion of both single chain mPEG-SH and the dimer mPEG-S-S-mPEG that can generate by oxidation as confirmed by dedicated tests performed using $mPEG_{2\ kDa}$-OH and and $mPEG_{5kDa}$-OH. Then PEG-SH conjugation degree to diblock was determined by ^{1}H-NMR and estimated to be ~ 60% with respect to the activated poly[GMA]-block-poly[ImHeMA]-S-S-pyridyl co-polymer. Figure 3.8 reports the ^{1}H-NMR spectrum of the expected poly[GMA]-block-poly[ImHeMA]-$PEG_{2\ kDa}$.

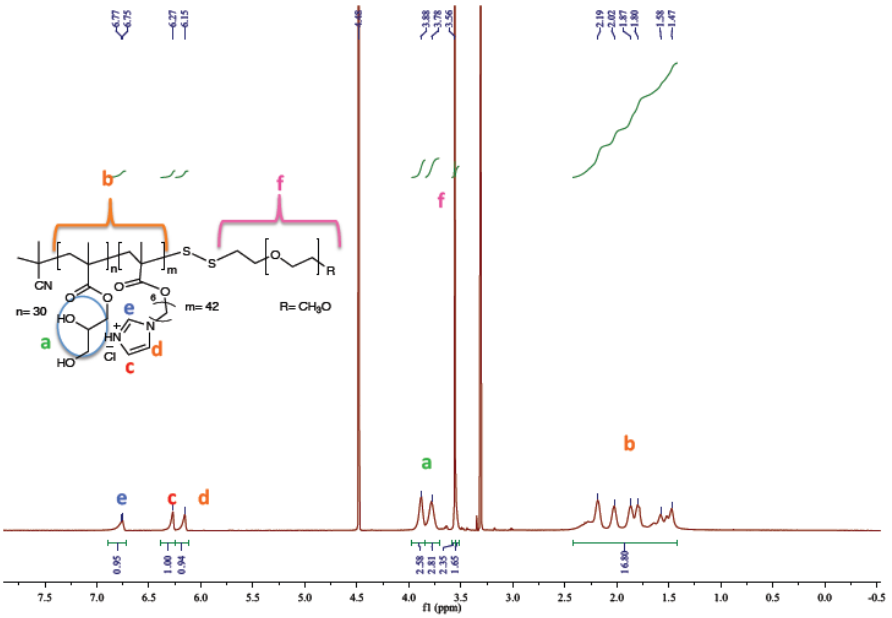

Figure 3.8. ^{1}H-NMR profile of poly[GMA]-block-poly[ImHeMA]–PEG_{2kDa} triblock co-polymer after purification.

3.4 ASSEMBLY OF COLLOIDAL SYSTEMS USING THE TRIBLOCK CO-POLYMER OF PEG_{2KDA}-POLY[GMA]-BLOCK-POLY[IMHEMA] AND TIME STABILITY INVESTIGATION

Nanoparticles using the triblock co-polymer PEG_{2kDa}-poly[GMA]-block-poly[ImHeMA] were physically assembled in 20 mM phosphate buffer, 150 mM NaCl, following the method previously described.The pH was gradually increased from pH 3 up to pH 7.4. The saline buffer was used to mimic the physiological environment, as salts influence the stability of charged polymersomes. The ions, in the media, can affect the particle

diffusion speed by changing the thickness of the electric double layer nameda Z- potential (211). Compared to a solely aqueous media, a higher conductivity media will suppress the electric double layer increasing the diffusion speed and resulting in a smaller measured hydrodynamic diameter by DLS and more stable polymersome assemblies. The slow increase of the pH performed in the assembling procedure, allowed the self-assembling of the polymer, as clearly confirmed by DLS (Figure 3.9).

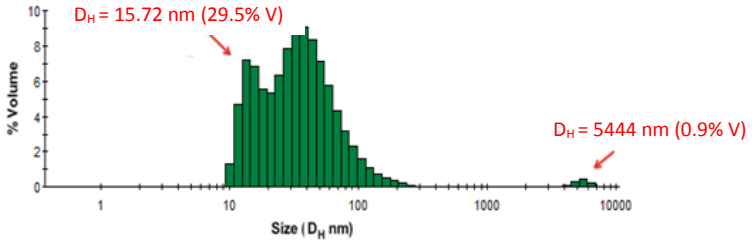

Figure 3.9. DLS analysis (Size distribution by % Volume) after the self-assembly of poly[GMA]-block-poly[ImHeMA]-$PEG_{1.9\ kDa}$.

The analysis showed the presence of a main population (67.6% Volume) of mean diameter of 49 ± 5 nm with a PDI of 0.397, which confirmed the ability of the triblock copolymer to assembly in colloidal structures at physiological pH although with a not high homogeneity. A population with hydrodynamic size of 15.72 nm (29.5% Volume) was also observed and it can be attributed to a minimum amount of non-assembled free polymer. Moreover, also a population with a size of 5444 nm, (0.9% Volume) was detected, perhaps related to a small ratio of aggregated polymer. In order to isolate the aggregated polymer and characterize the nanoparticles only, the suspension was filtered through a cellulose acetate (CA) filter with a 5 μm cut-off size and analyzed by DLS (Figure 3.10).

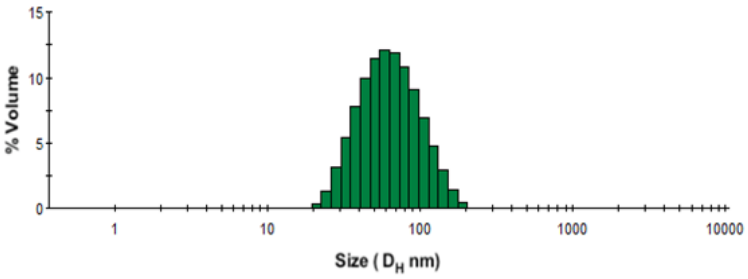

Figure 3.10. DLS analysis (Size distribution by %Volume) of colloidal assembled poly[GMA]-block-poly[ImHeMA]-PEG_{2kDa} after filtration.

Only one population (100% Volume) with a size of 42 ± 3 nm (PDI = 0.168) was detected after filtration, which indicated the nanoparticle sample is rather homogeneous even though a limited amount of the material does not self-organize in colloidal systems. Kinetic stability of the nanoparticles was also investigated by DLS at 25ºC. Particles size was recorded across pH ranges at scheduled times (Table 3.3). Samples were prepared using the method previously described, in buffers at pH 5, 6.5 and 7.4 to mimic the endosomal compartment, tumor interstitium and blood respectively.

Table 3.3. DLS analysis of nanoparticles assembled with poly[GMA]-block-poly[ImHeMA]-$PEG_{2\ kDa}$ at pH 5, 6.5 and 7.4, measured at different time intervals.

	pH 5		pH 6.5		pH 7.4	
time (h)	PDI	Volume (nm)	PDI	Volume (nm)	PDI	Volume (nm)
0	0.528	483.6	0.517	114.9	0.404	44.08
1	1.000	166.2	0.397	136.5	0.397	43.30
2	1.000	269.3	0.382	145.1	0.411	42.92
6	1.000	169.2	0.222	169.5	0.389	40.69
16	1.000	398.2	0.197	234.5	0.341	39.11
24	1.000	255.1	0.216	237.2	0.435	39.67
48	1.000	173.2	0.277	289.1	0.492	40.59
72					0.464	41.47
75			0.249	308.6	0.132	42.24
96			0.423	320.7	0.138	41.45

At pH 7.4 only one population with DH ~ 42 nm was recorded and particles resulted stable up to 72 hours. After 72 hours, only a small amount of aggregates (~3% in Volume) was found. At pH 6.5 the system rearranged in larger aggregates than at pH 7.4. A possible explanation for this behavior might be ascribed to the repulsion between positive charges originating from the partial protonation of the polymer pH responsive block (poly[ImHeMA]) at this pH which destabilize the system with respect to pH 7.4 but are not sufficient to promote the full dissolution of the polymer chains (the pH condition is very close to the pKa expected for the imidazole). Assemblies remained stable within 6 hours at this pH and afterwards their stability decreased, as it was shown by the enlargement in the diameter size. However, the PDI of the particles was comparable to the one of the particles at pH 7.4 showing the the rearrangement of the polymer does not

translate into macroscopic aggregation of the system. At pH 5 the polymer central block poly[ImHeMA] was mainly protonated since the pH is lower than the polyer apparent pKa, therefore the DLS analysis proved no colloidal assemblies were detectable as confirmed by the very high PDI. The value of PDI=1 indicated that the polymer was disperse in solution rather than in colloidal suspensions; therefore the size distribution displayed was very approximate. This result, in addition, suggested that the triblock copolymer loses its ability to assemble with other polymer chains at this pH and rather, being protonated, it induces the colloidal system to dissociate. This is a clear evidence that the polymer generated can respond to pH alterations with sharp conversion from an associated state to a dissociated state. This pH-responsive polymer possess the capacity to generate particulate carriers with good stability at physiological pH, and induce destabilization and break down of the carrier at slightly acidic pH, as required for the pH-triggered release of therapeutics in acidic pathological environment, as aimed in this work.

3.5 TRIBLOCK COPOLYMERS SYNTHESES

Evidences described in the previous section show that the ABC amphiphilic triblock copolymer poly[GMA]-block-poly[ImHeMA]-PEG_{2kDa} possesses a clear self-assembling behavior. This polymer was deemed adequate to generate nanovehicles for the delivery of drugs and siRNA. The polymer has been synthesized according to a two steps procedure: 1. Sequential RAFT polymerization of the poly-GMA block followed by the poly-ImHeMA; 2. Conjugation of mPEG-SH to the poly-ImHeMA after removal of the RAFT agent. However, this material was synthesized with a unsatisfying purity due to the low conjugation yield of the mPEG-SH to the diblock co-polymer. In order to obtain the the same three block co-polymer with predictable molecular weight and narrow molecular weight distribution (PDI), RAFT was the process chosen to successfully polymerize the materials. In this work, a small library of well-defined mPEG-block-poly(ImHeMA) diblock co-polymers was prepared by polymerization of N-alkyl imidazole monomers using either methoxy$PEG_{1.9kDa}$-OH or t-boc-NH-$PEG_{3.5kDa}$-OH dithiobenzoates as the macrotransfer agents, which were firstly synthesized. Chain extension with glycerol methacrylate (GMA) on m$PEG_{1.9kDa}$-block-poly(ImHeMA) and t-boc-NH-$PEG_{3.5kDa}$-block-poly(ImHeMA) co-polymers afforded the required ABC amphiphilic triblock mPEG-block-poly(ImHeMA)-block-poly(GMA) co-polymers. The two PEG derivative

were chosen to generate the major polymeric self-assembling component of the nanoparticles and the polymer for the ligand conjugation. $PEG_{3.5kDa}$ was chosen to provide flexibility and hydrophilicity to the targeting ligand and allow its exposure on the nanocarrier surface.

The chemical syntheses of the block copolymers used in this work are shown in Scheme 3.15.

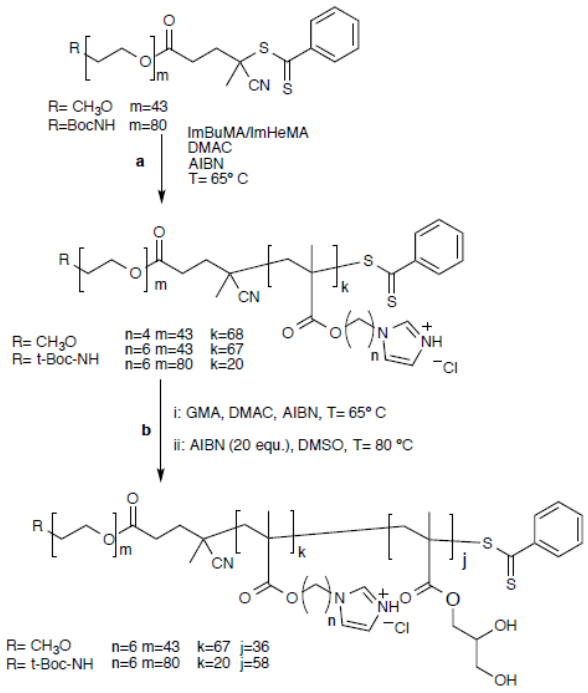

Scheme 3.15. Reagents and conditions for the syntheses of $mPEG_{1.9kDa}$-b-$[ImHeMA]_{67}$ –b-$[GMA]_{36}$ and t-Boc-NH-$PEG_{3.5kDa}$-b-$[ImHeMA]_{20}$–b-$[GMA]_{58}$ block co-polymers.

The syntheses of methoxy $PEG_{1.9kDa}$ and t-boc-NH-$PEG_{3.5kDa}$ dithiobenzoates were carried out following an adaption of the procedure reported by Yamago et al. (212) (Scheme 3.16)

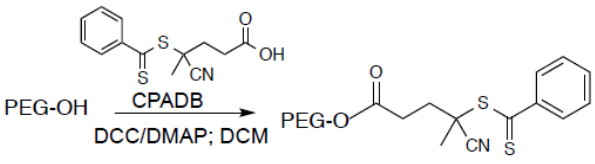

Scheme 3.16. Syntheses of $mPEG_{1.9kDa}$ and t-boc-NH-$PEG_{3.5kDa}$ dithiobenzoates; $mPEG_{1.9kDa}$-OH was dried by azeotropic distillation with toluene under reduced pressure before the reaction.

The t-boc-NH-terminated $PEG_{3.5kDa}$-OH was used to obtain a sub-family of block co-polymers with a protected amino functionality at the polymer chain-end as a chemical handle, amenable for subsequent functionalization with a targeting agent. This PEG agent was used in the reaction without further purification. Molar ratios used for reaction were: [PEG-OH]: [DCC]: [CPADB]= 1:3:3. PEG-OH terminated compounds reacted with CPADB in presence of DMAP, as catalyst, and DCC to obtain the dithiocarbonate macro-CTA at room temperature, under stirring, over 16 hours. The reaction was monitored by ^{1}H-NMR by observing the increasing of the signal corresponding to the two ester protons ($C(O)OCH_2$) at 4.26 ppm of the newly generated ester bond between PEG-OH and CPADB. The insoluble dicyclohexylurea (DCU) by-product was filtered and the polymer derivative precipitated several times in Et_2O until the complete elimination of unreacted DMAP (Scheme 3.17)

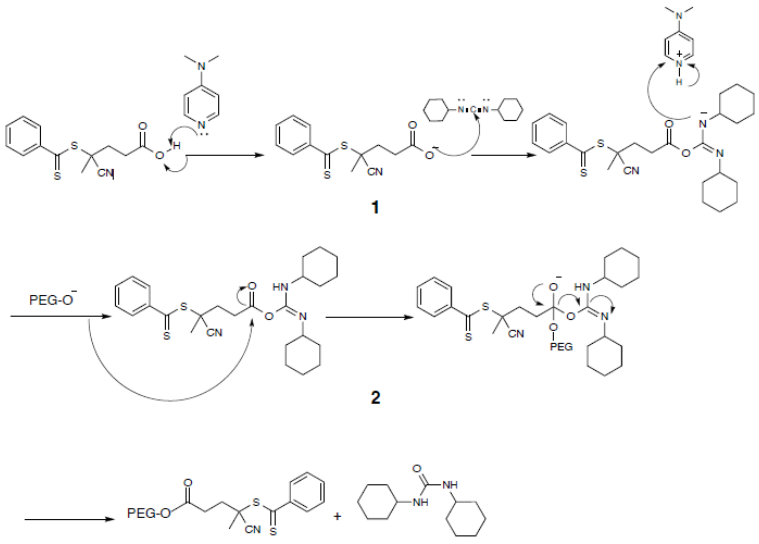

Scheme 3.17. Mechanism of the reaction to generate the PEG dithiobenzoates: 1) DMAP drives the deprotonation of CPADB, which reacts with DCC to give the reactive O-acyl isourea; 2) The binding of deprotonated PEG-OH provides the product and DCU as by-product.

The reaction is reported in the literature as "Steglich esterification" (213): the combination of DMAP, as catalyst, for carboxyl activation affords a useful method for in situ activation of the carboxylic acids for reaction with alcohols in mild conditions.

The polymerizations of all the materials were performed in DMAC as solvent and AIBN as radical initiator. Reaction conditions for the imidazolic monomers and the GMA were set-up according to the degree of polymerization (DP) required for each block to grow in

the co-polymer. Varying the ratio of ImHeMA and GMA monomers in the co-polymerizations process, it was possible to prepare different molecular masses of mPEG-block-poly(ImHeMA)-block-poly(GMA). The [PEG macro-CTA]: [AIBN] ratio was left the same in each polymerization as 1:1.

To profile the conversion rate, the reaction mixtures were monitored by ^{1}H-NMR at scheduled times.

The block co-polymers were isolated by precipitation in Et_2O/petroleum ether 1:1 several times, so residual CPADB and unreacted monomers were efficiently removed.

It has been reported (214) that the dithiobenzoate- CTA end-group confers a certain degree of toxicity to the polymers. Therefore, being the polymer intended for in in vitro/in vivo testing, the cleavage of this functional group was compulsory in order to perform further studies on these materials. The cleavage reactions were performed with an excess (1:20) of AIBN at 80 °C in DMSO for 3 hours (AIBN half time at 80ºC is 80 min) using the procedure developed by Perrier et al. (215) The block co-polymers were recovered by precipitation in THF several times. The structure of all materials was confirmed by ^{1}H-NMR spectra obtained in (D_2O).

Moreover, ^{1}H-NMR analyses, through the integral of each signal of the spectra, were used to determine the degree of polymerization (DP) of each block co-polymer synthesized and to calculate the theoretical molecular weight of each co-polymer and, therefore, the w/w% ratio of hydrophilic/hydrophobic sections (Table 3.4).

Table 3.4. Molar ratio of PEG/ ImHeMA/GMA blocks of diblock and triblock co-polymers.

Co-polymer	Final ratio[a]	M_n (theo)* (kDa)	M_n (theo)* (kDa)	M_n (theo)* (kDa)	w/w% hydrophilic	w/w% p(ImHeMA)*
$mPEG_{1900}$-b-p[ImHeMa]	44:67	2179	18291		11	89
$mPEG_{1900}$-b-p[ImHeMa]-p[GMA]	44:67:36	2179	18291	5760	30	70
t-Boc-$NHPEG_{3500}$-b-p[ImHeMa]	80:20	3779	5460		41	59
t-Boc-$NHPEG_{3500}$-b-p[ImHeMa]-p[GMA]	80:20:58	3779	5460	9280	70	30

[a] Calculated ^{1}H-NMR

*Theoretical molecular weight

Gel Permeation Chromatography (GPC) analyses to determine the molecular weight and polydispersity index (PDI) of the products were impossible to perform due, perhaps, to solubility problems of the materials in the eluents or to the polymer interactions with the GPC.

3.5.1 SYNTHESIS OF α-FOLATE-NH-PEG$_{3.5KDA}$-BLOCK-POLY[IMHEMA]$_{20}$-BLOCK-POLY[GMA]$_{58}$

t-boc-NH-PEG$_{3.5kDa}$-block-poly[ImHeMA]$_{20}$-bp[GMA]$_{58}$ was designed in order to be end functionalized with a targeting agent. Amphiphilic macromolecules bearing specific ligands conjugated to the hydrophilic polymer block end have been used as site-selective targeted nanocarriers. For example, Zhang and co-workers engineered Tet1-functionalized PEG-block-PCL polymersomes as drug delivery vehicles to the inner ear by targeting trisialoganglioside clostridial toxin (GT1b) receptors (216), while Upadhayand co-workers exploited poly(γ-benzyl L-glutamate)-block-hyaluronan polymersomes to promote intracellular uptake of doxorubicin in a murine model of Ehrlich Ascites Tumor (EAT) through CD44 receptor-mediated endocytosis (217). In few cases, efficient recognition/endocytic processes do not require high densities of ligands at the surface of drug carriers (218), and this can be advantageous when a specific ligand production is expensive (201). Furthermore, an excess of exposed ligands can negatively affect the 'stealth' properties conferred by hydrophilic polymer chains at the surface of nanoparticles and reduce the polymer flexibility and mobility. Ligand- and ligand-free block copolymers can therefore be combined in a suitable ratio to assemble nanoparticles, and in particular polymeric vesicles, and achieve the desired ligand surface density. Kokkoli and co-workers used this approach to formulate a mixture of ligand free poly(1,2-butadiene)-block-poly(ethylene oxide) with its azido-terminated analogue. The mixture spontaneously assembled in vesicle-like particles. The azide functionalities at the surface of the resulting polymersomes were then reacted with PR_b - a ligand for α5β1 integrin targeting – to provide targeted nanocarriers that were able to selectively deliver Orai3- specific siRNA to T47D breast cancer cells for tumor treatment (219).

Therefore, the chain ends of the t-Boc-protected polymer t-boc-NHPEG$_{3.5\ kDa}$-block-poly[ImHeMA]$_{20}$-block-poly[GMA]$_{58}$ were converted to a ligand-functionalized polymer, by acid hydrolysis in TFA, followed by coupling of the resulting terminal primary amine

with folic acid N-hydroxysuccinimide activated ester (Scheme 3.18). The reactions were carried out following a procedure mentioned elsewhere (194, 195).

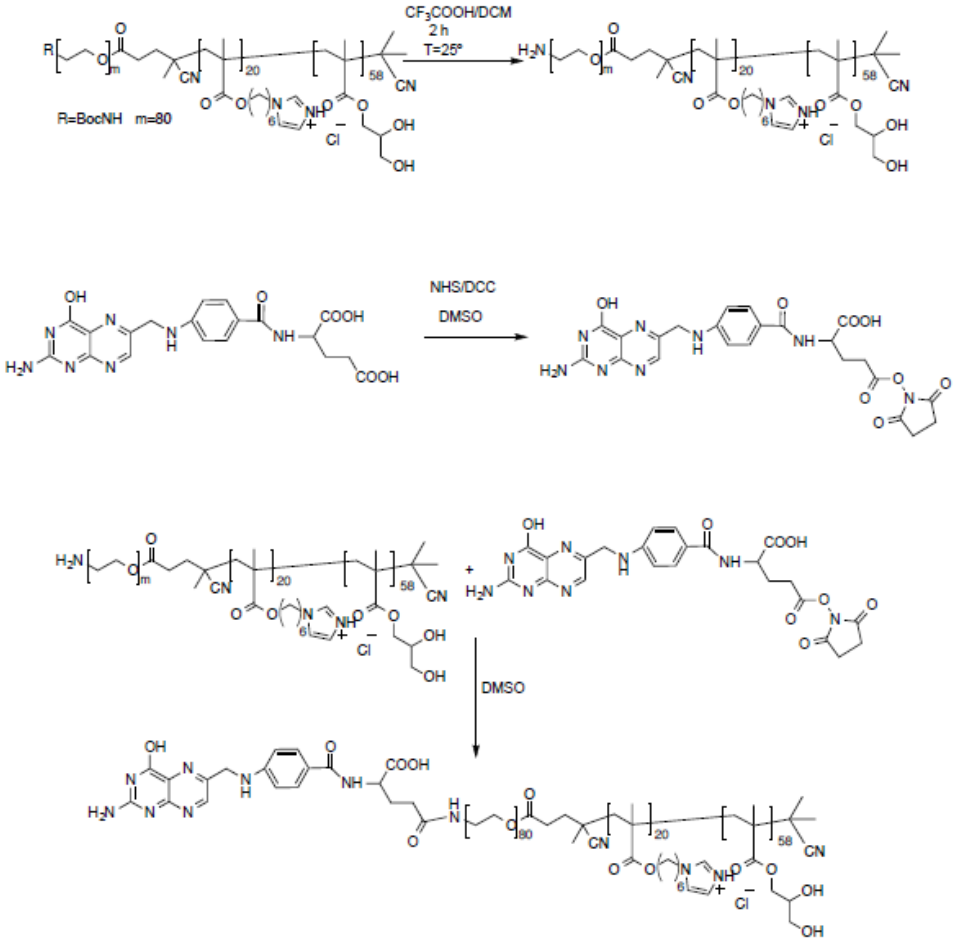

Scheme 3.18. t-boc removal and folic acid conjugation to t-boc-NH-$PEG_{3.5kDa}$-block-poly[ImHeMA]$_{20}$-block-poly[GMA]$_{58}$. Reagents and conditions: a. i) TFA/DCM 1:1 vol/vol, ambient temperature, 2 h; b. folic acid-NHS ester, DMSO, ambient temperature, 14 h.

The quantification tests by Uv-Vis spectroscopic analysis showed a conjugation yield of folic acid to the polymer of 96% and thus a 1 : 1 folate/polymer molar ratio.

The analysis of the polymer conjugate by reverse phase high-performance liquid chromatography (RP-HPLC) did not show the presence of free folic acid in the chromatogram confirming the high degree of purity of the conjugate folate-$PEG_{3.5\ kDa}$-block-poly[ImHeMA]$_{20}$-block-poly[GMA]$_{58}$.

3.6 POTENTIOMETRIC TITRATION AND TURBIDIMETRIC ASSAYS OF MPEG$_{1.9KDA}$-BLOCK-POLY[IMHEMA]$_{67}$-BLOCK-POLY[GMA]$_{36}$

In order to assess the pKa of the polymer, potentiometric acid/base titration and back titration were carried out on mPEG$_{1.9kDa}$-block-poly[ImHeMA]$_{67}$-block-poly[GMA]$_{36}$. The titration was performed by adding aliquots of 0.1 M NaOH, to a solution of the polymer at pH 3. The maximum of the first derivative titration curve allowed the calculation of the point of inflection ("equivalent point"). The "apparent" pKa were estimated as mid-points between the titration start pH and equivalence points, using the first derivatives of the titration curves to aid in measurement of equivalence points. Potentiometric titrations of mPEG$_{1.9kDa}$-block-poly[ImHeMA]$_{67}$-block-poly[GMA]$_{36}$ showed a suggested an apparent pKa of ~5.9 while the apparent pKa of diblock copolymers (1) and (2) were found to be ~7.5 and 7.8. These values should be interpreted with care as self-assembly of polymer chains and association of imidazolic units into the hydrophobic core/layer of a colloidal system devoid of water could potentially make proportion of the acid/base functionalities inaccessible for titration over the timescale of the experiment (Figure 3.11).

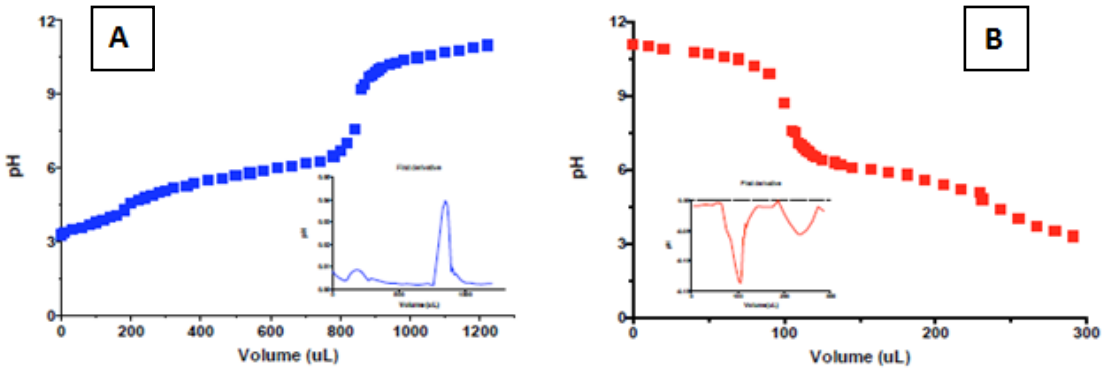

Figure 3.11. Titration (Panel A) and back titration (Panel B) of mPEG$_{1.9ka}$-b-p[ImHeMA]$_{67}$-b-p[GMA]$_{36}$. Adapted from (205) with DOI: 10.1039/c3py00744h - Reproduced by permission of the Royal Society of Chemistry.

Turbidimetric analyses were carried out to determine the cloud point of mPEG$_{1.9kDa.}$-block-poly[ImHeMA]$_{67}$-block-poly[GMA]$_{36}$. The cloud point was considered here as the pH at which the block co-polymers start to form aggregates. Turbidimetric assays were carried out by gradually increasing the pH from pH 3 of a solution of mPEG$_{1.9kDa}$-block-

poly[ImHeMA]$_{67}$-block-poly[GMA]$_{36}$ in 150 mM NaClaq. The triblock co-polymer showed a "cloud point" at ~pH 5.7 whereas the diblock co-polymers poly[GMA]-block-poly[ImHeMA] (1) and (2) exibited respectively a cloud point at ~pH 5.6 and ~pH 5.4 (Figure 3.12).

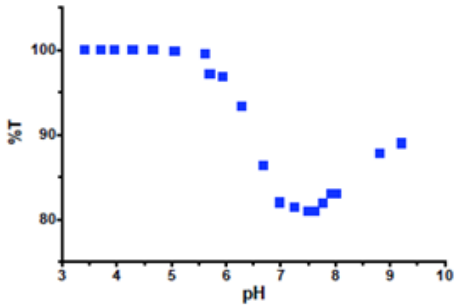

Figure 3.12. Turbidimetry titration profile of mPEG$_{1.9kDa}$-block-poly[ImHeMA]$_{67}$-block-poly[GMA]$_{36}$ showing the cloud point at ~ pH 5.7. Adapted from (205) with DOI: 10.1039/c3py00744h - Reproduced by permission of the Royal Society of Chemistry.

We observed that diblock copolymers poly[GMA]-block-poly[ImHeMA] (1) and (2), by addition of aqueous NaOH started from pH 3, was found to produce aggregates that precipitated rapidly without forming well defined particles. On the other hand, with the same procedure, the turbidimetric assays showed that the triblock copolymer mPEG$_{1.9ka}$-block-poly[ImHeMA]$_{67}$-block-poly[GMA]$_{36}$ could form nano assemblies.

To summerize, in Table 3.5 the main features of diblock polymers poly[GMA]-block-poly[ImHeMA] (1) and (2) and triblock copolymer mPEG$_{1.9kDa}$-block-poly[ImHeMA]-block-poly[GMA] are reported in order to better compare their chemico-physical behavior.

Table 3.5. Chemico-physical properties of diblock polymers poly[GMA]-block-poly[ImHeMA] (1) and (2) and triblock copolymer mPEG$_{1.9kDa}$-block-poly[ImHeMA]-block-poly[GMA

Polymers	pKa	cloud point	Hydrophilic block/polymer weight ratio %	Hydrophobic block/polymer weight ratio %	PEG/ImHeMA/GMA monomers
poly[GMA]-b-poly[ImHeMA] (1)	7.5	5.6	32	68	30/42
poly[GMA]-b-poly[ImHeMA] (2)	7.8	5.4	23	77	30/68
mPEG$_{1.9kDa}$-b-p[ImHeMA]-b-p[GMA]	5.9	5.7	32	68	44/67/36

Observing the above reported main properties of the synthesized polymers, the first difference we perceive between the diblock copolymers and the triblock copolymer is the value of the apparent pKa. Indeed, for the triblock copolymer $mPEG_{1.9kDa}$-block-poly[ImHeMA]-block-poly[GMA] pKa is lower with a value of ~5.9, compared to the diblock copolymers poly[GMA]-block-poly[ImHeMA] (1) and (2) which showed a pKa of ~7.5 and ~7.8. According to the results we obtained, it seemed that the triblock polymer that posses lower pKa could be the best candidate in order to obtain polymersomes with a response in the physiopathological pH range. However, the pKa is not the only difference between the produced copolymers. Although the w/w% ratio of hydrophilic/hydrophobic blocks of the three polymers is comparable, the disposition of the hydrophilic blocks is clearly different for the triblock copolymer. The higher weight ratio of the hydrophobic block in the diblock copolymer was expected to allow for the self assembly in vesicles (12). However, even though the diblock copolymers are soluble in acid conditions, their exposure to higher pH induces the deprotonation of the imidazole units at the pH close to the pKa value of the polymer, which induce the precipitation of the material. This behavior can be ascribed to the very high molecular weight of the hydrophobic blockwhich destabilize the whole system and does not allow the generation of vesicles. Thus ,we could assume that the presence of two hydrophilic blocks at the terminal ends of the triblock co-polymer better promote the polymer to arrange in vesicles once the environment pH is above the polymer pKa. As reported in the literature, for triblock copolymers assembled in vesicles, it was found that the polymer shorter hydrophilic block is mostly segregated to the outer surface of vesicles due to thermodynamic stabilization reasons (220); this conceivably takes place also for our triblock copolymer. On the other hand, the GMA segments are mostly segregated to the inner vesicle surface.

The information gained with the colloidal characterization studies of the triblock copolymers poly[GMA]-block-poly[ImHeMA] (1) and (2) allowed us to further synthesize triblock copolymers with physico-chemical properties and pH responsiveness suitable for the generation of performing vesicular systems as aimed in this project thesis.

3.7 BLOCK CO-POLYMERS COLLOIDAL RESPONSE TO PH ALTERATIONS

The block co-polymers, with different A, B, and C blocks alternating in hydrophilic/hydrophobic nature and block length, were intended to assemble in stable vesicular systems at neutral pH but would disassemble at lower pH (205). It was expected that these vesicles could encapsulate drug payloads while assembling and that possess the capacity to undergo pH-triggered controlled release.

The ^{1}H NMR spectrum of mPEG$_{1.9kDa}$-block-poly[ImHeMA]$_{67}$-block-poly[GMA]$_{36}$ copolymer was recorded in D_2O added of 150 mM NaCl, (conc. 1mg/mL) as shown in Figure 3.13.

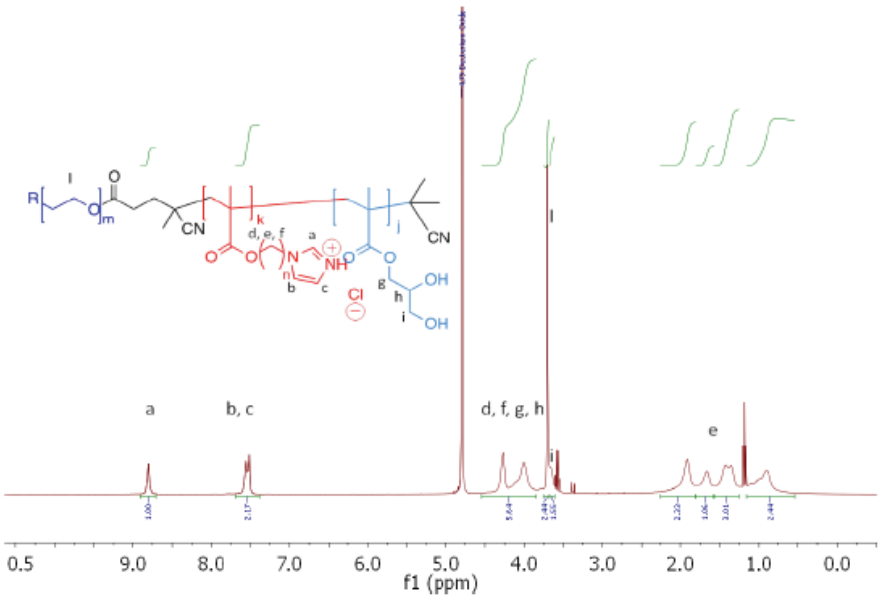

Figure 3.13. ^{1}H NMR spectrum of mPEG$_{1.9kDa}$-block-poly[ImHeMA]$_{67}$-block-poly[GMA]$_{36}$ co-polymer, 1.0 mg/mL in D_2O containing 150 mM NaCl. Traces of Et_2O from polymer precipitation are visible in the spectrum. Adapted from (205) with DOI: 10.1039/c3py00744h - Reproduced by permission of the Royal Society of Chemistry.

Self-assembly behavior of A-B-C amphiphilic triblock copolymers mPEG$_{1.9kDa}$-block-poly[ImHeMA]$_{67}$-block-poly[GMA]$_{36}$ and t-Boc-NHPEG$_{3.5kDa}$- block-poly[ImHeMA]$_{20}$-block-poly[GMA]$_{58}$ as a function of the pH was also investigated, as for the diblock co-polymer, by ^{1}H NMR and DLS. In the NMR spectrum, repeating units of ImHeMA were clearly detectable (a, b, c), indicating efficient solvation of the poly (ImHeMA) block

under these conditions. However, ^{1}H NMR analysis of mPEG$_{1.9kDa}$-block-poly[ImHeMA]$_{67}$-block-poly[GMA]$_{36}$ at different pH values revealed that, above pH 5.8, the area of the imidazole aromatic proton signals (a, b, c) ~7.9 - 9 ppm rapidly decreased, and disappeared completely at pH 7.0. This suggested that the polymer assembled into supramolecular structures wherein the poly(ImHeMA) domain was poorly solvated and therefore not visible in the ^{1}H-NMR spectra. This is consistent with a mechanism by which at pH > 5.8 corresponding to the apparent the protonated imidazole units were progressively deprotonated, loose their positive charge and converted into more hydrophobic free-base imidazole moieties, resulting in self-assembled structures as shown by the DLS analysis performed at increasing pH (Figure 3.14).

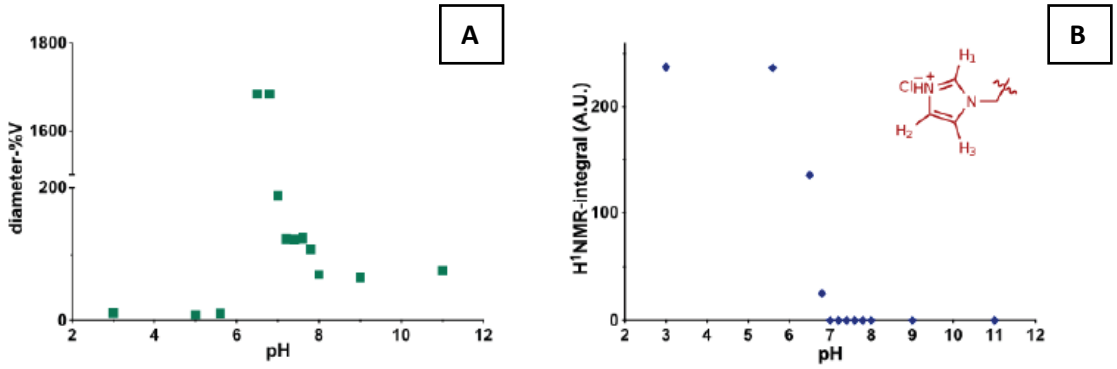

Figure 3.14. Panel A: size changes by DLS analysis of mPEG$_{1.9kDa}$-block-poly[ImHeMA]$_{67}$-block-poly[GMA]$_{36}$ co-polymer, 1 mg/mL at various pH values in D_2O, 150 mM NaCl. Panel B: Integral of H_1 proton (from C_1 of imidazole) in the pH-responsive poly[6-(1H-imidazol-1-yl)hexyl-methacrylate] block, expressed in arbitrary units, A.U.. Disappearance of the signal at pH >6.8 is indicative of the conversion of the deprotonated imidazolyl block into a poorly solvated hydrophobic core. Adapted from (205) with DOI: 10.1039/c3py00744h - Reproduced by permission of the Royal Society of Chemistry.

Dynamic light-scattering (DLS) carried out using the samples analyzed by NMR confirmed this hypothesis, showing that when the polymer solution pH increased from 3 to 5.6, the dissolved unimeric polymer chains of mPEG$_{1.9kDa}$-block-poly[ImHeMA]$_{67}$-block-poly[GMA]$_{36}$ started to aggregate, generating particles with a size of over 1 μm at pH ~ 6.5-6.8. The size sharply decreased under slightly higher conditions, reaching a stable size of ~70 nm at pH ≥ 8.0. DLS studies with mPEG$_{1.9kDa}$-block-poly[ImHeMA]$_{67}$-b-p[GMA]$_{36}$ in salt-free conditions showed a similar size trend, although the smaller aggregates (~70 nm) were observed in the 6.5-7.0 ranges with this polymer rather than at

higher pH values. Furthermore, $mPEG_{1.9kDa}$-block-$[ImHeMA]_{67}$-block-poly$[GMA]_{36}$ behavior at different pH and its stability over time was investigated by Dynamic Light Scattering analysis at 25ºC (Figure 4.13). The triblock co-polymer was dissolved in 10 mM PBS, 150 mM NaCl, and the pH was changed by adding small aliquots of 0.1 M NaOH or 0.1 M HCl. Figure 3.13 shows the results of this study. The polymer started to aggregate at pH from 5.6 and achieve a maximum at pH 6. At this pH value, big aggregates (DH~ 1 mm) were detectable in the polymer solution up to pH 6.5 (Figure 3.13, panel A). The size decreased by increasing the pH to 7.4 and 8, where smaller aggregates (DH ~ 200-250 nm) were observed. The size of $mPEG_{1.9kDa}$-block-poly$[ImHeMA]_{67}$-block-poly$[GMA]_{36}$ at all the pH conditions investigated were demonstrated to be stable over the time (Figure 3.15, panel B).

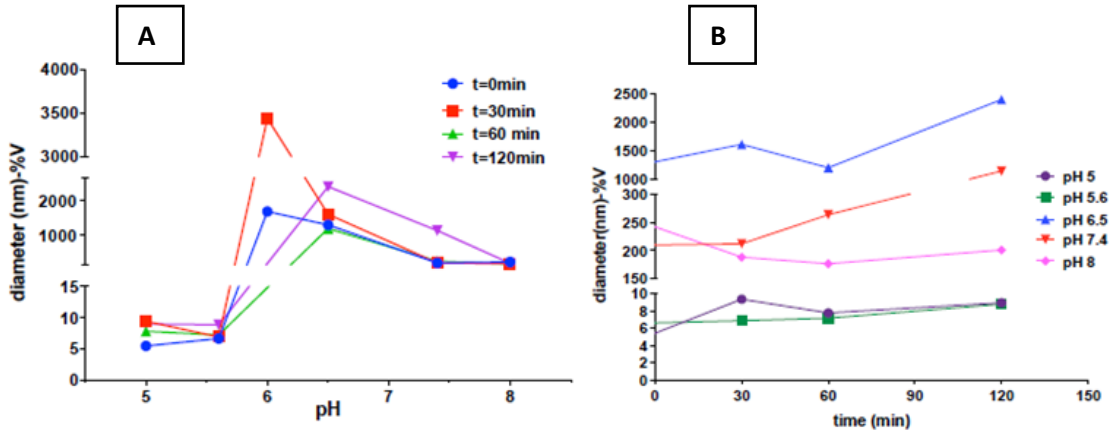

Figure 3.15. Kinetic profiles of $mPEG_{1.9kDa}$-block-poly$[ImHeMA]_{67}$-block-poly$[GMA]_{36}$ by Dynamic Light Scattering analysis at different pH, at 25ºC. Particle diameters were recorded across pH ranges at scheduled times (Panel A) and over increasing time periods at specified pH (Panel B). Adapted from (205) with DOI: 10.1039/c3py00744h - Reproduced by permission of the Royal Society of Chemistry.

The behavior of this polymer was agreed with the preliminary data found for the similar polymer poly[GMA]-block-poly[ImHeMA]-$PEG_{1.9kDa}$ reported in Table 3.3 that showed the assembly of particles with bigger size at pH 6.5 (about 200 nm), while the particles rearranged to about 50 nm when the medium pH was increased to 7.4. This behavior is very advantageous for in vivo applications. While the small particles can circulate in the blood stream at pH 7.4, they have a size that is adequate to extravasate in the tumor according to the EPR effect. The polymeric nanoparticles, however, can suddenly rearrange and increase in size at pH conditions of the tumour interstitium (pH 6.5-7), which induces the trapping of the particles after extravasation in the tumor. Since the

particles are decorated with targeting agent that stimulate the cancer cell uptake, they undergo receptor mediated endocytosis and migrate to acid cellular subcompartments such as the endosomes where the pH conditions (pH 5) induce the disassembly of the carrier and the release of the encapsulated drugs. The system disassembly at pH 5 is immediate as shown in Table 3.3 at time zero.

Under the same conditions (10 mM PBS, 150 mM NaCl) t-Boc-NHPEG$_{3.5kDa}$-block-poly[ImHeMA]$_{20}$-block-poly[GMA]$_{58}$ behaviour was also investigated by DLS. This co-polymer features a shorter hydrophobic p(ImHeMA) central block with respect to the above discussed mPEG$_{1.9kDa}$-block-poly[ImHeMA]$_{67}$-block-poly[GMA]$_{36}$, thus a slightly different behavior was expected. This polymer showed a very similar colloidal response to pH changes with respect to the previously discussed triblock but arranged in big aggregates at lower pH (pH 5). Thus, the different aggregation behavior to pH alterations was ascribed to the higher weight ratio of the hydrophilic blocks of t-boc-NHPEG$_{3.5kDa}$-block-poly[ImHeMA]$_{20}$-block-poly[GMA]$_{58}$ (70%) with respect to the mPEG$_{1.9kDa}$-block-poly[ImHeMA]$_{67}$-block-poly[GMA]$_{36}$ whose hydrophilic blocks weigh ratio is only 30%. Furthermore, the t-Boc terminating polymer generates smaller aggregates of only ~13 nm at pH 8.0 (Figure 3.14, panel A), which were stable over time (Figure 3.16, panel B).

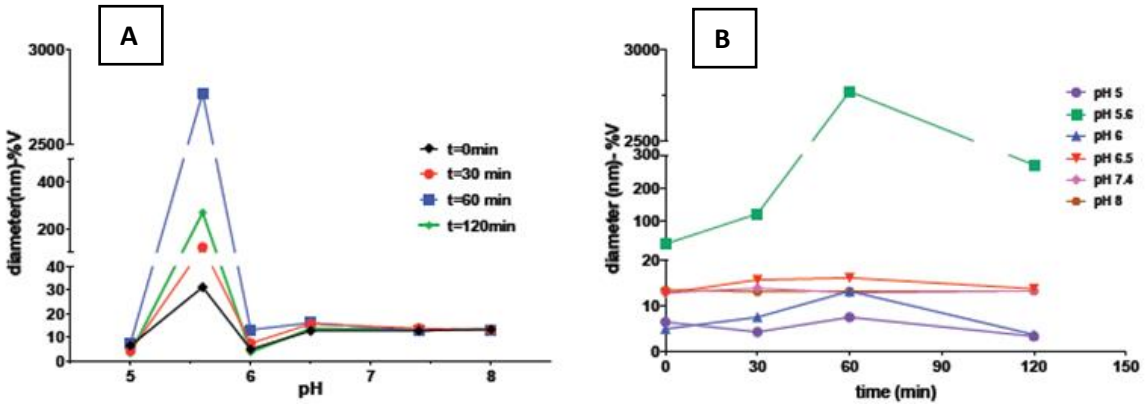

Figure 3.16. Kinetic stability profiles of t-boc-NH-PEG$_{3.5kDa}$-block-[ImHeMA]$_{20}$-block-poly[GMA]$_{58}$ by Dynamic Light Scattering analysis at different pH, at 25ºC. Particle diameters were recorded across pH ranges at scheduled times (Panel A) and over increasing time at a chosen pH condition (Panel B). Adapted from (205) with DOI: 10.1039/c3py00744h - Reproduced by permission of the Royal Society of Chemistry.

Dynamic light-scattering results were in agreement with the ^{1}H-NMR study performed over different pH conditions (Figure 3.17). ^{1}HNMR confirmed the arrangement of the polymer formation of the aggregates.

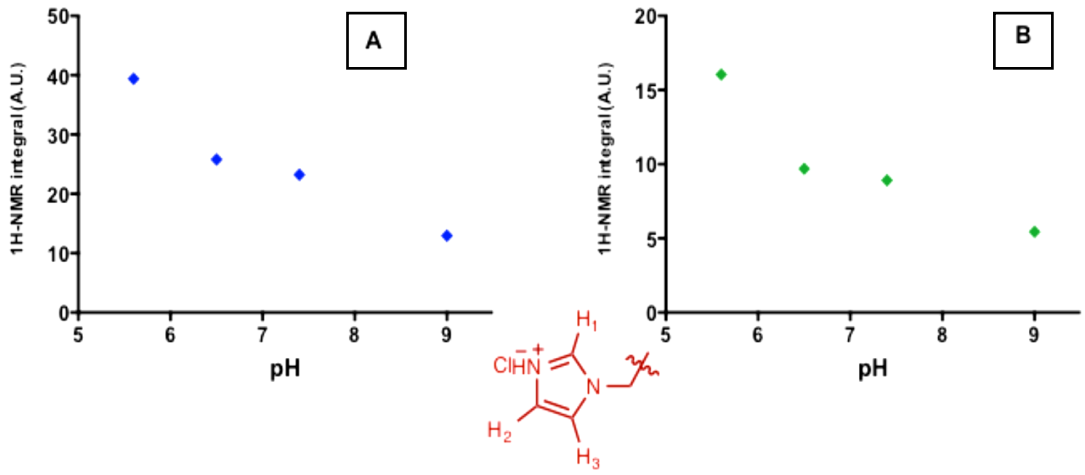

Figure 3.17. ^{1}H-NMR integral profile of aromatic protons, expressed in arbitrary units, A.U., of the imidazole moiety in the central block of t-Boc-NH-PEG$_{3.5kDa}$-block-[ImHeMA]$_{20}$-block-poly[GMA]$_{58}$ at different pH conditions. Panel A: protons analyzed in the "low field" range of the spectra (H_2-H_3 corresponding to C_2 and C_3 of imidazole). Panel B: protons in the "high field" of the spectra (H_1 corresponding to C_1 of imidazole).

3.8 CRITICAL AGGREGATION CONCENTRATION OF MPEG$_{1.9KDA}$-BLOCK-POLY[IMHEMA]$_{67}$-BLOCK-POLY[GMA]$_{36}$

The mPEG$_{1.9kDa}$-block-poly[ImHeMA]$_{67}$-block-poly[GMA]$_{36}$ was designed as amphiphilic block-copolymer to assemble polymeric vesicles for drug delivery purposes. According to previously reported studies for similar materials (12), it was expected that the hydrophilic blocks of the co-polymer (mPEG$_{1.9\ kDa}$ and poly(GMA block) participate to the inner and the outer face of the polymeric vesicles, and provide for stealth hydrated surfaces, whereas the hydrophobic poly(ImHeMA) block assembles to form the vesicle water free membrane core. The ability of the mPEG$_{1.9kDa}$-block-poly[ImHeMA]$_{67}$-block-poly[GMA]$_{36}$ co-polymer to self-assemble in aqueous physiological conditions (pH 7.4, 37 ºC) was investigated by the estimating the critical aggregation concentration (CAC). The experiment was performed as reported in section 2.3.6, following the procedure described by Kwon et al.(221). The triblock co-polymer was solubilized in 20 mM

phosphate buffer, 150 mM NaCl, at pH 4, and induced to assemble by the 'pH-switch' method (166, 198) at pH 7.4. Then, the dispersion was further diluted in phosphate buffer at pH 7.4, yielding different polymer concentrations. Pyrene was used as fluorescent probe. The CAC of co-polymer $mPEG_{1.9kDa}$-block-poly$[ImHeMA]_{67}$-b-p$[GMA]_{36}$ was estimated by spectrofluorimetry to be 21 µg/mL. (Figure 3.18).

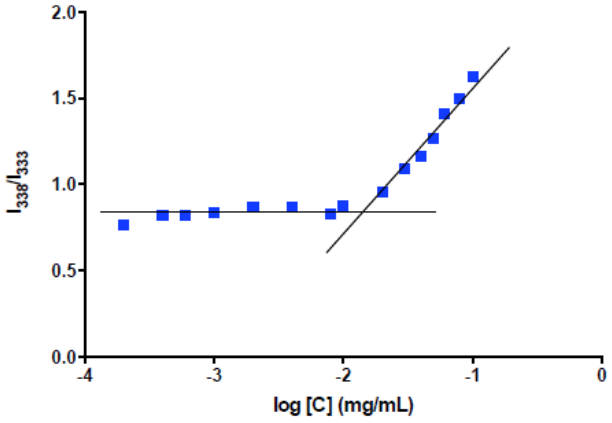

Figure 3.18. Pyrene emission intensity profile as a function of $mPEG_{1.9kDa}$-block-poly$[ImHeMA]_{67}$-b-p$[GMA]_{36}$ concentration. The net increase in fluorescence emission derived from the intercept of the two segments represent the CAC. Adapted from (205) with DOI: 10.1039/c3py00744h - Reproduced by permission of the Royal Society of Chemistry.3.9 Physical characterization of polymersome formulations.

Polymersomes were assembled with $mPEG_{1.9kDa}$-block-poly$[ImHeMA]_{67}$-block-poly$[GMA]_{36}$ at 1 mg/mL polymer concentration according to the "pH-switch" technique reported in chapter 2.3.3. The size distribution of the polymerosomes in physiological conditions was assessed by DLS above the CAC. As it is shown in Figure 3.19, the triblock co-polymer assembled into colloidal systems with DH ~130 nm. The polymersomes resulted stable at 25°C for about 24 hours which confirmed the results reported in chapter 3.4 (See Figure 3.9); the size only increased of about 10 nm. On the contrary, when vesicles were incubated at body temperature (37 °C) and monitored over time, they underwent instability phenomena and slight aggregation. After 90 minutes of incubation at 37°C, vesicle sizes were 400 nm, ~ 650 nm after 270 minutes and almost the same size after 24 hours, and showed also few bigger aggregates.

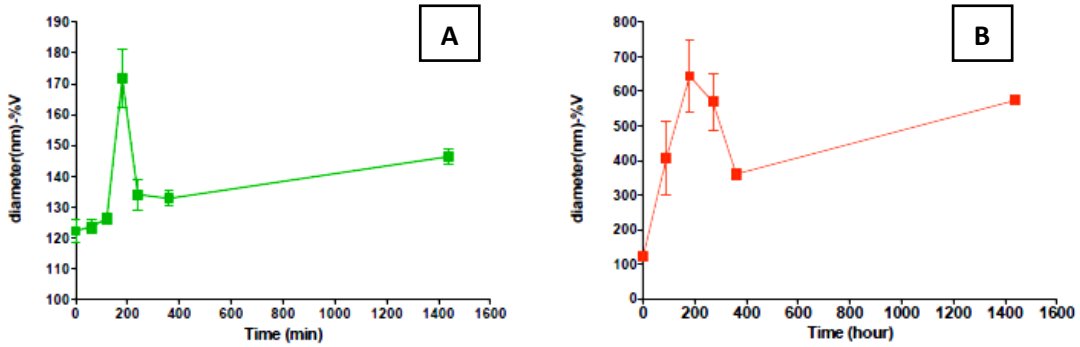

Figure 3.19. Kinetic stability profile of particles assembled with $mPEG_{1.9kDa}$-block-poly $[ImHeMA]_{67}$-block-poly$[GMA]_{36}$ by Dynamic Light Scattering at pH 7.4, at 25ºC (Panel A) and at 37ºC (Panel B).

This result was attributed to the short $mPEG_{1.9\ kDa}$ chains of the copolymer, which may be not adequate to generate a sufficiently stable hydrophilic coating on the top of the vesicles or may provoque an imbalanced hydrophilic/hydrophobic ratio within the co-polymer that was not suitable to guarantee the stability of the particles. Therefore, in order to stabilize the nanoparticles, vesicle formulations were prepared by mixing different weight ratio of $mPEG_{1.9kDa}$-block-poly$[ImHeMA]_{67}$-block-poly$[GMA]_{36}$ and t-boc-$NHPEG_{3.5kDa}$-block-poly$[ImHeMA]_{20}$-block-poly$[GMA]_{58}$. Three different formulations were prepared. In a preliminary screening, formulations assembled with $mPEG_{1.9kDa}$-block-poly$[ImHeMA]_{67}$-block-poly$[GMA]_{36}$/t-boc-NH-$PEG_{3.5kDa}$-block-poly$[ImHeMA]_{20}$-block-poly$[GMA]_{58}$ (1 mg/mL) at 99:1, 95:5 and 90:10 w/w% ratios were found to possess mean diameters of 165 ± 6, 162 ± 4 and 119 ± 2 nm, respectively at 25°C. (See Table 3.6). The analysis showed that the incorporation of the t- boc-NH-$PEG_{3,5kDa}$-b-p$[ImHeMA]_{20}$-b-p$[GMA]_{58}$ copolymer did not affect the size of the vesicles.

Table 3.6. Mean size of polymersomes obtained with different $mPEG_{1.9kDa}$-block-poly$[ImHeMA]_{67}$-block-poly$[GMA]_{36}$/t-boc-NH-$PEG_{3.5kDa}$-block-poly$[ImHeMA]_{20}$-block-poly$[GMA]_{58}$ (w/w %). The analisys was performed with freshly prepared polymersome (time = 0).

$mPEG_{1.9kDa}$-b-p$[ImHeMA]_{67}$-b-p$[GMA]_{36}$/t-Boc-NH-$PEG_{3.5kDa}$-b-p$[ImHeMA]_{20}$-b-p$[GMA]_{58}$ w/w%	**D_H (nm) - %V**
1%	165 ± 6
5%	162 ± 4
10%	119 ± 2

Particle charges were evaluated by Zeta potential (ζ) measurements. The vesicle formulations were diluted 10 times in mQ water at 25°C prior to the analysis. The z-potential profile of the three formulations was neutral (Figure 3.20). This result is rather expected since at pH 7.4 of the water (with 10% saline buffer) the poly-imidazolic block of the co-polymers result mostly deprotonated and thus devoid of charge. Moreover, the PEG chains or the GMA exposed on the surface would be expected to form a hydrophilic corona and PEG/p(GMA) are neutral blocks that shield the few charges associated with the hydrophobic membrane core.

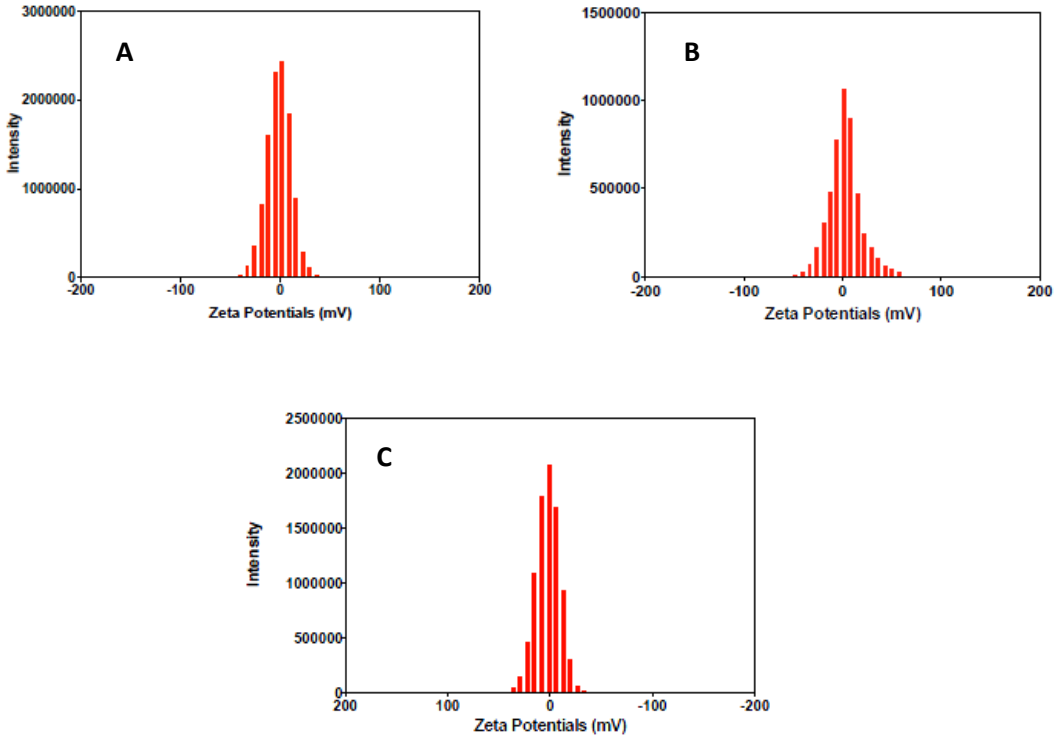

Figure 3.20. z-potential of vesicle formulations obtained with different $mPEG_{1900}$-block-poly[ImHeMA]$_{67}$-block-poly[GMA]$_{36}$/t-Boc-NH-PEG_{3500}-block-poly[ImHeMA]$_{20}$-block-poly [GMA]$_{58}$ w/w % ratios: 99:1:0 (panel A); 95:5:0 (panel B); 90:10:0 (panel C). Adapted from (205) with DOI: 10.1039/c3py00744h - Reproduced by permission of the Royal Society of Chemistry.

Incubation at 37 °C for 5 hours showed that the formulation obtained with 90:10 w/w % of $mPEG_{1900}$-block-poly[ImHeMA]$_{67}$-block-poly[GMA]$_{36}$ / t-boc-NH-PEG_{3500}-block-poly[ImHeMA]$_{20}$-block-poly[GMA]$_{58}$ was the most stable, with virtually no change in

particle size over time, whereas the 99:1 and 95:5 w/w% samples showed a 2-fold increase in size, as reported in Figure 3.21.

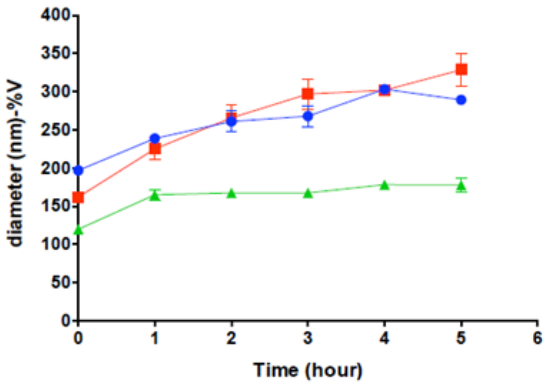

Figure 3.21. Kinetic stability profile of $mPEG_{1.9kDa}$-block-poly[ImHeMA]$_{67}$-block-poly[GMA]$_{36}$/t-Boc-NHPEG$_{3.5kDa}$-block-poly[ImHeMA]$_{20}$-b-p[GMA]$_{58}$ polymersomes at 37°C and increasing weight percentage of the t-BOC terminating polymer: 1% (●), 5% (■), 10% (▲). Adapted from (205) with DOI: 10.1039/c3py00744h - Reproduced by permission of the Royal Society of Chemistry.

Hence the presence of 10 % w/w t-boc-NH-PEG$_{3.5kDa}$-block-poly[ImHeMA]$_{20}$-block-poly[GMA]$_{58}$ was beneficial for the stability of the polymersomes over time. This was ascribed to the generation of a thicker, more flexibles hydrophilic coating on top pf the polymeric vesicles due to both longher PEG and poly-GMA blocks in the t-BOC terminating polymer compared to $mPEG_{1.9kDa}$-block-poly[ImHeMA]$_{67}$-block-poly[GMA]$_{36}$. It is reported in the literature that PEG and hydrophilic polymer coating of liposomes greatly enhance the colloidal formulation stability of this carrier and avoid the vesicle aggregation (222, 223). As is possible to imagine, it can be generalized that the same concept apply also to polymeric vesicles that possess structurally resembling features of the liposomes.

Consequently, the same formulation was tested by DLS in 20 mM phosphate, 150 mM NaCl at pH 7.4 in the presence of 10% of fetal bovin serum at 37°C to mimic a more physiological environment that plein saline buffer. These conditions will also be exploited further studies in vitro on cancer cells. Figure 3.22 display the kinetic stability profile of the polymersome suspension under these conditions.

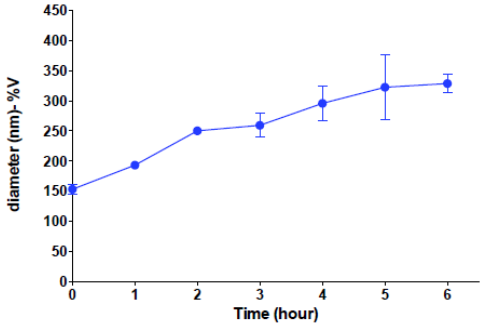

Figure 3.22. Kinetic stability profile of polymersomes obtained with 90:10 w/w% $mPEG_{1900}$-block-poly[ImHeMA]$_{67}$-block-poly[GMA]$_{36}$/t-Boc-NH-PEG_{3500}-block-poly[ImHeMA]$_{20}$-block-poly[GMA]$_{58}$ at 37 °C in saline buffer, pH 7.4, in the presence of 10% fetal bovin serum. Adapted from (205) with DOI: 10.1039/c3py00744h - Reproduced by permission of the Royal Society of Chemistry.

The formulation was stable for about 6 hours, presenting a negligible variation of the PDI. The mild size increase was only partially attributed to a rearrangement of block co-polymers at 37°C. As seen in the test performed withut serum, the vesicle formulation obtained with 90:10 w/w% $mPEG_{1900}$-block-poly[ImHeMA]$_{67}$-block-poly[GMA]$_{36}$/t-boc-NH-PEG_{3500}-block-poly[ImHeMA]$_{20}$-block-poly[GMA]$_{58}$ was rather stable. The size increase can be due to a limited adsorption of proteins on the vesicles surface or to the rearrangement of the polymer conformation in the presence of serum protein that traduce in a limited morphological change of the polymersomes. However, a stability of about 6-8 hours is desirable for in vivo applications, since a blood circulation time of about 6 hours is considered ideal for tumor accumulation (218).

α-Folate-$PEG_{3.5kDa}$-block-(ImHeMA)$_{20}$-block-(GMA)$_{58}$ was used to prepare folate-targeted polymeric dispersions. In order to set up a stable polymersome formulation, three different formulations of the triblock co-polymers were prepared in 20 mM phosphate, 150 mM NaCl, pH 7.4 to generate the targeted vesicles: 90:10 w/w% of $mPEG_{1.9kDa}$-block-poly[ImHeMA]$_{67}$-block-poly[GMA]$_{36}$ / α- folate-$PEG_{3.5kDa}$-block-poly[ImHeMA]$_{20}$-block-poly[GMA]$_{58}$, 90:5:5 w/w% $mPEG_{1.9kDa}$-block-poly[ImHeMA]$_{67}$-block-poly[GMA]$_{36}$/t-boc-NH-$PEG_{3.5kda}$-block-poly[ImHeMA]$_{20}$-block-poly[GMA]$_{58}$/ α-folate-PEG_{3500}-block-poly[ImHeMA]$_{20}$-block-poly[GMA]$_{58}$ and 90:10

polymers $mPEG_{1.9kDa}$-block-poly[ImHeMA]$_{67}$-block-poly[GMA]$_{36}$ / t-boc-NH-$PEG_{3.5kDa}$-block-poly[ImHeMA]$_{20}$-block-poly[GMA]$_{58}$). The different ratios were chosen on the basis of the previous results obtained with the different $mPEG_{1.9kDa}$-block-poly[ImHeMA]$_{67}$-block-poly[GMA]$_{36}$/t-Boc-NH-$PEG_{3.5kDa}$-block-poly[ImHeMA]$_{20}$-block-[GMA]$_{58}$ mixtures and that have shown how a 10 w/w% of the more hydrophilic polymer t-Boc-NH-$PEG_{3.5kDa}$-block-poly[ImHeMA]$_{20}$-block-[GMA]$_{58}$ generated vesicles with higher stability. The folate targeted formulations were compared for stability to the non-targeted formulation assembled with 90:10 w/w% of $mPEG_{1.9kDa}$-block-poly[ImHeMA]$_{67}$-block-poly[GMA]$_{36}$/t-Boc-NH-$PEG_{3.5kDa}$-block-poly[ImHeMA]$_{20}$-block-poly[GMA]$_{58}$ already discussed above for stability at 25°C (see Figure 3.21 for results). The samples were incubated at 37 °C and analysed by dynamic light scattering at scheduled times (Figure 3.23).

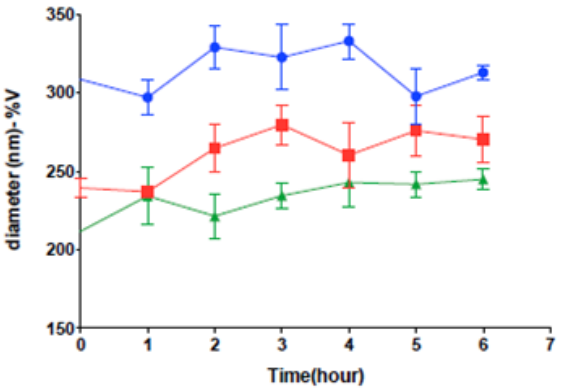

Figure 3.23. Kinetic stability profile of polymersomes obtained with 90:10 w/w% $mPEG_{1.9kDa}$-block-poly[ImHeMA]$_{67}$-block-poly[GMA]$_{36}$ / α-folate-$PEG_{3.5kDa}$-block-poly[ImHeMA]$_{20}$-block-poly[GMA]$_{58}$ (●), 90:5:5 w/w% $mPEG_{1.9kDa}$-block-poly[ImHeMA]$_{67}$-block-poly[GMA]$_{36}$/t-boc-NH-$PEG_{3.5kDa}$-block-poly[ImHeMA]$_{20}$-block-poly[GMA]$_{58}$ / α-folate-$PEG_{3.5kDa}$-block-poly[ImHeMA]$_{20}$-block-poly[GMA]$_{58}$ (■) and 90:10 w/w% $mPEG_{1.9kDa}$-block-poly[ImHeMA]$_{67}$-block-poly[GMA]$_{36}$/t-boc-NH-$PEG_{3.5kDa}$-block-poly[ImHeMA]$_{20}$-block-poly[GMA]$_{58}$ (▲) at 37°C. Adapted from (205) with DOI: 10.1039/c3py00744h - Reproduced by permission of the Royal Society of Chemistry.

This experiments showed that the non targeted 90:10 w/w% $mPEG_{1.9kDa}$-block-poly[ImHeMA]$_{67}$-block-poly[GMA]$_{36}$ / t-boc-NH-$PEG_{3.5kDa}$-block-poly[ImHeMA]$_{20}$-block-poly[GMA]$_{58}$ polymersomes were stabele over time even at 37°C. On the contrary, the presence of the folate on the vesicle surface induces the instantaneous rearrangement of the vesicles to particles with bigger size with respect to the folate-free formulation.

This can be ascribed to, at least in part, the hydrophobization of the vesicle surface by the exposure of the folate that is a vitamin with low water solubility. However, for this formulation, the particle size was not found to increase over time, which shows how the enlargement induced by the folate is rather limited and the flexibility of the PEG coating can control the particle aggregation. The formulation obtained with the 90:5:5 w/w% of polymers $mPEG_{1.9kDa}$-block-poly[ImHeMA]$_{67}$-block-poly[GMA]$_{36}$/t-boc-NH-$PEG_{3.5kDa}$-block-poly[ImHeMA]$_{20}$-block-poly[GMA]$_{58}$ / α-folate-$PEG_{3.5kDa}$-block-poly[ImHeMA]$_{20}$-block-poly[GMA]$_{58}$ lead to the smallest polymersomes. The size and kinetic stability profile of this formulation overlap the profiles of the non targeted polymersomes obtained with the 90:10 w/w% $mPEG_{1900}$-block-poly[ImHeMA]$_{67}$-block-poly[GMA]$_{36}$/t-boc-NH-$PEG_{3.5kDa}$-block-poly[ImHeMA]$_{20}$-block-poly[GMA]$_{58}$ showing that the presence of the t-boc terminating co-polymer, in virtue of its hidrophylic character, can counterbalance the particle enlargement tendency due to the folate. Therefore, the stability of this formulation was also tested in 20 mM phosphate, 150 mM NaCl at pH 7.4 in the presence of 10 v/v% of fetal bovine serum at 37 °C by DLS. Figure 3.24 shows the kinetic stability profile of the assembly obtained with 90:5:5 w/w % of $mPEG_{1.9kDa}$-block-poly[ImHeMA]$_{67}$-block-poly[GMA]$_{36}$ / t-boc-NH-$PEG_{3.5kDa}$-block-poly[ImHeMA]$_{20}$-block-poly[GMA]$_{58}$/α-folate-PEG_{3500}-block-poly[ImHeMA]$_{20}$-block-poly[GMA]$_{58}$ under this condition.

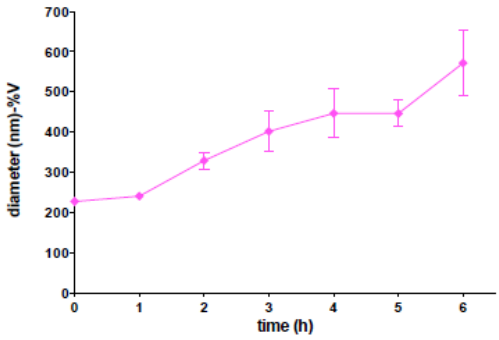

Figure 3.24. Kinetic stability profile at 37 °C in 10% serum of polymersomes obtained with 90:5:5 w/w% of $mPEG_{1.9kDa}$-block-poly[ImHeMA]$_{67}$-block-poly[GMA]$_{36}$/t-boc-NH-$PEG_{3.5kDa}$-block-poly[ImHeMA]$_{20}$-block-poly[GMA]$_{58}$/α-folate-$PEG_{3.5kDa}$-block-poly[ImHeMA]$_{20}$-block-poly[GMA]$_{58}$. Adapted from (205) with DOI: 10.1039/c3py00744h - Reproduced by permission of the Royal Society of Chemistry.

Similarly to what was found for the non targeted polymersomes containing 10 w/w% of t-boc-NH-$PEG_{3.5kDa}$-block-poly[$ImHeMA]_{20}$-block-poly[$GMA]_{58}$ (Figure Figure 3.22), the presence of the serum induces a comparable size increase of the targeted polymersome formulation over time that can be ascribed to a slow rearrangement of the polymer chain conformation in the presence of serum protein induced by the unspecific interaction of the polymer chains with the serum proteins.

3.10 ENCAPSULATION OF FLUORESCENT PROBES AND POLYMERSOMES LABELLING

The ability of the newly-synthesised block copolymers to spontaneously and reversibly assemble into colloidal particles over physiologic pH ranges was encouranging for the encapsulation of these systems with small drugs and oligonucleotides for tumour targeting.

With the aim of tracking the polymersomes in vitro studies, we first investigated the loading capacity of the vesicles generated in this work with model fluorescent probes with different chemical features. At this aim we chose a hydrophilic probe, namely 5(6)carboxyfluorescein, that may dispose in the aqueous core of the vesicles, and a hydrophobic alkylated molecule, namely N-(fluorescein-5- thiocarbamoyl)-1,2-dihexadecanoyl-sn-glycero-3-phospho-ethanolamine, triethyl-ammonium salt (fluorescein-DHPE), that may be associated in the hydrophobic shell core of the polymeric vesicles. Scheme 3.19 shows the chemical structures of the two fluorescent probes. Besides acting as fluorescent tags to label the polymersomes, these two molecules can also provide information on the capacity of polymersomes to load small model molecules with specific hydrophilic or hydrophobic properties. The two probes were tested with polymersomes assembled with 90:10 w/w% of $mPEG_{1.9kDa}$-block-poly[$ImHeMA]_{67}$-block-poly[$GMA]_{36}$ / t-boc-NH-$PEG_{3.5kDa}$-block-poly[$ImHeMA]_{20}$-block-poly[$GMA]_{58}$ mixture and the loading capacity (% LC) and encapsulation efficiency (% EE) were investigated.

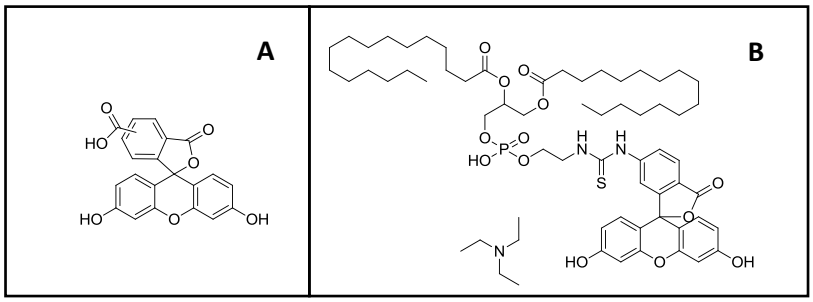

Scheme 3.19. Chemical structure of 5(6)carboxyfluorescein (A) and N-(fluorescein-5-thiocarbamoyl)-1,2-dihexadecanoyl-sn-glycero-3-phosphoethanol-amine, triethylammonium salt (fluorescein-DHPE, B).

The polymersome were induced to assemble by the "pH-switch" method and excess of non-loaded fluorescent labels was removed by extensive dialysis. The probe loaded polymersomes were analyzed by spectrofluorimetry to quantify fluoresceine. The analysis indicated a Loading Capacity (LC% = weight of loaded fluorophore / weight of polymer %) of 6.4 and 0.05 w/w% for fluorescein-DHPE and 5(6)-carboxyfluorescein, respectively. The Encapsulation Efficiency (EC%= loaded fluorophore /initial fluorophore concentration) was found to be 45.8 and 0.01 mol/mol% for Fluorescein-DHPE and 5(6) carboxyfluorescein, respectively. Fluorescein-DHPE displayed very high values for both the LC% and EC% with respect to the 5(6) carboxyfluorescein, which demonstrates that the phospholipid moiety of this fluorophore participated as an anchoring agent to the polymersomes external shell. The carboxyfluorescein was instead only marginally encapsulated in the aqueous core of the vesicle despite it was processed with the polymer at high concentration. However, it should also be mentioned that the low EC% of the 5(6) carboxyfluorescein was rather expected as consequence of the high concentration of this probe used in the polymersome assembly process.

This result also shows that, despite the anionic character of the 5(6) carboxyfluorescein that should promote its association to the imidazole containing blocks of the co-polymer at pH 5 and then its encapsulation in the assembled vesicles, the loading strategy is not adequate for this small molecule or the molecule is not sufficiently retained within the polymersome aqueous core. Further studies are required to assess the permeability of the vesicle polymeric shell to small molecule.

3.11 OLIGONUCLEOTIDE LOADING STUDIES

3.11.1 ELECTROPHORETIC MOBILITY SHIFT ASSAY

In order to investigate if the pH responsive triblock co-polymers selected for the assembly of the vesicles can associate with double strand siRNA by ionic interaction and if the association is affected by the pH conditions, a dsDNA 19-nucleotides model sequence was used. dsDNA was expected to display very similar physico-chemical properties as ds-siRNA but did not require formulation under rigorously RNAse-free conditions. dsDNA sequence underwent electrophoretic chromatography in the presence of increasing ratio of $mPEG_{1.9kDa}$-block-poly[ImHeMA]$_{67}$-block-poly[GMA]$_{36}$ at pH 5 mimicking the endosomal environment and at pH 7.4 mimicking the blood.

The Electrophoretic Mobility Shift Assay can also provide information about the stability of the DNA/polymer complexes and the extent of DNA/polymer dissociation. A polyacrylamide vertical gel with a reticulation degree (concentration of acrylamide/bis-acrylamide) of 12% w/v was used for this purpose to run the dsDNA polymer mixtures. The samples were prepared in citrate buffer at pH 5 using different N/P feed ratios (from 0.1:1 to 1:20 N/P molar ratios and the gel was run at pH 5 (citrate buffer) and at pH 7.4 (phosphate buffer). Figure 3.25 shows the electrophoretic profiles of the gels.

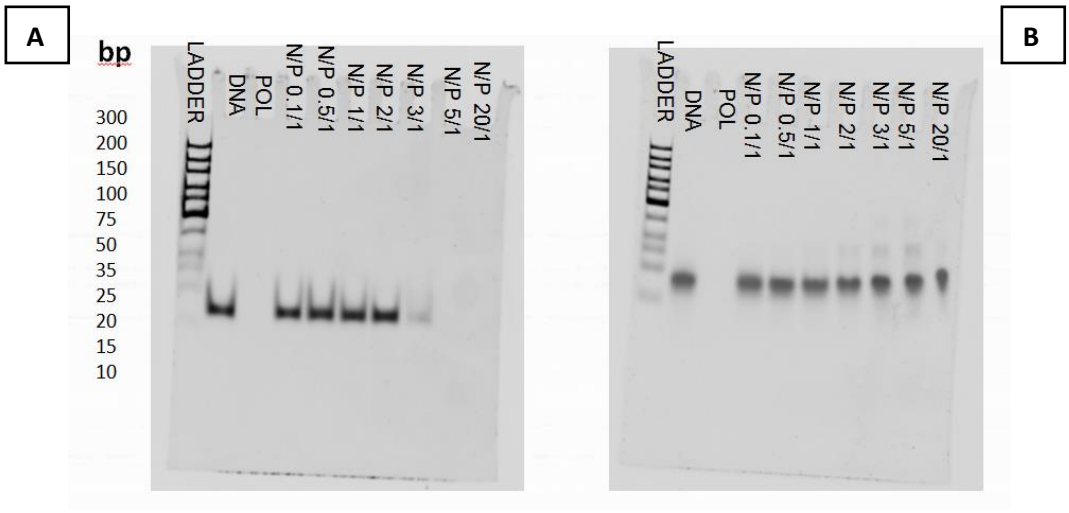

Figure 3.25. Electrophoretic Mobility profiles of dsDNA in the presence of $mPEG_{1.9kDa}$-block-poly[ImHeMA]$_{67}$ block-poly[GMA]$_{36}$ at pH 5 (Panel A) and pH 7.4 (Panel B).

At pH 5, the electophoretic migration do dsDNA shows that for low N/P feed ratios the dsDNA migrate along the gel, which confirms that for these feed ratios the polymer was not sufficient to complex the dsDNA. On the contrary, for N/P feed ratios above 2:1, the dsDNA is completely retained by the polymer and does not migrates along the gel, which confirms that for these feed ratios the polymer has sufficient positive charges to complex the DNA. The dsDNA retained by the polymer is thus retarded at the loading site where it is not detectable because many dsDNA/polymer complexes do not stain using GelRed™ Nucleic Acid Gel Stain (224) (Figure 3.28, panel A). Thus the poly-imidazol block, being the pH responsive component of the polymer, in virtue of its protonation at low pH, generate a polycationic block that is able to associate with dsDNA by charge charge interaction. This is expected to help the loading of dsDNA and ds-siRNA according to the assembly protocol through the "pH-shift".

At pH 7.4, the co-polymer is devoid of most of its charges according to the apparent pKa of the polymer (see chapter 3.6), and the dsDNA migrates along the gel regardless of the N/P feed ratio (Figure 3.28, panel B). This is ascribable to a net lower capacity of the polymer to complex the dsDNA and to retain the polyanionic macromolecule.

Overall, the retardation assay confirmed the capacity of the $mPEG_{1900}$-block-poly[ImHeMA]$_{67}$-block-poly[GMA]$_{36}$ co-polymer to complex the dsDNA at acid conditions, when it is fully protonated.

3.11.2 POLYMERSOME DNA LOADING

A short dsDNA 19-nucleotides was used as model oligonucleotide. $mPEG_{1.9kDa}$-block-poly[ImHeMA]$_{67}$-block-poly[GMA]$_{36}$ / t-boc-NH-$PEG_{3.5kDa}$-block-poly[ImHeMA]$_{20}$-block-poly[GMA]$_{58}$ were dissolved at a 90:10 weight ratio in buffer at pH 5, then dsDNA was added to achieve a 1:1 N/P feed ratio and the pH was raised to 7.4. Unentrapped oligonucleotide was removed by dialysis against PBS pH 7.4.

Firstly, the loading of the dsDNA was proved by inducing the dissociation of the colloidal aggregates at pH 5, and quantifying the encapsulated dsDNA with UV-Vis analysis. In this conditions the UV-Vis absorbance of the polymers was negligiable. The analysis showed a loading capacity (LC) of 14% mol/mol (mol of dsDNA/ mol of polymer chain), corresponding to 7 w/w%. Due to the relatively high encapsulation efficiency, we have

speculated that the dsDNA is not just encapsulated in a discrete "water pool" inside the polymeric vesicle (which would have yielded a lower LC due to the low concentration of the dsDNA in the loading medium), but was, at least partially, complexed with the polymer by electrostatic interactions, which drove the encapsulation of the polyanionic macromolecule.

DLS analysis proved the formation of colloidal aggregates with a mean size of 123 ± 11 nm and a PDI = 0.276, whilst the absence of smaller assemblies ascribable to the dsDNA (about 60 nm mean diameter) confirmed the total removal of free dsDNA (Figure 3.26).

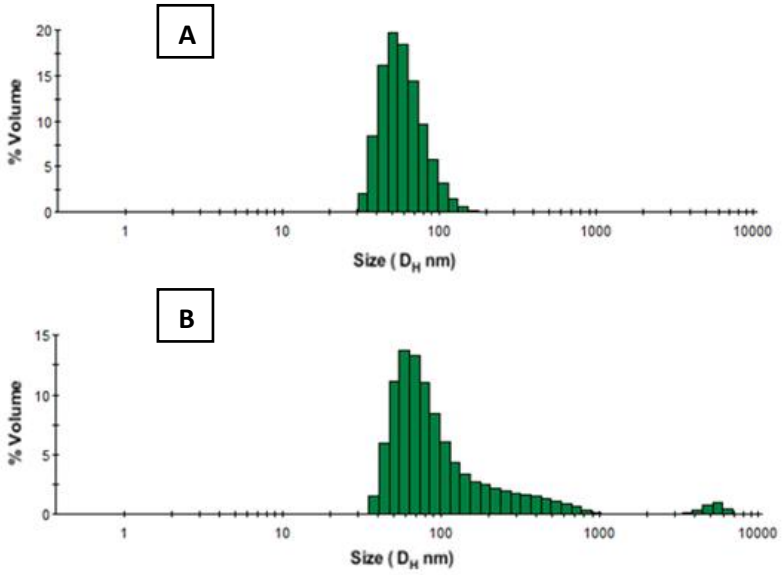

Figure 3.26. Dynamic light-scattering profile of the non loaded polymerosomes obtained with a 90:10 w/w% ratio of $mPEG_{1.9kDa}$-block-poly[ImHeMA]$_{67}$-block-poly[GMA]$_{36}$ / t-boc-NH-$PEG_{3.5kDa}$-block-poly[ImHeMA]$_{20}$-block-poly[GMA]$_{58}$ (Panel A, mean diameter ~ 50 nm, PDI = 0.097) and the dsDNA-loaded polymersomes assembled with the same polymers (Panel B). Adapted from (205) with DOI: 10.1039/c3py00744h - Reproduced by permission of the Royal Society of Chemistry.

The DLS analysis showed that the size of polymersomes was not dramatically affected by the loading of the dsDNA. However, with respect to unloaded polymersomes, the PDI was slightly higher, which can be ascribed to a rearrangement of the vesicles when a polyanionic macromolecules is loaded in the aqueous core or in proximity of the polymeric membrane.

When the polymer/dsDNA nanoassemblies were brought to pH 7.4, the overall charge associated to the particles was close to zero as shown by the zeta potenatial analysis in

Figure 3.27 indicating that there was no surface segregation and exposure of the polymer cationic blocks or anionic dsDNA. If any charge exist within the nanosystem, it is likely shielded by the hydrophilic neutral polymers (PEG and polyGMA). The stability of the particles in aqueous suspension was therefore attributable to a hydrophilic but non-charged outer polymer corona.

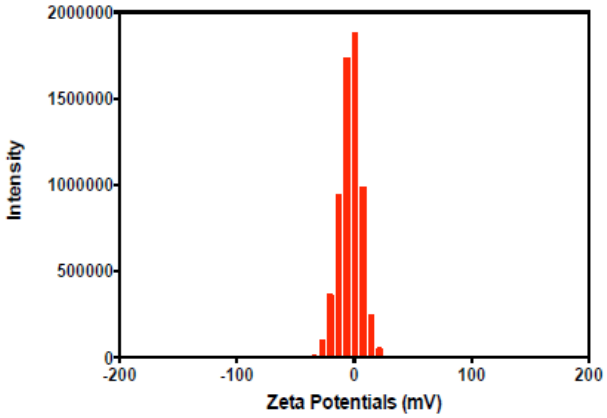

Figure 3.27. z-potential profile of the dsDNA/polymer formulation loaded using a 1:1 N/P feed ratio. The zeta potential, measured at neutral pH was found to be -0.172 mV. Adapted from (205) with DOI: 10.1039/c3py00744h - Reproduced by permission of the Royal Society of Chemistry.

A mechanism describing the dsDNA loading in the polymer nanoassemblies can be hypotized. At acid pH (pH 5) where the polymer and the dsDNA are dissolved, the imidazole containing block of the polymer is mostly in the cationic status, as dictated by the "apparent" pKa, which promotes the complexation with dsDNA strands. However, no physical crosslinking of the dsDNA strands and the positive polymer chains was observed at this pH, which can be ascribable to the steric hindrance of the two hydrophilic blocks of the co-polymer (PEG and poly-GMA block) that reduce the generation of macroaggregates at this condition. When the pH was slowly increased to induce the vesicle assembly, the central block of the polymer starts to lose its charges by deprotonation and becomes more hydrophobic thus increasing its surface energy that can only be thermodynamically minimized by reducing the exposed surface area and undergoing physical association with other polymer chains. However, despite the dsDNA/polymer interaction becomes weaker as the pH increases during the assembly process and the imidazole containing blocks loose part of their charges, dsDNA remains trapped within the aqueous core of the nanoparticles or within the hydrophobic membrane core of the vesicles.

3.11.3 DNA RELEASE FROM POLYMERSOMES

Release of the 19-mer dsDNA from 90:10 w/w% $mPEG_{1.9kDa}$-block-poly[ImHeMA]$_{67}$-block-poly[GMA]$_{36}$ / t-boc-NH-$PEG_{3.5kDa}$-block-poly[ImHeMA]$_{20}$-block-poly[GMA]$_{58}$ nanocarrier was investigated in buffer media at 37 °C at pH 7.4 and 5.0, to mimic the conditions found in systemic circulation and in late endosomal/lysosomal intracellular compartments respectively. The endosomal condition was chosen because endocitosed nanocarriers traffick to the endosomes and the short oligonucleotides loaded in the vehicles must be released within the endosomes for therapeutic activity. As apparent from Figure 3.28, release of the dsDNA was markedly pH-dependent, with 85% of the original encapsulated/complexed nucleic acid released at pH 5.0 after 8 hours, whilst only 15% of entrapped dsDNA was released by the nanocarriers at pH 7.4 over the same time.

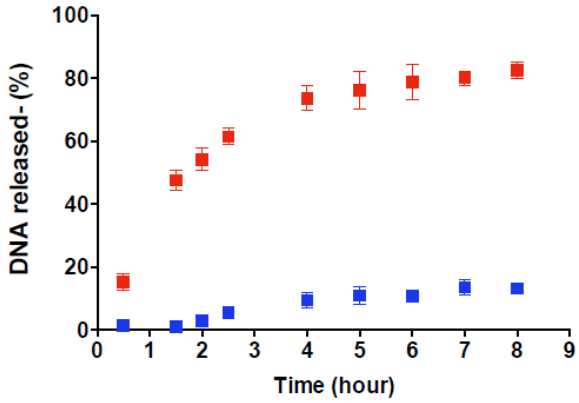

Figure 3.28. Kinetics of release of dsDNA from polymersomes formed by 90:10 w/w % mixture of $mPEG_{1.9kda}$-block-poly[ImHeMA]$_{67}$-block-poly[GMA]$_{36}$ / t-boc-NH-$PEG_{3.5kDa}$-block-poly[ImHeMA]$_{20}$-block-poly[GMA]$_{58}$ at pH 5 (■) and 7.4 (■), at 37°C. Adapted from (205) with DOI: 10.1039/c3py00744h - Reproduced by permission of the Royal Society of Chemistry.

The dsDNA release experiments were an important test of the polymer design criteria, as they implied that the imidazole containing blocks of the polymer were at a physico-chemically critical state over the key cytosol-endosome pH range. The fact that dsDNA could be reversibly associated with the co-polymer implied that not enough imidazole units in the block were protonated for the polymer as a whole to bind strongly to dsDNA at pH 5.0, yet there were nevertheless sufficient numbers of positive charges over the pH responsive blocks to repel each other at the lower pH and prevent self-association into polymersomes. Furthermore, the positive charges over the pH responsive blocks at acid

pH guided the approach of the polymer to the negative charged dsDNA during the association process, thus guaranteeing the encapsulation of the dsDNA.

3.11.4 siRNA LOADING STUDIES

The ds-siRNA sequence used in this study was 5'- CTT ACG CTG AGT ACT TCG A -3' with its complementary sequence. It was loaded in polymeric vesicles according the "pH-switch" method described previously for the dsDNA loading (Section 3.11.2). As mentioned above, dsDNA was used as model oligonucleotide to set up the loading and release protocols since it possess similar chemical features to ds-siRNA but higher stability than ds-siRNA and thus its handling is easier. Once the procols for efficient loading had been set up with dsDNA we moved to ds-siRNA.

Non targeted vesicles were obtained processing a 90:10 w/w % $mPEG_{1.9kDa}$-block-poly[ImHeMA]-block-poly[GMA]/t-boc-$PEG_{3.5}$kDa-block-poly[ImHeMA]$_{20}$-block-poly[GMA]$_{58}$ polymer mixture.

The siRNA loaded vesicles obtained after extensive dyalisis to remove siRNA non associated to the polymeric particles showed a main diameter of 236 ± 7 nm with a polydispersity index of 0.058 as shown in Figure 3.29.

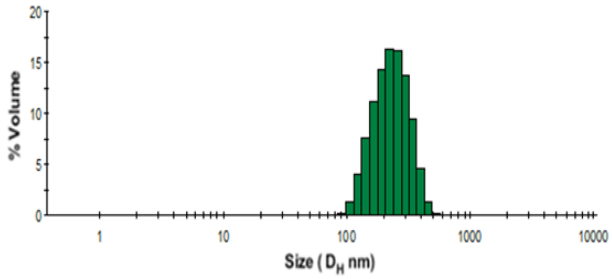

Figure 3.29. Dynamic light-scattering profile of the ds-siRNA loaded polymerosomes obtained with a 90:10 w/w% ratio of $mPEG_{1.9kDa}$-block-poly[ImHeMA]$_{67}$-block-poly[GMA]$_{36}$ / t-boc-NH-$PEG_{3.5kDa}$-block-poly[ImHeMA]$_{20}$-block-poly[GMA]$_{58}$.

The result is in agreement with the ones obtained with dsDNA loaded polymersomes (see Figure 3.26 B) showing that the assembling behavior of the ds-siRNA with the co-polymer mixture is comparable to the one of dsDNA.

The loading capacity of ds-siRNA in the polymersomes was assessed using a Quant-iT™ RiboGreen® kit. The ds-siRNA was not detectable by UV-Vis spectroscopy due to the very limited amount of the oligonucleotide processed for loading. The intercalating agent

provided with the kit for the detection of ds-siRNA is highly sensitive and has a minimum detection limit for ds-siRNA in solution equal to 0.25 ng/mL. In order to determine loading capacity of ds-siRNA in the polymersomes, the method involving Quant-iT™ RiboGreen® was set up. Indeed, the direct addition of the intercalating agent to the ds-siRNA loaded vesicle suspension was not efficient probably because polymersomes do not allow fluorescent probes to diffuse across the polymeric shell. Furthermore, evidences with the electrophoretic mobility shift assay (see chapter 3.11.1 for results) showed that dsDNA/polymer complexes were not efficiently stained by GelRed™ (that is an intercalating agent as well) when the polymer concentration was increased over the 2/1 N/P ratio. Thus, in order to quantify ds-siRNA after the dialysis process, vesicles were induced to disassemble in acidic conditions. The high sensitive intercalating agent can thus compete with the imidazole containing blocks of the polymer for the intercalation with the ds-siRNA. This procedure prove the best possible condition for the intercalating agent to approach the ds-siRNA since at pH 5 no vesicles are present and thus the ds-siRNA is not encapsulated. Afterwards, the mixture pH was increased to pH 7.4 which should favor the intercalation of the intercalating agent rather than the charge/charge complexation of the ds-siRNA with the imidazole containing blocks of the polymer. While the ds-siRNA/polymer strength depends on the pH conditions and is weaker at pH 7.4, the pH does not affect the association of the intercalating agent with the oligonucleotide.

The quantification of ds-siRNA was based on a calibration curve with known dilutions of the oligonucleotide as reported in Figure 3.30.

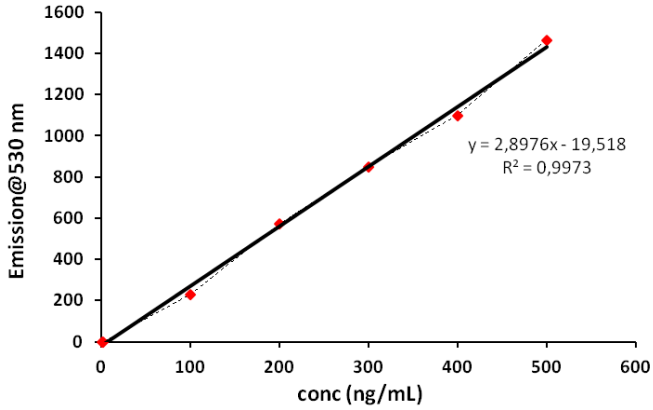

Figura 3.30. Calibration curve of ds-siRNA (0-1000 ng/mL) in RNAses free 10 mM Tris-HCl, 1 mM EDTA, pH 7.5.

The ds-siRNA concentration in the solutions derived from polymersome disassembly resulted to be of 2.4 μM.

The analysis indicated a Loading Capacity LC% = 3.2 w/w% and an Encapsulation Efficiency EC%= 34 mol/mol%. The relatively high value obtained for encapsulation efficiency confirmed the positive results obtained for the DNA loading an described in chapter 3.11.2. Since a very low PDI (0.002) was obtained for the ds-siRNA loaded polymersomes, we can suppose that partially positively charged polymers at pH 7.4 form a complex with the loaded ds-siRNA resulting in high homogeneous and spherical shaped vesicles.

3.12 TRANSMISSION ELECTRON MICROSCOPY (TEM)

The morphology of the different formulation of polimersomes was tested by Transmission Electron Microscopy (TEM). dsDNA-free and dsDNA-loaded polymersomes assembled with 90:10 w/w % of $mPEG_{1.9kDa}$-block-poly[ImHeMA]$_{67}$-block-poly[GMA]$_{36}$ / t-boc-NH-$PEG_{3.5kDa}$-block-poly[ImHeMA]$_{20}$-block-poly[GMA]$_{58}$ were prepared according to the "pH-shift" procedure at final concentration of 2 mg/mL in 20 mM phosphate, 150 mM NaCl, pH 7.4. TEM images of dsDNA free and dsDNA loaded polymersomes are are shown in Figure 3.31 and 3.32 respectively.

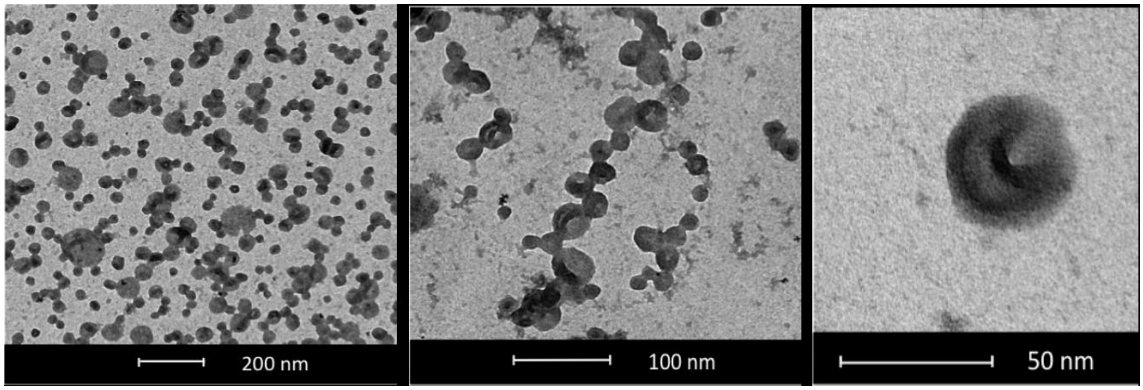

Figure 3.31. TEM images of dsDNA-free polymersomes assembled with 90:10 w/w % of $mPEG_{1.9kDa}$-block-poly[ImHeMA]$_{67}$-block-poly[GMA]$_{36}$ / t-boc-NH-$PEG_{3.5kDa}$-block-poly[ImHeMA]$_{20}$-block-poly[GMA]$_{58}$ at pH7.4. Adapted from (205) with DOI: 10.1039/c3py00744h - Reproduced by permission of the Royal Society of Chemistry.

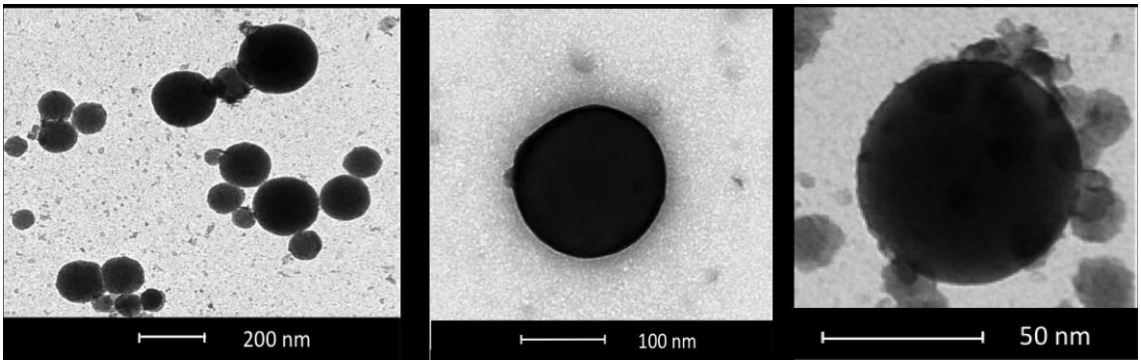

Figure 3.32. TEM images of dsDNA-loaded polymersomes assembled with 90:10 w/w % of $mPEG_{1.9kDa}$-block-poly[ImHeMA]$_{67}$-block-poly[GMA]$_{36}$ / t-boc-NH-$PEG_{3.5kDa}$-block-poly[ImHeMA]$_{20}$-block-poly[GMA]$_{58}$ at pH 7.4. Adapted from (205) with DOI: 10.1039/c3py00744h - Reproduced by permission of the Royal Society of Chemistry

TEM results provided supporting evidence of particle formation and also indicated a clear difference in nanoparticle structure. Dense, almost spherical, objects were observed in the polymer/dsDNA formulations, whereas hollow-looking vesicles were present in the samples assembled with polymers alone. Thus, the appearance of the dsDNA-free particles supports for the vesicle-like structure of the colloid that collapses when exposed to the TEM analytical conditions, which seems not to take place for ds-DNA loaded particles that possess a denser matrix. Although the TEM analysis itself can neither support nor eliminate the possibility of a polyplex assembly, these observed differences on volume and shape between the two particles might arise as a consequence of an active role of an additional electrostatic interaction DNA/polymer in the polymersome cohesion forces.

3.13 CO-POLYMER HEMOLYTIC ACTIVITY

The pH sensitive polymers designed for this work are aimed to deliver ds-siRNA to the cytosolic compartment of cancer cell for the silencing of the biological pathways involved in tumor progression. In order to achieve this, a nanocarriers must undergo active receptor mediated endocytosis by the cancer cell and then escape from the endosomal compartment where it is confined to release the siRNA payload in the cytosol. The "endosomal escape" of nanocarriers is paramount for ds-siRNA since its molecular target, namely the RISC protein complex, is on the cytosol and cytosol is the compartment

where the RNAi process will take place. Figure 3.33 schematizes the hypothesized pathway of ds-siRNA loaded polymersomes to guarantee the siRNA biological activity.

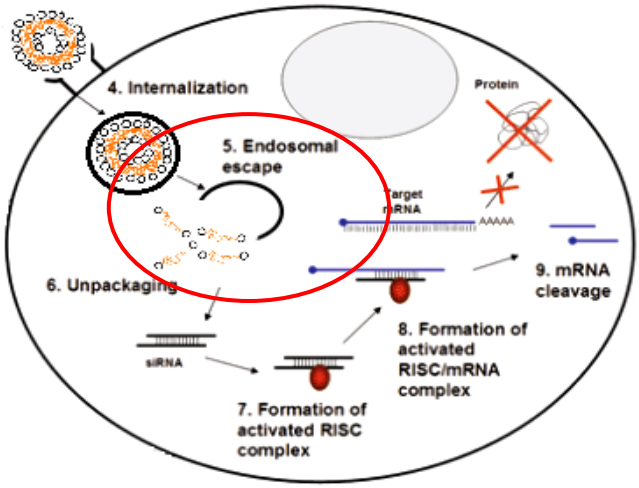

Figure 3.33. Pathway of ds-siRNA loaded polymersomes inside a cancer cell to achieve RNA silencing. In red the key step of the carrier endosomal escape.

The phenomenon of the endosomal escape is also known as "proton sponge effect" and can occur in virtue of the physic-chemical properties of the polymers that compose a specific nanocarrier. This effect has been observed for cationic polymers with a high pH buffering capability over a wide pH range. These polymers usually bear protonable secondary and/or tertiary amino groups with pKa close to endosomal/lysosomal pH. During the maturation of endosomes, the membrane-bound ATPase proton pumps actively transfer protons from the cytosol into the endosomes, which yield the acidification of endosomal compartments and the activation of hydrolytic enzymes. Polymers with ‘proton sponge’ feature will become protonated when exposed to the relatively low pH of endosomes and will buffer, up to a certain extent, the acidification of endosomes. As a result, more protons will be continuously pumped into the endosomes with the aim of decreasing the pH at the physiologic endosomal condition. The proton pumping activity is hyper regulated in endosomes engulfed with polymers with “proton sponge” feature and is accompanied by passive entry of chloride ions, which increases the endosomal ionic concentration and, as consequence, the water influx (Figure 3.34, panels B-C). Eventually the osmotic pressure causes swelling and rupture of endosomes, releasing their content to the cytosol (225).

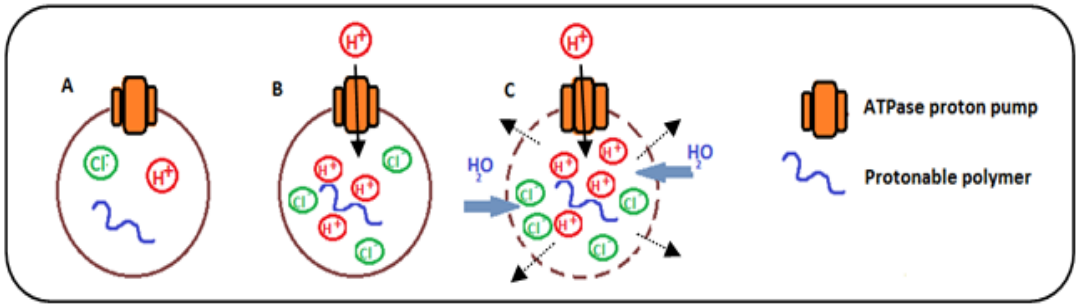

Figure 3.34. Mechanism of the "proton sponge" effect featured by certain cationic polymers and the consequent endosomal rupture.

The polymer we have synthesize in this project thesis is a good candidate for endosonal escape since it possesses imidazole containing blocks and a pKa of 5.9. The polymer is thus adequate to perform as a "proton sponge" once inside the endosomes where the pH is between ~ 5.5-6.5 (226).

A dedicated test was selected to evaluate the ability of the pH responsive polymers investigated in this project of potentially undergoing endosomal escape. The study was carried using red blood cells (RBC) and testing the hemolytic activity of the polymers in different pH conditions since a correlation between a polymer hemolytic activity at acidic pH and endosomal membrane disruption was reported in the literature (227).

Synthetic polymer with "proton sponge" features can destabilize the RBC membrane and generate pores at acidic pH that allow for the intra and extracellular solutes to diffuse in and out generating an osmotic imbalance that causes the red blood cell lysis.

The Figure 3.35 reports the results for the hemolytic assay carried out by incubating the RBC with increasing concentration of $mPEG_{1.9kDa}$-b-p[$ImHeMA]_{67}$-b-p$[GMA]_{36}$.

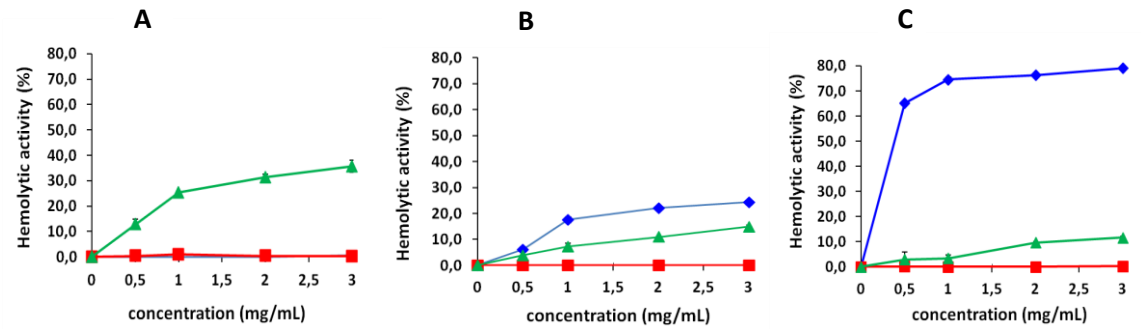

Figure 3.35. Hemolytic activity profiles of $mPEG_{1.9kDa}$-block-poly$[ImHeMA]_{67}$-block-poly$[GMA]_{36}$ (■), PEI (■), dextran (■) at pH 7.4 (panel A), 6.5 (panel B), 5.5 (panel C) at increasing concentration.

The hemolytic test was performed using the polymer dispersions at different concentration. The hemolytic profile shows that the pH responsive $mPEG_{1.9kDa}$-block-poly[ImHeMA]$_{67}$-block-poly[GMA]$_{36}$ does not possess any hemolytic activity at all concentrations tested at pH 7.4, that mimics the pH in bloodstream. The result is extremely encouraging since it shows that the polymer has no specific toxicity toward the red blood cells and cannot induce RBC membrane rupture in the blood conditions.

The hemolityc activity of the polymer was also tested at pH 6.5, that mimics the tumor interstitium. At this condition the vesicles tend to increase in size as reported in Figure 3.12 and 3.13. The size increase is beneficial to favor the entrapment of the vesicles in the tumor interstitium. At this pH condition the polymersomes are still stable but the morphological rearrangement that induces the size increase can partially induce unspecific interactions with biological membranes. This might promote a limited hemolytic activity of the polymer that was detected only at rather high concentrations (above 1 mg/mL).

Finally, at pH 5.5, that mimics the endosomal environment, the capacity of the polymer to induce the rupture of the RBC membrane is considerable even at the lowest concentration tested. Over 70% hemolysis was observed in this pH condition. The result confirmed that the polymer can induce cell membrane rupture selectively at pH 5.5, which translates in a reliable endosomal escape capacity that will not cause cell damage in the blood stream.

3.14 PHENOTYPIC CHARACTERIZATION OF CANCER CELLS AND FOLATE RECEPTOR EXPRESSION

Folic acid (vitamin B9) is an essential nutrient required by eukaryotic cells for survival. Cells physiologically acquire folic acid by specific transporters. However, few cells can also internalize folate receptor via receptor mediated endocytosis due to the presence on the cell surface of the folate receptors (FR). In particular, cells undergoing a high metabolic activity can up regulate FR expression. Among these cells, also many different human cancer cells, including ovarian, breast, cervical, renal, colorectal and nasopharyngeal cancer cells show significant up regulation of the FR as compared to normal tissues (228). As such, folic acid has been successfully exploited as a cancer specific targeting moiety for the efficient delivery of chemotherapeutic agents, drug carriers, photo sensitizers and diagnostic reporters.

The literature report the over expression of FR in a variety of cancer cells by Western blot assay that require the isolation of the protein pool from the cell, a gel electrophoretic fractionation and the staining of the specific FR (229). We decided to pursue a different strategy to characterize the expression of the FR by two cell line. For that purpose we performed a cytometric study on KB cells from human cervical carcinoma and MCF7 cells from human breast adenocarcinoma. The advantage of this method, if compared to the other techniques as Western blot, consists of no cells lisys and no possibility to overestimate the amount of folate receptor taking in account also the receptors inside the cells. It means that with cytofluorimetry we are sure of the effective presence of receptor expressed on the cell surface and that we need for our purpose.

The cell phenotypic profile was investigated by tagging alive cells with specific anti folate receptor antibody conventionally used in immunohistochemical settings. Cell samples were then treated with a secondary fluorescent antibody as labeling agent. Figure 3.36 shows the cytfluorimetric profiles of the two cell lines grown in different medium.

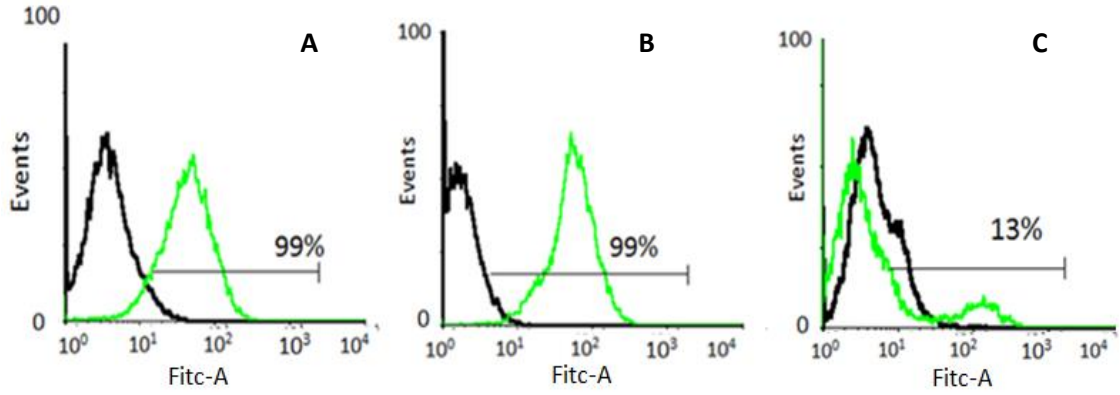

Figure 3.36. KB and MCF7 cell cytofluorimetric profile obtained by FACS analysis after treatment with only the secondary antibody (■**,** control untreated sample) and after treatment with anti FR Ig and secondary antibody (■). KB cells were grown in folate containing DMEM medium (A), and in folic free DMEM medium (B). MCF7 were grown in folate containing RPMI medium (Panel C).

The cytofluorimetric analysis shows that KB cells express high level of the folate receptor since almost 100% of cells resulted positive to this specific receptor (Panel A and B). Furthermore, the growth medium was not affecting the KB cells expression level of the receptor that is constitutive expressed in this cell line. The receptor expression is not

increased when cells are grown in folic acid depleted medium (Panel B) with respect to the same cell line grown in folic acid containing medium (Panel A).

Only 13% of the total MCF7 cell population resulted positive to folate receptor (Panel C). Notably, this cell line does not grow in folic acid depleted medium, which is conceivable being MCF7 devoided of the folate receptor that, in the other hand, supplies KB cells with the vitamin even in folate depleted medium (concentration of free folate in folate depleted DMEM = 2 nM). Overall the result confirmed that KB cells is an adequate cell model for investigating folate targeted nanocarriers and that MCF7 cells can be used as negative control being devoid of the folate receptor.

3.15 BIOCOMPATIBILITY STUDIES

Having established the primary utility of the polymers as nucleic acid carriers, the cytocompatibility of the materials was explored by MTS (3- (4,5- dimethylthiazol - 2-yl) - 5-(3- carboxymethoxyphenyl)-2-(4- sulfophenyl)-2H-tetrazolium, inner salt) cell viability assay (230). This test is based on the conversion through the mitochondrial activity of viable cells, incubated at 37ºC, of a tetrazolium salt into a colored formazan. The quantity of formazan produced by dehydrogenase activity is directly proportional to the number of living cells and it is measured at 492 nm.

The cell viability test showed that the selected untargeted polymersomes obtained with 90:10 w/w% of $mPEG_{1.9kDa}$-block-poly[ImHeMA]$_{67}$-block-poly[GMA]$_{36}$/ t-boc-$PEG_{3.5kDa}$-block-poly[ImHeMA]$_{20}$-block-poly[GMA]$_{58}$ and targeted polymersomes obtained with the 90:5:5 w/w% of $mPEG_{1.9kDa}$-block-poly[ImHeMA]$_{67}$-block-poly[GMA]$_{36}$ / t-boc-$PEG_{3.5kDa}$-block-poly[ImHeMA]$_{20}$-block-poly[GMA]58 / α-folate-PEG_{3500}-block-poly[ImHeMA]$_{20}$-block-poly[GMA]$_{58}$ were well-tolerated by a range of cell lines including KB human cervical carcinoma, MCF-7 breast cancer cells and B16-F10 mouse melanoma cell (Figure 3.37). No evident cytotoxicity was detected even for prolonged cell exposure to the polymersomes.

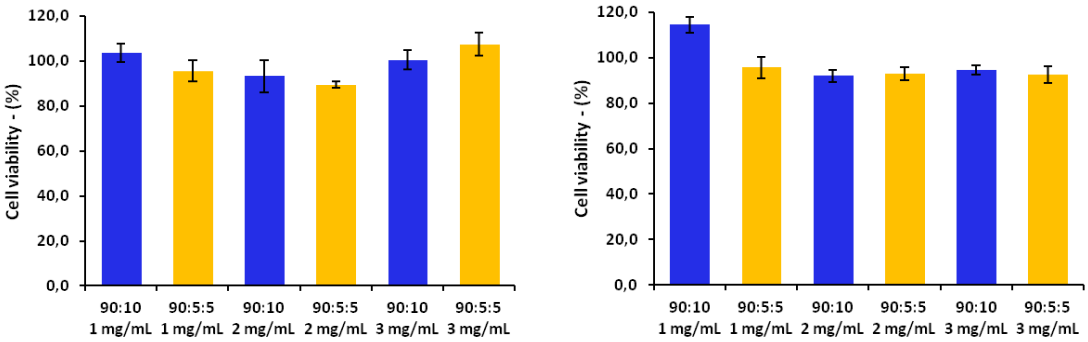

Figure 3.37. MTS cell availability assay on B16F10 cells at 1, 2, 3 mg/mL of 90:10 w/w% of $mPEG_{1.9kDa}$-block-poly[ImHeMA]$_{67}$-block-poly[GMA]$_{36}$ / t-boc-$PEG_{3.5kDa}$-block-poly [ImHeMA]$_{20}$-block-poly[GMA]$_{58}$ based polymersomes (■) and 90:5:5 w/w% of $mPEG_{1.9kDa}$-block-poly[ImHeMA]$_{67}$-block-poly[GMA]$_{36}$ / t-boc-$PEG_{3.5kDa}$-block-poly[ImHeMA]$_{20}$-block-poly[GMA]58 / α-folate-PEG_{3500}-block-poly[ImHeMA]$_{20}$-block-poly[GMA]$_{58}$ polymersomes (■), after 24 hours (Panel A) and 48 hours (Panel B) incubation at 37°C. Data are reported as mean values of 5 measurements with ± standard deviations.

3.16 CELLULAR UPTAKE OF POLYMERSOMES

Cell uptake studies were performed using the selected polymersomes formulations. The folate targeted polymersomes were constituted of 90:10 w/w% of $mPEG_{1.9k}$-block-poly[ImHeMA]$_{67}$-block-poly[GMA]$_{36}$/ t-boc-$PEG_{3.5kDa}$-block-poly[ImHeMA]$_{20}$-block-poly[GMA]$_{58}$ and the control non-targeted vesicles were assembled with 90:5:5 w/w% of $mPEG_{1.9kDa}$-block-poly[ImHeMA]$_{67}$-block-poly[GMA]$_{36}$ / t-boc-$PEG_{3.5kDa}$-block-poly[ImHeMA]$_{20}$-block-poly[GMA]58 / α-folate-$PEG_{3.5kDa}$-block-poly[ImHeMA]$_{20}$-block-poly[GMA]$_{58}$.

3.16.1 FLUORIMETRIC AND CYTOFLUORIMETRIC UPTAKE STUDIES

Folate-targeted polymeric formulations loaded with cyanine-DNA were incubated with B16F10 cells in order to investigate the time dependant cellular uptake by cytofluorimetric analysis. B16F10 cells were selected because they overexpress the folate receptor (199, 200) and were also used as model for the silencing studies being transfected with luciferase. The polymersomes uptake study was carried out at 37 °C and at 4 °C, in order to determine whether the main cell internalization mechanism was energy-dependent (231). Incubation at 4 °C allow to selectively inhibit any energy dependent process but not the diffusive uptake. Cell associated polymersomes were

quantified by flow cytometry. Figure 3.38 shows the cell uptake profile at the two different temperature conditions and at different time points of incubation.

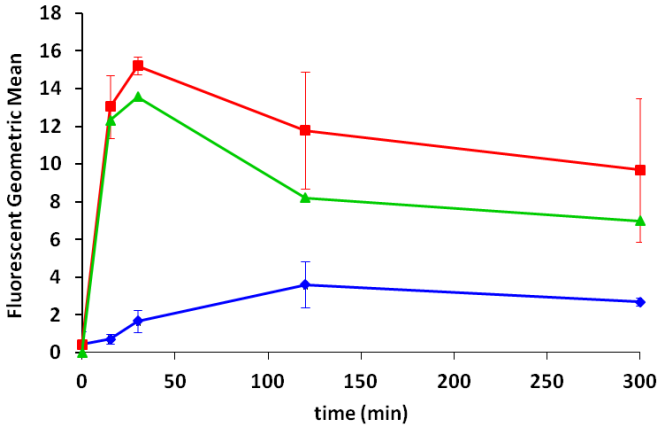

Figure 3.38. Kinetic B16F10 cells uptake profile of folate -targeted polymersomes loaded with cyanine-labelled DNA at 37°C (■) and 4°C (■). The normalized uptake was derived by subtracting cell associated fluorescence of cells incubated at 4°C from the cell associated fluorescence of cells incubated at 37°C (■).

The unspecific association of the targeted polymersomes obtained by incubating cells at 4 °C was subtracted from the fluorescence detected in cell samples incubated with polymersomes at 37°C to obtain the normalized uptake profile. The normalized uptake profile shows that folate tipped polymersomes internalization at 37°C is maximum after 30 minutes incubation with polymersomes. After this period, the uptake starts to slightly decrease, probably according a folate receptor saturation mechanism suggested from in vivo studies performed by Leamon and Low (232).

The kinetic uptake study confirmed that about 30 minutes of dsDNA loaded polymersome incubation is required to achieve significative cell internalization of the targeted nanosystem by folate receptor expressing cancer cells and that the cell uptake is rather saturated after this time frame.

Based on the outcome from the kinetic uptake study with B16F10 cells, polymer formulations with, and without, the folate-terminal functionality were also incubated with KB and MCF-7 cells to investigate feasibility for cell delivery by passive or receptor mediated internalization mechanisms. The folate-receptor (FR) mediate targeting used in this experiment, has been elsewhere reported, to be highly suitable for some cancer cell lines (228, 229). KB cancer cell line, as reported above, were shown to over-expresses the

folate receptor, while the MCF-7 does not. The polymer nanoparticles for these assays were prepared in the presence of cyanine-3 labelled dsDNA (with the same sequence as that used in the encapsulation assays) to facilitate cross-comparison. Quantification of polymer nanoparticles uptake was carried out via fluorescence intensities of cell lisates derived from the cyanine-3 dsDNA emission. The incubation time was selected based on the evidences acquired by the above discussed kinetic uptake study. KB and MCF7 cells were incubated with polymersome formulation for 30 minutes apparent from Figure 3.32, marked differences in cell association occurred dependent on whether the dsDNA loaed polymeric particles were ligand-functionalised and if the cells expressed the folate receptor. Results are reported in Figure 3.39.

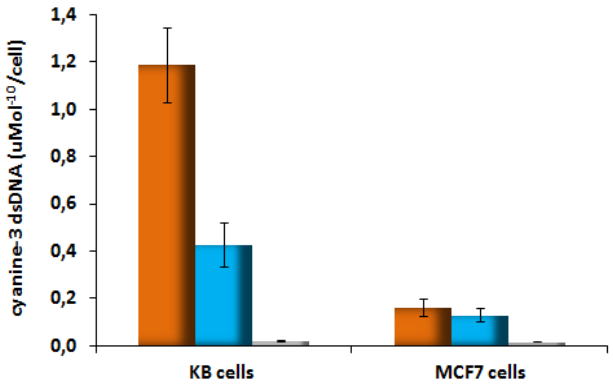

Figure 3.39. Amount of cyanine-3 dsDNA internalized by KB and MCF7 cells after 30 minuts incubation with polymersome formulations. Targeted nanoparticles were prepared from $mPEG_{1.9kda}$-block-poly[ImHeMA]$_{67}$-block-poly[GMA]$_{36}$ with 10 w/w% t-boc-NH-$PEG_{3.5kDa}$-block-poly[ImHeMA]$_{20}$-block-poly[GMA]$_{58}$ (■) or 5:5 w/w% t-boc-NH-$PEG_{3.5kDa}$-block-poly[ImHeMA]$_{20}$-block-poly[GMA]$_{58}$ and α-folate-$PEG_{3.5kDa}$-block-poly[ImHeMA]$_{20}$-block-poly[GMA]$_{58}$ (■). The blank consisted of phosphate saline buffer pH 7.4 (■).

Targeted polymersomes showed about 2.5-fold higher uptake with respect the non-targeted control polymersomes with the same cell line. No difference in the cell association was instead observed with MCF7 where a negligible unspecific association was only recorded. In general, uptake of the nanoparticles was higher in KB cells compared to MCF-7 cells, and the highest uptake overall was obtained for the polymer formulations containing 5% of the folate-tipped α-folate-$PEG_{3.5kDa}$-block-poly[ImHeMA]$_{20}$-block-poly[GMA]$_{58}$.

The selective uptake of polymersome with the same cell lines (KB and MCF7 cells) was also confirmed by cytofluorimetry analysis that provided comparable results in term of uptake profile, cell specificity, polymersomes selectivity (Figure 3.40 a) and 3.40 b)).

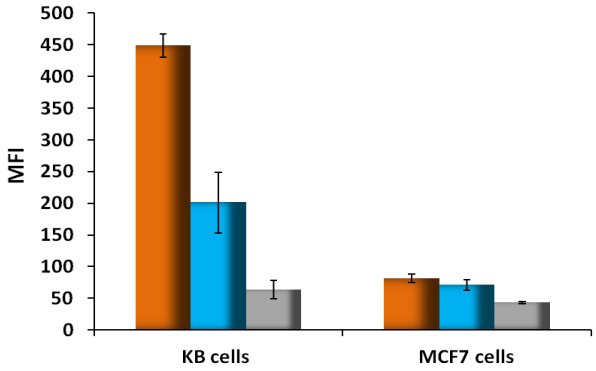

Figure 3.40 a). Mean Fluorescence Intensity of cells incubated with polymersomes loaded with cyanine-3 dsDNA. Targeted nanoparticles were prepared from mPEG$_{1.9kda}$-block-poly[ImHeMA]$_{67}$-block-poly[GMA]$_{36}$ with 10 w/w% t-boc-NH-PEG$_{3.5kDa}$-block-poly[ImHeMA]$_{20}$-block-poly[GMA]$_{58}$ (■) or 5:5 w/w% t-boc-NH-PEG$_{3.5kDa}$-block-poly[ImHeMA]$_{20}$-block-poly[GMA]$_{58}$ and α-folate-PEG$_{3.5kDa}$-block-poly[ImHeMA]$_{20}$-block-poly[GMA]$_{58}$ (■).The blank consisted of phosphate saline buffer pH 7.4 (■).

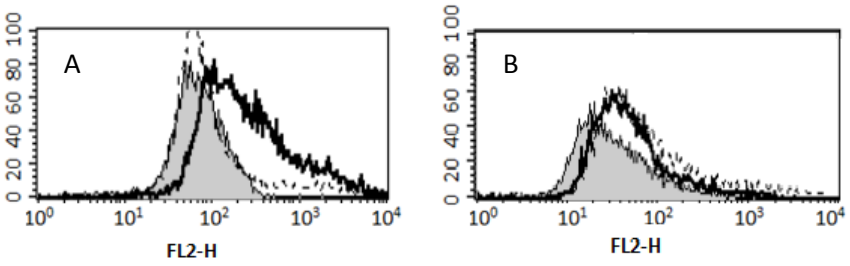

Figure 3.40 b). Histograms overlay of fluorescent positive KB (Panel A) and MCF7 cells (Panel B) to cyanine-3 dsDNA are reported for cells treated with PBS (■), cells treated with targeted vesicles (-) and cells treated with non targeted vesicles (- - -).

The fact that the polymer nanoparticles were of similar sizes and ζ-potential across the set of folate-tipped and non-folate tipped materials, when formulated with dsDNA, strongly suggests that the uptake pathways and kinetic profile, investigated with two folate receptor expressing cells and using fluorescence spectroscopy and cytofluorimetry, were unlikely to have been a function of the nanoparticle geometries. Thus, while specific inhibition studies with free folic acid to saturate any folate receptors on the KB cells were not carried out, the ability of these folate receptor positive cells to internalize the folate-

tipped polymers nevertheless was supportive of a specific uptake pathway for the folate polymer formulations. These experiments also highlighted the ability of mixed polymer formulations with relatively low ligand densities at their surfaces being able to enter cells via a receptor-mediated process.

3.17 CONFOCAL MICROSCOPY

Studies of confocal microscopy were performed on vesicles with/without targeting agent and loaded with dsDNA fluorescently labeled with cyanin-3 to acquire information about the intracellular deposition of the delivered dsDNA after vesicle uptake. As for the uptake analysis performed by fluorescence spectrometry and cytofluorimetry KB cells over expressing folate receptor and MCF7 as negative control were used.

In the following Figure 3.41, all the cell samples were obtained by incubating cells with polymersome formulations as described in section 2.3.18.

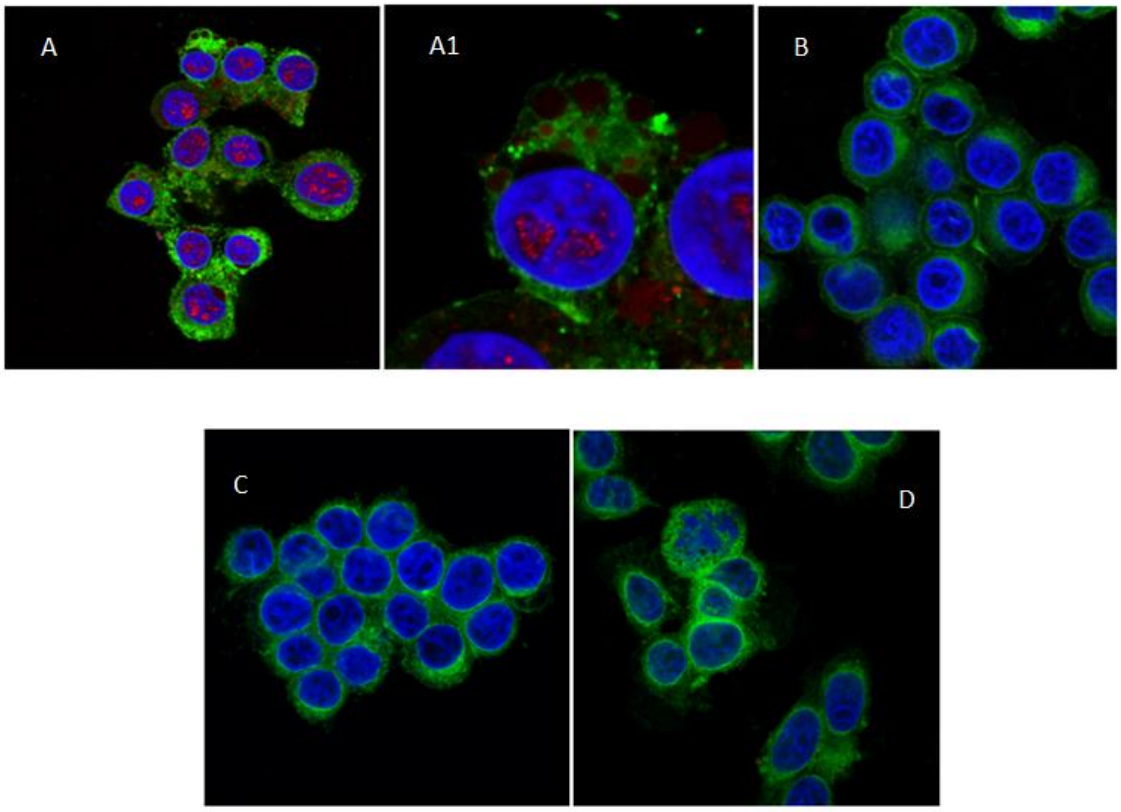

Figure 3.41. Images obtained by confocal microscopy of KB cells incubated with folate targeted Cyanin-3 labelled DNA polymersomes (panel A); KB cells incubated with non targeted Cyanin-3 labelled DNA polymersomes (panel B); MCF7 cells incubated with folate targeted Cyanin-3 labelled DNA polymersomes (panel C); MCF7 cells incubated with non targeted Cyanin-3 labelled DNA polymersomes (panel D) are reported. Panel A1 is a magnification of the panel A

showing details of KB cell nucleus and intracellular fluorescent organelles. Cell images were acquired using blue channel for nuclei detection after labelling with DAPI, green channel for cell membrane detection after labelling with fluorescein-DHPE, red channel for cyanin-3 labeled polymersome detection.

Panels A and the magnification (Panle A1) shows clear red spots consisting of cyanin-3 DNA labelled polymersomes or free cyanin-3 DNA that are detectable both in the cytosol of KB cells, and in the cell nucleus. The magnification (panel A1) also highlights that the dsDNA loaded polymersomes or the dsDNA alone is associated mostly in confinded in cytosolic sub-compartments of the or in the nuclei but spreading over the cytosol is also detectable. The red spot confined in the cytosolic compartment could be endosomes at some stage of development and migration even though more detailed studies are required to precisely confirm this hypothesis. Notably, tt was rather unexpected to find out red spots inside the nucleus. We have speculated that the folate can target the nanocarriers toward the nucleus; this has one first relevant implication: the vesicles undergo endosomal escape and can migrate elsewhere in the cell. A possible explanation of this unexpected disposition may be related to the roles of the folate that can operate as transcription factor (233) and is cofactor of the synthesis of nucleotides once inside the cell nucleus (234). Being both activities and the molecular targets of folate confined to the nucleous, it is conceivable that it can direct the migration towards the nucleous of conjugated macromolecules.

This evidence is confirmed by literature, where Chao Zhang managed to deliver minicircle DNA to cytosol and cell nucleus using folate–poly(ethylene glycol)–polyethylenimine polyplexes (235). The images obtained by the confocal analysis, together with the results of polymersomes uptake obtained by fluorimetric analysis on cell lisate, cytofluorimetry, confirm that targeted oligonucleotide loaded vesicles are internalized by receptor mediated endoycotosis and that the vesicle payload or the carriers as a whole undergo intracellular trafficking, which, at some extent, allow the deposition of the oligonucleotide in the nuclear compartment.

On the other hand, polymersomes without folate on surface were inefficient in triggering the cell uptake and do not cross the cell membrane by diffusion, as demonstrated in panel B and D that are devoid of red fluorescent spots.

To conclude, the selectivity of the polymersomes was further confirmed by both targeted and non targeted polymersomes incubation with MCF7 cells that were used as negative control. No internalization was observed with this cell line.

3.18 SILENCING STUDIES

To conclude polymersomes were also investigated to assess their biopharmaceutical properties and if the intracellular delivery of oligonucleotides allows for their biological activity to take place. Folate targeted polymersomes assembled according to the description reported in section 2.3.3 and loaded with ds-siRNA with a specific sequence to silence luciferase were incubated with B16F10 cells from mouse melanoma overexpressing folate receptor and that have been previously transfected with a plasmid encoding pGL3 luciferase under the SV40 (236). Luciferace is an ideal enzymatic model to test the intracellular delivery of the functional siRNA that silence the expression of the enzyme. Thus it is conventionally exploited to investigate the delivery efficiency of nanocarriers.

Luciferase has an apparent molecular weight of 62 kDa and requires luciferin, ATP, and O_2 as substrates for its enzymatic activity. The structure and physic-chemical properties of firefly luciferin is known and the chemical synthesis of this heterocyclic carboxylic acid has also been reported (237, 238). The reactions catalyzed by firefly luciferase are:

$$\text{luciferin} + \text{ATP} \rightarrow \text{luciferyl adenylate} + \text{PPi}$$

$$\text{luciferyl adenylate} + O_2 \rightarrow CO_2 + \text{oxyluciferin} + \text{AMP} + \text{light}$$

where ATP is Adenosine triphosphate, PPi is pyrophosphate and AMP is Adenosine monophosphate.

The first reaction involves the formation of an enzyme-bound luciferyl-adenylate. During the second reaction, the luciferyl-adenylate undergoes an oxidative decarboxylation which results in the production of CO_2, oxyluciferin, AMP, and light. When the luciferin substrates is provided in the reaction mixture, firefly luciferase produces a flash of light that is proportional to the quantity of luciferase (239).

A model representation of luciferase activity is reported in Figure 3.42.

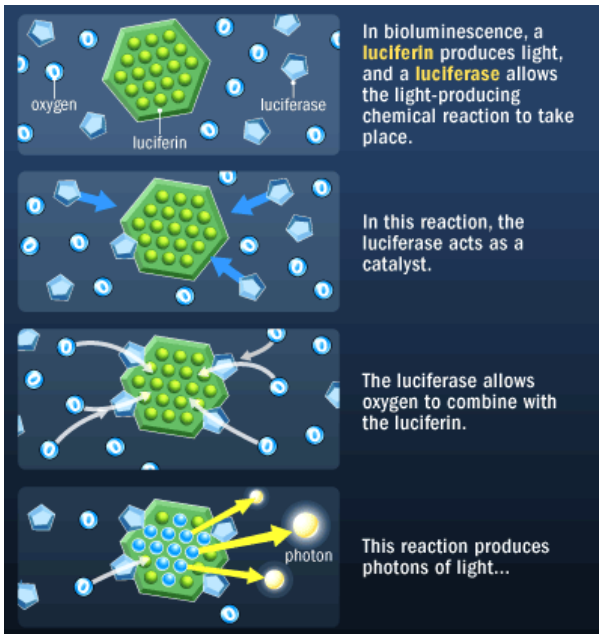

3.42. Schematic representation of luciferase activity.

The bioluminescence process can be monitored at λ_{em} 535 nm by spectrophotometric analysis.

The siRNA loaded inside polymersomes has a specific sequence that was selected to inhibit the luciferase expression by degradating the mRNA involved in the translation process responsible for the synthesis of this enzyme. This is indeed the RNAi process described in the introduction chapter 1.1.2.5. Studies reported in literature (240), showed that a cellular ds-siRNA anti-luciferase concentration of 25 nM is sufficient to carry out a silencing effect of the enzyme, which can be monitored by the decrease in the bioluminescence emitted at 535 nm.

Figure 3.43 reports the silencing profiles obtained by incubating luciferase transfected B16F10 cells with folate targeted polymersomes loaded with anti-luciferase ds-siRNA for 30 minutes.

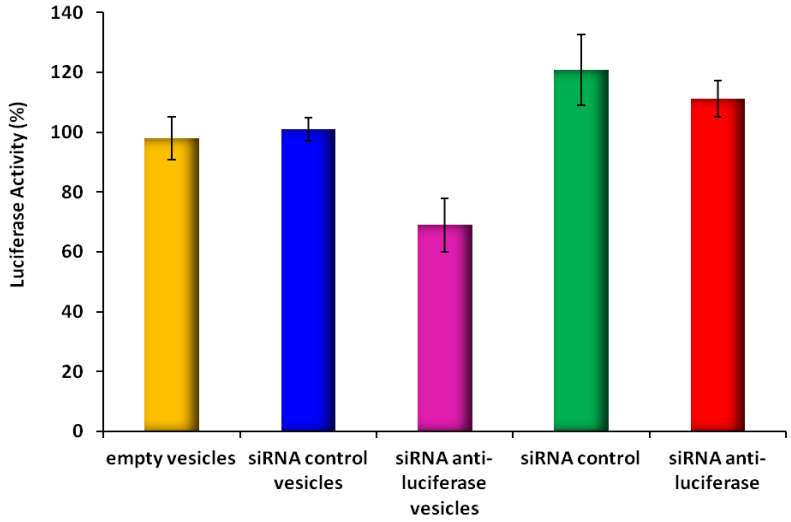

3.43. Luciferase silencing profiles in B16F10 cells treated with, from the left: folate targeted siRNA free vesicles (■), targeted vesicles loaded with scrambled siRNA (■), targeted vesicles loaded with anti-luciferase siRNA (■); unformulated scrambled siRNA (■), unformulated anti-luciferase siRNA (■).

According the luciferase silencing profile, after 30 minutes of incubation with cells, the folate targeted polymersomes loaded with anti-luciferase ds-siRNA induced an inhibition of the luciferase activity of almost 30%. No evidence of silencing effect was observed when cells were incubated with empty polymersomes and targeted polymersomes loaded with scrambled ds-siRNA. These controls confirmed that the silencing effect detected with the targeted vesicles can only be ascribed to the efficient intracellular delivery of the oligonucleotide, its release from the polymeric carrier and the endosomal escape in the biologically active form. The decrease of bioluminescence cannot be a consequence of nanocarrier toxicity since the bioluminescence was not altered by the cell incubation with solely the ds-siRNA free polymesomes. Notably, when anti-luciferase ds-siRNA was administered to the cells as free unformulated molecule, not effect on the bioluminescence was observed due to the inefficient permeability of the polyanionic macromolecules to freely permeate the biological membranes.

The protein expression inhibition achieved with the delivery strategy here discussed is unquestionable and promising for further silencing studies of proteins involved in the tumor progression for therapeutic purposes. It should be mentioned that the results reported in Figure 3.36 were referred to the bioluminescence generated by cells treated with the folate targeted ds-siRNA free polymersomes. This formulation, in fact, induced an increase in bioluminescence with respect to untreated cells. Studies performed by

Boshnjaku et all. (233) showed that [folic acid / folate recetor α] complex can operate as a transcription factor. Indeed, this complex translocates to the nucleus, where it can bind regulatory elements at regions of promoters and it may modulate the expression of the controlled proteins. Thus, a similar activation effect can induce the enhancement of the bioluminescence in cell samples treated with folate targeted polymersomes as consequence of the [folate-polymer / folate recetor α] complex binding the luciferase promoter. Furthermore, an hyper proliferation of cells incubated with folate targeted polymersomes was also observed, which can be a consequence of promoters activation. Hence, the normalization according folate targeted siRNA free formulation was required.

To conclude, the potential activation of nuclear promoters is in agreement with the massive deposition of the polymeric carrier or the loaded oligonucleotides in the cell nucleus opening up novel perspectives for sub-cellular targeting approaches.

4. CONCLUSIONS

In conclusion, this thesis project, in collaboration with University of Nottingham and Centro de Investigacion Principe Felipe in Valencia, was aimed at designing, synthesizing and characterizing in vitro few responsive AB and ABC block copolymers that changed conformation with varying the pH conditions. In particular, in order to develop targeted drug-delivery systems for antitumoral therapy, novel monomers with N-alkyl imidazole structure, have been successfully designed, synthesized and characterized. The monomers were chosen in virtue of their amphiphilic character: the alkyl chains allowed for intermingle association with other polymer chains by hydrophobic interaction, while the imidazole moiety allows for association/dissociation shift of the polymeric chains as consequence of the imidazole protonation equilibrium.

These monomers were subsequently used for the synthesis of pH responsive block co-polymers using RAFT polymerization technique. Moreover, polymersome formation tests were conducted. The diblock co-polymers responded to pH variations in a range close to the one of interest (pH 6.5-5), but early precipitation occurred. Although these materials were not all fully soluble in aqueous media at physiological pH, which limits their applications, they provided useful information for subsequent studies. It was clear that the high hydrophobicity of ImHeMA, needed to be balanced by a higher degree of hydrophilicity, potentially improving the solubility in aqueous media and favoring the formation of polymersomes over micelles that are more versatile for the loading of very hydrophilic macromolecules such as the oligonucleotides.

Bearing in mind this assumption, an ABC triblock co-polymer poly[GMA]-block-poly[ImHeMA]-block-$PEG_{1.9kDa}$ was first synthesized according to a two step procedure involving a first RAFT polymerization process and a subsequent performed PEG conjugation. This co-polymer showed a remarkably high solubility at physiological pH (pH 7.4) and the ability to form polymeric assemblies. These particles were reasonably hollow vesicles that are conventionally named polymersomes and were stable at pH 7.4 over three days, but they were easily destabilized at lower pH 6.5, i.e. a similar pH value found in the cellular endosomes.

Despite these results, reactions for a mPEG macroCTA were carried out to engineer a simpler ABC triblock co-polymer system, starting from the same materials used in these

early stage studies, but aiming an improvement of the yields obtained by the conjugation of the PEG to the di-block. The ability of the obtained polymers to change conformation over specific biologically relevant pH ranges has been shown by NMR and DLS studies and the pH-switching behavior has been used to encapsulate DNA and release the nucleic acid in a triggered fashion. Selected polymers and their formulations with DNA have been shown to be non-toxic, colloidally stable at ambient pH and temperature and even in the presence of serum protein, and able to transport DNA via folate receptor-mediated uptake pathway into specific cell lines.

The polymeric vesicles were thus loaded with a functional ds-siRNA sequence able to participate to the RNAi process and silence a model enzyme expressed in transfected cancer cells. The synthesis of the target protein was inhibited by the 30% as consequence of the efficient intracellular delivery of ds-siRNA by the folate targeted polymersomes. The promising result is in agreement with data obtained from cell uptake studies performed with the same polymeric vesicles loaded with a model fluorescently labeled dsDNA. The images obtained from confocal microscopy studies also confirmed the internalization of oligonucleotides loaded polymersomes inside the target cells.

The results of all studies were thus good indicators of the success of the design strategy for these pH-responsive materials. When considered in context, the described materials exhibit some key properties that are favorable for pharmaceutical applications. The ability to encapsulate biopolymers such as DNA and siRNA is clearly advantageous for emerging medical technologies, since many new therapeutic entities (proteins, siRNA) are biological in origin and need a delivery system to be used in practice. In addition, the ability to fine tune the polymer conformations across physiological pH ranges by mixed responsive monomer block combinations may allow control over tissue and cell localization. Significant size changes were observed for some of the self-assembled polymer structures over pH ranges varying from 5.5 - 6.5, 6.8 -7.0 and 7.2 -7.4, and these might in turn result in nanocarrier entrapment and retention in tumors through pH-dependent swelling (241), followed by intracellular uptake and drug release. From literature we have fascinating examples of shape and size polymer variation in response to pH (201) and particle shape itself can be investigated as a means to influence biodistribution and cell targeting (205, 242, 243). Finally, the facile route to ligand-functionalized formulations by mixing two or more co-polymers with different end-

groups potentially enables multi-modal targeting, whereby much more specific cell- or sub-cellular organelle- delivery might be addressed. As a corollary, it should be noted that while the imidazole ring on the responsive block components is present in natural molecules (e.g. purine, histamine, histidine) and is therefore considered to be cytocompatible and non toxic, there are many examples of polymers with positive charges (e.g. polylysine) which can be toxic (205, 244). Moreover, imidazole containing antifungal agents include potent inhibitors of the CYTP450 enzymes lanosterol α demethylase (CYP3A4) and Δ 22 desaturase (CYP2C19), leading to blocking of the ergosterol pathway and subsequent membrane destabilization and toxicity (205, 245, 246). Breakdown in vivo of the polymers used in this study would probably lead to PEG, polymethacrylic acid and imidazolic residues which may be tolerable for acute therapies but not acceptable for long-term treatments. Nevertheless, the design rules obtained for responsive materials as shown in this PhD project are important to inform further studies wherein specific components of each responsive block and/or polymeric amphiphile are re-formulated, re-engineered or synthesized from more pharmacologically acceptable materials.

Concluding, the positive results reported in this thesis using this novel pH sensitive vesicular system can be reasonably extended to specifically silence therapeutically relevant intracellular proteins for cancer therapy.

The structural rearrangement of the block co-polymers, which may be critical in determining their interactions with biological components, need also further investigations, as the detailed mechanisms underlying their behavior are still not clear and require further investigations involving the soft matter characterization techniques at molecular level. Initial results revealed some aspects, but full biological and biophysical understanding is still needed in order to maximize their effects in anticancer therapy.

REFERENCES

(1) Steichen SD, Caldorera-Moore M, Peppas NA. A review of current nanoparticle and targeting moieties for the delivery of cancer therapeutics. European Journal of Pharmaceutical Sciences. 2013;48:416-427.

(2) Adams G, Weiner L. Monoclonal antibody therapy of cancer. Nat Biotechnol. 2005;23:1147-1157.

(3) Davis ME, Chen Z(, Shin DM. Nanoparticle therapeutics: an emerging treatment modality for cancer. Nature Reviews Drug Discovery. 2008;7:771-782.

(4) Caldorera-Moore M, Peppas NA. Micro- and nanotechnologies for intelligent and responsive biomaterial-based medical systems. Adv Drug Deliv Rev. 2009;61:1391-1401.

(5) Bertrand N, Leroux J. The journey of a drug-carrier in the body: An anatomo-physiological perspective. J Controlled Release. 2012;161:152-163.

(6) Liechty WB, Peppas NA. Expert opinion: Responsive polymer nanoparticles in cancer therapy. European Journal of Pharmaceutics and Biopharmaceutics. 2012;80:241-246.

(7) Mellman I. Endocytosis and molecular sorting. Annu Rev Cell Dev Biol. 1996;12:575-625.

(8) Mukherjee S, Ghosh R, Maxfield F. Endocytosis. Physiol Rev. 1997;77:759-803.

(9) Pai S, Lin Y, Macaes B, Meneshian A, Hung C, Wu T. Prospects of RNA interference therapy for cancer. Gene Ther. 2006;13:464-477.

(10) Kim Y, Tewari M, Pajerowski JD, Cai S, Sen S, Williams J, et al. Polymersome delivery of siRNA and antisense oligonucleotides. J Controlled Release. 2009;134:132-140.

(11) Mann C, Honeyman K, Cheng A, Ly T, Lloyd F, Fletcher S, et al. Antisense-induced exon skipping and synthesis of dystrophin in the mdx mouse. Proc Natl Acad Sci U S A. 2001;98:42-47.

(12) Discher D, Eisenberg A. Polymer vesicles. Science. 2002;297:967-973.

(13) Antonietti M, Forster S. Vesicles and liposomes: A self-assembly principle beyond lipids. Adv Mater. 2003;15:1323-1333.

(14) Sugimura T. Multistep Carcinogenesis - a 1992 Perspective. Science. 1992;258:603-607.

(15) Berenblum, I., Schubik P., Ibid. 1947; 1:383.

(16) UNSCEAR (2000). Sources and Effects of Ionizing Radiation. Vol II, Effects. United Nations Scientific Committee on the Effects of Atomic Radiation, 2000 Report to the General Assembly. United Nations, New York.

(17) Upton A.C., Albert R.E., Burns F.J.. Radiation Carcinogenesis. Elsevier, 1986

(18) Hart I.R., Saini I... Biology of tumor metastasis. Lancet 1992, 339, 1453-1457.

(19) Perkins A..S and Stern D.F.. Molecular biology of cancer. In: V.T. DeVita, S. Hellman and S.A. Rosenberg (eds.). Cancer: Principles and Practice of Oncology, 1997, 5th ed., Lippincott Raven Publ., Philadelphia, pp. 79-102.

(20) Kastan MB. Molecular biology of cancer: the cell cycle. In: VT DeVita, S Hellman and SA Rosenberg (eds.), Cancer: Principles and Practice of Oncology, 1997. 5th edn. JB Lippincott, Philadelphia, Pp. 121-134.

(21) Hollstein MD, Sidransky B, Vogelstein B. P53 mutations in human. 1991

(22) FOLKMAN J, SHING Y. Angiogenesis. J Biol Chem. 1992;267:10931-10934.

(23) MATSUMURA Y, MARUO K, KIMURA M, YAMAMOTO T, KONNO T, MAEDA H. Kinin-Generating Cascade in Advanced Cancer-Patients and Invivo Study. Jap J Cancer Res. 1991;82:732-741.

(24) Wu J, Akaike T, Maeda H. Modulation of enhanced vascular permeability in tumors by a bradykinin antagonist, a cyclooxygenase inhibitor, and a nitric oxide scavenger. Cancer Res. 1998;58:159-165.

(25) Senger, D.R., Galli, S.J., Dvorak, A.M., Perruzzi, C.A. Harvey V.S. and Dvorak, H.F. (1983). Tumor cells secrete a vascular permeability factor that promotes accumulation of ascites fluid. *Science* **219**: 983-985.

(26) Leung, D.W., Cachianes, G., Kuang, W.J., Goeddel, D.V., and Ferrara, N. (1989). Vascular endothelial growth factor is a secreted angiogenic mitogen. *Science* **246**: 1306-1309.

(27) Wu, X., Li, H. Kang, L., Li, L. Wang, W. and Shan, B. (2002). Activated Matrix Metalloproteinase-2-A Potential Marker of Prognosis for Epithelial Ovarian Cancer, *Gynecologic Oncology*. **84**:126-134.

(28) Skinner, S.A., Tutton, P.J.M., and O'Brien, E., (1991). Microvascular architecture of experimental colon tumors in the rats. *Cancer Res.* **50:** 2411-2417.

(29) Matsumura, Y. and Maeda, H. (1986). A new concept for macromolecular therapeutics in cancer chemotherapy: mechanism of tumoritropic accumulation of proteins and the antitumor agent Smancs. *Cancer Res.* **46**: 6387-6392.

(30) Duncan R. The dawning era of polymer therapeutics. Nature Reviews Drug Discovery. 2003;2:347-360.

(31) Iwai, K. Maeda H. and Konno, T. (1984). Use of oily contrast medium for selective drug targeting to tumor: enhanced therapeutic effect and X-ray image. *Cancer Res.* **44**: 2115-2121.

(32) Maeda, H., Matsumoto, T., Konno, T., Iwai, K., and Ueda, M. (1984). Tailor-making of protein drugs by polymer conjugation for tumor targeting: A brief review on SMANCS. *J. Protein Chem.* **3:** 181-193

(33) Maeda, H., Matsumura, Y., Oda, T., and Sasamoto, K. (1986). Cancer selective macromolecular therapeutics: tailoring of antitumor protein drugs, pp. 353-382 in *Protein*

Tailoring for Food and Medical Uses (R. E. FEENEY and J. R. WHITAKER, eds.), Marcel Dekker Inc., New York, USA.

(34) Maeda, H., Ueda, M., Morinaga, T., and Matsumoto, T. (1985). Conjugation of poly(styrene-co-maleic acid) derivatives to antitumor protein neocarzinostatin: pronounced improvements in pharmacological properties. *J. Med. Chem.* **28**: 455-461.

(35) Duncan, R., Connors, T.A., and Maeda, H. (1996). Drug targeting in cancer therapy: the magic bullet, what next?. *J. Drug Target.* **3**: 317-319.

(36) Maeda, H., Matsumoto, T., Konno, T., Iwai, K., and Ueda, M. (1984). Tailor-making of protein drugs by polymer conjugation for tumor targeting: A brief review on SMANCS. *J. Protein Chem.* **3:** 181-193

(37) Sakata, Y., Akaike, T., Suga, M., Ijiri, S., Ando, M., and Maeda, H. (1996). Bradykinin generation triggered by *Pseudomonas* protease facilitates invasion of the systemic circulation by *Pseudomonas aeruginosa*. *Microbiol. Immunol.* **40**: 415-423.

(38) Okamoto, T., Akaike, T., Nagano, T., Miyajima, S., Suga, M., Ando, M., Ichimori, K., and Maeda, H. (1997). Activation of human neutrophil precollagenase by nitrogen dioxide and peroxynitrite: a novel mechanism for procollagenase activation involving nitric oxide. *Arch. Biochem. Biophys.* **342**: 261-274

(39) Matsumura, Y., Maruo, K., Kimura, M., Yamamoto, T., Konno, T., and Maeda, H. (1991). Kinin-generating cascade in advanced cancer patients and in vitro study. *Jpn. J. Cancer Res.* **82**: 732-741

(40) Lijnen, H.R., Ugwu, F., Bini, A., and Collen, D. (1998). Generation of an angiostatin-like fragment from plasminogen by stromelysin-1 (MMP-3). *Biochemistry* **14:** 4699-4702.

(41) Moreno, J.J., and Pryor, W. (1992). Inactivation of α_1-protease inhibitor by peroxynitrite. *Chem. Res. Toxicol.* **5**: 425-431.

(42) Jackson, J.R., Seed, M.P., Kirchen, C.H., Willoguhby, D.A., and Winkler, J.D. (1997). The codependence of angiogenesis and chronic inflammation. *FASEB J.* **11**: 457-465.

(43) Seymour, L.W., Miyamoto, Y., Maeda, H., Brereton, M., Strohalm, J., Ulbrich, K., and Duncan, R. (1995). Influence of molecular weight on passive tumor accumulation of a soluble macromolecular drug carrier. *Eur. J. Cancer* **31A**: 766-770.

(44) Haley B, Frenkel E. Nanoparticles for drug delivery in cancer treatment. Urologic Oncology-Seminars and Original Investigations. 2008;26:57-64.

(45) Phillips BE, Giannoukakis N. Drug delivery technologies for autoimmune disease. Expert Opinion on Drug Delivery. 2010;7:1279-1289.

(46) Rihova B. Receptor-mediated targeted drug or toxin delivery. Adv Drug Deliv Rev. 1998;29:273-289.

(47) ROBINSON M. The Role of Clathrin, Adapters and Dynamin in Endocytosis. Curr Opin Cell Biol. 1994;6:538-544.

(48) Lamaze, C. and Schmid, S.L. (1995). The emergence of clathrin-independent pinocytic pathways. *Curr. Opin. Cell Biol.* **7**: 573-580.

(49) Anderson, R.G.W., Kamen, B.A., Rothberg, K.G. and Lacy, S.W. (1992). Potocytosis: sequestration and transport of small molecules by caveolae. *Science*. **255**: 410-411.

(50) Stoovogel, W. Strous, G.J. Geuze, H.J. Oorsschot V. and Schwartz, A.L. (1991). Late endosome derive from early endosome by maturation. *Cell.* **65**: 417-427.

(51) Kato, Y. Seita, T. Kuwabara T. and Sugiyama, Y. (1996). Kinetic analysis of receptor-mediated endocytosis (RME) of proteins and peptides: use of RME as a drug delivery system. *J. Control. Release* **39**: 191-200.

(52) Leamon, C.P. and Low, P.S. (1991). Delivery of macromolecules into living cells: A method that exploits folate receptor endocytosis. *Proc.Natl. Acad. Sci. USA* **88**: 5572-5576.

(53) Huennekens F.M.: Folic acid coenzymes in the biosynthesis of purines and pyrimidines. Vitam Horm 1968, 26:375,.

(54) Antony, A.C. (1992). The biological chemistry of folate receptors. *Blood* **79**: 2807-2820.

(55) Kamen, B.A., and Capdevila, A. (1986). Receptor-mediated folate accumulation is regulated by the cellular folate content. *Proc. Natl. Acad. Sci. USA* **83**: 5983-5987.

(56) Antony, A.C. (1996). Folate receptors. *Ann. Rev. Nutr.* **16**: 501-521.

(57) Wang, X., Shen, F., Freisheim, J.H., Gentry, L.E., and Ratnam, M. (1992). Differential stereospecificities and affinities of folate receptor isoforms for folate compounds and antifolates. *Biochem. Pharmacol.* **44**: 1898-1901.

(58) Anderson, R.G.W., Kamen, B.A., Rothberg, K.G. and Lacy, S.W. (1992). Potocytosis: sequestration and transport of small molecules by caveolae. *Science*. **255**: 410-411.

(59) Lee, R.J., Wang, S., Low, P.S. (1996). Measurement of endosome pH following folate receptor-mediated endocytosis. *Biochim. Biophys. Acta* **1312**: 237-242.

(60) Weitman, S.D., Lark, R.H., Coney, L.R., Fort, D.W., Frasca, V., Zurawski, V.R. Jr, Kamen, B.A. (1992). Distribution of the folate receptor GP38 in normal and malignant cell lines and tissues. *Cancer Res.* **52**: 3396-3401.

(61) Reddy, J.A,. Haneline, L.S., Srour, E.F., Antony, A.C., Clapp, D.W,. and Low, P.S. (1999). Expression and functional characterization of the beta-isoform of the folate receptor on CD34+ cells. *Blood* **93**: 3940-3948.

(62) Garin-Chesa, P., Campbell, I., Saigo, P., Lewis, J., Old, L., and Rettig, W. (1993). Trophoblast and ovarian cancer antigen LK26. Sensitivity and specificity in immunopathology and molecular identification as a folate-binding protein. *Am. J. Path.* **142**: 557-567.

(63) Ross, J.F., Wang, H., Behm, F.G., Mathew, P., Wu, M., Booth, R., Ratnam, M. (1999). Folate receptor type beta is a neutrophilic lineage marker and is differentially expressed in myeloid leukemia. *Cancer*. **85**: 348-357

(64) Bottero, F., Tomassetti, A., Canevari, S., Miotti, S., Menard, S., and Calnagi, M.I. (1993). Gene transfection and expression of the ovarian carcinoma marker folate binding protein on NIH/3T3 cells increases cell growth in vitro and in vivo. *Cancer Res.* **53**: 5791-5796.

(65) Toffoli, G., Cernigio, C., Russo, A., Gallo, A., Bagnoli, M., and Boiocchi, M. (1997). Overexpression of folate binding protein in ovarian cancers. *Int. J. Cancer* **74**: 193-198.

(66) Leamon, C.P. and Low, P.S. (1991). Delivery of macromolecules into living cells: A method that exploits folate receptor endocytosis. *Proc.Natl. Acad. Sci. USA* **88**: 5572-5576

(67) Stella, B. Arpicco, S.,. Peracchia, M.T, Desmaele, D., Hoebeke, J., Renoir, M., d'Angelo, J., Cattel, L., Couvreur, P. (2000). Design of folic acid-conjugated nanoparticles for drug targeting. *J. Pharm. Sci.*, **89**:1452-1464.

(68) Yoo H, Park T. Folate receptor targeted biodegradable polymeric doxorubicin micelles. J Controlled Release. 2004;96:273-283.

(69) Feng S, Chien S. Chemotherapeutic engineering: Application and further development of chemical engineering principles for chemotherapy of cancer and other diseases. Chemical Engineering Science. 2003;58:4087-4114.

(70) Rowinsky E. The development and clinical utility of the taxane class of antimicrotubule chemotherapy agents. Annu Rev Med. 1997;48:353-374.

(71) Minotti G, Menna P, Salvatorelli E, Cairo G, Gianni L. Anthracyclines: Molecular advances and pharmacologic developments in antitumor activity and cardiotoxicity. Pharmacol Rev. 2004;56:185-229.

(72) WEISS R. The Anthracyclines - Will we Ever Find a Better Doxorubicin. Semin Oncol. 1992;19:670-686.

(73) Hurley L. DNA and its associated processes as targets for cancer therapy. Nature Reviews Cancer. 2002;2:188-200.

(74) Boulikas T, Vougiouka M. Cisplatin and platinum drugs at the molecular level (review). Oncol Rep. 2003;10:1663-1682

(75) Maeda H. The enhanced permeability and retention (EPR) effect in tumor vasculature: The key role of tumor-selective macromolecular drug targeting. Advances in Enzyme Regulation, Vol 41. 2001;41:189-207.

(76) Mitomo, K., Griesenbach, U..Toward gene therapy for cystic fibrosis using a lentivirus pseudotyped with Sendai virus envelopes. *Molecular therapy : the journal of the American Society of Gene Therapy* 18.6; **2010**; 1173-1182.

(77) Kay, M., Rothenberg, S.In vivo gene therapy of hemophilia B: sustained partial correction in factor IX-deficient dogs. *Science* 262.5130; **1993**; 117-119.

(78) Lozier, J. Gene therapy of the hemophilias. *Seminars in hematology* 41.4 **;2004**, 287-296.

(79) DelloRusso, C., Scott, J.M., et al. Functional correction of adult mdx mouse muscle using gutted adenoviral vectors expressing full-length dystrophin. *Proceedings of the National Academy of Sciences* 99.20; **2002**; 12979-12984.

(80) Chowdhury, J., Grossman, M., et al. Long-term improvement of hypercholesterolemia after ex vivo gene therapy in LDLR-deficient rabbits. *Science* 254.5039 **;1991**; 1802-1805.

(81) Cavazzana-Calvo, M., Payen, E., et al. Transfusion independence and HMGA2 activation after gene therapy of human beta-thalassaemia. *Nature* 467.7313 **;2010**; 318-322.

(82) Cavazzana-Calvo, M., Hacein-Bey, S., et al. Gene therapy of human severe combined immunodeficiency (SCID)-X1 disease. *Science (New York, N.Y.)* 288.5466; **2000;** 669-672.

(83) Ott, M.G., Schmidt, M., et al. Correction of X-linked chronic granulomatous disease by gene therapy, augmented by insertional activation of MDS1-EVI1, PRDM16 or SETBP1. *Nature medicine* 12.4; **2006;** 401-409.

(84) Caplen N. Gene therapy progress and prospects. Downregulating gene expression: the impact of RNA interference. Gene Ther. 2004;11:1241-1248.

(85) Dorsett Y, Tuschl T. siRNAs: Applications in functional genomics and potential as therapeutics. Nature Reviews Drug Discovery. 2004;3:318-329.

(86) Fire A, Xu S, Montgomery M, Kostas S, Driver S, Mello C. Potent and specific genetic interference by double-stranded RNA in Caenorhabditis elegans. Nature. 1998;391:806-811.

(87) J. C. Skou, Biochim. Biophys. Acta 1957, 23, 394.

(88) SWEADNER K. Isozymes of the Na+/k+-Atpase. Biochim Biophys Acta. 1989;988:185-220.

(89) Kaplan J. Biochemistry of Na,K-ATPase. Annu Rev Biochem. 2002;71:511-535.

(90) Liang M, Tian J, Liu L, Pierre S, Liu J, Shapiro J, et al. Identification of a pool of non-pumping Na/K-ATPase. J Biol Chem. 2007;282:10585-10593.

(91) Xie Z. Molecular mechanisms of Na/K-ATPase-mediated signal transduction. Na,k-Atpase and Related Cation Pumps: Structure, Function, and Regulatory Mechanisms. 2003;986:497-503.

(92) Mijatovic T, Roland I, Van Quaquebeke E, Nilsson B, Mathieu A, Van Vynckt F, et al. The alpha 1 subunit of the sodium pump could represent a novel target to combat non-small cell lung cancers. J Pathol. 2007;212:170-179.

(93) Mobasheri A, Avila J, Cozar-Castellano I, Brownleader M, Trevan M, Francis M, et al. Na+, K+-ATPase isozyme diversity; Comparative biochemistry and physiological implications of novel functional interactions. Biosci Rep. 2000;20:51-91.

(94) Blanco G. Na,K-ATPase subunit heterogeneity as a mechanism for tissue-specific ion regulation. Semin Nephrol. 2005;25:292-303.

(95) Shen SS, Hamamoto ST, Bern HA, Steinhardt RA. Alteration of sodium transport in mouse mammary epithelium associated with neoplastic transformation. *Cancer Res* 1978;**38:**1356–1361.

(96) GONTAGRABIEC K, ROSSOWSKI W, SZUMIEL I. Properties of Na+/k+ Atpase and Alkaline-Phosphatase Alter during Spontaneous and Radiation-Induced Leukemogenesis in Mice. Neoplasma. 1986;33:141-155.

(97) AKOPYANZ N, BROUDE N, BEKMAN E, MARZEN E, SVERDLOV E. Tissue-Specific Expression of Na,k-Atpase Beta-Subunit - does Beta-2 Expression Correlate with Tumorigenesis. FEBS Lett. 1991;289:8-10.

(98) Boukerche H, Su Z, Kang D, Fisher P. Identification and cloning of genes displaying elevated expression as a consequence of metastatic progression in human melanoma cells by rapid subtraction hybridization. Gene. 2004;343:191-201.

(99) Davis ME, Chen Z.,Shin DM. Nanoparticle therapeutics: an emerging treatment modality for cancer. Nature Reviews Drug Discovery. 2008;7:771-782.

(100) Zamboni W. Liposomal, nanoparticle, and conjugated formulations of anticancer agents. Clinical Cancer Research. 2005;11:8230-8234.

(101) Proceedings of the AACR-NCI-EORTC International Conference: Molecular Targets and Cancer Therapeutics; 2011 Nov 12-16; San Francisco, CA. Philadelphia (PA): AACR; Mol Cancer Ther 2011;10(11 Suppl):Abstract nr B115.

(102) Langer R. Drug delivery and targeting. Nature. 1998;392:5-10.

(103) Duncan R. Polymer conjugates as anticancer nanomedicines. Nature Reviews Cancer. 2006;6:688-701.

(104) Mura S, Nicolas J, Couvreur P. Stimuli-responsive nanocarriers for drug delivery. Nature Materials. 2013;12:991-1003

(105) Tagami T, Foltz WD, Ernsting MJ, Lee CM, Tannock IF, May JP, et al. MRI monitoring of intratumoral drug delivery and prediction of the therapeutic effect with a multifunctional thermosensitive liposome. Biomaterials. 2011;32:6570-6578.

(106) Al-Ahmady ZS, Al-Jamal WT, Bossche JV, Bui TT, Drake AF, Mason AJ, et al. Lipid-Peptide Vesicle Nanoscale Hybrids for Triggered Drug Release by Mild Hyperthermia in Vitro and in Vivo. Acs Nano. 2012;6:9335-9346.

(107) Zhang L, Wang T, Yang L, Liu C, Wang C, Liu H, et al. General Route to Multifunctional Uniform Yolk/Mesoporous Silica Shell Nanocapsules: A Platform for Simultaneous Cancer-Targeted Imaging and Magnetically Guided Drug Delivery. Chemistry-a European Journal. 2012;18:12512-12521.

(108) Hua M, Liu H, Yang H, Chen P, Tsai R, Huang C, et al. The effectiveness of a magnetic nanoparticle-based delivery system for BCNU in the treatment of gliomas. Biomaterials. 2011;32:516-527.

(109) Plassat V, Wilhelm C, Marsaud V, Menager C, Gazeau F, Renoir J, et al. Anti-Estrogen-Loaded Superparamagnetic Liposomes for Intracellular Magnetic Targeting and Treatment of Breast Cancer Tumors. Advanced Functional Materials. 2011;21:83-92.

(110) Zhang F, Braun GB, Pallaoro A, Zhang Y, Shi Y, Cui D, et al. Mesoporous Multifunctional Upconversion Luminescent and Magnetic "Nanorattle" Materials for Targeted Chemotherapy. Nano Letters. 2012;12:61-67.

(111) Park JW, Bae KH, Kim C, Park TG. Clustered Magnetite Nanocrystals Cross-Linked with PEI for Efficient siRNA Delivery. Biomacromolecules. 2011;12:457-465.

(112) Prijic S, Prosen L, Cemazar M, Scancar J, Romih R, Lavrencak J, et al. Surface modified magnetic nanoparticles for immuno-gene therapy of murine mammary adenocarcinoma. Biomaterials. 2012;33:4379-4391.

(113) Schroeder A, Honen R, Turjeman K, Gabizon A, Kost J, Barenholz Y. Ultrasound triggered release of cisplatin from liposomes in murine tumors. J Controlled Release. 2009;137:63-68.

(114) Kheirolomoom A, Mahakian LM, Lai C, Lindfors HA, Seo JW, Paoli EE, et al. Copper-Doxorubicin as a Nanoparticle Cargo Retains Efficacy with Minimal Toxicity. Molecular Pharmaceutics. 2010;7:1948-1958.

(115) Rapoport NY, Kennedy AM, Shea JE, Scaife CL, Nam K. Controlled and targeted tumor chemotherapy by ultrasound-activated nanoemulsions/microbubbles. J Controlled Release. 2009;138:268-276.

(116) Zhao L, Kim T, Huh KM, Kim H, Kim SY. Self-assembled photosensitizer-conjugated nanoparticles for targeted photodynamic therapy. J Biomater Appl. 2013;28:434-447.

117) Yang J, Lee J, Kang J, Oh SJ, Ko H, Son J, et al. Smart Drug-Loaded Polymer Gold Nanoshells for Systemic and Localized Therapy of Human Epithelial Cancer. Adv Mater. 2009;21:4339-+.

(118) You J, Zhang R, Xiong C, Zhong M, Melancon M, Gupta S, et al. Effective Photothermal Chemotherapy Using Doxorubicin-Loaded Gold Nanospheres That Target EphB4 Receptors in Tumors. Cancer Res. 2012;72:4777-4786.

(119) Ge J, Neofytou E, Cahill,Thomas J.,,III, Beygui RE, Zare RN. Drug Release from Electric-Field-Responsive Nanoparticles. Acs Nano. 2012;6:227-233.

(120) Yan Q, Yuan J, Cai Z, Xin Y, Kang Y, Yin Y. Voltage-Responsive Vesicles Based on Orthogonal Assembly of Two Homopolymers. J Am Chem Soc. 2010;132:9268-9270.

(121) Kim H, Jeong S, Park J. Electrical Switching between Vesicles and Micelles via Redox-Responsive Self-Assembly of Amphiphilic Rod-Coils. J Am Chem Soc. 2011;133:5206-5209.

(122) Kim JA, Lee WG. Role of weakly polarized nanoparticles in electroporation. Nanoscale. 2011;3:1526-1532.

(123) Wang S, Zhang X, Yu B, Lee RJ, Lee LJ. Targeted nanoparticles enhanced flow electroporation of antisense oligonucleotides in leukemia cells. Biosens Bioelectron. 2010;26:778-783.

(124) Deng Z, Zhen Z, Hu X, Wu S, Xu Z, Chu PK. Hollow chitosan-silica nanospheres as pH-sensitive targeted delivery carriers in breast cancer therapy. Biomaterials. 2011;32:4976-4986.

(125) Min KH, Kim J, Bae SM, Shin H, Kim MS, Park S, et al. Tumoral acidic pH-responsive MPEG-poly(beta-amino ester) polymeric micelles for cancer targeting therapy. J Controlled Release. 2010;144:259-266.

(126) Griset AP, Walpole J, Liu R, Gaffey A, Colson YL, Grinstaff MW. Expansile Nanoparticles: Synthesis, Characterization, and in Vivo Efficacy of an Acid-Responsive Polymeric Drug Delivery System. J Am Chem Soc. 2009;131:2469-+.

(127) You J, Auguste DT. Nanocarrier cross-linking density and pH sensitivity regulate intracellular gene transfer. Abstracts of Papers of the American Chemical Society. 2010;240.

(128) Zhu S, Lansakara-P DSP, Li X, Cui Z. Lysosomal Delivery of a Lipophilic Gemcitabine Prodrug Using Novel Acid-Sensitive Micelles Improved Its Antitumor Activity. Bioconjug Chem. 2012;23:966-980.

(129) Du Y, Chen W, Zheng M, Meng F, Zhong Z. pH-sensitive degradable chimaeric polymersomes for the intracellular release of doxorubicin hydrochloride. Biomaterials. 2012;33:7291-7299.

(130) Ren D, Kratz F, Wang S. Protein Nanocapsules Containing Doxorubicin as a pH-Responsive Delivery System. Small. 2011;7:1051-1060.

(131) Kang HC, Bae YH. Co-delivery of small interfering RNA and plasmid DNA using a polymeric vector incorporating endosomolytic oligomeric sulfonamide. Biomaterials. 2011;32:4914-4924.

(132) Su X, Fricke J, Kavanagh DG, Irvine DJ. In Vitro and in Vivo mRNA Delivery Using Lipid-Enveloped pH-Responsive Polymer Nanoparticles. Molecular Pharmaceutics. 2011;8:774-787.

(133) Zhou T, Xiao C, Fan J, Chen S, Shen J, Wu W, et al. A nanogel of on-site tunable pH-response for efficient anticancer drug delivery. Acta Biomaterialia. 2013;9:4546-4557.

(134) Auguste DT, Furman K, Wong A, Fuller J, Armes SP, Deming TJ, et al. Triggered release of siRNA from poly(ethylene glycol)-protected, pH-dependent liposomes. J Controlled Release. 2008;130:266-274.

(135) Lee S, O'Halloran TV, Nguyen ST. Polymer-Caged Nanobins for Synergistic Cisplatin-Doxorubicin Combination Chemotherapy. J Am Chem Soc. 2010;132:17130-17138.

(136) Li J, Huo M, Wang J, Zhou J, Mohammad JM, Zhang Y, et al. Redox-sensitive micelles self-assembled from amphiphilic hyaluronic acid-deoxycholic acid conjugates for targeted intracellular delivery of paclitaxel. Biomaterials. 2012;33:2310-2320.

(137) Li Y, Xiao K, Luo J, Xiao W, Lee JS, Gonik AM, et al. Well-defined, reversible disulfide cross-linked micelles for on-demand paclitaxel delivery. Biomaterials. 2011;32:6633-6645.

(138) Kurtoglu YE, Navath RS, Wang B, Kannan S, Romero R, Kannan RM. Poly(amidoamine) dendrimer-drug conjugates with disulfide linkages for intracellular drug delivery. Biomaterials. 2009;30:2112-2121.

(139) Ong W, Yang Y, Cruciano AC, McCarley RL. Redox-Triggered Contents Release from Liposomes. J Am Chem Soc. 2008;130:14739-14744.

(140) Wang B, Ma R, Liu G, Li Y, Liu X, An Y, et al. Glucose-Responsive Micelles from Self-Assembly of Poly(ethylene glycol)-b-Poly(acrylic acid-co-acrylamidophenylboronic acid) and the Controlled Release of Insulin. Langmuir. 2009;25:12522-12528.

(141) Kim H, Kang YJ, Kang S, Kim KT. Monosaccharide-Responsive Release of Insulin from Polymersomes of Polyboroxole Block Copolymers at Neutral pH. J Am Chem Soc. 2012;134:4030-4033.

(142) Kim H, Kong YJ, Jeong ES, Kong S, Kim KT. Glucose-Responsive Disassembly of Polymersomes of Sequence-Specific Boroxole-Containing Block Copolymers under Physiologically Relevant Conditions. Acs Macro Letters. 2012;1:1194-1198.

(143) Okhapkin I, Makhaeva E, Khokhlov A. Water solutions of amphiphilic polymers: Nanostructure formation and possibilities for catalysis. Conformation-Dependent Design of Sequences in Copolymers i. 2006;195:177-210.

(144) LAU K, DILL K. A Lattice Statistical-Mechanics Model of the Conformational and Sequence-Spaces of Proteins. Macromolecules. 1989;22:3986-3997.

(145) WEST M, HECHT M. Binary Patterning of Polar and Nonpolar Amino-Acids in the Sequences and Structures of Native Proteins. Protein Science. 1995;4:2032-2039.

(146) KAMTEKAR S, SCHIFFER J, XIONG H, BABIK J, HECHT M. Protein Design by Binary Patterning of Polar and Nonpolar Amino-Acids. Science. 1993;262:1680-1685.

(147) Okhapkin I, Makhaeva E, Khokhlov A. Two-dimensional classification of amphiphilic monomers based on interfacial and partitioning properties. 1. Monomers of synthetic water-soluble polymers. Colloid Polym Sci. 2005;284:117-123.

(148) Discher DE, Ahmed F. Polymersomes. Annu Rev Biomed Eng. 2006;8:323-341.

(149) Cornelissen J, Fischer M, Sommerdijk N, Nolte R. Helical superstructures from charged poly(styrene)-poly(isocyanodipeptide) block copolymers. Science. 1998;280:1427-1430.

(150) Discher B, Won Y, Ege D, Lee J, Bates F, Discher D, et al. Polymersomes: Tough vesicles made from diblock copolymers. Science. 1999;284:1143-1146.

(151) Aranda-Espinoza H, Bermudez H, Bates F, Discher D. Electromechanical limits of polymersomes. Phys Rev Lett. 2001;87:208301.

(152) Dimova R, Seifert U, Pouligny B, Forster S, Dobereiner H. Hyperviscous diblock copolymer vesicles. European Physical Journal E. 2002;7:241-250.

(153) Lee J, Bermudez H, Discher B, Sheehan M, Won Y, Bates F, et al. Preparation, stability, and in vitro performance of vesicles made with diblock copolymers. Biotechnol Bioeng. 2001;73:135-145.

(154) Lee J, Santore M, Bates F, Discher D. From membranes to melts, rouse to entangled: Diffusion in polymersome versus lipid bilayers. Biophys J. 2002;82:551A-551A.

(155) Bermudez H, Brannan A, Hammer D, Bates F, Discher D. Molecular weight dependence of polymersome membrane structure, elasticity, and stability. Macromolecules. 2002;35:8203-8208.

(156) Hammer D, Discher D, Bates F, Discher B, Lee C, Bermudez H, et al. Polymersomes: Tough vesicles made from block copolymers. Abstracts of Papers of the American Chemical Society. 2000;220:U258-U258.

(157) BANGHAM A. Liposomes - the Babraham Connection. Chem Phys Lipids. 1993;64:275-285.

(158) Lipowsky R., Sackmann E. Structure and dynamics of membranes-from cells to vesicles. Science, 1995.

(159) Chambon P, Blanazs A, Battaglia G, Armes SP. Facile Synthesis of Methacrylic ABC Triblock Copolymer Vesicles by RAFT Aqueous Dispersion Polymerization. Macromolecules. 2012;45:5081-5090.

(160) Blanazs A, Massignani M, Battaglia G, Armes SP, Ryan AJ. Tailoring Macromolecular Expression at Polymersome Surfaces. Advanced Functional Materials. 2009;19:2906-2914.

(161) Murdoch C, Reeves KJ, Hearnden V, Colley H, Massignani M, Canton I, et al. Internalization and biodistribution of polymersomes into oral squamous cell carcinoma cells in vitro and in vivo. Nanomedicine. 2010;5:1025-1036.

(162) Lomas H, Canton I, MacNeil S, Du J, Armes SP, Ryan AJ, et al. Biomimetic pH sensitive polymersomes for efficient DNA encapsulation and delivery RID E-5399-2010. Adv Mater. 2007;19:4238-+.

(163) Du F, Wang Y, Zhang R, Li Z. Intelligent nucleic acid delivery systems based on stimuli-responsive polymers. Soft Matter. 2010;6:835-848.

(164) Lomas H, Du J, Canton I, Madsen J, Warren N, Armes SP, et al. Efficient Encapsulation of Plasmid DNA in pH-Sensitive PMPC-PDPA Polymersomes: Study of the Effect of PDPA Block Length on Copolymer-DNA Binding Affinity. Macromolecular Bioscience. 2010;10:513-530.

(165) Meng F, Zhong Z, Feijen J. Stimuli-Responsive Polymersomes for Programmed Drug Delivery. Biomacromolecules. 2009;10:197-209.

(166) Du J, Tang Y, Lewis A, Armes S. pH-sensitive vesicles based on a biocompatible zwitterionic diblock copolymer. J Am Chem Soc. 2005;127:17982-17983.

(167) Soo P, Eisenberg A. Preparation of block copolymer vesicles in solution. Journal of Polymer Science Part B-Polymer Physics. 2004;42:923-938.

(168) Marsden HR, Gabrielli L, Kros A. Rapid preparation of polymersomes by a water addition/solvent evaporation method. Polymer Chemistry. 2010;1:1512-1518.

(169) Ghoroghchian P, Li G, Levine D, Davis K, Bates F, Hammer D, et al. Bioresorbable vesicles formed through spontaneous self-assembly of amphiphilic poly(ethylene oxide)-block-polycaprolactone. Macromolecules. 2006;39:1673-1675.

(170) Rodriguez N, Pincet F, Cribier S. Giant vesicles formed by gentle hydration and electroformation: A comparison by fluorescence microscopy. Colloids and Surfaces B-Biointerfaces. 2005;42:125-130.

(171) You Shusen, Yang Wantai, Yin Meizhen. Synthesis and Applications of Stimulus-Responsive Functional Polymers. Progress in Chemistry. 2012;24:2198-2211.

(172) Pangburn TO, Georgiou K, Bates FS, Kokkoli E. Targeted Polymersome Delivery of siRNA Induces Cell Death of Breast Cancer Cells Dependent upon Orai3 Protein Expression. Langmuir. 2012;28:12816-12830.

(173) Carthew RW, Sontheimer EJ. Origins and Mechanisms of miRNAs and siRNAs. Cell. 2009;136:642-655.

(174) Vogelstein B, Kinzler K. Cancer genes and the pathways they control. Nat Med. 2004;10:789-799.

(175) Panta G, Nwariaku F, Kim L. RET signals through focal adhesion kinase in medullary thyroid cancer cells. Surgery. 2004;136:1212-1216.

(176) Chen L, Le H, Qin R, Kumar M, Du Z, Xia R, et al. Reversal of the phenotype by K-ras(val12) silencing mediated by adenovirus-delivered siRNA in human pancreatic cancer cell line Panc-1. World Journal of Gastroenterology. 2005;11:831-838.

(177) Brummelkamp T, Bernards R, Agami R. Stable suppression of tumorigenicity by virus-mediated RNA interference. Cancer Cell. 2002;2:243-247.

(178) Aharinejad S, Paulus P, Sioud M, Hofmann M, Zins K, Schafer R, et al. Colony-stimulating factor-1 blockade by antisense oligonucleotides and small interfering RNAs suppresses growth of human mammary tumor xenografts in mice. Cancer Res. 2004;64:5378-5384.

(179) Pal A, Ahmad A, Khan S, Sakabe I, Zhang C, Kasid U, et al. Systemic delivery of RafsiRNA using cationic cardiolipin liposomes silences Raf-1 expression and inhibits tumor growth in xenograft model of human prostate cancer. Int J Oncol. 2005;26:1087-1091.

(180) Easton J., Lincoln F..Modified Cyclodextrins: Scaffolds and Templates for Supramolecular Chemistry, 1999.

(181) Hu-Lieskovan S, Heidel J, Bartlett D, Davis M, Triche T. Sequence-specific knockdown of EWS-FLI1 by targeted, nonviral delivery of small interfering RNA inhibits tumor growth in a murine model of metastatic Ewing's sarcoma. Cancer Res. 2005;65:8984-8992.

(182) Bartlett DW, Su H, Hildebrandt IJ, Weber WA, Davis ME. Impact of tumor-specific targeting on the biodistribution and efficacy of siRNA nanoparticles measured by multimodality in vivo imaging. Proc Natl Acad Sci U S A. 2007;104:15549-15554.

(183) Bartlett DW, Davis ME. Impact of tumor-specific targeting and dosing schedule on tumor growth inhibition after intravenous administration of siRNA-containing nanoparticles. Biotechnol Bioeng. 2008;99:975-985.

(184) Heidel JD, Yu Z, Liu JY, Rele SM, Liang Y, Zeidan RK, et al. Administration in non-human primates of escalating intravenous doses of targeted nanoparticles containing ribonucleotide reductase subunit M2 siRNA. Proc Natl Acad Sci U S A. 2007;104:5715-5721.

(185) Chiefari J, Chong Y, Ercole F, Krstina J, Jeffery J, Le T, et al. RID A-9022-2010 RID A-1984-2008. Macromolecules. 1998;31:5559-5562.

(186) Moad G, Chiefari J, Chong Y, Krstina J, Mayadunne R, Postma A, et al. Living free radical polymerization with reversible addition-fragmentation chain transfer (the life of RAFT). Polym Int. 2000;49:993-1001.

(187) Moad G, Rizzardo E, Thang S. Living radical polymerization by the RAFT process. Aust J Chem. 2005;58:379-410.

(188) Braunecker WA, Matyjaszewski K. Controlled/living radical polymerization: Features, developments, and perspectives. Progress in Polymer Science. 2007;32:93-146.

(189) Jones MW, Mantovani G, Blindauer CA, Ryan SM, Wang X, Brayden DJ, et al. Direct Peptide Bioconjugation/PEGylation at Tyrosine with Linear and Branched Polymeric Diazonium Salts. J Am Chem Soc. 2012;134:7406-7413.

(190) De Luca L. Naturally occurring and synthetic imidazoles: Their chemistry and their biological activities. Curr Med Chem. 2006;13:1-23.

(191) Kim D, Lee ES, Oh KT, Gao ZG, Bae YH. Doxorubicin-Loaded Polymeric Micelle Overcomes Multidrug Resistance of Cancer by Double-Targeting Folate Receptor and Early Endosomal pH. Small. 2008;4:2043-2050.

(192) Boyer C, Bulmus V, Davis TP. Efficient Usage of Thiocarbonates for Both the Production and the Biofunctionalization of Polymers RID A-5436-2009 RID B-6395-2008. Macromolecular Rapid Communications. 2009;30:493-497.

(193) Yin M, Habicher W, Voit B. Preparation of functional poly(acrylates and methacrylates) and block copolymers formation based on polystyrene macroinitiator by ATRP. Polymer. 2005;46:3215-3222.

(194) Yoo H, Park T. Folate-receptor-targeted delivery of doxorubicin nano-aggregates stabilized by doxorubicin-PEG-folate conjugate. J Controlled Release. 2004;100:247-256.

(195) KRANZ D, PATRICK T, BRIGLE K, SPINELLA M, ROY E. Conjugates of Folate and Anti-T-Cell-Receptor Antibodies Specifically Target Folate-Receptor-Positive Tumor-Cells for Lysis. Proc Natl Acad Sci U S A. 1995;92:9057-9061.

(196) Sims G.E., and Snape T.J, A method for the estimation of polyethylene glycol in plasma protein fractions. *Anal Biochem.;* **107**: 60-3, 1980.

(197) Caliceti, P.; Salmaso, S.; Semenzato, A.; Carofiglio, T.; Fornasier, R.; Fermeglia, M.; Ferrone, M.; Pricl, S. Synthesis and physicochemical characterization of folate-cyclodextrin bioconjugate for active drug delivery. Bioconjug. Chem. 2003, 14, 899-908.

(198) Fernyhough C, Ryan AJ, Battaglia G. pH controlled assembly of a polybutadiene-poly(methacrylic acid) copolymer in water: packing considerations and kinetic limitations. Soft Matter. 2009;5:1674-1682.

(199) Urbiola K, Garcia L, Zalba S, Garrido MJ, Tros de Ilarduya C. Efficient serum-resistant lipopolyplexes targeted to the folate receptor. European Journal of Pharmaceutics and Biopharmaceutics. 2013;83:358-363.

(200) Kurosaki T, Morishita T, Kodama Y, Sato K, Nakagawa H, Higuchi N, et al. Nanoparticles Electrostatically Coated with Folic Acid for Effective Gene Therapy. Molecular Pharmaceutics. 2011;8:913-919.

(201) Massignani M, LoPresti C, Blanazs A, Madsen J, Armes SP, Lewis AL, et al. Controlling Cellular Uptake by Surface Chemistry, Size, and Surface Topology at the Nanoscale. Small. 2009;5:2424-2432.

(202) Wang Z, Cui Y, Xu Z, Qu J. Hot water-promoted ring-opening of epoxides and aziridines by water and other nucleopliles. J Org Chem. 2008;73:2270-2274.

(203) Fujioka H, Kubo O, Senami K, Minamitsuji Y, Maegawa T. Remarkable effect of 2,2 '-bipyridyl: mild and highly chemoselective deprotection of methoxymethyl (MOM) ethers in combination with TMSOTf (TESOTf)-2,2 '-bipyridyl. Chemical Communications. 2009:4429-4431.

(204) Scriven E. F. V. ,4-Dialkylaminopyridines: super acylation and alkylation catalysts, Chemical Society Reviews, vol. 12, no. 2, pp. 129–161 , (1983).

(205) Matini, T.; Francini, N.; Battocchio, A.; Spain, S.G.; Mantovani, G.; Vicent, M.J.; Sanchis, J.; Gallon, E.; Mastrotto, F.; Salmaso, S.; Caliceti, P. and Alexander C., (2014) Polym. Chem., DOI: 10.1039/c3py00744h

(206) Weber WG, McLeary JB, Sanderson RD. Facile preparation of bis(thiocarbonyl)disulfides via elimination. Tetrahedron Lett. 2006;47:4771-4774.

(207) Mata J, Majhi P, Guo C, Liu H, Bahadur P. Concentration, temperature, and salt-induced micellization of a triblock copolymer Pluronic L64 in aqueous media. J Colloid Interface Sci. 2005;292:548-556.

(208) Valade D, Boyer C, Davis TP, Bulmus V. Synthesis of siRNA Polyplexes Adopting a Combination of RAFT Polymerization and Thiol-ene Chemistry. Aust J Chem. 2009;62:1344-1350.

(209) Liu J, Bulmus V, Barner-Kowollik C, Stenzel MH, Davis TP. Direct synthesis of pyridyl disulfide-terminated polymers by RAFT polymerization. Macromolecular Rapid Communications. 2007;28:305-314.

(210) G. T. Hermanson, Bioconjugate techniques, 1996.

(211) MALLAMACE F, MICALI N, VASI C. Viscoelastic Properties of Charged Colloids, Polystyrene, and Silica-Water Suspensions. Physical Review a. 1990;42:7304-7311.

(212) Yamago S, Yamada T, Togai M, Ukai Y, Kayahara E, Pan N. Synthesis of Structurally Well-Defined Telechelic Polymers by Organostibine-Mediated Living Radical Polymerization: In Situ Generation of Functionalized Chain-Transfer Agents and Selective omega-End-Group Transformations. Chemistry-a European Journal. 2009;15:1018-1029.

(213) B. Neises and W. Steglich, Angewandte Chemie-International, Edition in English, 1978, 17, 522-524.

(214) Soeriyadi AH, Boyer C, Burns J, Becer CR, Whittaker MR, Haddleton DM, et al. High fidelity vinyl terminated polymers by combining RAFT and cobalt catalytic chain transfer (CCT) polymerization methods. Chemical Communications. 2010;46:6338-6340.

(215) Perrier S, Takolpuckdee P. Macromolecular design via reversible addition-fragmentation chain transfer (RAFT)/Xanthates (MADIX) polymerization. Journal of Polymer Science Part A-Polymer Chemistry. 2005;43:5347-5393.

(216) Zhang Y, Zhang W, Johnston AH, Newman TA, Pyykko I, Zou J. Targeted delivery of Tet1 peptide functionalized polymersomes to the rat cochlear nerve. International Journal of Nanomedicine. 2012;7:1015-1022.

(217) Upadhyay KK, Mishra AK, Chuttani K, Kaul A, Schatz C, Le Meins J, et al. The in vivo behavior and antitumor activity of doxorubicin-loaded poly(gamma-benzyl L-glutamate)-block-hyaluronan polymersomes in Ehrlich ascites tumor-bearing BalB/c mice. Nanomedicine-Nanotechnology Biology and Medicine. 2012;8:71-80.

(218) Cavallaro G, Mariano L, Salmaso S, Caliceti P, Gaetano G. Folate-mediated targeting of polymeric conjugates of gemcitabine. Int J Pharm. 2006;307:258-269.

(219) Petersen MA, Yin L, Kokkoli E, Hillmyer MA. Synthesis and characterization of reactive PEO-PMCL polymersomes. Polymer Chemistry. 2010;1:1281-1290.

(220) Yang X, Grailer JJ, Rowland IJ, Javadi A, Hurley SA, Matson VZ, et al. Multifunctional Stable and pH-Responsive Polymer Vesicles Formed by Heterofunctional Triblock Copolymer for Targeted Anticancer Drug Delivery and Ultrasensitive MR Imaging. Acs Nano. 2010;4:6805-6817.

(221) KWON G, NAITO M, YOKOYAMA M, OKANO T, SAKURAI Y, KATAOKA K. Micelles Based on Ab Block Copolymers of Poly(ethylene Oxide) and Poly(beta-Benzyl L-Aspartate). Langmuir. 1993;9:945-949.

(222) NEEDHAM D, MCINTOSH T, LASIC D. Repulsive Interactions and Mechanical Stability of Polymer-Grafted Lipid-Membranes. Biochim Biophys Acta. 1992;1108:40-48.

(223) Immordino ML, Dosio F, Cattel L. Stealth liposomes: review of the basic science, rationale, and clinical applications, existing and potential. International Journal of Nanomedicine. 2006;1:297-315.

(224) Huang Q, Baum L, Fu W. Simple and Practical Staining of DNA with GelRed in Agarose Gel Electrophoresis. Clin Lab. 2010;56:149-152.

(225) Cho Y, Kim J, Park K. Pollycation gene delivery systems: escape from endosomes to cytosol. J Pharm Pharmacol. 2003;55:721-734.

(226) Sorkin A, von Zastrow M. Signal transduction and endocytosis: Close encounters of many kinds. Nature Reviews Molecular Cell Biology. 2002;3:600-614

(227) Murthy N, Robichaud J, Tirrell D, Stayton P, Hoffman A. The design and synthesis of polymers for eukaryotic membrane disruption. J Controlled Release. 1999;61:137-143.

(228) LEAMON C, LOW P. Delivery of Macromolecules into Living Cells - a Method that Exploits Folate Receptor Endocytosis. Proc Natl Acad Sci U S A. 1991;88:5572-5576.

(229) Sonvico F, Dubernet C, Marsaud V, Appel M, Chacun H, Stella B, et al. Establishment of an in vitro model expressing the folate receptor for the investigation of targeted delivery systems. Journal of Drug Delivery Science and Technology. 2005;15:407-410.

(230) Malich G, Markovic B, Winder C. The sensitivity and specificity of the MTS tetrazolium assay for detecting the in vitro cytotoxicity of 20 chemicals using human cell lines. Toxicology. 1997;124:179-192.

(231) Barz M, Arminan A, Canal F, Wolf F, Koynov K, Frey H, et al. P(HPMA)-block-P(LA) copolymers in paclitaxel formulations: Polylactide stereochemistry controls micellization, cellular uptake kinetics, intracellular localization and drug efficiency. J Controlled Release. 2012;163:63-74.

(232) Paulos C, Reddy J, Leamon C, Turk M, Low P. Ligand binding and kinetics of folate receptor recycling in vivo: Impact on receptor-mediated drug delivery. Mol Pharmacol. 2004;66:1406-1414.

(233) Boshnjaku V, Shim K, Tsurubuchi T, Ichi S, Szany EV, Xi G, et al. Nuclear localization of folate receptor alpha: a new role as a transcription factor. Scientific Reports. 2012;2:980.

(234) Stover PJ, Field MS. Trafficking of Intracellular Folates. Advances in Nutrition. 2011;2:325-331.

(235) Zhang C, Gao S, Jiang W, Lin S, Du F, Li Z, et al. Targeted minicircle DNA delivery using folate-poly(ethylene glycol)-polyethylenimine as non-viral carrier. Biomaterials. 2010;31:6075-6086.

(236) Fan X, Roy E, Zhu L, Murphy T, Kozlowski M, Nanes M, et al. Nitric oxide donors inhibit luciferase expression in a promoter-independent fashion. J Biol Chem. 2003;278:10232-10238.

(237) Baldwin T. Firefly luciferase: The structure is known, but the mystery remains. Structure. 1996;4:223-228.

(238) Suzuki, N. & Goto, T.. Studies on firefly bioluminescence — II.Identification of oxyluciferin as a product in the bioluminescence offirefly lanterns and in the chemiluminescence of firefly luciferin.Tetrahedron, 1972, 28, 4075–4082.

(239) DEWET J, WOOD K, DELUCA M, HELINSKI D, SUBRAMANI S. Firefly Luciferase Gene - Structure and Expression in Mammalian-Cells. Mol Cell Biol. 1987;7:725-737.

(240) Elbashir S, Harborth J, Lendeckel W, Yalcin A, Weber K, Tuschl T. Duplexes of 21-nucleotide RNAs mediate RNA interference in cultured mammalian cells. Nature. 2001;411:494-498.

(241) Vaupel P, Kelleher D, Thews O. Microtopology of local perfusion, oxygenation, metabolic and energetic status, and interstitial pH in malignant tumors: Techniques and characterization. Experimental Oncology. 2000;22:15-25.

(242) Petros RA, DeSimone JM. Strategies in the design of nanoparticles for therapeutic applications. Nature Reviews Drug Discovery. 2010;9:615-627.

(243) Yoo J, Irvine DJ, Discher DE, Mitragotri S. Bio-inspired, bioengineered and biomimetic drug delivery carriers. Nature Reviews Drug Discovery. 2011;10:521-535.

(244) Hunter AC, Moghimi SM. Cationic carriers of genetic material and cell death: A mitochondrial tale. Biochimica Et Biophysica Acta-Bioenergetics. 2010;1797:1203-1209.

(245) Matsui H, Sakanashi Y, Oyama TM, Oyama Y, Yokota S, Ishida S, et al. Imidazole antifungals, but not triazole antifungals, increase membrane Zn2+ permeability in rat thymocytes - Possible contribution to their cytotoxicity. Toxicology. 2008;248:142-150.

(246) Edward D.L., Kerns H., Drug-like properties: concepts, structure design and methods, Academic Press, Elsevier, London, UK, 2008.